REMARKS

Reexamination and reconsideration in light of the foregoing amendment and following remarks is respectfully requested.

Claims 1, 21, 23, 24, 26, 30-32 and 34-49 are pending in this application. Claims 2-20, 22, 25, 27-29 and 33 have been canceled without prejudice or disclaimer. Claims 1, 21, 23, 24, 26 and 30-32 have been amended and new claims 34-49 have been added. No new matter has been added to the application. Support for the amendments to the claims and for the new claims can be found in the specification as follows:

Claim 1:	The group insulin receptor (IR), IGF-1 receptor (IGF-1R) and insulin receptor related receptor (IRR): page 6, lines 14-17. Step (C) (i): page 7, lines 20-23. Step (C) (ii): page 17, lines 28-34.
Claim 21:	The group IR, IGF-1R and IRR: page 6, lines 14-17.
Claim 23:	Original claim 23 and page 7, lines 20-23.
Claim 24:	Original claim 24, page 17, lines 28-34 and page 13, lines 15-20.
Claim 26:	Original claim 26, page 17, lines 28-34 and page 13, lines 15-20.
Claim 34:	Page 17, lines 28-34.
Claim 35:	Page 28, line 28-33.
Claim 36:	Page 6, lines 14-17 and page 28, lines 28-34.
Claim 37:	Page 29, lines 1-3.
Claim 38:	Page 6, lines 14-17 and page 29 lines 1-3.
Claim 39:	Original claim 4.
Claim 40:	Original claim 4 and page 7, lines 5-6.

Claim 41: Page 7, lines 2-5.

Claim 42: Page 6, lines 14-17 and page 7, lines 2-5.

Claim 43: Original claim 2.

Claim 44: Original claim 13, page 17, lines 28-34 and page 13, lines 15-20.

Claim 45: Original claim 14, page 17, lines 28-34 and page 13, lines 15-20.

Claim 46: Original claim 15, page 6, lines 14-17.

Claim 47: Original claim 1, page 7, lines 13-15 and page 7, lines 23-24.

Claim 48: Page 7, lines 13-15.

Claim 49: Page 7, lines 23-24.

Applicants note the Examiner's consideration of the art cited in the Information Disclosure Statement filed May 26, 2000 as acknowledged in the Office Action Summary. Applicants further note the Examiner's acknowledgment of Applicant's claim of foreign priority under 35 U.S.C. §119 and receipt of the certified priority document.

Applicants want to thank the Examiner for granting the interview on June 24, 2003. The interview provided a greater understanding of the Examiner's position with respect to the following rejections.

REJECTION UNDER 35 U.S.C. § 101

Claims 1-20 were rejected under 35 U.S.C. § 101 as being directed to non-statutory subject matter because "the only steps set forth in claims 1-20 are manipulation of data." Claims 2-20 have been canceled, thereby rendering the rejection moot as to these claims. Claim 1 has been amended to recite a method that is more than a manipulation of data. The claim as amended requires (i) assessing the stereochemical complementarity between a compound and a molecule, (ii) obtaining a

compound that possesses stereochemical complementarity to the molecule; and (iii) testing the compound. For the foregoing reason, it believed that the amendment to claim 1 overcomes the rejection and it is respectfully requested that the rejection be reconsidered and withdrawn.

REJECTION UNDER 35 U.S.C. § 112, FIRST PARAGRAPH

Claims 1-33 were rejected under 35 U.S.C. § 112, first paragraph, for lack of enablement. The Examiner at the interview indicated that the rejection comports with the guidelines set forth in the Trilateral Project WM4 "Report on comparative study on protein 3-dimensional (3-D) structure relating claims" and that the claims need to be restructured to overcome this rejection.

Claims 2-20, 22, 25, 27-29 and 33 have been canceled, thereby rendering the rejection as to these claims moot. As for the remaining claims, claim 1 has been amended to recite a method of "identifying" a compound as opposed to "designing" or selecting a compound. Claim 1 has been further amended to require that the method is directed to identifying a compound that (i) modulates binding of a natural ligand to the insulin receptor (IR), IGF-1 receptor (IGF-1R) or insulin receptor related receptor (IRR) or (ii) modulates signal transduction via IR, IGF-1R or IRR.

Applicants' position is that the level of skill of those working in the field of *in silico* screening at around the priority date of the present application (i.e., around November 1997) was relatively high. More specifically, the average capabilities of those working in this field included the ability to identify candidate binding pockets within any given 3D structure using standard methodologies.

Computer algorithms that may be used for this purpose, include, for example, PASS (evidence: Brady, G.P., Jr. et al., "Fast prediction and visualization of protein binding pockets with PASS," *J. Comput Aided Mol. Des.*, vol. 14, 383-401 (2001); copy attached as Exhibit A). The

PASS algorithm involves coating the surface of the protein structure model with sets of probe spheres, retaining those with low solvent accessibility and identifying some of these as likely centers of binding pockets. A person skilled in this field would have been fully familiar with the implementation of a range of docking programs (such as those listed in the patent application) to screen for candidate binding ligands. Evidence of the techniques that would be well within the capabilities of those skilled in this field are described in the following publications:

(1) Li et al., "Structure-based design of parasitic protease inhibitors," *Bioorg Med Chem*, 1996 Sep, 4(9):1421-7. Copy attached as Exhibit B.

(2) Ring et al., "Structure-based inhibitor design by using protein models for the development of antiparasitic agents," *Proc Natl Acad Sci USA*, 1993 Apr 15, 90(8):3583-7. Copy attached as Exhibit C.

(3) Li et al., "Anti-malarial drug development using models of enzyme structure," *Chem Biol.*, 1994 Sep, 1(1):31-7. Copy attached as Exhibit D.

As mentioned above, Applicants submit that any competent researcher working in the field of *in silico* screening would be able to identify candidate binding pockets in any given 3D structure. In the present case, however, the patent application actually identifies specific "topographic regions" which represent preferred "binding pockets" within the IGF-1R structure. These binding pockets can be used in screening methods to identify potential ligands. For example, the fragment which includes residues 191-290 forms part of the cys-rich region of the ectodomain of IGF-1R. This region is important in determining ligand binding specificity. The specificity determinant can be further limited to residues 223-274 (see page 28, line 12 to page 29, line 15).

The patent application provides further guidance for selecting regions within the identified binding pockets at page 6, line 26 to page 7, line 12. For example, it is stated that the ligand may interact with (i) a region of the L1 domain-cys-rich interface, thereby causing an alteration in the positions of the domains relative to each other; (ii) a hinge region between the L2 domain and the cys-rich domain causing an alteration in the positions of these domains relative to each other; or (iii) the β-sheet of the L1 domain causing an alteration in the position of the L1 domain relative to the position of the cys-rich domain or L2 domain.

The patent application goes even further by specifying two sites on the lower β-sheet of the L1 and L2 domains as suitable targets for screening. See, for example, the specification at page 6, lines 9-14.

Accordingly, the patent application not only identifies the binding pockets within the IGF-1R structure, but also suggests preferred regions within these binding pockets to use in screening for ligands.

Armed with the atomic coordinates of the IGF-1R provided in the patent application and the information regarding preferred regions within specified binding pockets, it would have been a matter of routine for a person skilled in the area of *in silico* screening to utilize any one of the well known docking programs to screen for potential ligands.

On page 3 of the Office Action, the Examiner states that it is unknown and cannot be predicted from the information presented in the specification what degree of stereochemical complementarity is required. Stereochemical complementarity between a chemical compound and the target protein structure is a cumulative effect of the hydrogen bonds, favorable electrostatic interactions, and favorable van der Waals contacts between the compound molecule and the protein

molecule. Depending on the nature of the compound molecule, one factor may predominate over others in contributing to the overall complementarity. Those skilled in the art can visually examine on a computer graphics monitor a compound molecule docked into the binding site of the receptor and assess the source of the complementarity. All docking programs have scoring functions which are used to dock and then rank the molecules with a score indicating how well a particular chemical compound molecule binds to the receptor.

The top-ranking compounds can then be further assessed visually and computationally. For example, a computer program such as XSCORE (evidence: Wang, R. et al., "Further development and validation of empirical scoring functions for structure-based binding affinity prediction," *J. Compu Aided Mol. Design*, Vol 16, 11-26(2002); copy attached as Exhibit E) has a scoring function which predicts the dissociation constant for a given ligand-protein complex structure (for example, the docked compound-receptor complex). This scoring function was derived by fitting the function to the experimentally determined dissociation constants of a set of 200 ligand-protein complexes. As a general rule, stereochemical complementarity is not discussed in terms of degree. *In silico* screening requires certain parameters to be set to determine whether or not any given molecule will register as a stereochemical "fit" with the binding site of interest. A person of skill in this area would be able to set appropriate parameters through trial and error to select for suitable stereochemical complementarity to a binding site described in the patent application.

On page 3 of the Office Action, the Examiner points out that claim 1 requires that the selected compound bind to any molecule of the insulin receptor family and modulate any activity mediated by the molecule. Claim 1 has been amended to make it clear that the compound is tested

for its ability to either modulate binding of a natural ligand to or to modulate signal transduction via a member of the insulin family selected from IGF-1R, IR and IRR.

For all of the foregoing reasons, the specification provides sufficient guidance that a person having ordinary skill in the art would have been able to practice the invention without undue experimentation. Accordingly, claims 1, 21, 23, 24, 26, 30-32 satisfy the requirement of 35 U.S.C. § 112, first paragraph. It is respectfully requested that the rejection be reconsidered and withdrawn.

REJECTION UNDER 35 U.S.C. § 112, SECOND PARAGRAPH

Claims 1-33 were rejected under 35 U.S.C. § 112, second paragraph, as being indefinite. The Examiner objected to language specifically recited in claims 1, 3-6, 16-20 and 21. Claims 2-20 have been canceled, thereby rendering any rejection under 35 U.S.C. § 112, second paragraph, as to these claims moot.

In claim 1, the Examiner objected to the phrase "assessing the stereochemical complementarity between the compound and receptor site of the molecule" in that she did not know "what delimits a topographical region." The phrase has been deleted from the claim. It is believed that by this amendment, the rejection is overcome.

Also in claim 1, the Examiner objected to the phrases "substantially as shown" and "forms an equivalent." With respect to the term "substantially," Applicants submit that a person skilled in the art would have understood that the coordinates set out in Fig. 1 need not be strictly adhered to in order to generate a three dimensional structure *in silico* for screening for ligands of the IR, IGF-1R or IRR. See Section 2173.05(b) of MPEP, and in particular, the discussion on the term "substantially." This Section refers to a decision in which the phrase "which produces substantially equal E and H plane illumination patterns" was considered definite because one of ordinary skill in

the art would know what is meant by "substantially equal". *Andrew Corp v Gabriel Electronics*, 847 F.2d 819, 6 USPQ2d 2010 (Fed. Cir. 1988). In the present case, given the nature of the invention and the experience of those skilled in the art of *in silico* screening, the phrase "substantially as shown in Figure 1" in relation to coordinates would have been clearly understood. Applicants also point out that this phrase is present in a method claim which involves numerous steps including obtaining a compound with requisite stereochemical complementarity and testing the compound for its ability to modulate binding of a natural ligand to or signal transduction via the IR, IGF-1R or IRR. Within the context of this screening process, a person skilled in the art would have understood the flexibility in variation from the exact coordinates shown in Fig. 1 which would allow generation of a structure with sufficient identity to the IGF-1R receptor coordinates listed in Fig. 1 to allow screening for ligands.

With respect to the phrase "forms an equivalent" in claim 1, this phrase has now been amended to refer to an amino acid sequence of IR or IRR that forms an equivalent structure to that formed by amino acids 1-462 or IGF-1R. In light of the information provided in the specification, and in particular, the sequence alignment information provided in Fig. 9, a person skilled in the art would have clearly understood what is meant by this phrase.

With regard to claim 21, the Examiner found the phrase "which are structurally similar to a portion" to be indefinite because "it is unknown what degree of similarity is required to meet this limitation." It is Applicants' position that the phrase would have been clearly understood by a person skilled in the art. In the context of the claim, it would have been clear to such a person that the selected chemical structures must be similar to a sufficient portion of the criteria data set to allow binding of the actual compound to a member of the insulin receptor family.

For all of the foregoing reasons, it is respectfully requested that the rejection of claims 1 and 21 under 35 U.S.C. § 112, second paragraph, be reconsidered and withdrawn.

REJECTION UNDER 35 U.S.C. § 103(a)

Claims 1-20 and 29-34 were rejected under 35 U.S.C. § 103(a) as being unpatentable over Hendry et al. (U.S. Patent No. 5,705,335).[1] Claims 2-20, 29 and 33 have been canceled, thereby rendering the rejection as to these claims moot.

The Examiner finds that the claims are obvious in light of Hendry et al. This reference relates to a computer based method for creating a pharmacophore which involves determining the optimal fit of compounds into nucleic acid sequences such that the lowest energy of interaction and best steric fit are obtained. In support of this rejection, the Examiner refers to the Trilateral Project WM4 "Report on comparative studies on protein 3-dimensional (3-D) structure related claims." This report states that if the difference between the prior art and the claimed invention as a whole is limited to descriptive material stored on or employed by a machine, it is necessary to determine whether the descriptive material is functionally descriptive or non-functionally descriptive material.

Applicants submit that the difference between amended claim 1 and the prior art is not merely limited to descriptive material stored on or employed by a machine. In particular, claim 1 as proposed to be amended not only involves the step of assessing stereochemical complementarity between a compound and the 3-dimensional structure of a molecule of the insulin receptor family,

[1] The inclusion of claim 34 in this rejection is in error since as of the date of the Office Action, there were only 33 claims. It is believed that the Examiner intended the rejection to encompass claims 1-20 and 29-33.

but also involves the step (B) of obtaining a compound which possesses stereochemical complementarity to the molecule; and step (C) of testing the compound for its ability to (i) modulate binding of a natural ligand to the IR, IGF-1R or IRR, or (ii) modulate signal transduction via the IR, IGF-1R or IRR.

Steps (B) and (C) of claim 1 are clearly not merely descriptive material stored on or employed by a machine. These steps involve physical testing of compounds for their ability to modulate a specified activity of a member of the insulin receptor family. Hendry et al. do not disclose or suggest a method of screening for a compound which binds to a molecule of the insulin receptor family followed by testing of compounds identified for their ability to modulate either binding of natural ligands or signal transduction via a member of the insulin receptor family.

Claims 30 and 32 have been amended to be dependent on claim 1 while claim 31 has been amended to be further dependent on claim 30. It is respectfully submitted, therefore, that claims 1 and 30-32 as amended are clearly novel and non-obvious over Hendry et al. It is requested that the rejection be reconsidered and withdrawn.

NEW CLAIMS

New claims 34-49 are presented for examination. Claims 34-46 are dependent on base claim 1. For the reasons set forth above for patentability of claim 1, it is believed that new claims 34-46 are allowable. New claim 47, and its dependent claims, claims 48 and 49, are directed to the method steps (A) and (B) as in claim 1, but also require in step (C) "selecting a compound that has a K_b or K_i of less than 10^{-6} M for IR, IGF-1R or IRR." Hendry et al. does not teach or suggest step (C) as required by claim 47. For all of the foregoing reasons, it is believed that claims 34-49 are patentable.

Conclusion

It is submitted that the claims 1, 21, 23, 24, 26, 30-32 and 34-49 are patentable over the teachings of the prior art relied upon by the Examiner as well as comply with the requirements of 35 U.S.C. § 112, first and second paragraphs. Accordingly, favorable reconsideration of the claims is requested in light of the preceding amendments and remarks. Allowance of the claims is courteously solicited.

To the extent necessary, a petition for a three-month extension of time under 37 C.F.R. 1.136 is hereby made. Please charge any shortage in fees due in connection with the filing of this paper, including extension of time fees, to Deposit Account 500417 and please credit any excess fees to such deposit account.

Respectfully submitted,

McDERMOTT, WILL & EMERY

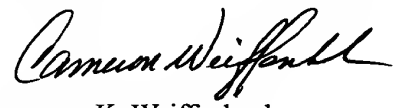

Cameron K. Weiffenbach
Registration No. 44,488

600 13th Street, N.W.
Washington, DC 20005-3096
(202) 756-8000 CKW:jdj
Facsimile: (202) 756-8087
Date: August 6, 2003

APPENDIX

Replacement sheets of the drawings and annotated sheets showing changes in original Figs. 1 and 9 are attached hereto.

Fast Pr diction and Visualization of Protein Binding Pockets with PASS

G. Patrick Brady, Jr.[*] and Pieter F.W. Stouten[1]

DuPont Pharmaceuticals Company

[*]Experimental Station E500
Route 141 & Henry Clay Road
Wilmington, DE 19880-0500
G.Patrick.Brady@dupontpharma.com
Phone: (302)-695-3834
Fax: (302)-695-2209

[1]Present address:
Pharmacia & Upjohn
Viale Pasteur 10
20014 Nerviano (Mi)
Italy

Summary

PASS (Putative Active Sites with Spheres) is a simple computational tool that uses geometry to characterize regions of buried volume in proteins and to identify positions likely to represent binding sites based upon the size, shape, and burial extent of these volumes. PASS'S utility as a predictive tool for binding site identification is tested by predicting known binding sites of proteins in the PDB using both complexed macromolecules and their corresponding apo-protein structures. The results indicate that PASS can serve as a front-end to fast docking. The main utility of PASS lies in the fact that it can analyze a moderate-size protein (~ 30 kD) in under twenty seconds, which makes it suitable for interactive molecular modeling, protein database analysis, and aggressive virtual screening efforts. As a modeling tool, PASS (i) rapidly identifies favorable regions of the protein surface, (ii) simplifies visualization of residues modulating binding in these regions, and (iii) provides a means of directly visualizing buried volume, which is often inferred indirectly from curvature in a surface representation. PASS produces output in the form of standard PDB files, which are suitable for any modeling package, and provides script files to simplify visualization in Cerius2®, InsightII®, MOE®, Quanta®, RasMol®, and Sybyl®. PASS is freely available to all.

Keywords: protein active site, binding site, cavity detection, buried volume, molecular modeling, computer-aided drug design

Introduction

The identification and visualization of protein cavities is the starting point for many structure-based drug design (SBDD) applications. Sites of activity in proteins usually lie in cavities, where the binding of a substrate typically serves as a mechanism for triggering some event, such as a chemical modification or conformational change. Consequently, binding sites are often targeted in attempts to interrupt molecular processes via therapeutics. Although binding site locations are often furnished by x-ray data or fold recognition, tools that automatically predict these locations have become quite popular in SBDD, especially as front-ends to molecular docking or when alternate binding sites are sought [1, 2]. The size and shape of protein cavities dictates the three-dimensional geometry of ligands that can strongly bind there; i.e. they must fit like a hand in glove. Thus, a minimal requirement for drug activity is that the molecule sterically fit the region of buried volume inscribing the active site cavity, with some allowance for induced fit. The determination and visualization of these volumes is critical in drug design, particularly since manual intervention is still fruitfully employed in most design scenarios. An ordinary stick representation of a protein, unfortunately, provides little insight regarding the location, shape, or size of its buried volumes. While surface representations [3, 4] are a step in the right direction, they still fall short in that they require the user to infer buried volumes from often-occluded void space. Consequently, methods for direct display of regions of buried volume in proteins have

become prevalent in recent years [5-11]. Moreover, as molecular docking and virtual screening become more predictive and prevalent, the possibility of interfacing such tools with functional genomics via threading or homology modeling becomes increasingly tempting. A versatile tool that can rapidly predict binding sites should, therefore, find a niche as a front-end to such automated screening efforts. This paper describes a program called PASS (Putative Active Sites with Spheres), which may serve both as an interface to virtual screening and as a visualization aid for manual molecular modeling.

Methods

The PASS algorithm is designed to fill the cavities in a protein structure with a set of spheres and to identify a few of these spheres (called "active site points", ASPs) that most likely represent the centers of binding pockets. Crevice filling is performed in layers using three-point Connolly-like [3] sphere geometry. An initial coating of probe spheres is calculated with the protein as substrate, then additional layers of probes are accreted onto the previously found probe spheres. Only probes with low solvent exposure are retained, and the routine finishes when an accretion layer produces no new buried probe spheres. Although physical arguments can be made to substantiate PASS'S success in binding site prediction, the algorithm itself is purely geometrical (see Figure 1).

Figure 1 - PASS Algorithm

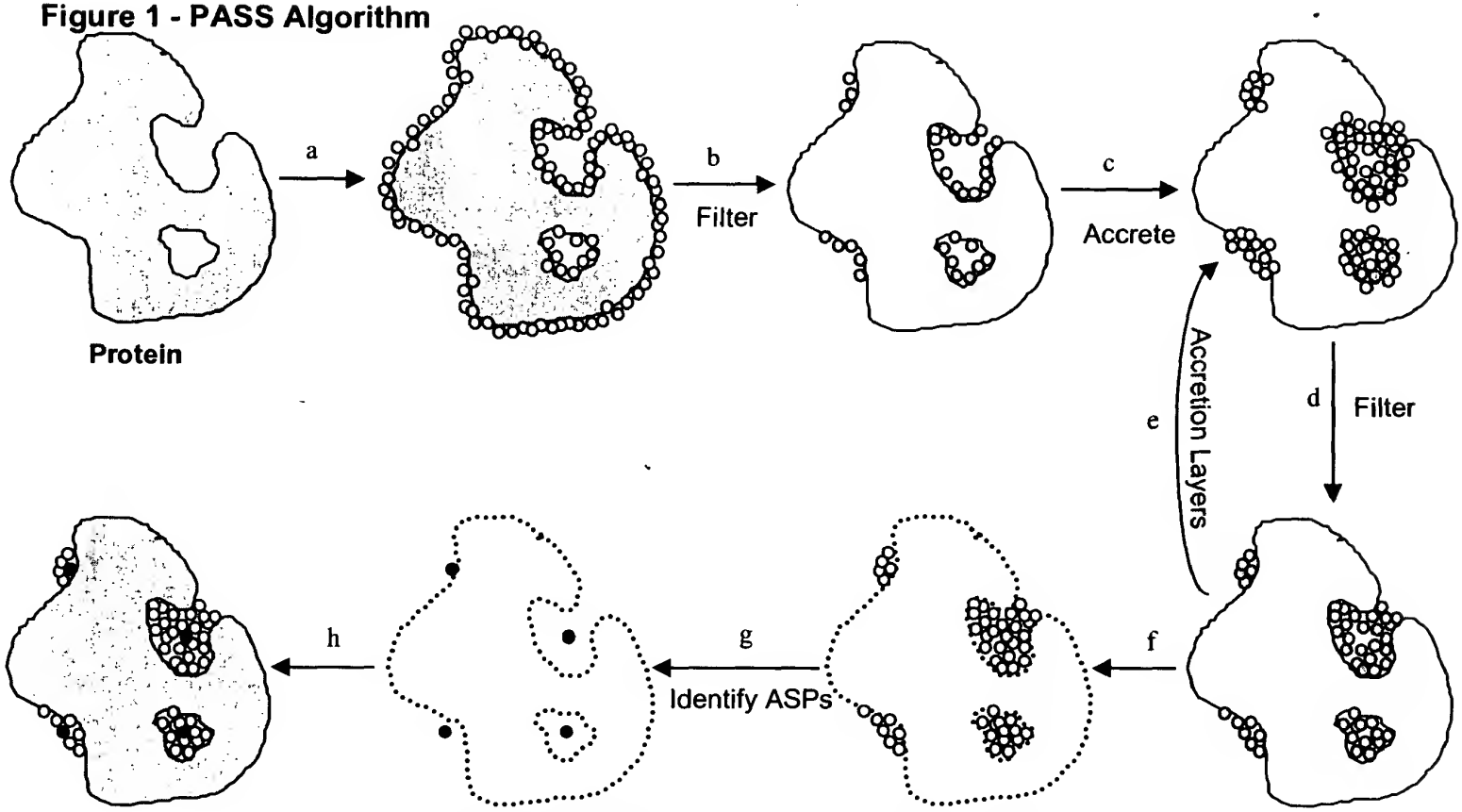

a. PASS uses three-point geometry to coat the protein with an initial layer of spherical probes. b. These probes are filtered to eliminate those that (i) clash with the protein, (ii) are not sufficiently buried, and (iii) lie within 1Å of a more buried probe. c. A new layer of spheres (white) is accreted onto a scaffold consisting of all previously-identified probes (shaded). d. The probes are filtered as described in step b. e. Accrete a new layer of spheres onto the existing probes, as in step c. f. Accretion and filtering (steps e and d) are repeated until a layer is encountered in which no newly-found probes survive the filters. This leaves the final set of probe spheres. g. Probe weights (PW) are computed for each sphere and active site points (ASPs) are identified from amongst the final probes. h. The final PASS visualization is produced. By default, the final probe spheres are first smoothed, leaving only clusters of four or more.

Calculation of Probe Spheres

PASS begins by reading the Protein Data Bank (PDB) coordinates of a target protein and assigning elemental atomic radii (Table 1). Since a protein with explicitly represented hydrogen atoms contains less interstitial volume than one without hydrogen, PASS assigns a few different parameter values in the two cases. By default, if less that 20% of the atoms in the protein PDB file are hydrogen, then all hydrogen atoms are removed and hydrogen-free parameters are assigned; otherwise, hydrogen is retained and hydrogen-inclusive parameters are assigned (Table 1). The first layer of probe spheres is computed by looping over all unique triplets of protein atoms and, if they are close enough together, calculating the two locations at which a probe sphere (of radius R_{probe}) may lie tangential to all three protein atoms (Fig. 1; Step a). Appendix A elucidates this three-point geometry, which is nontrivial since the radii are not necessarily equal. To be retained, a putative probe sphere must survive several filters (Fig. 1; Step b). The first condition is that it cannot overlap with any atoms of the accretion substrate. The second filter explicitly prohibits the probe from clashing with any protein atoms, while the third ensures that the probe be somewhat buried within the protein (i.e. in a binding-site-like region). In particular, each probe sphere is ascribed a "burial count" (BC) representing the extent to which it is excluded from solvent (Figure 2). The BC of a probe is computed by counting the number of protein atoms that lie within a radius R_{BC}=8Å of it, and the probes are filtered such that any probe sphere with BC less than a threshold value ($BC_{threshold}$) is rejected. This threshold value was determined empirically, as were many of the PASS parameters, by visual inspection of

results for a few test systems. Our experience has been that PASS'S predictions are largely insensitive to the precise values of any of its parameters. Finally, probe spheres are "weeded" such that no two probe centers lie any closer together than R_{weed} = 1Å. This keeps the distribution of probe spheres from becoming clumped, which enables reliable prediction of active site points from the final set of probes.

Table 1 - PASS Parameters

Parameter	
R_{probe} hydrogen-free	1.8 Å
$BC_{threshold}$ hydrogen-free	55
R_{probe} with hydrogen	1.5 Å
$BC_{threshold}$ with hydrogen	75
R_{BC}	8.0 Å
R_{weed}	1.0 Å
$R_{accretion}$	0.7 Å
R_o	2.0 Å
D_o	1.0 Å
R_{ASP}	8.0 Å
PW_{min}	1100
Elemental Radii [40]	
Hydrogen	1.20 Å
Oxygen	1.52 Å
Nitrogen	1.55 Å
Carbon	1.70 Å
Sulfur	1.80 Å

Values of PASS parameters, which are defined as follows. R_{probe} - Radius of a probe sphere. $BC_{threshold}$ - Threshold burial count (BC) distinguishing a buried probe from an exposed one. R_{BC} - Radius used to compute burial counts. R_{weed} - Minimal separation between probe spheres. $R_{accretion}$ - Radius of probes as they are accreted onto existing probes. R_o, D_o - Parameters defining the probe weight (PW) envelope function (see Fig. 2). R_{ASP} - Minimal distance between active site points (ASPs). PW_{min} - Minimal PW for an ASP.

Figure 2 - Burial Counts and Probe Weights

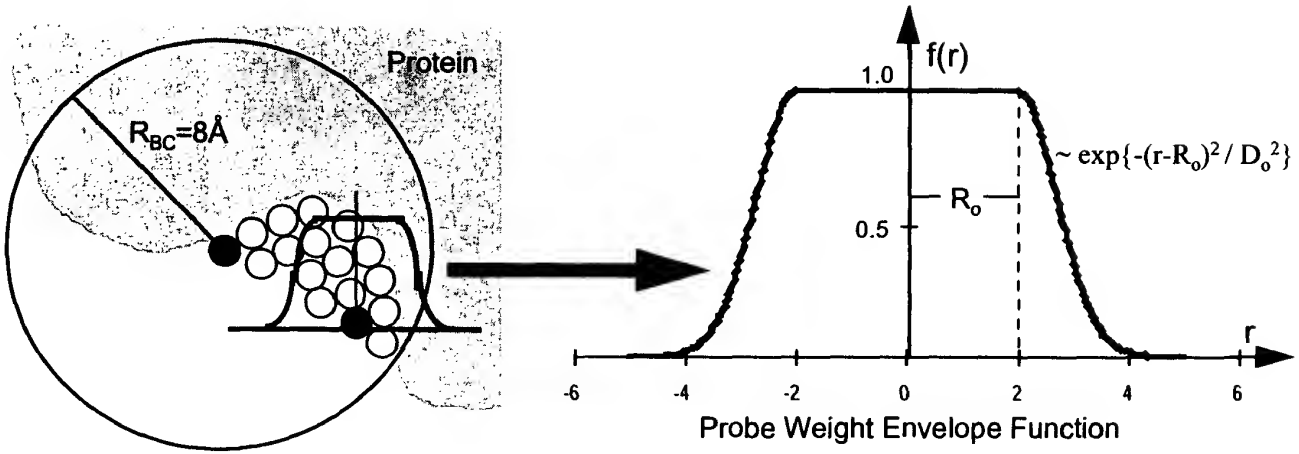

The burial count (BC) of a probe sphere is obtained by counting the number of protein atoms that lie within R_{BC}=8Å of it. The probe weight (PW) of a sphere is obtained by summing the BCs of neighboring probe spheres, scaled by the distance-dependent envelope function shown above. R_o = 2.0 Å and D_o = 1.0 Å.

After the seminal layer of probes is computed, additional layers of spheres are iteratively accreted onto the existing probe spheres. At each iteration, a set of new probe spheres is computed as described above (Fig. 1; Steps c,e), but with a smaller probe radius ($R_{accretion}$ = 0.7Å) and with the set of all probe spheres retained from previous layers as the accretion substrate. New probes, however, must still maintain a center-to-center distance of at least $R_{probe}+ \sigma_i$ from each protein atom, i (of radius σ_i). The aforementioned filters are imposed when the newly-found spheres are combined with those retained from previous layers (Fig. 1; Step d). PASS continues the accretion phase until a layer is encountered in which none of the newly-found probe spheres survives the filters (Fig. 1; Step f). The result of this procedure is that the cavities, invaginations, and internal voids in the protein are filled with a set of fairly evenly-spaced probe spheres, all of which are buried and none of which sterically clashes with the protein. Furthermore, probes lying along the protein surface are packed in ideal steric contact with three protein atoms.

Active Site Point (ASP) Determination

PASS subsequently identifies a small number of "active site points" (ASP) from amongst the final set of probe spheres (Fig. 1; Step g). These ASPs are meant to represent potential binding sites (i.e. centers of putative active sites) for ligands of arbitrary shape and polar character. Thus, PASS conservatively views a protein binding site as simply an invagination in the protein surface that is large enough to accomodate a ligand and possesses substantial solvent-excluded volume in which

hydrophobic ligand moieties may be buried. ASPs are accordingly selected by identifying the central probes in regions that contain many spheres with high BCs. In particular, each probe is assigned a "probe weight" (PW), which is proportional to the number of probe spheres in the vicinity and the extent to which they are buried. The probe weight of the ith probe is given by $PW(i) = \sum_{j=1}^{Nprobes} BC(j) f(|\mathbf{r}_i - \mathbf{r}_j|)$, where the envelope function, f(r), is shown in Figure 2. This is conceptually similar to the solvation term of Stouten et al. [12], the premise of which is that the solvation energy of an atom varies linearly with its exposure which, in turn, is proportional to the unoccupied volume around it. The final ASPs are determined by cycling through the probes in descending order of PW, keeping only those with PW $\geq$ PW_{min} (=1100) that are separated by a minimum distance R_{ASP} (= 8Å) from the ASPs already identified. Finally, the set of ASPs is rank-ordered according to PW values. These are PASS'S predicted binding sites.

PASS Output

The default PASS output consists of (i) a PDB file containing the final set of probe spheres, (ii) a PDB file of the ASPs, and (iii) a separate PDB file for each ligand that was optionally read in (see below). By default, PASS "smoothes" the probe spheres before writing the final set of "display" probes to a PDB file. In particular, only probes with at least 4 display probes lying within 2.5Å are written to file by default. Smoothing removes all but appreciable groupings of probe spheres, leaving the final

visualization less cluttered. Smoothing can be suppressed via the command-line flag [-all]. PASS also produces visualization scripts for several popular molecular modeling packages; namely, Cerius2®[13], InsightII®[14], MOE®[15], Quanta®[16], RasMol®[17], and Sybyl®[18]. These scripts, which are optionally produced via command-line flags (e.g. [-InsightII]), simplify visualization by automatically loading, rendering, and coloring the protein, probe spheres, ASPs, and ligands. PASS also displays detailed runtime information, including parameter settings, an account of sphere calculation and filtering (e.g. Table 2), and final probe sphere and ASP data, including BCs and PWs. PASS can also read the coordinates of bound ligands, either automatically from the protein PDB file (as HETATM entries with different residue names), or as separate files via the command-line flag [-ligand <filename.pdb>]. For each ligand, PASS computes the distance from each ASP to the nearest ligand atom and to the ligand center of mass. Other command-line options enable the user to (i) produce an enhanced set of probe spheres and ASPs ([-more]), (ii) repress production of the probe sphere PDB file ([-noprobes]), (iii) treat water molecules as part of the protein ([-water]), rather than ignoring them (which is the default behavior), (iv) specify an explicit output path ([-outdir <directory_path>]), (v) produce a set of PDB files containing subsets of the final probe spheres that were produced in the various layers of sphere calculation ([-layers]), and (vi) compute the volumes of all groupings of probe spheres left after smoothing ([-volume]). None of these options slows PASS noticeably except the volume calculation, which proceeds as follows. After probe smoothing, the final set of display probes is agglomeratively clustered [19] by iteratively merging pairs of overlapping groups of probes until an iteration attempts to join two non-overlapping clusters. This determines

both the optimal number of probe groups and the identities of spheres in these groups. Group volumes are subsequently computed by looping over probe spheres and estimating the volume increments statistically. If ligand(s) are present, distances are computed from the center of each group (i.e. the cluster center) to (i) the nearest ligand atom (D_{near}), and (ii) the ligand center of mass (D_{COM}).

Results

Table 2 shows the numbers of probe spheres retained at various stages of a PASS calculation on thermolysin (1hyt) and is meant to provide an impression of the practical operation of the algorithm. In layer #1 of the probe sphere calculation, the protein atoms constitute the accretion substrate, and every set of three protein atoms lying close enough together to be simultaneously touched by a single sphere (of radius R_{probe}) must be identified and used to determine two putative probe sphere positions. The number of atomic triples that must be tried is reduced by first identifying atomic neighborhoods. The "neighborhood" of atom "i" is the set of atoms lying close enough to "i" to be bridged by a single probe sphere. In layer #1, 769,205 triples of protein atoms satisfied the neighborhood criterion, and 1,154,010 "bridging spheres" were located using these triplets. The number of bridging spheres is less than twice the number of atomic triples because not all triples of atoms in the accretion substrate that satisfy the neighborhood criterion can actually be bridged by a sphere of radius R_{probe}. The set of bridging spheres is then filtered according to (i) clash with the accretion

Table 2 - PASS Probe Sphere Algorithm Applied to Thermolysin (1hyt)

	Layer #1	Layer #2	Layer #3	Layer #4	Layer #5	Layer #6	Layer #7
Accretion Substrate	Protein	Probes	Probes	Probes	Probes	Probes	Probes
Triplets of Substrate Spheres Tried	769,205	384	1,320	2,138	1,852	1,067	1,194
Bridging Spheres Found	1,154,010	560	2,120	3,386	2,954	1,690	1,898
... after substrate clash filter	2,151	306	430	370	222	104	108
... after protein clash filter	2,151	118	115	88	53	16	14
... after burial filter	811	98	64	32	12	7	0
... after weeding filter (New Probes)	360	60	41	21	7	3	0
Total Probe Spheres	360	420	461	482	489	492	492
Comment	Seminal Protein Coat	Accretion	Accretion	Accretion	Accretion	Accretion	Completion

The numbers of spheres retained at various stages of a PASS calculation on thermolysin (1hyt). Protein atoms form the substrate in the first layer; previously identified probe spheres form the substrate in all subsequent layers. A triplet of substrate spheres is tried if each substrate pair can be bridged by a probe sphere. There are two possible probe sphere positions for each valid triplet of substrate spheres. The number of bridging spheres found is always less than twice the number of triplets tried because of exceptional cases (e.g. one sphere lying inside the other two). The bridging spheres are then subjected to a series of filters. The number of probes surviving the filters are shown. Accretion procedes until a layer produces no new probes, which occurs in the seventh layer in this case.

substrate, (ii) clash with the protein, (iii) burial count, and (iv) proximity to other probe spheres, in that order. After the substrate clash filter, 2,151 putative probe spheres remain and, since the protein is the accretion substrate in layer #1, the same number remains after the protein clash filter. All but 811 putative probes are discarded based upon insufficient burial, and 360 remain after these 811 are "weeded" to maintain a mutual separation of at most R_{weed}=1.0 Å. Thus, 360 probe spheres are found in the first layer. The accretion substrate for the second and subsequent "accretion" layers is the set of probe spheres. In layer #2, the substrate of 360 probe spheres requires that 384 substrate triples be tested, from which 560 bridging spheres are identified. After applying the four filters, only 60 new probe spheres remain, bringing the total number of probes to 420 after layer #2. This process is repeated until layer #7, in which no new probe spheres are identified, signalling the completion of probe sphere determination. Note that although the number of probe spheres continually grows as accretion procedes, the number of accretion substrate triples that must be tried in each layer plateaus. This is because PASS is written such that only triples of substrate atoms incorporating a newly-found probe sphere (or the neighbor of a freshly-weeded probe) are tried. As a result, PASS'S performance scales favorably with protein size (approximately $MW^{3/2}$ over the molecular weight range in Table 3).

PASS was first tested for its ability to identify known binding sites. Table 3 shows the results of applying PASS to 30 protein-ligand complexes drawn from the PDB. The structures were chosen based upon diversity, resolution, inclusion in previous theoretical studies, and the existence of corresponding apo-protein x-ray structures in the PDB. In each case, hydrogen-free PASS parameters were assigned

Table 3 - PASS Results for PDB Complexed Proteins[a]

PDB Code	Protein	Ligand(s)[b]	Size (kD)	Layers	Probes	ASPs[c]	Binding Site Hits[d]	D_{Near} (Å)[e]	D_{COM} (Å)[f]	CPU Time (sec)[g]
1abe	l-arabinose binding protein	l-arabinose	31	8	468	4	3	1.1	0.5	12
1bid	thymidylate synthase	DUMP	28	10	572	4	1	3.0	6.3	10
1cdo	alcohol dehydrogenase[h]	NAD	37	8	760	7	2,3,5	1.4,3.2,0.9	4.2,11.3,9.8	13
1dwd	alpha thrombin + hirudin	NAPAP	31	7	664	7	1	0.6	4.7	11
1etr	epsilon thrombin	MQPA	32	6	774	16	2,15,16	0.8,1.3,2.4	5.1,5.5,6.6	11
1fbp	fructose-1,6 bisphosphatase[h,i]	F6P	32	6	593	5	3	1.8	3.9	12
		AMP					- (4)	- (1.1)	- (1.2)	
1gca	galactose binding protein	d-galactose	32	5	575	9	1	0.7	0.8	11
1hew	lysozyme	NAG	13	8	211	1	1	0.7	6.9	5
1hvr	HIV 1 protease[j]	XK263	20	10	385	2	1,2	1.2,0.8	2.3,6.3	8
1hyt	thermolysin	BZS	32	6	492	4	1	0.8	2.2	13
1inc	elastase	benzoxazinone	24	9	403	4	4	1.9	5.7	8
1jst	CDK2 - cyclin A complex[h,i]	ATP	59	7	1326	15	2	1.4	1.5	27
1pbe	p-hydroxybenzoate hydroxylase	FAD	41	10	935	10	1,2,6	1.5,1.0,0.8	7.2,12.6,2.5	16
		PHB					- (9)	- (1.8)	- (1.7)	
1phf	cytochrome p450-cam[k]	C4PI	43	7	723	6	1	0.7	0.9	17
1ppc	trypsin	NAPAP	22	5	304	2	1	1.0	4.8	6
1rbp	retinol binding protein	retinol	19	7	377	4	1,2	0.6,0.4	3.2,5.5	7
1rob	ribonuclease A	cytidylic acid	13	9	236	2	2	0.5	2.4	4
1stp	streptavidin	biotin	12	7	197	2	1	0.4	1.1	3
1ulb	purine nucleoside phosphorylase[i]	guanine	30	9	596	3	1	1.3	3.1	10
2er6	endothiapepsin	H256	31	7	487	3	1,2,3	1.9,1.0,0.8	8.7,7.6,1.2	11
2ifb	fatty acid binding protein	palmitic acid	14	6	292	3	1,2	0.4,0.8	1.8,6.6	5
2ptc	beta trypsin	PTI	22	5	305	2	1,2	1.1,2.6	19.4,19.8	7
2ypi	triose phosphate isomerase[h]	PGA	25	9	486	5	4	3.4	5.7	8
3aah	methanol dehydrogenase[h,j]	PQQ	64	7	997	8	4	0.5	3.1	30
3ptb	beta trypsin	benzamidine	22	6	290	2	1	0.9	0.8	7
4dfr	dihydrofolate reductase[h]	methotrexate	17	8	366	3	1	3.9	8.1	5
4mbn	myoglobin	heme	16	5	297	3	1,2	0.8,0.5	5.4,5.9	5
4phv	HIV 1 protease	VAC	20	7	397	2	1,2	0.7,0.7	2.1,7.1	6
5cna	concanavalin A[m]	MMA	24	6	309	2	- (3)	- (0.3)	- (1.4)	8
7cpa	carboxypeptidase A	FVF	32	6	481	3	2,3	0.6,1.0	6.5,3.1	14

[a]Default PASS parameters used; bound waters removed. Molecular weights do not include hydrogen. Parenthetical entries were obtained in "more" mode (see text). [b]Ligand abbreviations: DUMP = 2'-deoxyuridine 5'-monophosphate, NAD = nicotinamide adenine dinucleotide, NAPAP = N==a==-(2-naphthyl-sulfonyl-glycyl)-DL-P-amidinophenylalanyl-piperidine, MQPA = (2r,4r)-4-methyl-1-[Nalpha-(irs)-3-methyl-1,2,3,4-tetrahydro-8-quinolinesulfonyl)-L-arginyl]-2-piperidine carboxylic acid,F6P = fructose 6-phosphate, AMP = adenosine monophosphate, NAG = tri-n-acetylchitotriose, BZS = benzylsuccinic acid, ATP = adenosine-5'-triphosphate, FAD = flavin-adenine dinucleotide, PHB = p-hydroxybenzoic acid, C4PI = camphor 4-phenyl imidazole, cytidylic acid = cytidine 2'-monophosphate, PTI = pancreatic trypsin inhibitor, PGA = 2-phosphoglycolic acid, PQQ = pyrroloquinoline quinone, VAC = n,n-bis-2(r)-hydroxy-1(s)-indanyl-2,6-(r,r)-diphenylmethyl-4-hydroxy-1,7-heptandiamide, MMA = alpha-methyl-d-mannopyranoside, FVF = bz-phe-val==p==(o)-phe. [c]Number of active site points (ASPs). [d]Rank of ASP(s) lying within 4 Å of the ligand. [e]Distances from binding site hits to the nearest atom in the ligand. [f]Distances from binding site hits to the center of mass of the ligand. [g]CPU Times in seconds on a single Silicon Graphics R10000 processor running at 194 MHz. [h]Dimer truncated to a monomer. [i]No water in the PDB file. [j]Phosphorylated protein. [k]Heme treated as part of the protein. [m]Tetramer truncated to a monomer.

and bound water molecules were ignored. For each PDB complex, Table 3 shows the number of layers of probes PASS computed prior to convergence, the final number of probe spheres, the number of ASPs identified for each protein structure, and the required CPU time. Coordinates of the known ligand(s) are used to define a binding site "hit." In particular, for each ASP of a particular protein, two quantities are computed: (i) D_{Near}, the distance from the ASP to the nearest ligand atom, and (ii) D_{COM}, the distance from the ASP to the ligand center of mass (COM). Any ASP with $D_{Near} \leq 4$Å is considered a binding site "hit." The Binding Site Hits column lists the rank order of the ASP(s) that are considered hits, and the values in the D_{Near} and D_{COM} columns correspond to these hits. For instance, the "1hvr" row in Table 3 indicates that both the top ASP and the second-ranked ASP lie near the site in HIV-1 protease known to bind XK263. In particular, the top ASP lies 1.2 Å from the nearest XK263 atom and 2.3 Å from the COM, while the second-ranked ASP lies 0.8 Å from the nearest atom and 6.3 Å from the COM. Note that ligand size impacts the D_{COM} values, as evidenced by the trypsin-PTI system, which has the largest ligand (a protein) and, correspondingly, the largest D_{COM} values (~ 19 Å).

Table 3 shows that PASS is able to successfully identify the locations of known binding sites in complexed x-ray structures. PASS located the pocket containing a known ligand in all but three of the 32 trials, often finding multiple binding site hits for a given ligand (11 times). In addition, the top-ranking ASP identified by PASS represents a binding site hit in 19 of the 32 trials, and one of the top three ASPs is a hit in 26 trials. These observations indicate that PASS can usually identify the protein cavity to which a ligand will bind with maximal affinity in a matter of seconds. There is a strong, but not

perfect, correlation between ASP rank (i.e. PW) and the volume of the corresponding group of probe spheres. In fact, volume is approximately as predictive of binding sites (results not shown) as ASP rank for the systems in Table 3. However, the calculation of volumes slows PASS noticeably for systems requiring many probe spheres (e.g. 92, 40, and 24 seconds for 1jst, 3aah, and 1etr, respectively).

From a drug design perspective, the analysis presented in Table 3 is somewhat immaterial, since the existence of complexed coordinates implies that at least one binding site location is already known. Intuition suggests that the presence of a ligand in a complex might induce a more pronounced binding site cavity than would be present in an apo-protein structure, thereby biasing a cavity-detection algorithm like PASS to succeed on complexed systems. Thus, the postdiction of binding sites in PDB complexes does not establish the predictive utility of a tool for drug design, where one is lucky to have an apo x-ray structure or reliable homology model.

A more realistic test of PASS as a tool for prediction is to try to locate known binding sites on the structures of proteins that are not complexed with a ligand. We address this predictability issue by using PASS to compute ASPs for the set of apo-protein structures from the PDB that correspond to complexed PDB structures in Table 3. Apo structures were identified for as many of the systems in Table 3 as possible (20), and default PASS parameters were used in all calculations. A few of these PDB correspondences are not identical residue-by-residue because the molecules either were obtained from different sources (1npc/1hyt; 2apr/2er6), had residue additions or deletions at the termini (1swb/1stp; 1hxf/1dwd), or had incomplete or missing residues due to poor electron density (5dfr/4dfr; 1hxf/1dwd). For comparison, the results

displayed in Table 4 are presented in the same order as in Table 3, and corresponding PDB codes are shown. "Known" binding site positions are determined by superposing the native and complexed structures and computing the proximity of the ASPs (from the native PASS calculation) to the known ligand (from the complexed crystal structure). This enables binding site "hits" to be computed as in Table 3, along with the distances D_{Near} and D_{COM} relating the position of the known ligand to the binding site hits. Only backbone atoms {C,O,C_α,N} were superposed and, in all but a few cases (see Table 4 caption), all residues in the chain were used. To quantify how severely the ligand deforms the protein in the binding site, we computed the RMSD between superposed structures using only residues lying in this region. In particular, we identified both the set $\{C_i\}$ of residues lying within 4 Å of the ligand in the complex and the set $\{A_i\}$ of corresponding residues in the superposed apo structure. The RMSD between $\{C_i\}$ and $\{A_i\}$ was then computed, using both side chain and backbone atoms for identical amino acids and only the backbone atoms otherwise.

Table 4 shows that PASS can reliably predict binding site locations when only an apo x-ray structure is known. PASS correctly identifies the binding site in 17 of the 21 trials in Table 4. The top-ranked ASP hits the binding site in 12 trials, and one of the top three ASPs is a hit in 16 trials. These observations imply that PASS may be a suitable front-end to virtual high throughput screening and fast docking routines. Furthermore, the similarity of observed hit rates between the apo-protein and complexed systems refutes the hypothesis that the presence of a ligand in the structural data is a crucial determinant of success for a cavity detection algorithm.

Table 4 - PASS Results for PDB Apo-Proteins[a]

Apo PDB Code	Protein	Complex PDB Code	Probes	ASPs[b]	Binding Site RMSD[c]	Binding Site Hits[d]	D_{Near} (Å)[e]	D_{COM} (Å)[f]
3tms	thymidylate synthase	1bid	577	4	1.7	1	3.9	6.8
8adh	alcohol dehydrogenase	1cdo[g]	656	3	1.2	1,2	0.2,3.1	5.1,12.0
1hxf	alpha thrombin + hirudin	1dwd	627	8	0.7[n]	1,4	0.7,1.4	3.7,5.0
2fbp[g]	fructose-1,6 bisphosphatase	1fbp[g]	564	7	1.3	- (9)	- (1.9)	- (4.8)
						- (5)	- (0.7)	- (2.2)
1gcg	galactose binding protein	1gca	471	3	0.4	1	0.5	1.0
1hel	lysozyme	1hew	219	1	0.7	1	1.0	6.9
1npc	thermolysin	1hyt	455	3	1.7[n]	1	1.7	2.2
1esa	elastase	1inc	349	1	1.1	- (4)	- (0.3)	- (4.6)
1brq	retinol binding protein	1rbp	401	2	2.2	1	0.9	3.4
8rat	ribonuclease A	1rob	216	2	0.6	1	0.3	1.8
1swb[h]	streptavidin	1stp	199	1	0.7[n]	1	0.8	2.4
1ula	purine nucleoside phosphorylase	1ulb	637	7	2.6	7	3.9	5.8
2apr	endothiapepsin	2er6	531	5	1.2[n]	2,5	1.5,0.9	2.6,9.0
1ifb	fatty acid binding protein	2ifb	291	4	0.6	1,2	2.5,0.9	4.6,4.1
3ptn	beta trypsin	3ptb	322	2	0.5	2	0.5	2.6
1ypi[g]	triose phosphate isomerase	2ypi[g]	508	7	2.4	3	2.2	2.0
5dfr	dihydrofolate reductase	4dfr[g]	283	2	1.3[n]	1	2.3	6.7
3phv[j]	HIV 1 protease[m]	4phv	348	1	3.2	- (1)	- (1.0)	- (5.1)
2ctv	concanavalin A	5cna[b]	361	4	1.1	2	0.6	1.0
5cpa[k]	carboxypeptidase A	7cpa[k]	448	3	2.0	1	1.2	4.6

[a]Default parameters used; bound waters removed. Parenthetical entries were obtained in "more" mode (see text). [b]Number of active site points (ASPs). [c]All residues in the proteins were superposed (heavy backbone atoms only), except where noted by superscript n. Binding site RMSDs are computed between all residues that lie within 4 Å of the ligand in the complexed structure and the corresponding residues in the apo structure (heavy atoms only). Notation: 1abc (10,2) indicates that, for structure 1abc, the binding-site RMSD calculation involved 12 residues, 10 of which included both backbone and sidechain atoms, while 2 included only backbone atoms (since corresponding residues were not of the same type). 3tms (12,0), 8adh (27,11), 1hxf (18,0), 2fbp (28,0), 1gcg (15,0), 1hel (11,0), 1npc (14,0), 1esa (14,0), 1brq (16,0), 8rat (8,0), 1swb (16,0), 1ula (8,0), 2apr (18,5), 1ifb (12,0), 3ptn (11,0), 1ypi (13,0), 5dfr (16,0), 3phv (26,0), 2ctv (9,0), 5cpa (18,0). [d]Rank of ASP(s) lying within 4 Å of the superposed ligand. [e]Distances from binding site hits to the nearest atom in the superposed ligand. [f]Distances from binding site hits to the center of mass of the superposed ligand. [g]Dimer truncated to a monomer. [h]Tetramer truncated to a monomer. [j]3phv dimer explicitly created via symmetry operators. [k]Zn was considered part of the protein. [m]PASS performed on dimer. [n]Residue superpositions- 1hxf: {A44,F199,E217}; 1npc: {T2,G3,T4,F282,K308,V316} of 1npc with {T2,G3,T4,F281,K307,V315} of 1hyt; 1swb: all residues except {K134,P135} of 1swb (chain A) and {A13,E14,A15} of 1stp; 2apr: {S39,W42,I130} of 2apr with {S36,W39,L128} of 2er6; 5dfr: {A6,N23,V93}.

One additional option available in PASS is the generation of an enhanced set of probes and ASPs by running PASS in "more" mode via the [-more] command-line flag. In "more" mode, the burial count threshold is slightly reduced (by 10), which typically has the effect of enhancing the number of probe spheres by about a factor of two and ASPs by a factor of two or three, at the expense of about 20-30% in cpu time. When the systems in Tables 3 and 4 are analyzed in "more" mode, the binding site is detected in every case, with no ASP hit ranking worse than ninth. Tables 3 and 4 show (in parentheses) the ASP hits obtained in "more" mode for the few binding sites that the default PASS calculation failed to locate. Detailed inspection revealed that several of these default-mode misses contained an accumulation of probe spheres that fell just beneath the threshold defining an ASP. Running PASS in "more" mode is suggested when broad binding sites are anticipated (e.g. protein-protein association).

The work of Mattos and Ringe [1, 20] constitutes the experimental analog of PASS and enables the most direct comparison of PASS to experimental data. In particular, Mattos and Ringe have soaked elastase crystals with a variety of small organic solvents and crystallographically determined the corresponding protein structures, including bound solvent molecules. These bound organic probes are meant to map out potential binding hot spots on the protein and suggest favorable ligand moieties. This raises the question of whether their organic probes tend to cluster in regions identified via PASS ASPs, which are likewise meant to identify possible hot spots. To address this, PASS was run on elastase and the resulting ASPs were graphically superimposed with Ringe et al.'s organic probes, along with a set of bound ligands drawn from the PDB. Figure 3 shows these results. Several clusters of organic

probes are observed, most notably a large grouping in the active site (S1 pocket). Although only one organic probe lies within 8Å of the top- or second-ranked ASPs, PASS places an ASP near four of the five largest clusters of probes. The inset to Figure 3 shows that the third-ranked ASP (pale blue) lies in the active site about 5Å above the catalytic triad (whose surface is colored green).

Figure 3 also addresses the question of whether clusters of these experimentally derived organic probes are more predictive of binding sites than PASS ASPs. Superposition of the ligands from nineteen elastase PDB complexes enables this comparison. All but three ligands bind in the S1 region of the known active site. The other three stick solely to an alternate site about 10Å away (near S3'), while four molecules employ both sites. PASS identifies this alternate binding site via the fourth-ranked ASP (white); however, since only one organic probe lies in this region, this site cannot be identified solely on the basis of organic probe clusters. Conversely, there is a cluster of organic probes near the S4 binding pocket, but no ASP is placed there (this region is too close to the ASP in the S1 pocket). Thus, clusters of the organic probes of Ringe et al. and the ASPs of PASS appear comparably predictive of the known binding sites in elastase. It should be noted that the physical nature of the probes employed by PASS and by Ringe et al. are drastically different, so one should not expect identical distributions of binding hot-spots in the two cases. Ringe et al. probe the protein surface with small, often quite polar, molecules, precisely the opposite of PASS ASPs, which can be thought of as large and apolar. ASPs are effectively apolar in that they are identified solely on the basis of cavity size, shape and burial, with no regard for e.g. electrostatics and hydrogen bonding. Moreover, the PASS parameters have been

tuned such that only a cavity of a certain critical size can sustain an ASP. Over the set of systems in Table 3, the smallest regions of buried volume containing an ASP are approximately the size of a benzene ring, while ASP regions that bind a ligand are typically three- to ten-fold larger than that. It is gratifying, however, that the central binding site (S1) is unambiguously identified by both methods.

Figure 3 – C mparison to Crystallographically-Determined Organic Probes

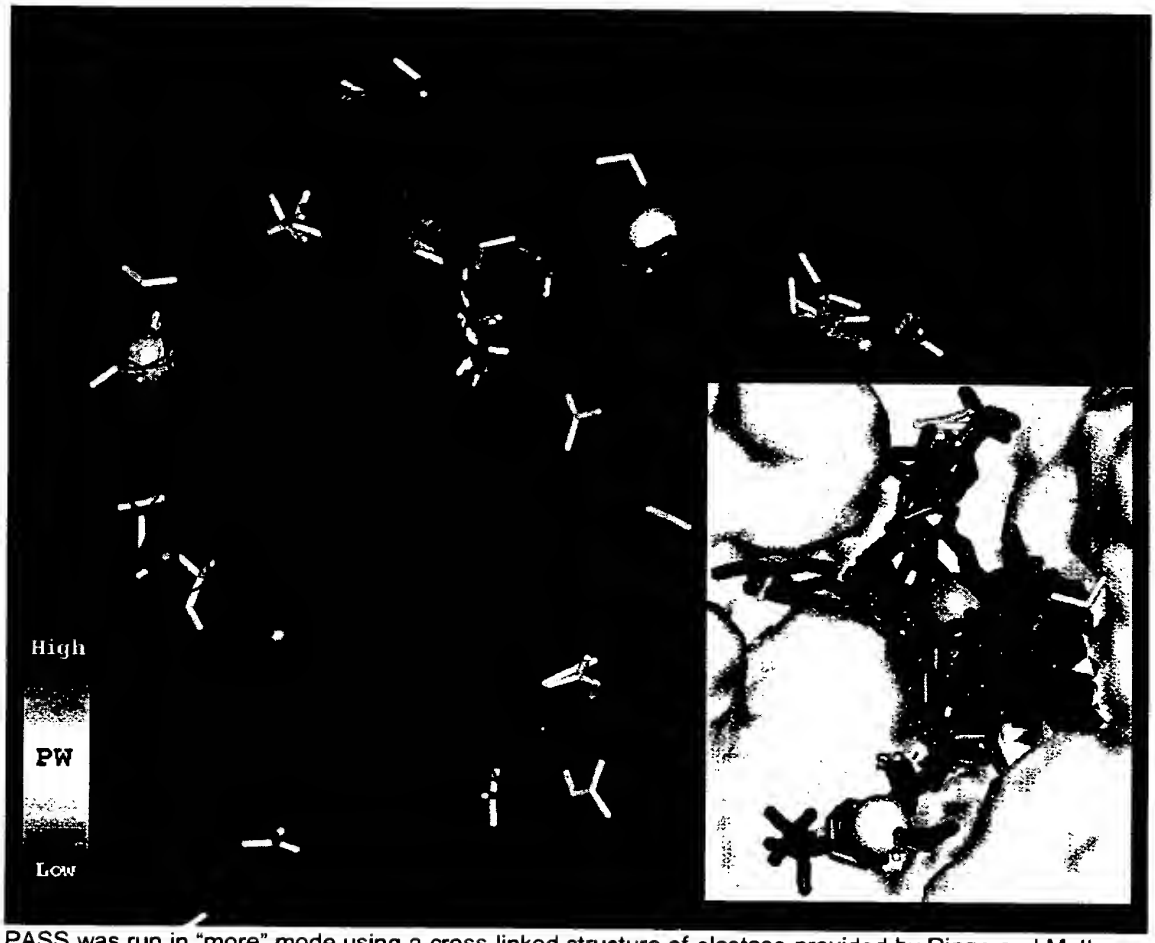

PASS was run in "more" mode using a cross-linked structure of elastase provided by Ringe and Mattos. The resulting ASPs are rendered as large spheres and colored according to probe weight, PW (see scale). Crystallographically determined organic probes (acetonitrile, dimethylformamide, acetone, ethanol, isopropanol, hexenediol) are displayed as solid yellow sticks. Although only one organic probe lies within 8Å of the top- or second-ranked ASP, four of the five largest clusters of organic probes lie in a region identified as a potential binding site by PASS. Every E.C.3.4.21.36 elastase complex in the PDB (19 structures, 20 ligands: 1bma, 1btu, 1eai, 1eas, 1eat, 1eau, 1ela, 1elb, 1elc, 1eld, 1ele, 1elf, 1elg, 1esb, 1fle, 1inc, 1jim, 1nes, 9est) was superposed onto the cross-linked elastase structure, and the resulting ligand overlays are shown as orange, blue, and magenta sticks (except for two protein-bound structures, 1eai and 1fle). The inset shows a top view of the protein surface at the active site, with the portion of the surface defined by the catalytic triad colored green. The third-ranked ASP (pale blue) is centrally located in the active site (S1 region), while the fourth-ranked ASP (white) identifies an alternate binding site about 10Å away (S3' region). Only 4 ligands (two of which are proteins) bind to both sites (colored blue). Thirteen of the twenty ligands (colored orange) bind in the S1 pocket but not in the alternate site. The other three ligands (1elf, 1elg, 1nes; colored magenta) bind only to the alternate site. Since only one organic probe lies in this region, probe clusters alone cannot identify this as a potential small molecule binding site. Conversely, a cluster of three organic probes lies in the S4 region, in a pocket that PASS failed to identify because it lies too close (i.e. < R_{ASP}=8 Å) to the S1 ASP.

Discussion

PASS in a Virtual Screening Environment

The hit rates shown in Table 4 indicate that PASS may serve as a front-end to virtual screening when the binding site is unknown or when alternative binding sites are sought. If the screening tool is fast enough that docking against multiple sites is permissible, then separate screening calculations can be run with the search space centered on the top few PASS ASPs. This strategy should enable identification of the optimal binding mode in most cases, as evidenced by the 71% hit rate to the top two ASPs in Table 4. A number of other screening strategies incorporating PASS are also possible. For instance, a more rigorous procedure could be used to select the "true" binding site from amongst the full set of ASP predictions. Using a docking routine with a more detailed scoring function, the affinity of a ligand for the different ASP regions can be directly compared. Thus, screening a small set of diverse probe molecules or fragments against all the ASPs might enable one to identify the stickiest region of the protein by comparing the scores of the top binders to each ASP region. A large database of ligands could then be computationally screened against this region. Since ASPs are determined using only steric size and shape, the electrostatic (ES) and hydrogen-bonding (HB) character of the ASP sites is arbitrary. One might, thus, search these sites for novel pharmacophores and construct focused combinatorial libraries designed to hit them. Conversely, one could use ES and HB characterization of ASP

regions to select sites most likely to possess affinity for a given class of compounds. Perhaps the most alluring aspect of PASS'S speed is that it (i) permits the expeditious analysis of entire structural databases (e.g. PDB, corporate), and (ii) could provide a suitable bridge between 3D structural modeling and ligand docking in a future drug design project designed to make use of genomic data.

PASS as an Interactive Visualization Tool

A PASS calculation on a moderate-sized protein (~ 30 kD) takes less than twenty seconds on a single Silicon Graphics R10000 processor (Table 3). PASS is, therefore, fast enough to be used interactively in a molecular modeling environment, and has particular utility as a visualization tool for drug design. By default, PASS produces PDB files of probes, ASPs, and ligand(s) (when specified), which can be loaded and rendered separately using any molecular modeling package. Alternately, a full display of the PASS output can be produced in a single step (in supported modeling suites) by executing a PASS visualization script, which loads, renders, and colors the protein, probe spheres, ASPs, and ligand(s). ASP coloring denotes probe weight (PW), while the probe spheres can be colored according to either (i) burial count (BC), (ii) group identity (optionally invoked via [-group]), or (iii) the layer of accretion in which each was identified. Color values (0-50) are encoded onto the B-factor column of the output PDB files containing the probes and ASPs. In runs for which the probes are smoothed and grouped, an integer specifying the group membership of each probe sphere is encoded onto the occupancy column of the probe PDB file. Figure 4 shows a

Figure 4 - PASS Visualization of RNAse A

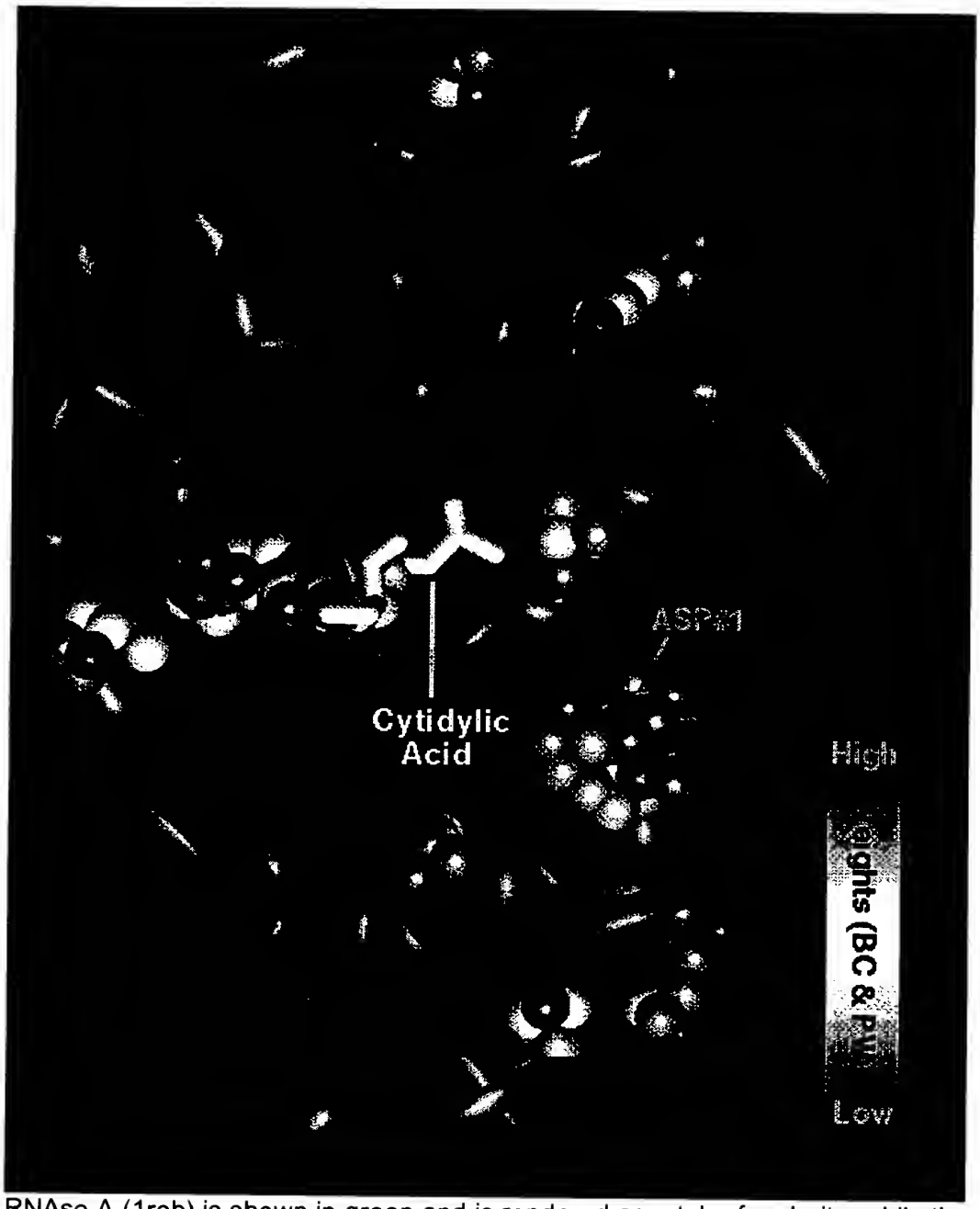

RNAse A (1rob) is shown in green and is rendered as a tube for clarity, while the cytidylic acid ligand is rendered in white sticks and is barely visible. The final probe spheres, which have been smoothed, are represented by small spheres and colored according to burial count. Active site points (ASPs) are rendered as larger spheres and colored by probe weight. The second-ranked ASP lies in the binding site.

standard PASS visualization in InsightII® for RNAse A (1rob), which is rendered as a tube for clarity. The probes are rendered as small spheres and colored according to BC, while the two ASPs are rendered as larger spheres and colored by PW. The ligand, cytidylic acid, is shown in white and is mostly occluded by probes and the second-ranked ASP. Because the ligand binds to a long groove in the RNAse surface rather than a deep pocket, the ASP lying in the true binding site has a lower PW than the one shown at the right, which lies in a rounder cavity.

One advantage of PASS as a visualization tool is that displaying the ASPs relative to the protein enables immediate identification of regions likely to be of interest in drug design. Since the ASPs are centrally located in cavities, one can use the displayed ASPs and a distance-based criterion to quickly identify the residues modulating binding in these regions. For the modeling suites that support subseting (e.g. InsightII), the PASS visualization scripts automatically define 6 Å, 8Å, and 10 Å residue-based subsets around each ASP, which facilitate the coloring and specific display of these regions. Figure 5 shows the 8 Å subset of protein residues around the top-ranked ASP of trypsin (3ptb). The ASP is shown in magenta, while the probe spheres are colored by burial count. The residues involved in benzamidinium binding are captured in this subset; e.g. hydrogen-bond partners are indicated by yellow lines. The probe coloring clearly indicates that the mouth of the binding pocket lies to the right, where the probe spheres have lowest burial counts. Because PASS ASPs are centrally located in cavities, 6-10 Å radial subseting almost always enables selective visualization of all the residues defining a protein cavity.

Figure 5 - Residues Modulating the Binding of Benzamidinium to Trypsin

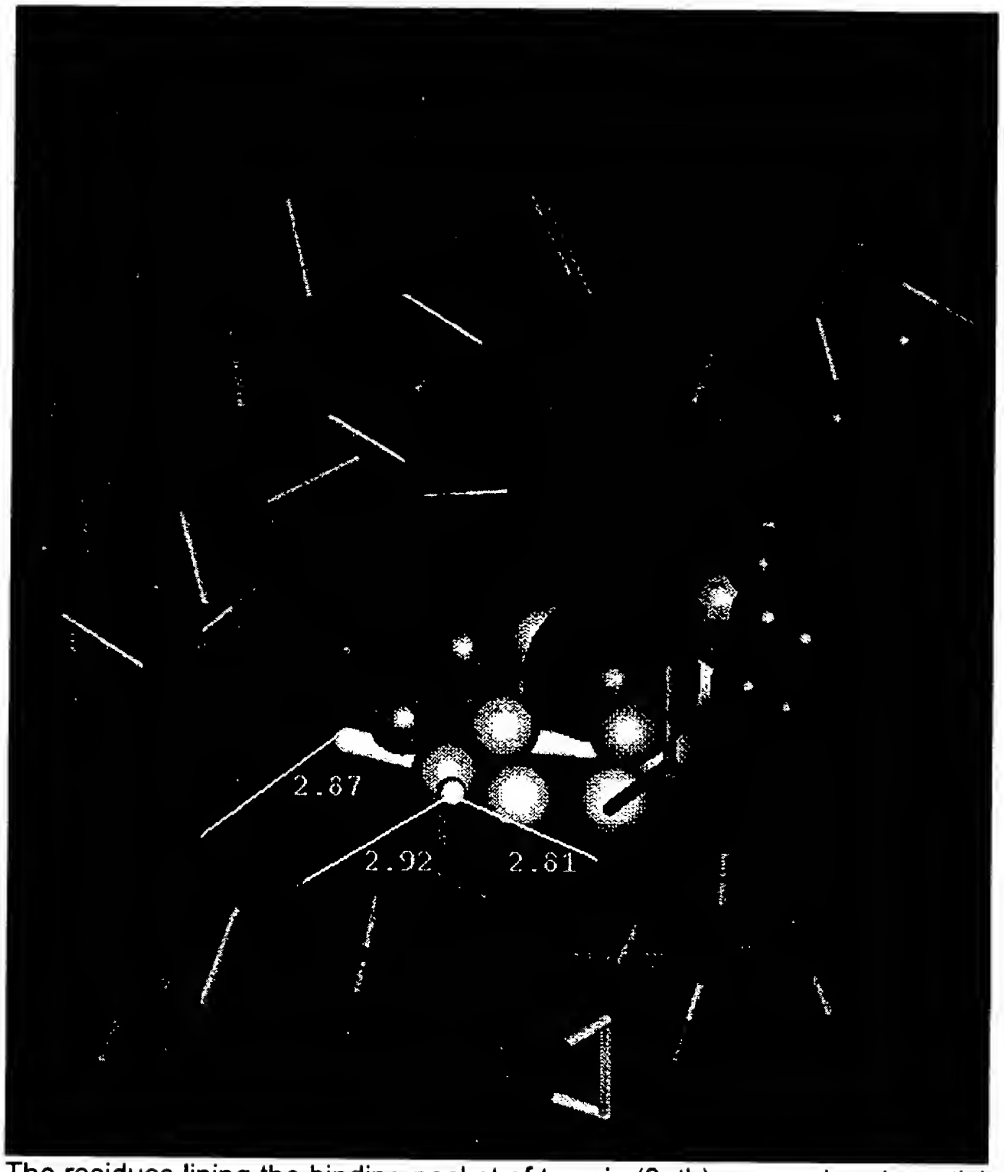

The residues lining the binding pocket of trypsin (3ptb) are rendered as sticks and colored according to atom type. They were selected by defining an 8 Å residue-based zone centered on the top-ranked PASS active site point, shown in magenta. The bound benzamidinium is shown in white, while the probe spheres near the pocket are rendered as small spheres and colored according to burial count (BC). The BC color scale runs from blue (high BC) to red (low BC), with muted colors denoting intermediate values. Dashed lines represent hydrogen bonds between benzamidinium and trypsin residues (D189 and G219), with distances measured in Angstroms.

By identifying multiple ASPs, PASS also suggests alternate binding sites in proteins for which a primary site(s) of binding has already been established. The pursuit of alternate binding sites is becoming increasingly prevalent in light of the mounting realization that many proteins have more than one biochemical role [21] and are likely to employ separate binding sites in performing distinct biochemical tasks. In addition, many enzymes have allosteric binding sites that effect catalytic activity or substrate binding via the induction of conformational changes upon cofactor binding [22]. PASS can suggest the locations of such sites. Finally, the disruption of protein-protein interactions forms the basis of many drug design efforts, and PASS can be used to identify interfacial pockets that may be suitable targets for drug binding. In particular, interfaces may be identified by using probe spheres to compute a difference map between the bound and unbound forms. This approach can be extended to quickly identify and visualize packing contacts in protein crystals or multimeric forms.

PASS also facilitates the visualization of buried volumes in a protein in that the space occupied by the manifold of probe spheres represents this volume, which can be viewed and manipulated as a solid object by rendering the probes in a space-filling model. Mesh or solid representations of various surfaces (molecular, van der Waals, Connolly) are often used to visualize the shape complementarity of a protein surface for putative ligands or functional groups. Often these surfaces are colored according to some other receptor-based property, such as electrostatics, hydrogen bond propensity, or surface curvature. The idea is that a modeler can use this sort of display to look for likely ligand hot-spots on the protein by visually searching the surface for voluminous invaginations that are colored to indicate favorable complementarity in, say,

electrostatic potential. In reality, ligands only bind to regions possessing enough buried volume to significantly accomodate them. Hence, buried volume is a quantity of central importance in drug design, and the development of methods for informatively displaying such regions should be accorded due attention. Surface representations fail to capture buried volumes directly in that the user is left to infer the buried volume from void space, much of which is obscured from view by the surface. Likewise, colored surface quantities are of most interest near deep invaginations, precisely where the surface is most difficult to see. Unfortunately, user expertise is typically required to overcome such difficulties. PASS takes a more direct approach by filling the buried volumes with a set of unbonded atoms that represent the ASPs and probe spheres. This enables both the size and shape of the buried volumes to be viewed directly, either with or without the protein, using any molecular visualization tool. Rendering the buried volumes as solid allows the user to eyeball the fit of certain ligands and groups to potential hot-spot regions. Figure 6 shows the region of buried volume (orange) lying in the binding cavity of retinol binding protein (1rbp), along with the bound retinol (white), some surrounding residues, and the top- and third-ranked ASPs (in magenta), on the left and right, respectively. Information equivalent to what is color-coded onto protein surface displays can, in principle, be captured by property-based coloring of probe spheres. For instance, the user could perform a finite-difference Poisson-Boltzmann calculation and color the probe spheres according to electrostatic potential, ϕ_{es}. Directly displaying ϕ_{es} in the region of interest, rather than having to infer it from ϕ_{es} at the protein surface, provides a more meaningful view of electrostatics than a surface

Figure 6 - Buried Volume in the Binding Pocket of Retinol Binding Protein

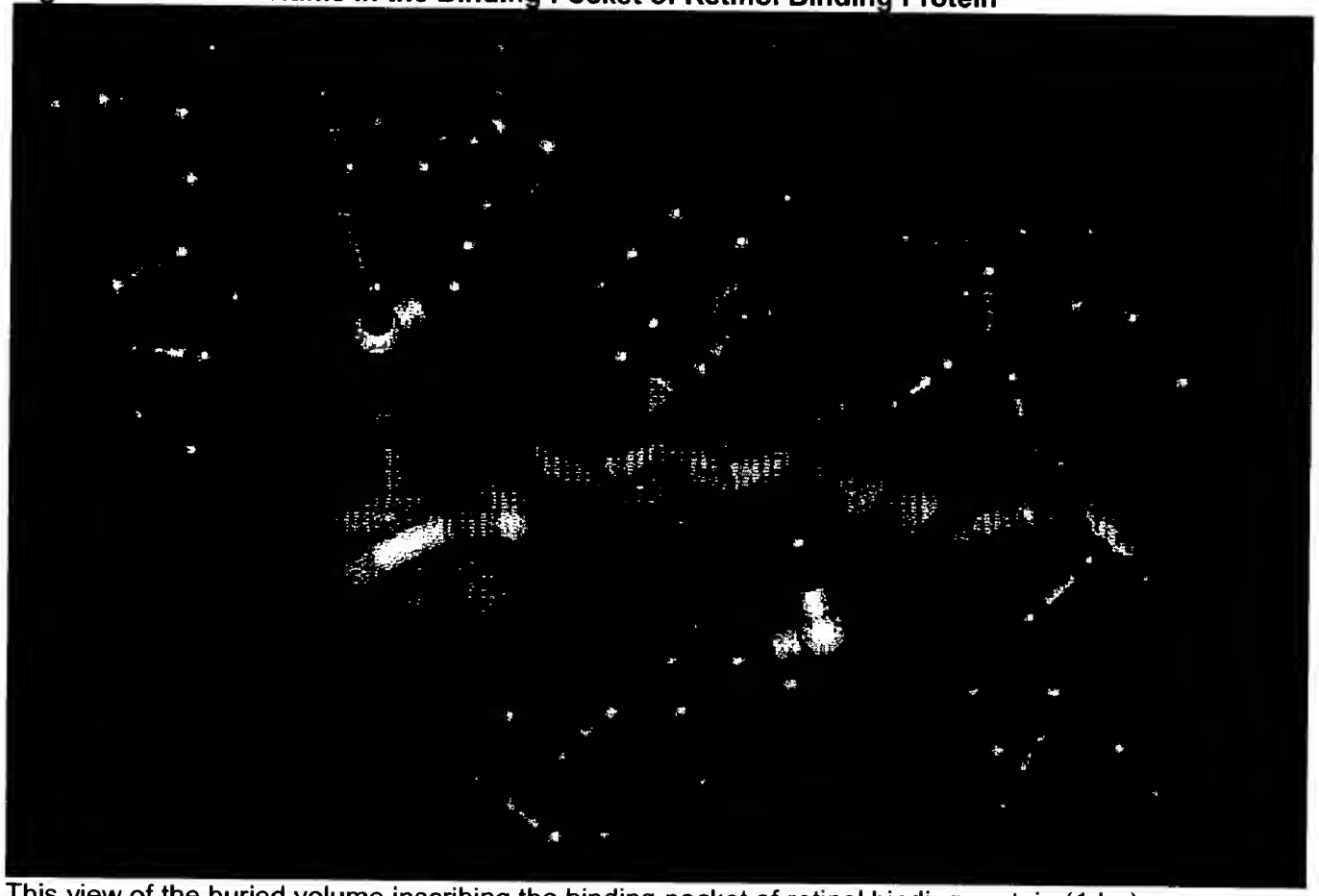

This view of the buried volume inscribing the binding pocket of retinol binding protein (1rbp) was obtained by rendering PASS probe spheres at 1.8 Å radius and coloring them orange. The probes were rendered with slight transparency in order to show the bound ligand (retinol) in white. The top- and third-ranked ASPs, shown in magenta, appear on the left and right, respectively. Protein residues lying within 8 Å of the two ASPs are diplayed in ball-and-stick style and colored according to atom type.

representation. Favorable hydrogen-bond donor and acceptor positions can likewise be more meaningfully defined within the manifold of probe spheres than on a protein surface. Interaction-based coloring schemes are not presently automated within PASS, however.

Comparative Study

Many procedures for characterizing and visualizing protein cavities have been presented in the past and, while all differ substantially from PASS, comparative study serves to highlight some of PASS'S strengths and weaknesses. First, almost all prior methods identify cavity regions using some type of regular grid [2, 5, 6, 8-11, 23-26]. A grid simply provides the coordinates of points lying in cavities, which are then used in some fashion to identify boundaries with the protein and, for all but internal voids, with empty space. One disadvantage of using a grid is that its storage consumes memory unnecessarily. Likewise, uncertainties arise relating to the possible dependence of results upon grid spacing or positioning. Orientational dependence was indeed found in the program POCKET [9, 24]. The advantage of implementing a grid is purely algorithmic, as there is no physical reason to use regular geometry when it is well known that protein packing and protein surfaces are extremely irregular [27], if not fractal [28]. The PASS algorithm captures this irregularity by using geometry to project outward from the known atomic coordinates in order to inscribe cavity regions. Although this sort of protein-based approach has been taken by other groups [7, 8, 29, 30], the geometry employed in these studies differ significantly from PASS. Every point in a protein cavity may be thought to represent a sphere that lies exactly tangential to the protein surface. The radius of this sphere is the distance of closest approach, and

the sphere generally touches the protein at one, two, or three points (i.e. atoms). Several authors have used this correspondence (in reverse) to define points lying in cavity regions by specifying a set of probe spheres and using geometry (one-, two-, and/or three-point) to project outward from the protein atoms into the cavity region. For instance, cavity points have been obtained by placing tangential spheres midway between atoms [8, 30] and by rolling a probe sphere over the set of atomic spheres representing the protein [7, 10]. The resulting probe coordinates usually correspond to one or two points of tangency with the protein. However, the sterically optimal packing of a spherical probe against the protein has the probe lying tangent to exactly three atoms, just as a marble that is dropped onto a pile of other marbles will come to rest touching exactly three. Unlike any previous method, PASS uses only three-point geometry to obtain points lying in cavity regions. Consequently, the shape of the rendered manifold of PASS probes represents maximally favorable sterics. One might expect that positioning the probe spheres using only three-point geometry would give rise to a spotty distribution of probes and poorly-shaped buried volume. Practical experience has shown, however, that PASS produces smooth well-shaped buried volume manifolds (e.g. Figure 6), and that using only three-point geometry helps minimize the number of points required to fill protein cavities.

The most ambiguous aspect of cavity characterization lies in deciding where to place the boundary between the pocket and free space; i.e. determining "sea-level" [8]. Several studies appearing in the literature [5, 6, 10] operate by filling fully-enclosed volumes (e.g. "flood fill") and, thus, require an artificial means of closing-off the mouths of cavities in order to define sea-level. With many other methods [8, 9, 23, 24], the definition of sea-level arises as a biproduct of the algorithm itself and has no physical significance. The work of Kuntz et al. [7] is closest in spirit to the present study with

regard to sea-level definition. Their method uses the Connolly surface as a substrate for sphere growth and rejects spheres based upon two criteria: (1) an angular condition, which essentially selects concave regions over flat or convex ones, and (2) a 5Å upper bound on radial sphere growth. Their radial constraint is expected to generate sea-level boundaries similar to those found with PASS. Unlike any other method of cavity detection, however, PASS explicitly defines sea-level according to a quantity of known physical significance, solvent accessibility, as quantified by burial counts (BC).

Computational speed and ease of use are also important criteria for comparison and, in these categories, PASS rates favorably with all published methods. Although reliable speed comparison is difficult since few studies report CPU times [2, 8, 10, 26, 30] and others report times on old processors [5, 7, 11, 29], the fastest CPU times reported in the literature belong to the LIGSITE program of Hendlich et al. [24], which can analyze a moderate-sized protein (at 0.5 Å grid spacing) in about 15 seconds. This is approximately the same speed demonstrated by PASS; however, the LIGSITE CPU time ramps-up very steeply as the grid spacing is reduced (twelve-fold slower at 0.25 Å), and the authors provide only a cursory investigation of the dependence of their results upon grid scale. PASS also excels in useability in that it requires no startup cost to use because the inputs are simple and the outputs are standard. A few programs in the literature appear to have shared this design perspective [8, 23, 24, 29]. The input to PASS is restricted to a PDB file(s) specifying the protein(s) coordinates plus a few optional command-line flags that can be used to control more detailed behavior. PASS produces versatile output in the form of standard PDB files, which allows the user to immediately view the results using whatever modeling tool is already familiar.

Although the roots of the PASS algorithm are geometrical, not statistical mechanical, it is useful in light of PASS'S success in identifying known binding sites to examine *a posteriori* which physical interactions (if any) are mimicked in PASS. PASS takes the philosophy that the task of binding site prediction is to identify regions of space along the protein where an arbitrary ligand might tightly bind. A physically well-designed algorithm should incorporate as many contributions to binding affinity as possible without sacrificing applicability over a wide range of ligands. Binding affinity is dictated by the free energy change induced by the binding process, ΔG_{bind}, which is known to have numerous contributions, both enthalpic and entropic. While there is disagreement regarding some factors [31-33], sterics, electrostatics, hydrogen-bonding, and solvation are known to be major players [34-38]. Of course, the fine details of ligand size, shape, flexibility, hydrogen-bonding propensity, and polar character are crucial determinants of ΔG_{bind}; however, the observation that proteins usually bind ligands strongly at only a few sites suggests that one might be able to use coarse details of ligand character (e.g. size) to identify these few binding sites. Thus, PASS must make its predictions using only binding affinity contributions that depend upon coarse ligand character. Two important contributions to ΔG_{bind} fit this description: solvation and sterics. Ligand binding is always favored entropically by the desolvation of molecular moieties, regardless of polarity [39]. This is because the hydration of any atomic group causes net ordering in the first few solvation shells of surrounding water. The PASS algorithm mimics this desolvation effect via the rejection of probe spheres based upon burial count. Likewise, the formation of steric (i.e. enthalpic van der Waals)

contacts between ligand and protein is generally favorable, regardless of the ligand. Although the steric contribution to ΔG_{bind} depends upon detailed molecular shape, the hardness of the steric interaction precludes any ligand from binding tightly to the protein without adopting a configuration consistent with the size and shape of the buried volume. PASS includes sterics by imposing an implicit size and shape criterion upon which regions of buried volume can be identified as active site points (ASPs). In particular, a region of buried volume that is either too small or too narrow to contain even a small ligand without steric clash will never contain an ASP because too few probe spheres will lie in the region for any one to have a large enough probe weight to be selected as an ASP. The PASS parameters (esp. R_o and PW_{min}) have been empirically tuned to make this distinction reliably.

Similar arguments cannot be made regarding the electrostatic interaction, for instance, which may contribute either attractively or repulsively to ΔG_{bind}, depending upon ligand charge and polarity. Several other programs in the literature, however, implement energetics in an effort to use other factors (e.g. hydrophobicity, electrostatics) to help identify and rank potential binding site cavities [2, 5, 26]. Most notably, Ruppert et al. present the most impressive results in the literature with regard to accuracy in locating binding sites [2]. Their method uses an in-house empirical forcefield to dock three different types of probes (steric, H-bond donor, H-bond acceptor) against the protein binding site. This maps out a set of favorable "probe" positions and permits the identification of "sticky spots" on the protein, which are used as central points to carve-out individual pockets. Although they provide no CPU times, their algorithm requires significant docking and, thus, is probably considerably slower than PASS or LIGSITE. They apply this method to the prediction of binding sites in a

set of 11 PDB complexes and find that their top-ranked pocket contains the ligand in every case. Nine of these eleven cases, however, are included in the PASS test set (Table 3), and strikingly similar results are obtained with PASS. The top-ranked ASP is a binding site hit in eight of the nine overlapping trials, and the second ASP is a hit in the other case. Although factors such as electrostatics and hydrogen-bonding certainly contribute to the affinity of a ligand for a particular cavity, the perspective taken in PASS is that only the most ligand-independent contributions to binding (i.e. size, shape, and burial extent of cavities) should contribute to binding site prediction. Energetic factors that strongly modulate specificity should be addressed case-by-case, either manually by the user or via downstream software (e.g. docking). Thus, the PASS ASP regions are completely inclusive with regard to electrostatic and hydrogen-bonding character, with the intention that each will be reinvestigated individually in light of a particular application or desired complementarity. PASS'S success in predicting binding sites without electrostatics and hydrogen-bonding constitutes a remarkable restatement of the importance of solvation and sterics in binding.

Conclusions

PASS is a simple cavity detection tool that has utility in both virtual screening and interactive molecular modeling environments. PASS was shown to reliably predict the locations of known binding sites using a set of 20 apo-protein x-ray structures from the PDB, thereby establishing its utility as a front-end to fast docking and virtual screening. Furthermore, for the price of a thirty-second investment, PASS provides the user a meaningful view of the buried volumes in a protein, suggests alternate binding

sites, and simplifies detailed visualization of potential binding hot-spots. PASS is freely available in unix executable form (SGI Irix, SunOS, Linux) to all users via the Protein Data Bank web site under "PDB-related Software" (http://www.pdb.bnl.gov/pdb-docs/software.html).

Acknowledgements

The authors thank Carla Mattos and Dagmar Ringe for providing their elastase structure with bound organic probes and Zelda Wasserman for critical review of the manuscript. GPB thanks the DuPont Pharmaceuticals Company for postdoctoral support during this work.

App ndix A - Three-Point Sph r G ometry

The sphere placement algorithm in PASS hinges upon solution of the following geometry problem. Given three "base" spheres (i, j, and k) of known positions ($\mathbf{R}_i$, $\mathbf{R}_j$, $\mathbf{R}_k$) and radii (σ_i, σ_j, and σ_k), at what two positions ($\mathbf{R}_p$) can a "probe" sphere of radius σ_p be placed so as to be exactly tangential to all three base spheres? We seek the general solution, in which none of the radii are necessarily equal and the coordinates of the base spheres are unconstrained. Figure A1 illustrates the situation: sphere perimeters are outlined, base sphere centers are labelled "i", "j", "k", the "base plane" (i-j-k) is shaded, the probe sphere is shaded and labelled "p", and vectors are denoted with uppercase lettering while points and distances are in lowercase. The global origin coordinates is labelled "O", while a local frame is defined by unit vectors {**x**′, **y**′, **z**′}. There are, in general, two solutions for $\mathbf{R}_p$, one on either side of the base plane. However, one must first impose several conditions to ensure the existence of a solution. If any pair {i,j} of base spheres are too far apart, the probe will be unable to bridge the gap, so one must first ensure that $|\mathbf{R}_j - \mathbf{R}_i| \le \sigma_i + \sigma_j + 2\sigma_p$, and likewise for pairs {i,k} and {j,k}. One must also make sure that no base sphere lies entirely within the volume occupied by the other two. With these conditions satisfied, the coordinates $\mathbf{R}_p$ of the two valid probe sphere positions may be written

$$\mathbf{R}_p = \mathbf{R}_b \pm h\mathbf{z}', \qquad \text{(A.1)}$$

where h is the height of the probe above the base plane, and **z**′ is a unit normal to this plane. To be precise, the local coordinate frame {**x**′, **y**′, **z**′} is right-handed, with **x**′

lying along $\mathbf{R}_j$-$\mathbf{R}_i$ and $\mathbf{z}'$ pointing out of the base plane in the direction of $\mathbf{x}'$ x ($\mathbf{R}_k$-$\mathbf{R}_i$).

The right triangle i-b-p gives the height

$$h=\sqrt{(\sigma_i+\sigma_p)^2-|\mathbf{R}_b-\mathbf{R}_i|^2}\quad . \tag{A.2}$$

The vector $\mathbf{R}_b$ from O to the point of projection of the probe onto the base plane, b, can be written vectorially as

$$\mathbf{R}_b=\mathbf{R}_i+(\mathbf{T}_{ij}-\mathbf{R}_i)+\mathbf{U}\,, \tag{A.3}$$

which leaves $\mathbf{T}_{ij}$ and $\mathbf{U}$ undetermined. In general, point b need not lie on the interior of triangle i-j-k, as drawn, but the equations are the same in either case. $\mathbf{U}$ can be eliminated from Eqn. (A.3) by observing that

$$\mathbf{U}\cdot(\mathbf{T}_{ik}-\mathbf{R}_i)=\mathbf{V}\cdot(\mathbf{T}_{ik}-\mathbf{R}_i), \tag{A.4}$$

where $\mathbf{V}\equiv\mathbf{T}_{ik}-\mathbf{T}_{ij}$, and $\mathbf{U}$ points in the direction of $\mathbf{y}'$. Solving Eqn. (A.4) for $\mathbf{U}$ yields

$$\mathbf{U}=\frac{(\mathbf{T}_{ik}-\mathbf{T}_{ij})\cdot(\mathbf{T}_{ik}-\mathbf{R}_i)}{(\mathbf{T}_{ik}-\mathbf{R}_i)\cdot\mathbf{y}'}\mathbf{y}'\,. \tag{A.5}$$

The remaining vectors $\{\mathbf{T}_{ij}, \mathbf{T}_{ik}, \mathbf{T}_{jk}\}$, which run from O to points $\{t_{ij}, t_{ik}, t_{jk}\}$, are found by considering the triangles formed by two base spheres and the probe sphere. For instance, the triangle i-j-p comprises two right triangles, i-t_{ij}-p and j-t_{ij}-p. Applying the Pythagorean theorem to each enables determination of the distance from i to t_{ij} via a quadratic equation, which yields the desired vector

$$\mathbf{T}_{ij}=\tfrac{1}{2}(\mathbf{R}_i+\mathbf{R}_j)+\frac{(\sigma_i+\sigma_p)^2-(\sigma_j+\sigma_p)^2}{2|\mathbf{R}_j-\mathbf{R}_i|^2}(\mathbf{R}_j-\mathbf{R}_i). \tag{A.6}$$

Swapping indices in Eqn. A.6 gives analogous equations for $\mathbf{T}_{ik}$ and $\mathbf{T}_{jk}$. The normal vector, $\mathbf{n}$, to the plane of tangency (α-β-γ) may also be of interest:

$$\mathbf{n}=C\cdot\left[\sigma_{kp}^{+}\mathbf{r}_i\times\mathbf{r}_j+\sigma_{ip}^{+}\mathbf{r}_j\times\mathbf{r}_k+\sigma_{jp}^{+}\mathbf{r}_k\times\mathbf{r}_i+(\sigma_{kj}^{-}\mathbf{r}_i+\sigma_{ik}^{-}\mathbf{r}_j+\sigma_{ji}^{-}\mathbf{r}_k)\times\mathbf{r}_p\right], \tag{A.7}$$

where $\sigma_{ab}^{\pm} \equiv \sigma_b \pm \sigma_a$, $C \equiv \sigma_p / \sigma_{ip}^{+} \sigma_{jp}^{+} \sigma_{kp}^{+}$, and **n** is not of unit magnitude.

Figure A1 - Sphere Geometry

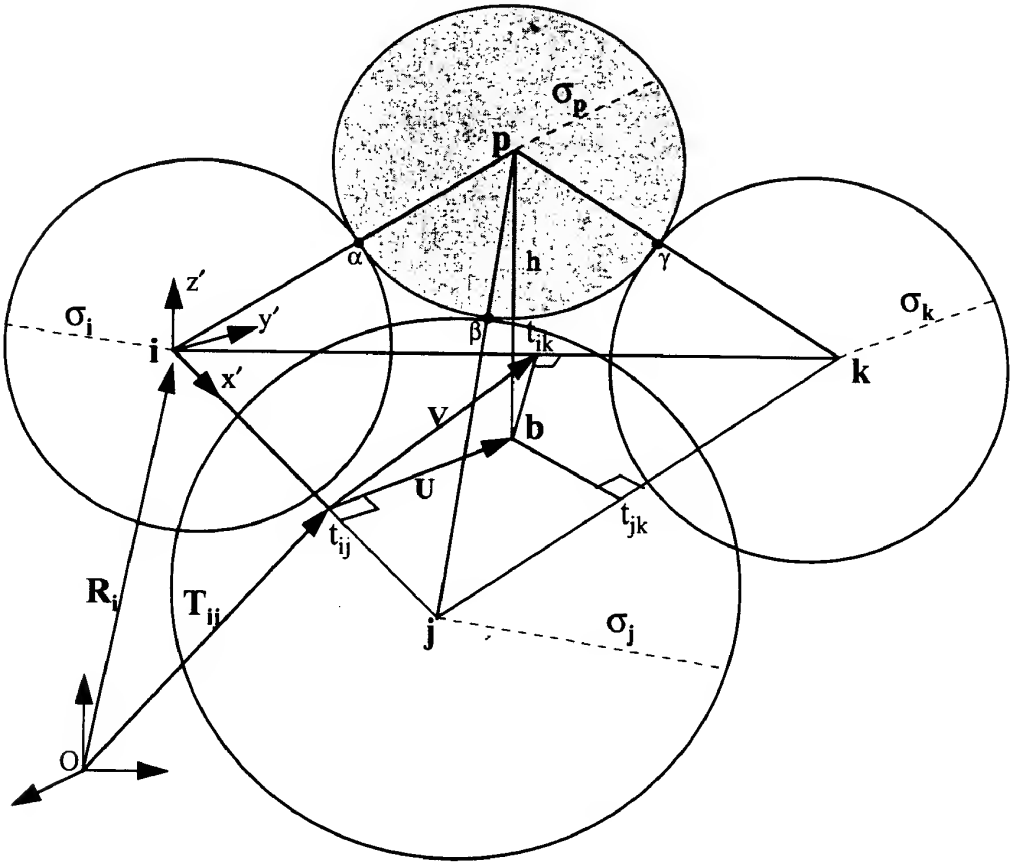

References

1 Ringe, D., Cur. Op. Struct. Biol., 5 (1995) 825.

2 Ruppert, J., Welch, W. and Jain, A.N., Prot. Sci., 6 (1997) 524.

3 Connolly, M. L., J. Appl. Crystallogr., 16 (1983) 548.

4 Nicholls, A., Bharadwaj, R. and Honig, B., Biophys. J., 64 (1993) A166.

5 Ho, C. M. W. and Marshall, G.R., J. Comput.-Aided Mol. Design, 4 (1990) 337.

6 Kleywegt, G. J. and Jones, T.A., Acta Cryst., D50 (1994) 178.

7 Kuntz, I. D., Blaney, J.M., Oatley, S.J., Langridge and R., Ferrin, T.E., J. Mol. Biol., 161 (1982) 269.

8 Laskowski, R. A., J. Mol. Graphics, 13 (1995) 323.

9 Levitt, D. G. and Banaszak, L.J., J. Mol. Graphics, 10 (1992) 229.

10 Masuya, M. and Doi, J., J. Mol. Graphics, 13 (1995) 331.

11 Voorintholt, R., Kosters, M.T., Vegter, G., Vriend, G. and Hol, W.G.J., J. Mol. Graphics, 7 (1989) 243.

12 Stouten, P. F. W., Froemmel, C., Nakamura, H. and Sander, C., Molecular Sim., 10 (1993) 97.

13 Cerius2 v3.8, Molecular Simulations Inc., San Diego, 1998.

14 InsightII v97.2, Molecular Simulations Inc., San Diego, 1998.

15 MOE v1997.09, Chemical Computing Group Inc., Montreal, 1997.

16 Quanta v97.1003, Molecular Simulations Inc., San Diego, 1997.

17 RasMol v2.6, Roger Sayle, Hertfordshire U.K., 1997.

18 Sybyl v6.5, Tripos Inc., St. Louis, 1998.

19 Kurita, T., Pattern Recognition, 24 (1991) 205.

20 Mattos, C., and Ringe, D., Nature Biotechnology, 14 (1996) 595.

21 Ringe, D., Personal Communication, 1998.

22 Hurley, J. H., Cur. Op. Struct. Biol., 6 (1998) 770.

23 Delany, J. S., J. Mol. Graphics, 10 (1992) 174.

24 Hendlich, M., Rippmann, F. and Barnickel, G., J. Mol. Graphics and Modelling, 15 (1997) 359.

25 Kisljuk, O. S., Kachalova, G.S. and Lanina, N.P., J. Mol. Graphics, 12 (1994) 305.

26 Young, L., Jernigan, R.L. and Covell, D.G., Protein Science, 3 (1994) 717.

27 Kurochkina, N. and Privalov, G., Prot. Sci., 7 (1998) 897.

28 Lewis, M. and Rees, D.C., Science, 230 (1985) 1163.

29 Del Carpio, C. A., Takasashi, Y. and Sasaki, S., J. Mol. Graphics, 11 (1993) 23.

30 Williams, M. A., Goodfellow, J.M. and Thornton, J.M., Prot. Sci., 3 (1994) 1224.

31 Brady, G. P. and Sharp, K.A., Cur. Op. Struct. Biol., 7 (1997) 215.

32 Holtzer, A., Biopolymers, 35 (1995) 595.

33 Murphy, K. P., Xie, D., Thompson, K.S., Amzel, L.M. and Freire, E., Protein Struct. Funct. Gen., 18 (1994) 63.

34 Ajay, Murcko, M.A. and Stouten, P.F.W., In Charifson, P. S. (ed.) Practical Application of Computer-Aided Drug Design , Marcel Dekker, New York, 1997, pp. 355.

35 Brady, G. P. and Sharp, K.A., Biophys. J., 72 (1997) 913.

36 Gilson, M. K., Given, J.A., Bush, B.L. and McCammon, J.A., Biophys. J., 72 (1997) 1047.

37 Kauzmann, W., Adv. Prot. Chem., 14 (1959), 1.

38 Makhatadze, G. I. and Privalov, P.L., Adv. Prot. Chem., 47 (1995) 307.

39 Madan, B. and Sharp, K.A., J. Phys. Chem., 100 (1996) 7713.

40 Bondi, A., J. Phys. Chem., 68 (1964) 441.

Pergamon *Bk~organic & Medicinal Chemistpy,* Vol. 4, No. 9, pp 1421-1427, 1996

PII: S0968-0896(96)00136-8 0968-08%/96 $15.00+0.00

Structure-Based Design of Parasitic Protease Inhibitors

Rongshi Li/Xiaowu Chen/Baoqing Gong/Paul M. S e i z e r , b Zhe Li,* Eugene Davidson, ~
Gary Kurzban/Robert E. Miller," Edwin O. Nuzum, f James H. McKerrow, ~'b
'Robert J. F l e t t e r i c k , "'~ Sarah A. G i l l m o r / ' ~ C h a r l e s S. Craik, a'~ Irwin D. Kuntz,"
F r e d E. Cohen a'd and George L. Kenyon a'*
Departments" of "Pharmaceutical Chemistry and hPathology, Veterans Affairs Medical Center, ~Department of Biochemistry
and Biophysics, and aPharmacology and Medicine, Universi~ of California, San Francisco, CA 94143-0446, U.S.A.
"Department of Biochemistry and Molecular Biolog); Georgetown University, Washington DC 20007, U.S.A.
tDivision of Experirnental Therapeutics, Walter Reed Army Institute of Research, Washington, DC 20307-5100, U.S.A.

Abstract--To streamline the preclinical phase of pharmaceutical development, we have explored the utility of structural data on
the molecular target and synergy between computational and medicinal chemistry. We have concentrated on parasitic infectious
diseases with a particular emphasis on the development of specific noncovalent inhibitors of proteases that play a key role in the
parasites' life cycles. Frequently, the structure of the enzyme target of pharmaceutical interest is not available. In this setting we
have modeled the structure of the relevant enzyme by virtue of its sequence similarity with proteins of known structure. For
example, we have constructed a homology-based model of falcipain, the trophozoite cysteine protease, and used the computa-
tional ligand identification algorithm DOCK to identify in compuo enzyme inhibitors including oxalic bis(2-hydroxy-l-naphthyl-
methylene)hydrazide (1) [Ring, C. S.; Sun, E.; McKerow, J. H.; Lee, G.; Rosenthal, P. J., Kuntz, I. D.; Cohen, F. E., *Proc. Natl*
Acad. Sci. U.S.A. 1993, *90,* 3583]. Compound 1 inhibits falcipain (IC,~, 6 ~M) and the organism in vitro as judged by hypoxanthine
uptake (ICs~, 7 ~tM). Following this lead, to date, we have identified potent bis arylacylhydrazides (ICs. 150 nM) and chalcones
(IC~o 200 nM) that are active against both chloroquine-sensitive and chloroquine-resistant strains of malaria. In a second
example, cruzain, the crystallographically determined structure of a papain-like cysteine protease, resolved to 2.35 A., was avail-
able. Aided by DOCK, we have identified a family of bis-arylacylhydrazides that are potent inhibitors of cruzain (ICso 600 ~tM).
These compounds represent useful leads for pharmaceutical development over strict enzyme inhibition criteria in a structure-
based design program. Copyright © 1996 Elsevier Science Ltd

Introduction

More and more successful examples of the design of new ligands based on knowledgc of target protein structure have been reported. These include design of noncovalent antiparasitic agents,' 3 rational design of sialidase-based inhibitors of influenza virus replication, 4 design of nonpeptide cyclic ureas as HIV protease inhibitors, ~ structure-based discovery of inhibitors of thymidylate synthase, ~ and structure-based design of inhibitors of purine nucleoside phosphorylase. 7 10 Most structure-based drug design relies on X-ray crystallo-

graphy/NMR spectroscopy" to obtain the appropriate structures to identify new leads and guide lead optimization. Our work on the structure-based drug design of parasitic protease inhibitors has relied upon X-ray crystal structures when available (e.g., cruzain n13 for anti-Chagas disease agents), but has relied on a homology-based model structure I ' if neither X-ray nor NMR data are available (e.g., falcipain for antimalarials) to generate leads and guide our lead optimization.

Proteases are involved in many important biological processes including protein turnover, blood coagulation, complement activation, 1~ hormone processing, ~

*Present address: Ar Qule Pharmaceuticals, Inc., 200 Boston Avenue, Medford. MA [)2155. U.S.A.

and cancer cell invasion, l" Thus, they are frequently chosen as targets for drug design and discovery. A potential strategy for the treatment of diseases caused by parasites is the design of compounds which selectively inhibit enzymes that are pivotal for survival of the parasite within the host that are part of biochemical pathways that are specific to the parasite. Parasite proteases are attractive target enzymes because of their roles in replication, metabolism, survival and pathology.~7

In the most simple terms, structure-based drug design methods identify favorable and unfavorable interactions between a potential inhibitor and target receptor and maximize the beneficial interactions to increase binding affinity. Although X-ray crystallography continues to be the source of high-resolution information about protein structures, considerable delays often exist between determining the sequence of a protein and solving its structure. Difficulties in protein expression and more commonly in protein crystallization are often responsible for such delays. Currently, no general method exists to predict tertiary structure from amino acid sequences. However, when a protein target is relatively highly homologous to another protein or group of proteins of known structure, a sensible model structure can be proposed. ~s

The World Health Organization estimates that 280 million people are infected with malaria ~9 and 1-2 million deaths are reported annually. 2° While various classes of antimalarial agents are available, chloroquine and its derivatives remain the mainstay of therapy against malaria. Unfortunately, the emergence of malarial parasite strains resistant to chloroquine has eroded its efficacyfl I This increases the urgency of the search for novel and cost-effective agents to treat chloroquine-resistant malaria.

Chagas disease is caused by *Trypanosoma cruzi, a* protozoan parasite that afflicts more than 24 million people in South and Central America. It is the leading cause of heart failure in many Latin American countries. Currently, there is no satisfactory treatment for this parasitic infection. Cruzain, the major cysteine

protease present in T. *cruzi,* is pivotal for the development and survival of the parasite within the host cells. This makes the enzyme a target for potential trypanocidal drugs.

In our previous reports, 1-3 we described a structure-based approach to inhibitor design for antimalarial drug development using models of falcipain, a malaria trophozoite cysteine protease structure. Here, we summarize our progress to date in the structure-based drug design of parasitic protease inhibitors.

Results and Discussion

Lead discovery and optimization

A structure for the malaria cysteine protease, falcipain, was proposed using the X-ray structures of papain and actinidin, two cysteine proteases from plant sources, as a basis for homology modeling? Falcipain has 33% sequence identity with both papain and actinidin. Moreover, ~60% of the conserved sequence centers around the active site regions. The homology-based model of the enzyme provides the template and the DOCK 22 algorithm calculates a set of spheres with approximately atom sized radii to fill the active site cleft. Within DOCK, the quality of a given compound's fit into the binding cleft can be evaluated based on its shape complementarity (contact score) or molecular mechanics interaction energy (AMBER force-field score).

The model structure was then used as a template for a DOCK search of the Fine Chemicals Directory of commercially available small molecules for putative ligands (the Fine Chemicals Directory distributed by Molecular Design Limited Information System, San Leandro, California, is currently known as the Available Chemical Directory). When searching a database of compounds, DOCK examines only the 'best' orientation of the small molecule within the binding cleft (DOCK database screening mode). When a. single compound is studied, multiple possible binding modes can also be examined (DOCK single mode). Of course, the initial orientation of the compound is dictated in part by the irregular lattice of sphere centers identified originally. To overcome some of the scoring distortion that this bias could impart, a rigid body minimization algorithm has been developed to move the ligand within the binding cleft and optimize the shape or forcefield scores. 23 Compound 1 [oxalic *bis((2-hydroxy-*1-naphthylmethylene)hydrazide)] was selected based on its score for shape complementarity. Thirty-one compounds were finally tested and a lead compound 1 was identified as the best inhibitor of the protease. The IC5o value for enzyme inhibition against the substrate benzyloxycarbonyl-Phe-Arg-(7-amino-4-methylcoumarin) was 6 I.tM. 3 More importantly, this compound inhibits the growth of parasites in culture. Malaria lacks some of the enzymes required for *de novo* purine biosynthesis and thus depends on purine salvage

pathways for DNA replication. Compound 1 inhibits parasite growth as judged by its ability to block hypoxanthine uptake, with an apparent IC5o value of 7 pM.3 Compound 1 fits a model of the active site of the malarial cysteine protease as shown in Figure 1. I-3 The DOCK 22 program placed this lead compound 1 into the enzyme's active site, presumably filling three of the substrate side-chain specificity pockets (subsites $2, $1' and to a lesser extent Sa). Beginning with compound 1 as shown in Scheme 1, the following chemical modifications were made in an attempt to identify more active agents: (i) The length of the backbone linking the aromatic rings of 1 was shortened via the construction of asymmetric acylhydrazides, which could have less conformational heterogeneity than the symmetric hydrazides, yet still could fill at least two of the three putative subsites (5 in Table 1). Compounds can be constructed by attaching a third aryl group to the center aromatic moiety to fill all three putative subsites (6 in Table 1). (ii) Heterocyclic acylhydrazides were generated by incorporating nitrogen atoms into aromatic rings both to improve water solubility of the compounds and potentially to enhance electrostatic interactions with His67 in the $2 site. (iii) To increase the chemical/metabolic stability of the compounds, a four-atom hydrazide linker was replaced with a three-atom ~,13-unsaturated ketone bridge (7 and 8 in Table 1). (iv) Naphthalene, quinoline or isoquinolinc rings were exchanged for substituted phenyl rings on both acylhydrazide and a,13-unsaturated ketone linkers to explore the effective size and electronic character of the putative subsite specificity pocket.

Chemistry, antiparasitic activity and inhibition specificity

Since cost of production is a critically important consideration if the resulting antimalarials and other antiparasitic agents are ever to be developed into therapeutic agents for the world's developing countries, one of our guidelines for the development of antiparasitic agents is that these compounds should be inexpensive to produce. Hence, we developed relatively simple chemistry to prepare both arylacylhydrazide and chalcone derivatives. For both series, the final step is the condensation of an aldehyde with either acylhydrazines via imine formation 2 or substituted methylketones

via a Claisen-Schmidt condensation. 1 Since there are a variety of commercially available aldehydes and methylketones as starting materials, a large number of target compounds can be produced relatively inexpensively. For preparation of the key acylhydrazine intermediates, a published procedure was followed)

After some 400 bis arylacylhydrazide and chalcone derivatives were synthesized, they were screened against three different antiparasitic screening systems. Antimalarial activities were evaluated based on an

assay of parasitemia of red blood cells quantitated by a fluorescence-activated cell sorter (FACS) analysis 24 and the more classical assay of metabolic viability, hypoxanthine uptake, 1 described below.

For the FACS analysis, synchronized trophozoite-stage parasites were cultured in human blood at various inhibitor concentrations. The parasites were allowed to mature, the host cell was lysed and parasite invasion of

'Figure 1. A putative binding orientation of the 'lead' compound (1) bound to the active site of the malarial cysteine protease. Key residues and the binding subsites of the protease are colored as cyan (S; site), yellow (S/catalytic site), and purple (SJS~ site). For the lead compound, carbon is shown in green, oxygen in red, and nitrogen in blue.

flesh red blood cells was investigated. Using propidium iodide to stain DNA, the FACS can discriminate between infected and uninfected cells and between stages of intraerythrocytic parasite development as only infected red blood cells contain DNA. 24 The hypoxanthine uptake system assessed the intrinsic antimalarial activity in vitro against the erythrocytic asexual life cycle (blood schizontocides). Two *Plasmodium falciparum* clones, CDC/Indochina III (W2) and CDC/Sierra Leone I (D6), 2~ were used for all antimalarial assays. W2 is resistant to chloroquine, quinine, and pyrimethamine and susceptible to mefloquine. D6 is resistant to mefloquine and susceptible to chloroquine, quinine and pyrimethamine. The resistance indexes are defined as ratios of the IC5, of a compound against W2 to the IC5. of the same compound against D6. This index is used as a factor to evaluate whether or not novel antimalarials are potential agents against chloroquine-resistant parasites. Chloroquine and mefloquine were used as controls in the assays. The third screening system involved the assay of two cysteine proteases, cruzain and cathepsin B. ~ Enzymatic activity of these two proteases was measured by following the cleavage of fluorogenic substrates. Structure-activity relationships (SAR) for some bis arylacylhydrazide and chalcone derivatives were reported previously, t2 Here, we summarize antiparasitic activity and enzyme inhibition of a group of hydrazide and chalcone derivatives. As shown in Table 1, the lead compound 1 showed little specificity in both antimalarial activity and enzyme inhibition. Cathepsin B is a mammalian cysteine protease from bovine spleen with 87% sequence identity to a human cathepsin B and papain is a cysteine protease from papaya. For comparison, inhibition activities of both cathepsin B and papain by hydrazide and chalcone derivatives are included in Table 1. Compound 2 is a more specific inhibitor of cruzain, with an IC~, value of 600 nM, than the rest of the compounds shown in Table 1. Compound 5 is the best in vitro antimalarial found in the acylhydrazide series with an IC~. value of 150 riM. The most noteworthy example is compound 6. The ICs0 value as an antimalarial is 450 nM while the IC~, value as a cathepsin B inhibitor is at least 400-fold higher (Table 1). This suggests that compound 6 is a more

specific inhibitor of the malarial cysteine protease and will be less likely to be toxic to the host. Compound 7 is the best in vitro antimalarial compound found in the chalcone series to date with an IC~, value of ~ 200 nM. The differences in inhibitory specificity shown above may stem from the fact that the active site residues of these cysteine proteases are quite different, as shown

H

',~ N'~. N N~ N.'~

H

(1)

l vary size of rings

vary size of tinker

H ~ O R

improve water solubility

o

Y< H '~z,;~"- OR~

RZ ~ vary size of rings

R 3 ~ RI O .OR6

R~"]R 5 v H "~z~OR7

RI--R 5 = H, OH, OCH3, N(CH3) 2

R6, R7 = H, CH 3

Scheme I. Lead' optimization by chemical modification.

change

original lead

found by DOCK

Rl = H, OH, OCH 3

R 2 = H, OH, OCH 3

R 3 = H, OH, OCH 3

R4= H, C1

R5 = H, CH 3

R6 = H, CH3, CH2Ar

X, YorZ=N orCH

X~. RI ¢~Z ..,~...~ R6

Y-f~' 6 R~

R4

vary size of rings X, Y or Z = N or CH

R2 R

R3~RI/£ RI0~ R8

R 4 ~ R 7

R 5 O R6

RI--Rlo = H, F, C1, Br, NO2, CF3, OH, OCH3, N(CH3)2

R~ = H, CH 3

to N-containing heterocycles

I improve metabolic stability

R1 = H, C1, OH, OCH 3

R2 = H, C1, OH, OCH 3

R 3 = H, CH 3

R4 =H, C1

R5 = H, OCH 3

R6 = H, OCH 3, imidazole

Parasitic protease inhibitors 1,125

in Table 2, especially the residues from the SiS3 site and part of the Sdcatalytic site. The most likely binding orientations of inhibitors involve extensive interactions between inhibitor molecules and the three binding subsites. The highly conserved SI' and catalytic binding

subsites provide basic interactions for binding, while the diverse residue types in the SiS3 binding subsite among different proteases result in binding specificity. A thorough discussion of structural implications of binding specificity will be presented in a separate manuscript. '~

Conclusions

Structure-based drug design typically depends upon the experimental determination of the target structure by either X-ray crystallography or NMR spectroscopy. We have circumvented this step and relied exclusively on the amino acid sequence homology between the

Table 1. Antiparasitic activity and enzyme inhibition of some hydrazide and chalcone derivatives

Compds	Structure	Antimalarial	Cruzain b	Cathepsin B"	Papain ~' activity
1	~ . ~ @ 7	' 0 (1)	22 (1)	19 (1)	
%	:',~"'~.,,-.~	91 (20)	78 (20)	74 (2(I)	
2	(~ ' ~ "~ ~ - 0.6 ~	20'	50'		
om					
4	**> 10' 30' 20'**				
'	**- ~ ND NO ND**				
6	~o 2.() ~	200'	ND		
7	**ND ND ND**				
>	l&				
ND	~				
ND					
0.15(J	**~' ~ 2**				
(i.450~,.	r..~				
o . : 3 0					
~ ~	0.19@ ...				
8	**i 0.. 10 .... 0 (1) 3 (I**				
0.720	~. ~				
6(1)					

"FACS assay. lC~, in j.iM.

~'% Enzyme inhibition 0.1M inhibitor).

~**ND:** not determined.

aHypoxanthine uptake assay, IC~,, of W2 (chloroqulne-resistance strain) in laM.

"Hypoxanthine uptake assay, lC~,, of D6 (chh)roquine-sensitive strain) in [aM.

'IC~. In I~M.

malaria enzyme and other cysteine proteases of known structure to support our antimalarial program. A homology based model of the malaria enzyme served as the template for a computer-based ligand docking calculation that identified a useful lead compound for a group of cysteine proteases in our antiparasitic program. Lead optimization was achieved by a combined approach of computational and synthetic analysis. Derivatives of the lead were first optimized for fit using the computer docking program, and then numerous candidate compounds were synthesized and tested experimentally. Despite the lack of a detailed experimental structure of the target enzyme or the enzyme-inhibitor complex, we have been able to identify compounds with increased potency. To date, we have identified a potent bis arylacylhydrazide, 5 (IC50 150 nM), and a chalcone, 7 (IC~0 ~200 nM), that are active against both chloroquine-sensitive and chlor-

oquine-resistant strains of malaria. Due to the ~30% sequence identity between cruzain and falcipain, a subgroup of compounds generated in the malaria project (selected using DOCK as a guide) were also screened against cruzain. The best cruzain inhibitor so far, hydrazidc 2, had an IC_{s_0} value of 600 nM.

Experimental

Melting points were measured on a Thomas-Hoover 'Unimelt apparatus and are uncorrected. TLC (silica gel 60 GF254, Merck, Darmstadt) was used to monitor reactions and check product homogeneity. NMR spectra at 300 MHz for ~H and 75 MHz for ~3C (tetramethylsilane as internal standard) were recorded on a General Electric QE-300 spectrometer. Chemical ionization mass spectrometry (CIMS) spectra were obtained at the UCSF Mass Spectrometry Facility, A. L. Burlingame, Director. Elemental analyses were performed by the University of California, Berkeley, Microanalytical Laboratory and were within _+0.4% of the theoretical values. All starting materials were purchased from Aldrich Chemical Company, Inc.

General procedure for condensation of aldehyde with hydrazine (Method A for 2 - 6)

To a solution of the aldehyde (1 mmol) in methanol (20 mE) was added the corresponding acylhydrazine (1 mmol). The resulting mixture was heated at reflux at 65 °C for 3 h. In most cases, a precipitate was observed after 10 min. The precipitate was filtered, washed with

Table 2. Active site residues of cysteine proteases

Sl S~/catalytic site	*82/,3*											
Proteases	19	177	175	25	159	67	68	69	133	160	205	207
Papain	Gin	Trp	Ash	Cys	His	Tyr	Pro	Trp	Val	Ala	Set	Phe
Actinidin	--~'	-	-	.	.	.	.	lie	Thr	Ala	-	-
Falcipain	.	.	.	.	.	His	-	-	Phe	Asn	Ser	Glu
Cruzain	.	.	.	.	.	Leu	Met	Asn	Ala	Gly	Glu	Ser
Cathepsin B	.	.	.	.	.	Glu	-	-	Ser	Ala	-	-

"Same residue wpe as papain..

hot methanol (50 mL) and dried under vacuum to give a solid (usually yellow). If needed, additional purification was performed by recrystallization using appropriate solvents.

Preparation of acylhydrazines from the corresponding acid or ester (Method A1)

A mixture of the acid (10 mmol) and concd H2SO 4 (5 mL) in MeOH (25 mL) was heated at reflux for 12-24 h. The mixture was poured onto ice (100 mL). The resulting precipitates were collected, washed with HzO and recrystallized from EtOH:H20 to give the pure methyl ester. The methyl ester was then dissolved in EtOH (80 mL) and treated with hydrazine monohydrate (5.01 g, 100.0 mmol). The resulting mixture was stirred overnight at 20°C and then concentrated to give the corresponding acylhydrazine, which was further purified by recrystallization from EtOH/H20. Compound 1 [oxalic bis(2-hydroxy-l-naphthylmethylene)hydrazide] was reported previously. 2 Chalcone

derivatives 7 [1-(2,5-dichlorophenyl)-3-(4-quinolinyl)-2-propen-l-one] and 8 [1-(3,4-dimethoxyphenyl)-3-(3-(2-chloroquinolinyl))-2-propen- 1-one] were prepared via a Claisen-Schmidt condensation also described previously)

2'-Hydroxy-6'-methoxynaphthylacyl-(2.hydroxy-l.naphthylmethylene)hydrazide (2). A 70% yield; mp >280 °C; ~H NMR (DMSO-d6): 8 12.84 (s, 1 H), 12.20 (br s, 1 H), 11.20 (br s, 1 H), 9.59 (s, 1 H), 8.46 (s, 1 H), 8.36 (d, 1 H, J= 8.4 Hz), 7.96 (d, 1 H, J= 9.0 Hz), 7.91 (d, 1 H, J=8.1 Hz), 7.74 (d, 1 H, J=9.0 Hz), 7.63 (t, 1 H, J=.6 Hz), 7.43 (t, 1 H, J=7.5 Hz), 7.28 (d, 1 H, J=9.0 Hz), 7.22 (dd, 1 H, J=2.0, 9.1 Hz), 3.90 (s, 3 H); ~3C NMR (DMSO-d6): 8 163.08, 158.14, 155.73, 152.16, 147.48, 132.89, 131.71, 131.48, 129.25, 128.93, 127.81, 127.76, 127.72, 127.44, 123.56, 121.31, 121.00, 119.94, 118.21, 110.94, 108.65, 106.45, 55.17; CIMS: *m/z* (MH ÷) 387.3. Anal. (C23H18N204): ealcd: C, 71.49; H, 4.70; N, 7.25. Found: C, 71.09; H, 4.84; N, 7.23%.

2'-Hydroxynaphthylacyl. (2, 8-dihydroxy- 1-naphthylmethylene)hydrazide (3). A 88% yield; mp 274 °C (dec); IH NMR (DMSO-d6): 8 14.03 (s, 1 H), 12.54 (br s, 1 H), 11.31 (br s, 1 H), 10.47 (s, 1 H), 10.37 (s, 1 H), 8.53 (s, 1 H), 7.96 (d, 1 H, J=8.1 Hz), 7.87 (d, 1 H, J =9.0 Hz), 7.80 (d, 1 H, J= 8.4 Hz), 7.54 (t, 1 H, J = 7.5 Hz), 7.39 (m, 3 H), 7.22 (m, 2 H), 7.08 (d, 1 H, J = 7.2 Hz); **13C** NMR (DMSO-d6): 8 163.80, 159.39, 154.34, 153.30, 153.02, 135.93, 133.51, 130.26, 130.06, 128.66, 128.28, 126.73, 125.91, 123.82, 123.71, 121.72, 120.50, 119.80, 119.43, 112.51, 110.67, 108.87; CIMS: *m/z* (MH') 373.3. Anal. (C=H16N204"0.2H20): calcd: C, 70.28; H, 4.40; N, 7.45. Found: C, 70.45; H, 4.58; N, 7.40%.

2'-Hydroxynaphthylacyl-(2, 5-dihydroxy- 1 -naphthylmethylene)hydrazide (4). A 74% yield; mp >280 °C; ~H NMR (DMSO-d6): 8 12.81 (s, 1 H), 12.23 (s, 1 H), 11.29 (s, 1 H), 10.22 (s, 1 H), 9.52 (s, 1 H), 8.52 (s, 1 H), 8.20 (d, 1 H, J=9.2 Hz), 7.59 (d, 1 H, *J=8.1* Hz), 7.80 (d, 1 H, J=8.2 Hz), 7.71 (d, 1 H, J=8.6 Hz), 7.54 (t, 1 H, J=7.5 Hz), 7.41 (m, 3 H), 7.16 (d, 1 H, J - 9 . 2 Hz), 6.80 (d, 1 H, J=7.5 Hz); 13C NMR (DMSO-d6) 8 163.04, 158.38, 154.10, 153.89, 148.09, 135.93, 133.39, 130.52, 128.66, 128.52, 128.32, 127.01, 126.78, 125.84, 123.85, 119.84, 118.93, 117.08, 111.40, 110.60, 108.29, 106.46; CIMS: *rn/z* (MH +) 373.2. Anal. (C22Ht6N204"0.5H20): calcd: C, 69.28; H, 4.49; N, 7.35. Found: C, 69.35; H, 4.54; N, 7.27%.

2',4'-Dihydroxyphenylacyl- (2-hydroxy-l-naphthylmethylene)hydrazide (5). A 81% yield; mp >280°C; ~H NMR (DMSO-d6): 8 12.83 (s, 1 H), 12.18 (br s, 1 H), 12.01 (br s, 1 H), 10.35 (br s, 1 H), 9.54 (s, 1 H), 8.32 (d, 1 H, J = 8.6 Hz), 7.88 (m, 3 H), 7.62 (t, 1 H, J= 7.6 Hz), 7.42 (t, 1 H, J = 7.4 Hz), 7.26 (d, 1 H, J=8.9 Hz), 6.47 (d, 1 H, J=8.8 Hz), 6.43 (s, 1 H); ~3C NMR

(DMSO-d6): 8 164.58, 162.94, 161.90, 158.02, 146.90, 132.72, 131.67, 129.96, 128.94, 127.80, 127.71, 123.54, 120.87, 178.92, 108.66, 107.78, 106.14, 102.93; CIMS: *m/z* (MH +) 323.1. Anal. (C18HI4N204): calcd: C, 67.08; H, 4.38; N, 8.69. Found: C, 67.04; H, 4.53; N, 8.91%.

2' - Hydroxy-4'- (4-nitrobenzyloxy) phenyacyl- (2,4-dihydroxy-l-naphthylmethylene)hydrazide (6). A 91% yield; mp >270 °C; 1H NMR (DMSO-d6): 8 12.82 (s, 1 H), 12.46 (br s, 1 H), 11.90 (br s, 1 H), 11.03 (br s, 1 H), 9.39 (s, 1 H), 8.25 (d, 1 H, J=8.1 Hz), 8.17 (d, 1 H, J=8.6 Hz), 8.10 (d, 1 H, J=8.3 Hz), 7.91 (d, 1 H, J=8.8 Hz), 7.71 (d, 1 H, J=8.2 Hz), 7.58 (t, 1 H, J = 7.6 Hz), 7.34 (t, 1 H, J= 7.5 Hz), 6.91 (d, 1 H, J= 8.8 Hz), 6.61 (s, 1 H), 6.60 (s, 1 H), 5.33 (s, 2 H); ~3C NMR (DMSO-d6): 8 164.23, 162.47, 162.10, 160.37, 157.62, 147.94, 147.07, 144.41, 132.92, 129.41, 128.27, 128.27, 123.66, 123.66, 122.93, 122.50, 120.67, 120.28, 107.75, 107.10, 102.39, 101.34, 100.46, 68.23; CIMS: *m/z* (MH +) 474.2. Anal. (C2sH19N307"2/3H20): calcd: C, 61.85; H, 4.12; N, 8.66. Found: C, 61.77; H, 4.33; N, 8.67%.

Biological assays

The previously published FACS assay protocol was followed for in vitro antimalarial testing. 24 Hypoxanthine uptake and enzyme (cruzain, cathepsin B and papain) inhibition procedures were also published previously?

Acknowledgments

This work was supported by grants from the Advanced Research Projects Agency (MDA-972-91-J1013; N00014-90-2032), the National Institute of Allergy and Infectious Disease (P01AI35707) and the World Health Organization (WHO 940104). The authors thank Margaret Brown from the Department of Veterans Affairs Medical Center, San Francisco, for excellent technical assistance.

References

1. Li, R.; Chen, X.; Gong, B.; Dominguez, J. N.; Davidson, E.; Kurzban, G.; Miller, R. E.; Nuzum, E. O.; Rosenthal, P. J.; McKerrow, J. H.; Kenyon, G. L.; Cohen, *F. E. J. Med. Chem.* 1995, *38,* 5031.
2. Li, Z.; Chen, X.; Davidson, E.; Zwang, O.; Mendis, C.; Ring, C. S.; Roush, W. R.; Fegley, G.; Li, R.; Rosenthal, P. J.; Lee, G. K.; Kenyon, G. L.; Kuntz, I. D.; Cohen, F. E. *Chem. Biol.* 1994, 1, 31.
3. Ring, C. S.; Sun, E.; McKerrow, J. H.; Lee, G.; Rosenthal, P. J.; Kuntz, I. D.; Cohen, F. E. *Proc. Natl Acad. Sci. U.S.A.* 1993, *90,* 3583.
4. yon ltzstein, M.; Wu, W.-Y.; Kok, G. B.; Pegg, M. S.; Dyason, J. C.; Jin, B.; Phan, T. V.; Smythe, M. L.; White, H. F.; Oliver, S. W.; Colman, P. M.; Vargheses, J. N.; Ryan, D. M.; Woods, J. M.; Bethell, R. C.; Hotham, V. J.; Cameron, J. M.; Penn, C. R. *Nature (London)* 1993, *363,* 418.
5. Lam, P. Y. S.; Jadhav, P. K.; Eyermann, C. J.; Hodge, C.

N.; Ru, Y.; Bacheler, L. T.; Meek, J. L.; Otto, M. J.; Rayner, M. M.; Wong, Y. N.; Chang, C.-H.; Weber, P. C.; Jackson, D. A.; Sharpe, T. R.; Erickson-Viitanen, S. *Science 1994, 263,* 380.
6. Shoichet, B. K.; Stroud, R. M.; Santi, D. V.; Kuntz, I. D.; Perry, K. M. *Science* 1993, *259,* 1445.
7. Montgomery, J. A.; Niwas, S.; Rose J. D.; Secrist, III, J. A.; Babu, Y. S.; Bugg, C. E.; Erion, M. D.; Guida, W. C.; Ealick, *S. E. J. Med. Chem.* 1993, *36,* 55.
8. Secrist, III, J. A.; Niwas, S.; Rose, J. D.; Babu, Y. S.; Bugg, C. E.; Erion, M. D.; Guida, W. C.; Ealick, S. E.; Montgomery, J. A. J. *Med. Chem.* 1993, *36,* 1847.
9. Erion, M. D.; Niwas, S.; Rose J. D.; Ananthan, S.; Allen, M.; Secrist, III, J. A.; Babu, Y. S.; Bugg, C. E.; Guida, W. C.; Ealick, S. E.; Montgomery, *J. A. J. Med. Chem.* 1993, *36,* 3771.
10. Guida, W. C.; Elliott, R. D.; Thomas, H. J.; Secrist, III, J. A.; Babu, Y. S.; Bugg, C. E.; Erion, M. D.; Ealick, S. E.; Montgomery, J. A. J. *Med. Chem. 1994, 37,* 1109.
11. Fesik, S. W.J. *Biomol. NMR* 1993,3, 261.
12. McGrath, M. E.; Eakin, A. E.; Engel, J. C.; McKerrow, J. H.; Craik, C. S.; Fletterick, *R. J. J. Mot Biol.* 1995, *247,* 251.
13. Chen, X.; Li, R.; Gong, B.; Davidson, E.; Dominguez, J. N.; McKerrow, J. H.; Kenyon, G. L.; Cohen, F. E. manuscript in preparation.
14. Stryer, L. *Biochemistry;* Freeman: New York, 1988.
15. Thomas, L.; Leduc, R.; Thorne, B. A.; Smeekens, S. P.; Steiner, D. F.; Thomas, G. *Proc. Natl. Acad. Sci. US,4.* 1991, *88,* 5297.
16. Cohen, R. L.; Xi, X. P.; Crowley, C. W.; Lucas, B. K.; Levinson, A. D.; Shuman, M. A. *Blood* 1991, *72,* 479.
17. McKerrow, J. H.; Sun, E.; Rosenthal, P. J.; Bouvier, J. *Annu. Rev. Microbiol.* 1993, *47,* 821.
18. Ring, C. S.; Cohen, F. E. *FASEB J.* 1993, 7, 783.
19. Gibbons, A. *Science* 1992, *256,* 1135.
20. Walsh, J.A. *Ann. N. Y. Acad. Sci.* 1989, *569, 1.*
21. World Health Organization Malaria Action Program. *Trans. R. Trop. Med. Hyg.* 1986, *80, 1.*
22. Kuntz, I. D. *Science* 1992, *257,* 1078; DOCK V 3.0 was used in all initial phases of this work. The current release is DOCK V 3.5. Contact I.D. Kuntz for distribution information.
23. Meng, E. C.; Gschwend, D. A.; Blaney, J. M.; Kuntz, I. *D. Proteins* 1993, *17,* 266.
24. Clark, D. L.; Chrisey, L. A.; Campbell, F. R.; Davidson, *E. A. Molec. Biochem. Parasitol.* 1994, 63, 129.
25. Oduola, A. M.; Weatherly, N. F.; Bowdre, J. H.; Desjardins, R. E. *In Vitro. Exp. Parasitol.* 1988, *66,* 86.
(Received in U.S~4. 3 October 1995)

Proc. Natl. Acad. Sci. USA
Vol. 90, pp. 3583–3587, April 1993
Biophysics

Structure-based inhibitor design by using protein models for the devel pment of antiparasitic agents

CHRISTINE S. RING*, EUGENE SUN†, JAMES H. MCKERROW*†‡, GARSON K. LEE†, PHILIP J. ROSENTHAL†, IRWIN D. KUNTZ*§, AND FRED E. COHEN*†§¶

*Departments of *Pharmaceutical Chemistry, §Biochemistry and Biophysics, ‡Pathology, and †Medicine, University of California, San Francisco, CA 94143-0446

Communicated by Seymour J. Klebanoff, December 24, 1992 (received for review October 30, 1992)

ABSTRACT **The lack of an experimentally determined structure of a target protein frequently limits the application of structure-based drug design methods. In an effort to overcome this limitation, we have investigated the use of computer model-built structures for the identification of previously unknown inhibitors of enzymes from two major protease families, serine and cysteine proteases. We have successfully used our model-built structures to identify computationally and to confirm experimentally the activity of nonpeptidic inhibitors directed against important enzymes in the schistosome [2-(4-methoxybenzoyl)-1-naphthoic acid, K_i = 3 μM] and malaria {oxalic bis[(2-hydroxy-1-naphthylmethylene)hydrazide], IC_{50} = 6 μM} parasite life cycles.**

Proteases are involved in many important biological processes including protein turnover, blood coagulation, complement activation (1), hormone processing (2), and cancer cell invasion (3). Thus, they are frequently chosen as targets for drug design and discovery. Noteworthy examples include the design of angiotensin-converting enzyme inhibitors for the treatment of hypertension (4) and programs to develop human immunodeficiency virus protease inhibitors to block proliferation of the AIDS virus (5). The critical role proteases play in the life cycle of parasitic organisms also makes them attractive drug-design targets for these infectious diseases (6).

In the most simple terms, structure-based drug design methods identify favorable and unfavorable interactions between a potential inhibitor and target receptor and maximize the beneficial interactions to increase binding affinity. Obtaining an accurate structure for the receptor or ligand–receptor complex is a logical step in this process. X-ray crystallography continues to be the source of high-resolution information about protein structures. However, considerable delays often exist between determining the sequence of a protein and solving its structure. Difficulties in protein expression and more commonly in protein crystallization can delay x-ray structure determination.

Currently, no general method exists for predicting tertiary structure from amino acid sequences. However, when a protein target is homologous to another protein or group of proteins of known structure, a sensible model structure can be proposed. Recent comparisons between model and crystal structures permit an assessment of the overall accuracy expected from homology model-built structures (7–9). For a sequence that is 80% identical to a protein of known structure, the expected rms deviation of the core residues is ≈0.6 Å (10). The expected rms deviation increases to 1.8 Å when the sequences are only 20% identical. However, model-built structures could still be useful in finding previously unknown lead compounds despite the uncertainties in the lower part of this range if the errors cluster far away from the enzyme active site.

The proteases targeted for inhibitor design in this study are important in establishing schistosome infection or necessary for the maintenance of malarial infection. Schistosomiasis is a snail-borne disease that is contracted by individuals who come into contact with the parasites in infested waters. Infectious larvae (cercariae) secrete an elastase to invade the skin of the human host and initiate infection. Once in the circulatory system, the schistosomes mature and reproduce. Thousands of eggs become trapped in the portal circulation of the liver, and the host immune response leads to portal hypertension. The protease that is implicated in skin penetration has been purified and characterized, and preliminary studies suggest that cutaneous application of an inhibitor of the cercarial elastase might prevent infection (11).

The increased incidence of drug-resistant strains of malaria (especially *Plasmodium falciparum*) necessitates the search for new therapies. Malaria infection includes an erythrocytic phase that is responsible for all the clinical manifestations of the disease (12). During this phase, erythrocytic trophozoites degrade hemoglobin as a principal source of amino acids. Rosenthal and coworkers (13, 14) have identified a critical cysteine protease that appears to be involved in the degradation of hemoglobin, the parasites' primary source of amino acids. Blocking this enzyme with cysteine protease inhibitors [L-*trans*-epoxysuccinylleucylamido-(4-guanidino)butane (E64), benzyloxycarbonyl-Phe-Arg-fluoromethyl ketone] in culture arrests further growth and development (15). Thus, this enzyme is a promising target for new modes of antimalarial chemotherapy.

METHODS

Model Construction. Three-dimensional models of the structures of cercarial elastase and trophozoite cysteine protease were built following the approach of Blundell and coworkers (16, 17). Seven mammalian serine proteases, bovine chymotrypsin (18), porcine pancreatic elastase (19), rat mast cell protease (20), human neutrophil elastase (21), rat tonin (22), porcine kallikrein (23), and bovine trypsin (24), were used to derive a structural alignment for cercarial elastase (25). Papain (26) and actinidin (27) were used for trophozoite cysteine protease. The conformations of side chains were retained when possible, and the statistically most likely rotamer was selected when no conformational information was available (17). Loops were placed by using a combination of the loop dictionary and key residue approaches (28, 29). The resulting models were refined by

The publication costs of this article were defrayed in part by page charge payment. This article must therefore be hereby marked "*advertisement*" in accordance with 18 U.S.C. §1734 solely to indicate this fact.

Abbreviations: P1 and S1, amino acid residues on the acyl side of the scissile bond are denoted P1, P2, . . . P*n*, and those on the leaving group side of the scissile bond are denoted as P1′, P2′, . . . P*n*′; corresponding binding sites on the enzyme are S1, S2, . . . S*n* and S1′, S2′, . . . S*n*′.

¶To whom reprint requests should be addressed.

energy minimization with the AMBER potential function (30). Models were validated with several computational strategies, including QPACK to probe side-chain volume (31), the profile method of Luthy *et al.* (32), a Ramachandran map analysis of backbone geometry, and solvent-accessibility calculations (33).

Screening the Fine Chemicals Directory Using DOCK3.0. The two protease model structures were used as receptors for ligand docking. DOCK3.0 is an automatic method to screen small-molecule data bases for ligands that could bind to a given receptor (34). DOCK3.0 characterizes the grooves and invaginations of the active site with sets of overlapping spheres. The generated sphere centers constitute an irregular grid that can be matched with the atom centers of a potential ligand. The quality of fit of a ligand to the binding site is judged either by shape complementarity or by a simplified molecular mechanics force-field energy (estimated interaction energy).

DOCK 3.0 was used to search the Fine Chemicals Directory (Molecular Design Limited, San Leandro, CA) of 55,313 commercially available small molecules. The structures of the small molecules were obtained computationally by using a heuristic algorithm, CONCORD, developed by R. Pearlman at the University of Texas. CONCORD-generated structures are estimated to be ≈90% in agreement with those structures optimized by molecular mechanics calculations (35). The Fine Chemicals Directory was chosen over the Cambridge Structural Database of experimentally determined structures because of the ease with which interesting compounds could be obtained.

In a typical DOCK search, the top-scoring 100–200 molecules are examined with 10–50 of these selected for experimental testing (36). Because model protein structures were used instead of crystallographically determined structures, an arbitrarily large number of small molecules were saved. For each enzyme system, the 2200 molecules with the best shape-complementarity scores and the 2200 with the best force-field scores were saved. The resulting 8800 compounds were visually screened in the context of the active site by using the molecular display software MIDASPLUS (37).

Because of the uncertainties inherent in model-built structures, the scores generated by DOCK3.0 did not influence the visual screening process. Instead, compounds were judged solely on how they might interact with the active site in the putative ligand–receptor complex. In an effort to be self-consistent, the resulting 8800 compounds were screened three times. No compounds were selected during the first screening in an attempt to get acquainted with the systems. During the second and third passes, compounds that filled the site and had potential hydrogen-bonding and electrostatic interactions were selected for further inspection. Only compounds that were chosen on both the second and third screenings were considered further. From this list, an effort was made to choose compounds that were chemically diverse and that appeared to interact with the receptor in different ways. Fifty-two compounds were ultimately chosen for testing against the cercarial elastase, and 31 compounds were chosen for testing against the trophozoite cysteine protease. This screening process took ≈1 week of effort. As the enzyme-active sites became more familiar with each successive pass, the time needed to examine the ligand–receptor complex shortened.

Of the 52 compounds selected for the cercarial elastase, 33 compounds were from the force-field list, 10 compounds were from the shape list, and 9 compounds appeared on both lists. Of the 31 compounds selected for the malarial protease, 20 compounds were from the shape list, and 11 compounds were from the force-field list. These compounds were ranked as high as 4th and as low as 1939th (out of 2200) by the scores generated by DOCK3.0.

K_i Determination for the Inhibitors Against Cercarial Elastase, Chymotrypsin, and Elastase. Cercarial elastase was purified as described (38). Initial reaction velocities were determined at room temperature for each enzyme by using tetrapeptide thiobenzyl ester substrates in the presence of 20 μM 4,4'-dithiopyridine and following the absorbance at 324 nM for 1 min after enzyme addition (39). Enzyme concentrations were determined by active-site titration with chloromethyl ketone inhibitors, and used at 1/100th of the lowest substrate concentration. The reaction buffer was 100 mM glycine-NaOH, pH 9.0/2 mM $CaCl_2$. The specific substrates used were *N*-succinylalanylalanylprolylphenylalanyl thiobenzyl ester for cercarial elastase and chymotrypsin, and *N*-succinylalanylalanylprolylalanyl thiobenzyl ester for pancreatic elastase at concentrations from 25 to 500 μM. Inhibitors were prepared as 100 mM stock solutions in dimethyl sulfoxide and used at concentrations from 0 to 100 μM. Reaction velocities were determined in triplicate for each point and plotted by using the method of Dixon. Data were also plotted using the Hanes transformation of the Michaelis–Menten equation to ascertain the competitive nature of inhibition. K_i was determined directly from the Dixon plot (40) and confirmed by replots of K_m^{app}/V^{app} from the Hanes plot (41).

The Trophozolte Cysteine Protease Inhibitor Studies. Enzyme activity was measured with the fluorogenic substrate benzyloxycarbonyl-Phe-Arg-(7-amino-4-methylcoumarin) as described (15). Trophozoite extracts were incubated with reaction buffer (in 0.1 M sodium acetate/10 mM dithiothreitol, pH 5.5) and an appropriate concentration of inhibitor for 30 min at room temperature. Benzyloxycarbonyl-Phe-Arg-(7-amino-4-methylcoumarin) (50 μM final concentration) was then added, and fluorescence (380 nM excitation, 460 nM absorbance) was measured continuously over 30 sec. The slope of fluorescence over time for each inhibitor concentration was compared with that of controls in multiple assays,

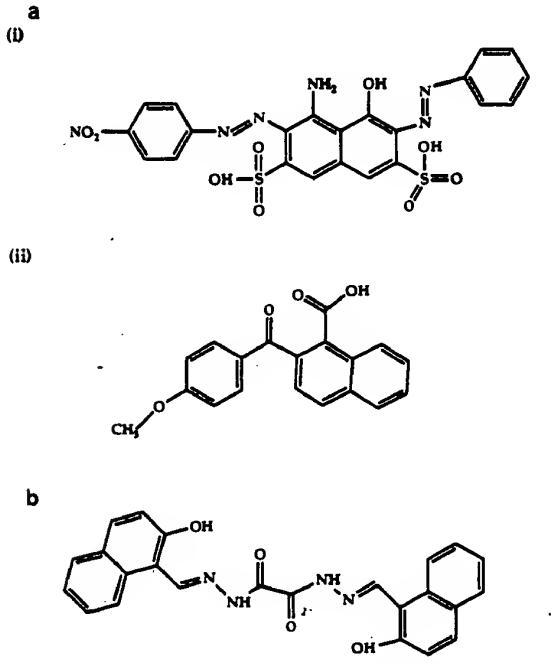

FIG. 1. (*a*) (*i*) Naphthol blue-black. (*ii*) 2-(4-Methoxybenzoyl)-1-naphthoic acid. (*b*) Oxalic bis[(2-hydroxy-1-naphthylmethylene)hydrazide].

Table 1. K_i values for compounds that inhibit cercarial elastase

Inhibitor	Cercarial elastase, K_i	Chymotrypsin, K_i	Pancreatic elastase, K_i
Naphthol blue-black	6 μM	6 μM	200 μM
2-(4-Methoxybenzoyl)-1-naphthoic acid	3 μM	30 μM	146 μM

and the IC_{50} was determined from plots of percent control activity over inhibitor concentration.

Effect of Oxalic Bis[(2-hydroxy-1-naphthylmethylene)hydrazide] on [^{3}H]Hypoxanthine Uptake as a Measure of Parasite Metabolism. [^{3}H]Hypoxanthine uptake was measured based on a modification of the method of Desjardins *et al.* (42). Microwell cultures of synchronized ring stage *P. falciparum* parasites were incubated with inhibitor in dimethyl sulfoxide (10% final concentration) for 4 hr. [^{3}H]Hypoxanthine was added (1 μCi per microwell culture; 1 Ci = 37 GBq), and the cultures were maintained for an additional 36 hr. The cells were then harvested and deposited onto glass-fiber filters that were washed and dried with ethanol. [^{3}H]Hypoxanthine uptake was quantitated by scintillation counting. The uptake at each inhibitor concentration was compared with that of controls, and the IC_{50} value was determined from plots of percent control uptake over inhibitor concentration.

RESULTS AND DISCUSSION

Nonpeptidic inhibitors were identified for both the cercarial elastase and the malarial cysteine protease. Approximately 10% of the compounds tested, 5 of 52 for the cercarial elastase and 4 of 31 for the malarial protease, displayed activity against the enzymes at concentrations <100 μM. Among these, three compounds were inhibitors at concentrations <10 μM (Fig. 1). 2-(4-Methoxybenzoyl)-1-naphthoic acid and naphthol blue-black inhibited the cercarial elastase with K_i values of 3 and 6 μM, respectively (Table 1 and Fig. 2). These two compounds also displayed specificity for the cercarial elastase, as evidenced by the generally higher K_i values against chymotrypsin and pancreatic elastase (Table 1). Because the S1 specificity pocket of cercarial elastase is more similar to chymotrypsin than to pancreatic elastase, it is not surprising that both 2-(4-methoxybenzoyl)-1-naphthoic acid and naphthol blue-black are also good inhibitors of chymotrypsin. (Note that the amino acid residues on the acyl side of the scissile bond are denoted P1, P2, . . . P*n*, and those on the leaving group side of the scissile bond are denoted as P1', P2', . . . P*n*'. The corresponding binding sites on the enzyme are S1, S2, . . . S*n* and S1', S2', . . . S*n*'.) Presumably, the application of standard medicinal chemistry strategies to these lead compounds will yield more potent and selective inhibitors of the schistosome enzyme. Topical application of peptide-based inhibitors has already been demonstrated to block parasite migration through the skin (11).

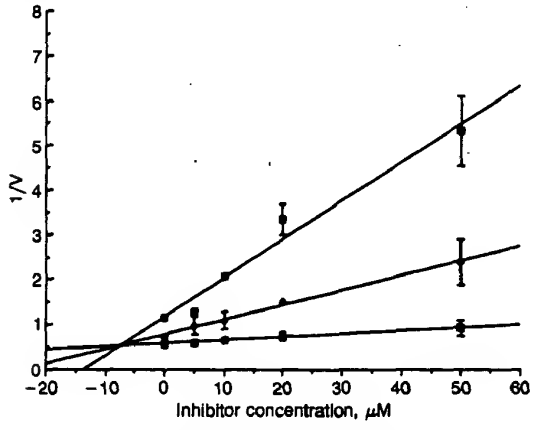

FIG. 2. Representative K_i determination using the Dixon plot. In this example, the K_i is determined for naphthol blue-black against cercarial elastase. Each point was determined in triplicate. Each line represents a different substrate concentration (■, 500 μM; ◆, 200 μM; □, 50 μM). Some error bars are too small to be graphed on this plot. V, velocity.

Oxalic bis[(2-hydroxy-1-naphthylmethylene)hydrazide] inhibited the trophozoite cysteine protease with an IC_{50} of 6 μM (Fig. 3*a*). When tested against cultured *P. falciparum*, this compound also inhibited the incorporation of hypoxanthine, a standard marker of parasite metabolism, at approximately the same concentration (Fig. 3*b*). Because this compound can inhibit the protease and the parasite, efforts are underway to synthesize analogs of oxalic bis[(2-hydroxy-1-naphthylmethylene)hydrazide] and examine their therapeutic potential.

The visual screening process was reexamined for the most active compounds in an attempt to find the relevant factors responsible for their selection. An interesting dichotomy was observed in the DOCK shape-based and force-field scores. All

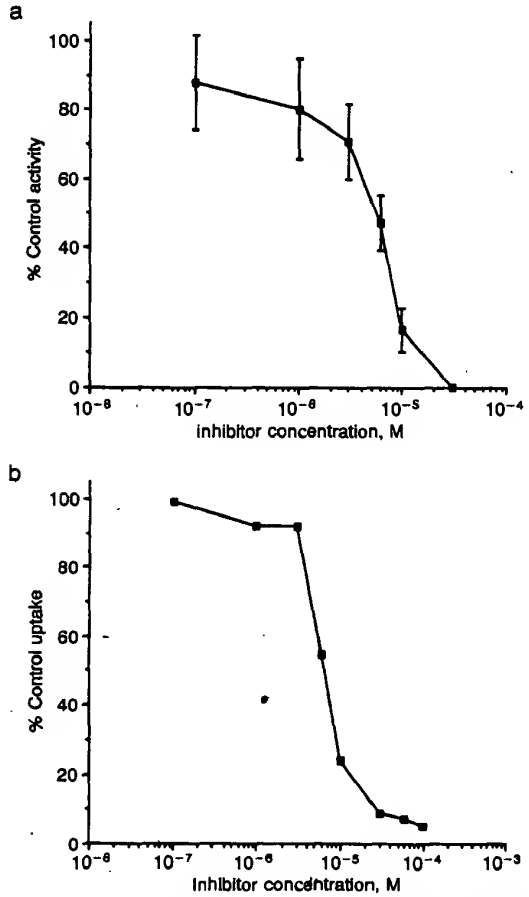

FIG. 3. (*a*) IC_{50} curve for oxalic bis[(2-hydroxy-1-naphthylmethylene)hydrazide] against malarial cysteine protease. The points are the means of eight assays, and the error bars are the SDs of the samples. (*b*) Inhibition of parasite uptake of [^{3}H]hypoxanthine by oxalic bis[(2-hydroxy-1-naphthylmethylene)hydrazide].

but one of the five inhibitors of the cercarial elastase were members of the force list with the following rankings: 85th, 2-(4-methoxybenzoyl)-1-naphthoic acid; 122nd, plasmocorinth B; 627th, naphthol blue-black; and 918th, α-phenethylphthalamic acid. The fifth compound, 9-fluorenone-4-carboxylic acid, appeared on both lists, ranking 561st on the force-field list and 1783rd on the shape-based list. The two best cercarial elastase inhibitors, 2-(4-methoxybenzoyl)-1-naphthoic acid and naphthol blue-black, ranked 85th and 627th, respectively, on the force-field list. By contrast, all four of the malarial protease inhibitors were members of the shape-based list, ranking as follows: 7th, 3,3′-diethyloxatricarbocyanine iodide; 13th, oxalic bis[(2-hydroxy-1-naphthylmethylene)hydrazide]; 793rd, cephaloglycin; and 1193rd, 1-(2-methoxyphenyl)-6-(4-trifluoromethylphenyl)-5-thiobiurea. The best inhibitor, oxalic bis[(2-hydroxy-1-naphthylmethylene)hydrazide], ranked 13th. These results may reflect the environmental differences in the active site. The active site of the malarial protease consists of a large hydrophobic cleft. Because of the absence of charged residues in the vicinity of the putative binding site, the shape-based scores for hydrophobic ligands that fill the site may adequately estimate the enthalpy of interaction between ligand and receptor. By contrast, the active site of the cercarial elastase contains both a hydrophobic S1 pocket and charged amino acids in the vicinity of the active site. Consequently, the force-field scores, which include both van der Waals and electrostatic components, better estimate the interaction energy of the ligands with the active site of the cercarial elastase.

The DOCK-generated enzyme–inhibitor complex structures for naphthol blue-black and oxalic bis[(2-hydroxy-1-naphthylmethylene)hydrazide] are shown in Fig. 4. Naphthol blue-black fits into the groove defined by the S1, S2, and S3 subsites of the cercarial elastase. In the model complex, ligand binding is stabilized by the interaction of a phenyl group with the hydrophobic S1 pocket. The sulfonic acid groups could hydrogen-bond with arginines in a nearby loop or possibly with the solvent. Similarly, oxalic bis[(2-hydroxy-1-naphthylmethylene)hydrazide] interacts with S2 and S1′ sites of the malarial protease. The hydrophobic specificity site, S2, is filled by a naphthol group. The other naphthol group participates in a stacking interaction with the indole ring of Trp-177 at the S1′ site. In addition, each hydroxyl group on the naphthol rings appears to hydrogen-bond to Ser-160 at S2 and Gln-19 at S1′. These complexes are useful starting points for modeling ligand–receptor interactions, but other possible binding modes should also be considered.

At micromolar concentrations, it is likely that the inhibitors will have multiple modes of binding to the enzyme. Because these different binding modes are approximately isoenergetic, discriminating among the plausible alternatives with current scoring functions is difficult. Assumptions, such as rigid ligands and rigid receptors, are necessary for computational tractability but are also presumably responsible for the loss of resolution in these scores. The x-ray structures of thymidylate synthase complexed with two different inhibitors that were

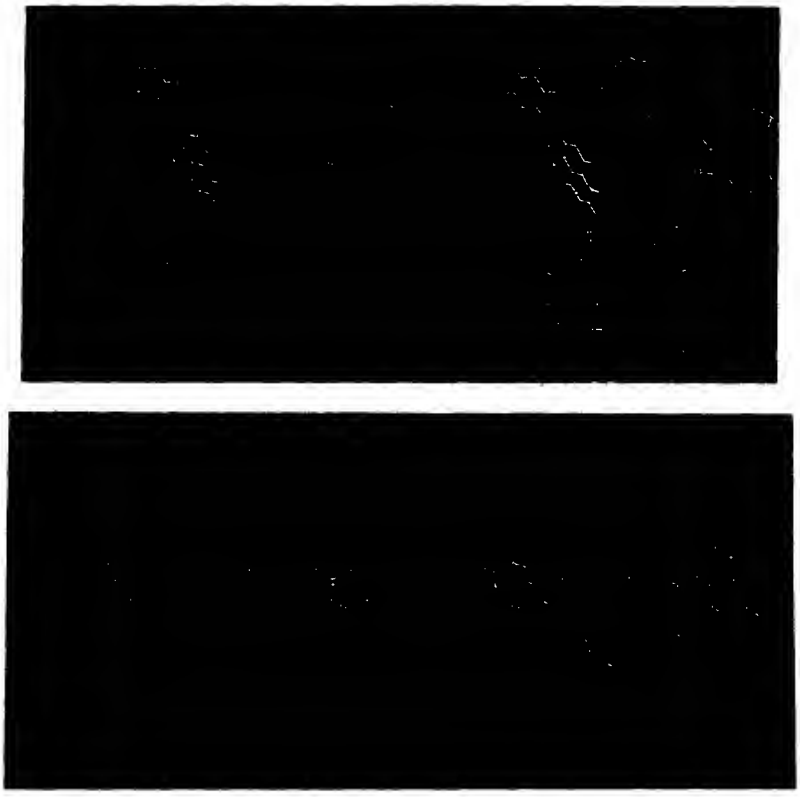

FIG. 4. (*Upper*) Stereo image of naphthol blue-black docked into the active site of cercarial elastase. (*Lower*) Stereo image of oxalic bis[(2-hydroxy-1-naphthylmethylene)hydrazide] docked into the active site of trophozoite cysteine protease. Catalytic residues are colored purple and labeled for orientation. The atoms on the inhibitors are color-coded: carbons are white, oxygens are red, nitrogens are blue, and sulfurs are cyan.

suggested by DOCK illustrate the challenges presented in accurately predicting the ligand–receptor complexes (43). For sulisobenzone, the failure to anticipate the binding of a counterion in the binding site led to an inaccurate prediction of the complex. In the case of phenolphthalein, a conformational change by an arginine between unbound and bound states of the enzyme and the presence of two waters in the bound state led to a slightly different conformation of the ligand than the one anticipated by DOCK (43). These examples highlight the importance of crystallography to the structure–based drug-design process. Ligand-induced conformational changes and the presence of bound waters and counterions are details that may be necessary for successful lead optimization.

The quality of the model structure is directly related to the percentage sequence identity between the relevant sequences. The trophozoite cysteine protease is ≈33% identical to both papain and actinidin, and the cercarial elastase is 20–25% identical to the seven mammalian serine proteases of known structure. Thus, we anticipate errors of 1–3 Å rms deviation in the model atomic coordinates, although errors in the vicinity of the active site are probably substantially smaller, reflecting selective sequence conservation. Two explanations of the success of our modeling/docking approach are plausible. (*i*) The modeling errors in the active site are small, and the major determinants of molecular recognition are faithfully recreated. (*ii*) Alternatively, the modeling process was irrelevant, and a homologous structure could have been substituted for computational ligand-binding studies to identify lead compounds. To address the latter possibility, two homologous serine proteases, chymotrypsin and trypsin, were used as receptors for ligand docking. Chymotrypsin was chosen because it shares with cercarial elastase a similar P1 specificity for hydrophobic residues. Trypsin was chosen because its S1 pocket is sterically similar, despite its different peptide specificity. With the same method, DOCK3.0 was used to search the Fine Chemicals Directory, and the top 2200 shape-complementarity scoring compounds and the top 2200 force-field scoring compounds were saved.

The best two inhibitors of the cercarial elastase were not included in either list of 4400 compounds predicted to inhibit chymotrypsin or trypsin, although each shape-based list included one of the less effective inhibitors. Due to unfavorable interactions seen in the model of 9-fluorenone-4-carboxylic acid docked to chymotrypsin (negative charge in hydrophobic S1 pocket), this compound would have been rejected during the visual-screening evaluation. Consequently, none of the five inhibitors identified for the cercarial elastase would have been found in a DOCK3.0 search by using the chymotrypsin active site, and only one of the 100 μM inhibitors, α-phenethylphthalamic acid, would have been found by using the trypsin active site. Although we cannot rule out finding other low-micromolar inhibitors from the lists of compounds generated by the chymotrypsin and trypsin searches, our results indicate that the modeling process was not irrelevant and that this method for inhibitor discovery is sensitive enough to differentiate between similar active sites in homologous structures.

Despite the inherent limitations of computer model-built structures, these structures are helpful in finding nonpeptidic inhibitors active at low-micromolar concentrations. Although these compounds are far from being drugs, they are sensible starting points for the process of drug development. Because these enzymes are members of two major protease families, our work suggests that computer models and structure-based drug-design methods can be applied to identify inhibitors of proteases that are relevant to other pathophysiologic processes.

We thank Elaine Meng and Cynthia Corwin for helpful suggestions and discussions and K. C. Lim for technical assistance. This work was supported by grants from the Defense Advanced Research Projects Agency (MDA-972-91-J1013 to F.E.C.) and the National Institutes of Health (GM07175 to C.S.R.; AI20452 to J.H.M.; F32AI08311 to E.S.; AI00870 to P.J.R.).

1. Stryer, L. (1988) *Biochemistry* (Freeman, New York).
2. Thomas, L., Leduc, R., Thorne, B. A., Smeekens, S. P., Steiner, D. F. & Thomas, G. (1991) *Proc. Natl. Acad. Sci. USA* **82**, 5297–5301.
3. Cohen, R. L., Xi, X. P., Crowley, C. W., Lucas, B. K., Levinson, A. D. & Shuman, M. A. (1991) *Blood* **72**, 479–487.
4. Navia, M. A. & Murcko, M. A. (1992) *Curr. Opin. Struct. Biol.* **2**, 202–210.
5. DesJarlais, R. L., Seibel, G. L., Kuntz, I. D., Furth, P. S., Alvarez, J. C., Ortiz de Montellano, P. R., DeCamp, D. L., Babe, L. M. & Craik, C. S. (1990) *Proc. Natl. Acad. Sci. USA* **87**, 6644–6648.
6. McKerrow, J. H. (1989) *Exp. Parasitol.* **68**, 111–115.
7. Read, R. J., Brayer, G. D., Jurasek, L. & James, M. N. G. (1984) *Biochemistry* **23**, 6570–6575.
8. Zuiderweg, E. R. P., Henkin, J., Mollison, K. W., Carter, G. W. & Greer, J. (1988) *Proteins* **3**, 139–145.
9. Weber, I. T. (1990) *Proteins* **7**, 172–184.
10. Chothia, C. & Lesk, A. M. (1986) *EMBO J.* **5**, 823–826.
11. Cohen, F. E., Gregoret, L. M., Amiri, P., Aldape, K., Railey, J. & McKerrow, J. H. (1991) *Biochemistry* **30**, 11221–11229.
12. Bruce-Chwatt, L. J. (1985) *Essential Malariology* (Wiley, New York).
13. Rosenthal, P. J., McKerrow, J. H., Aikawa, M., Nagasawa, H. & Leech, J. H. (1988) *J. Clin. Invest.* **82**, 1560–1566.
14. Rosenthal, P. J. & Nelson, R. G. (1992) *Mol. Biochem. Parasitol.* **51**, 143–152.
15. Rosenthal, P. J., McKerrow, J. H., Rasnick, D. & Leech, J. H. (1989) *Mol. Biochem. Parasitol.* **35**, 177–183.
16. Sutcliffe, M. J., Haneef, I., Carney, D. & Blundell, T. L. (1987) *Protein Eng.* **1**, 377–384.
17. Sutcliffe, M. J., Hayes, F. R. F. & Blundell, T. L. (1987) *Protein Eng.* **1**, 385–392.
18. Tsukada, H. & Blow, D. M. (1985) *J. Mol. Biol.* **184**, 703–711.
19. Meyer, E., Cole, G., Radhakrishnan, R. & Epp, O. (1988) *Acta Crystallogr.* **44**, 26–38.
20. Remington, S. J., Woodbury, R. G., Reynolds, R. A., Matthews, B. W. & Neurath, H. (1988) *Biochemistry* **27**, 8097–8105.
21. Navia, M. A., McKeever, B. M., Springer, J. P., Lin, T. Y., Williams, H. R., Fluder, E. M., Dorn, C. P. & Hoogsteen, K. (1989) *Proc. Natl. Acad. Sci. USA* **86**, 7–11.
22. Fujinaga, M. & James, M. N. G. (1987) *J. Mol. Biol.* **195**, 373–396.
23. Bode, W., Chen, Z., Bartels, K., Kutzbach, C., Schmidt, G. & Bartunik, H. (1983) *J. Mol. Biol.* **164**, 237–282.
24. Walter, J., Steigemann, W., Singh, T. P., Bartunik, H., Bode, W. & Huber, R. (1982) *Acta Crystallogr.* **38**, 1462–1472.
25. Greer, J. (1990) *Proteins* **7**, 317–334.
26. Kamphuis, I. G., Kalk, K. H., Swarte, M. B. A. & Drenth, J. (1984) *J. Mol. Biol.* **179**, 233–256.
27. Baker, E. N. & Dodson, E. J. (1980) *Acta Crystallogr.* **36**, 559–572.
28. Jones, T. A. & Thirup, S. (1986) *EMBO J.* **5**, 819–822.
29. Chothia, C. & Lesk, A. M. (1987) *J. Mol. Biol.* **196**, 901–917.
30. Singh, U. C., Weiner, P. K., Caldwell, J. W. & Kollman, P. A. (1986) AMBER (Dept. of Pharmaceutical Chemistry, Univ. of California, San Francisco), Version 3.0.
31. Gregoret, L. M. & Cohen, F. E. (1990) *J. Mol. Biol.* **211**, 959–974.
32. Luthy, R., Bowie, J. U. & Eisenberg, D. (1992) *Nature (London)* **356**, 83–85.
33. Chothia, C. (1976) *J. Mol. Biol.* **105**, 1–14.
34. Meng, E. C., Stoichet, B. M. & Kuntz, I. D. (1992) *J. Comp. Chem.* **13**, 505–524.
35. Rusinko, A., Sheriden, R. P., Nilakantan, R., Haraki, K. S., Bauman, N. & Venkataraghavan, R. (1989) *J. Chem. Inf. Comput. Sci.* **29**, 251–255.
36. Kuntz, I. D. (1992) *Science* **257**, 1078–1082.
37. Ferrin, T., Huang, C., Jarvis, L. & Langridge, R. (1988) *J. Mol. Graphics* **6**, 13–37.
38. McKerrow, J. H., Pino-Heiss, S., Lindquist, R. & Werb, Z. (1985) *J. Biol. Chem.* **260**, 3703–3707.
39. Grassetti, D. R. & Murray, J. F. (1967) *Arch. Biochem. Biophys.* **119**, 41–49.
40. Dixon, M. (1953) *Biochem. J.* **55**, 170–171.
41. Hanes, C. S. (1932) *Biochem. J.* **26**, 1406–1421.
42. Desjardins, R. E., Canfield, C. J., Haynes, J. D. & Chulay, J. D. (1979) *Antimicrob. Agents Chemother.* **16**, 710–718.
43. Shoichet, B. K., Stroud, R. M., Santi, D. V., Kuntz, I. D. & Perry, K. M. (1993) *Science*, in press.

Journal of Computer-Aided Molecular Design, **16**: 11–26, 2002.
KLUWER/ESCOM

Further development and validation of empirical scoring functions for structure-based binding affinity prediction

Renxiao Wang[a], Luhua Lai[b] & Shaomeng Wang[a,*]
[a]*Medical Chemistry and Comprehensive Cancer Center, University of Michigan, 1500 E. Medical Center Drive, Ann Arbor, MI 48109-0934, U.S.A.;* [b]*Institute of Physical Chemistry, Peking University, Beijing 100871, P.R. China*

Received 27 August 2001; Accepted 7 February 2002

Key words: binding affinity prediction, consensus scoring, empirical scoring molecular docking, structure-based drug design

Summary

New empirical scoring functions have been developed to estimate the binding affinity of a given protein-ligand complex with known three-dimensional structure. These scoring functions include terms accounting for van der Waals interaction, hydrogen bonding, deformation penalty, and hydrophobic effect. A special feature is that three different algorithms have been implemented to calculate the hydrophobic effect term, which results in three parallel scoring functions. All three scoring functions are calibrated through multivariate regression analysis of a set of 200 protein-ligand complexes and they reproduce the binding free energies of the entire training set with standard deviations of 2.2 kcal/mol, 2.1 kcal/mol, and 2.0 kcal/mol, respectively. These three scoring functions are further combined into a consensus scoring function, X-CSCORE. When tested on an independent set of 30 protein-ligand complexes, X-CSCORE is able to predict their binding free energies with a standard deviation of 2.2 kcal/mol. The potential application of X-CSCORE to molecular docking is also investigated. Our results show that this consensus scoring function improves the docking accuracy considerably when compared to the conventional force field computation used for molecular docking.

Introduction

Considerable advances in structure-based drug design have made a significant impact on drug discovery processes in the past decade [1–5]. By utilizing the essential structural properties of the target macromolecule, a variety of methods now exist for suggesting potential ligand molecules either by screening large chemical databases [6–10] or by assembling molecular fragments inside the binding site [11–18]. These methods usually suggest a large number of molecules rapidly, far too many for organic synthesis and biological experiments. Therefore, a structure-based drug design approach tends to arrive at the bottleneck where it is necessary to select only the most promising candidates for further experimental characterization. The basic assumption underlying structure-based drug design is that a good ligand molecule should bind tightly to its target. Thus, it is extremely valuable to predict the binding affinity of a given ligand to its target and use it as a criterion for selection. This is known as the 'scoring problem' and has attracted great interests in developing methods for binding affinity calculation [19–21].

A large group of methods calculate binding affinities through force fields. In early years, attempts have been made to calculate the direct interactions, e.g. steric and electrostatic interactions, between a ligand and its target molecule and relate the force field energies to binding affinities [22]. This method is still popular nowadays especially among molecular docking studies. However, as many researchers have pointed out, the interaction energy computed in this

*To whom correspondence should be addressed. E-mail: shaomeng@med.umich.edu

way is only an approximation to the enthalpy change in the binding process, therefore the application of this method is usually restricted to the analysis of a congeneric series of ligands. Some researchers have supplemented standard force fields with an additional term to address the solvation effect with either PB/SA or GB/SA method [23]. More ambitious methods, such as free energy perturbation [24] and linear response approximation [25, 26], try to consider solvent molecules explicitly and deal with ensemble averages. In theory these methods are expected to give more accurate predictions. However, in practice they do not always meet this expectation due to the deficiency in the force field as well as in the sampling procedure. In addition, these methods are still computationally expensive even for today's computers, which has limited their popularity in structure-based drug design practice.

Following the pioneering work of Böhm [27], a number of so-called empirical scoring functions have emerged as an alternative [28–32]. These approaches assume that the overall receptor-ligand binding free energy can be decomposed into basic components, which can be written out conceptually as:

$$\Delta G_{\text{bind}} = \Delta G_{\text{motion}} + \Delta G_{\text{interaction}} + \Delta G_{\text{desolvation}} + \Delta G_{\text{configuration}}.$$

Usually those factors which are known to be important for the binding process are included in the above function. Unlike force fields, empirical scoring functions are not derived from 'first principle'. Instead, they are directly calibrated with a set of protein-ligand complexes with experimentally determined structures and binding affinities through multivariate regression analysis. Empirical scoring functions have several appealing features. Firstly, since they are calibrated with diverse protein-ligand complexes, their applications are not limited to a certain congeneric series of ligands or a particular target receptor. Secondly, each term in an empirical scoring function has a clear physical meaning. Studying the regression coefficients before each term sheds lights on the understanding of the receptor-ligand binding process. Thirdly, at a lightning speed, the accuracy level (~2 kcal/mol) that a current empirical scoring function can achieve in binding affinity prediction is acceptable for structure-based drug design approaches. In recent years, empirical scoring functions have become more and more popular among structure-based drug design applications in which very accurate binding affinity predictions are not necessary, such as virtual database screening and *de novo* ligand generation.

We have extensive experience in applying several empirical scoring functions, including Bohm's scoring function [27], ChemScore [30] and SCORE [32], to structure-based drug design projects. Despite of all the encouraging results we have obtained with these empirical scoring functions, it is clear that there is still plenty of room for improvement in terms of accuracy as well as robustness. In this paper, we will describe our work on further development and validation of empirical scoring functions. Firstly, we have derived three scoring functions, each of which has only five adjustable parameters. These scoring functions are calibrated with a diverse set of 200 protein-ligand complexes, which is the largest one ever used by an empirical scoring function approach. Secondly, inspired by the consensus scoring strategy [33], we combine these three scoring functions into a consensus scoring function, X-CSCORE, to ensure converged results in binding affinity prediction. This consensus scoring function is tested on an independent set of 30 protein-ligand complexes. Thirdly, we have also explored the potential application of X-CSCORE to molecular docking. When compared to conventional force field computation, this consensus scoring function performs considerably better in identifying the experimentally determined protein-ligand complex structures.

Methods and results

Training set construction

Developing an empirical scoring function requires a set of receptor-ligand complexes for calibration. Both the size and the quality of the training set will affect the final form of the scoring function. In our selection of receptor-ligand complexes, we used the following five criteria to ensure the quality of the training set. (1) Only protein-ligand complexes are considered. Complexes involving other types of receptors, such as nucleic acids, are not included. (2) The ligand molecule should be a 'normal' organic compound and bind to the receptor non-covalently. Therefore, complexes containing covalently bound ligands, complex ligands (such as Heme), or large ligands (MW > 1000) are excluded. (3) There should be no cofactor binding beside the ligand. (4) Crystal structure of the complex with a resolution better than 3.0 Å should be available from the Protein Data Bank (PDB) [34]. Complex

structures solved by NMR techniques are currently not included in our selection. (5) The dissociation equilibrium constant (K_i or K_d) of the complex has been determined experimentally and can be found in literature. Complexes with only IC_{50} values are not accepted.

The resulting training set has 200 protein-ligand complexes, which comprises more than 70 different types of proteins. Basically, this training set is an assembly of the training sets used by other empirical scoring functions [27–32] plus our own collections. The experimentally determined binding affinities are cited either from those previous approaches or the references listed in the relevant PDB files. All binding affinities are expressed in the negative logarithms of dissociation constants, i.e. pK_d, for convenience. In this training set, the pK_d values range from 1.48 to 11.42, covering nearly 10 orders of magnitude. Here we neglect the potential inconsistence in the dissociation constants related to experiment conditions, such as PH level, temperature, and salt concentration. A complete list of the training set can be found in the *supplementary material* section in this paper.

Coordinates of the complex structure in the training set are downloaded from PDB. No minimization is performed to further adjust the structure. For the convenience of processing, each complex structure is processed in SYBYL [35]. First, the ligand is extracted from the complex, assigned proper atom and bond types, and then written out as a separate file in the MOL2 format. The remaining part of the complex, i.e. the protein, is written out into another file in the PDB format. Metal ions located inside the binding site are left with the protein and treated as part of it. All crystallographic water molecules and other cofactors are removed.

Scoring functions

We assume that the overall free energy change in a protein-ligand binding process can be dissected into the following terms:

$$\Delta G_{bind} = \Delta G_{vdw} + \Delta G_{H\text{-}bond} + \Delta G_{deformation} + \Delta G_{hydrophobic} + \Delta G_0 \quad (1)$$

Here, ΔG_{vdw} accounts for the van der Waals interaction between the ligand and the protein; $\Delta G_{H\text{-}bond}$ accounts for the hydrogen bonding between the ligand and the protein; $\Delta G_{deformation}$ accounts for the deformation effect; $\Delta G_{hydrophobic}$ accounts for the hydrophobic effect; ΔG_0 is the regression constant which implicitly includes the effects due to the translational and rotational entropy loss in the binding process. Detailed algorithms for calculating each term will be described below.

(1) Atom classification. Besides element type and hybridization state, both ligand and protein atoms need to be classified to compute some of the terms in our scoring functions. The atom types defined in our study are: (i) H-bond donor. Oxygen and nitrogen atoms bonded to hydrogen atom(s) and metal ions located inside the binding site of the protein. (ii) H-bond acceptor. Oxygen and sp^2 or sp hybridized nitrogen atoms with lone pair(s). (iii) H-bond donor/acceptor. Oxygen and nitrogen atoms which may act as either H-bond donor or H-bond acceptor, such as the oxygen atom in a hydroxyl group. (iv) Polar atom. Oxygen and nitrogen atoms that are neither H-bond donor nor H-bond acceptor, sulfur and phosphorus atoms, and carbon atoms bonded to hetero-atom(s). (v) Hydrophobic atom. Carbon atoms that do not belong to the 'polar atom' group and halogen atoms.

The following set of atomic radii are used in computation: carbon, 1.9 Å; nitrogen, 1.8 Å; oxygen, 1.7 Å; sulfur, 2.0 Å; phosphorus, 2.1 Å; fluorine, 1.5 Å; chlorine, 1.8 Å; bromine, 2.0 Å; iodine, 2.2 Å; metals, 1.2 Å. This radii set is applied to both ligands and proteins.

(2) Van der Waals interaction. The van der Waals interaction is one of the essential non-covalent interactions. We employ the Lennard-Jones equation to reflect the balance between the short-range repulsion and the long-range attractive dispersion force:

$$VDW = \sum_{i}^{ligand} \sum_{j}^{protein} VDW_{ij} = \sum_{i}^{ligand} \sum_{j}^{protein} \left[\left(\frac{d_{ij,0}}{d_{ij}} \right)^8 - 2 \times \left(\frac{d_{ij,0}}{d_{ij}} \right)^4 \right] \quad (2)$$

Here *VDW* denotes for the van der Waals interaction energy, which is calculated by considering all the atom pairs between the ligand and the protein; d_{ij} denotes for the distance between the ligand atom i and the protein atom j; $d_{ij,0} = r_i + r_j$, i.e. the sum of van der Waals radius of atom i and j. Note that we use a 'softer' form in Equation 2 instead of the standard 12–6 equation. Furthermore, in our algorithm, (i) only heavy atoms contribute. Hydrogen atoms are neglected. (ii) All heavy atoms are weighted equally. No weight factor is used to differentiate them. (iii) To avoid the huge repulsion raised by overlapped atom

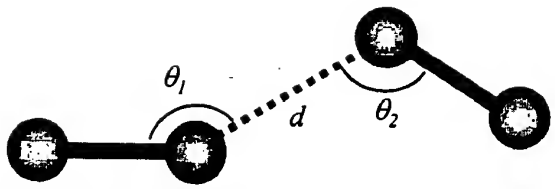

Figure 1. Illustration of the three geometric parameters used in characterizing a hydrogen bond.

pairs, we set an upper limit of 100 for VDW_{ij} in Equation 2. For any pair of atoms, if VDW_{ij} exceeds this limit, it will be cut flat to 100.

(3) Hydrogen bonding. Hydrogen bonding is perhaps the most important factor for the specific binding of a ligand to its receptor. Such interaction happens when two atoms get close enough and form a donor-acceptor pair. The geometry of a hydrogen bond, D–H· · ·A, is typically described by the bond length, i.e. the distance between the hydrogen atom (H) and the acceptor (A), and the bond angle, i.e. ∠DHA. However, hydrogen atoms are normally not revealed in X-ray crystallography analysis. Although hydrogen atoms can be added later, energy minimization is usually required to set them into position. This practice could become problematic especially when the hydrogen atoms can take multiple low-energy positions, such as the one in a hydroxyl group. Furthermore, minimized structures will depend on force field parameters and they may be incompatible with the initial experimentally determined ones. Therefore, we choose not to consider hydrogen atoms explicitly. Here we introduce the concept of 'root': the root of an atom is its non-hydrogen neighboring atom. When an atom bonds with more than one non-hydrogen atom, its root locates at the geometric center of all its non-hydrogen neighboring atoms. Let DR denotes for the donor's root and AR for the acceptor's root. In our algorithm, the geometry of a hydrogen bond is described by: (i) the distance (d) between D and A; (ii) the angle (θ_1) between DR, D and A; and (iii) the angle (θ_2) between D, A and AR (Figure 1).

We assume that a hydrogen bond has an ideal geometry and any deviation from it will weaken the strength of the hydrogen bond. The strength of a hydrogen bond is then computed by considering these three geometric descriptors:

$$HB_{ij} = f(d_{ij})\, f(\theta_{1,ij})\, f(\theta_{2,ij}). \qquad (3)$$

The distance function $f(d)$ and the angular functions $f(\theta_1)$ and $f(\theta_2)$ in Equation 3 are written in the following simple linear fuzzy forms:

$$\begin{aligned}
f(d) &= 1.0 && d_0 \le d_0 - 0.7\ \text{Å} \\
&= (1/0.7) \times (d_0 - d) && d_0 - 0.7\text{Å} < d \le d_0 \\
&= 0.0 && d > d_0 \\
f(\theta_1) &= 1.0 && \theta_1 \ge 120° \\
&= (1/60) \times (\theta_1 - 60) && 120° > \theta_1 \ge 60° \\
&= 0.0 && \theta_1 < 60° \\
f(\theta_2) &= 1.0 && \theta_2 \ge 120° \\
&= (1/60) \times (\theta_2 - 60) && 120° > \theta_2 \ge 60° \\
&= 0.0 && \theta_2 < 60°
\end{aligned}$$

Here $d_0 = r_i + r_j$, i.e. the van der Waals distance between the donor and the acceptor. These functions are derived from the analysis of all the potential hydrogen bonding pairs presented in the training set. The observed distribution of the donor-acceptor distance (d) is shown in Figure 2a. In this figure, one can see that the peak value appears around 2.8Å, which can be interpreted as the ideal length of a hydrogen bond. As d increases, the population decreases. But after d exceeds 3.4 ~ 3.5 Å, it passes the bottom and begins to rise again, which can be interpreted as the turning point from a hydrogen bond to a normal van der Waals contact. Therefore, it is reasonable to define that $f(d) = 1.0$ when $d = 2.8$ Å while $f(d) = 0.0$ when $d = 3.5$ Å. Considering the atomic radii of oxygen and nitrogen atoms, 2.8 Å corresponds to $d_0 - 0.7$ Å while 3.5 Å corresponds to d_0, approximately. By assuming that the distance dependence of the strength of a hydrogen bond is linear within this range, one will obtain the function listed above. The angular functions $f(\theta_1)$ and $f(\theta_2)$ are also derived similarly by interpreting the observed distributions of θ_1 and θ_2 from the training set (Figures 2b and 2c).

The hydrogen bonding interaction between the ligand and the protein is calculated by summing up all the hydrogen bonds:

$$HB = \sum_{i}^{ligand} \sum_{j}^{protein} HB_{ij} \qquad (4)$$

All types of hydrogen bonds, i.e. O-O, O-N, and N-N, are equally weighted so that no extra parameter is necessary. Special attention has been paid to the saturation in hydrogen bonding if one donor or acceptor atom contacts with multiple donor or acceptor atoms. For a given donor or acceptor atom, we define that (i) the maximal number of hydrogen bonds that a donor atom can form should not exceed the number of hydrogen atoms on that donor atom; and (ii) the maximal number of hydrogen bonds that an acceptor atom can

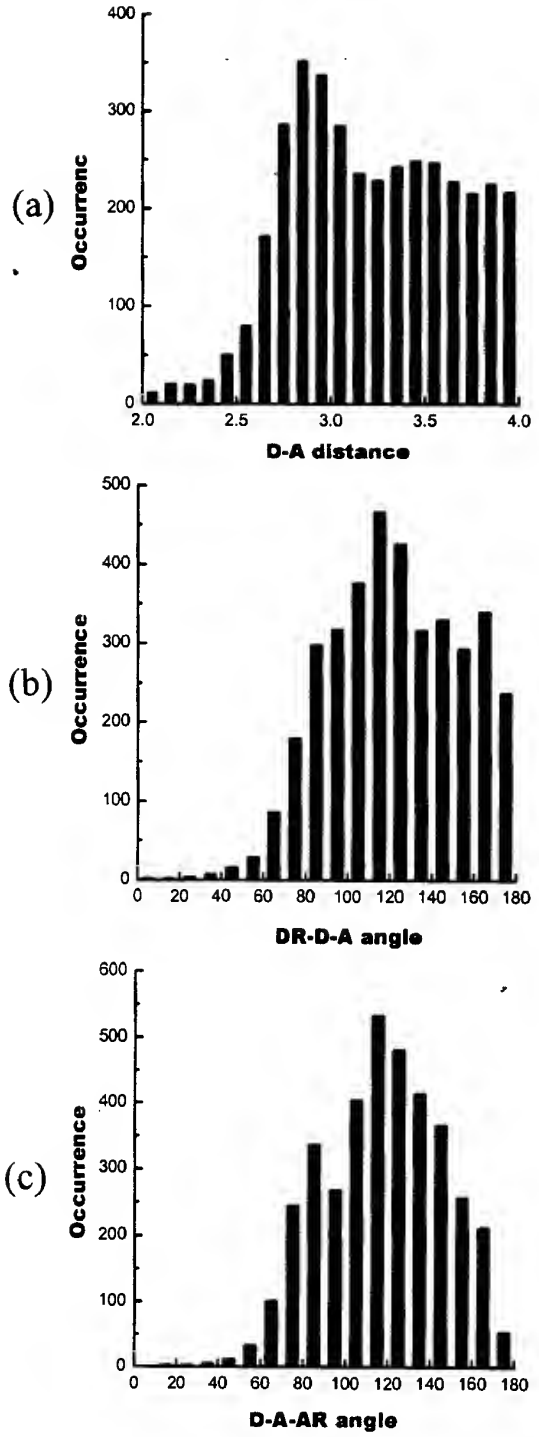

Figure 2. Distribution of the three geometric parameters in a hydrogen bond observed in the training set: (a) the donor-acceptor distance (in angstroms); (b) the DR-D-A angle (in degrees); (c) the D-A-AR angle (in degrees).

form should not exceed the number of lone pairs on that acceptor atom. If an atom could be a donor and an acceptor at the same time, such as the oxygen atom in a hydroxyl group, both rules apply.

As implied above, charged and neutral hydrogen bonds are not treated separately in our scoring functions since we find that the improvement of *our scoring functions* in the training set regression is totally negligible by separating them.

In some cases, metal ions are found inside the binding site of the protein. They may form coordinated bonds with atoms with lone pairs in the ligand and thus also contribute to the binding affinity. We include this kind of interaction in the hydrogen bonding term since it is the same as hydrogen bonding in nature, i.e. Lewis acid-base pair. Note that technically we define metal ions as 'donor' so that the metal-ligand coordinated bonds are calculated with exactly the same distance and angular functions of hydrogen bonding.

(4) Deformation effect. Upon binding, both the ligand and the protein will be constrained in conformation as compared to their free states in solvent. This will raise adverse entropic changes, which is a negative effect that must be overcome during the binding process. In other empirical scoring functions, the deformation effect of the ligand is often estimated by counting the number of rotatable bonds (rotors) that become frozen during the binding process, assuming that each rotor is associated with a discrete number of low-energy conformations and thus a certain amount of conformational entropy. If there are more than one rotor in the ligand, their contributions are assumed to be additive. This assumption is reasonable when all the rotors are isolated and free to rotate, so the low-energy conformations associated with each rotor will multiply to build up the entire conformational space. However, when two or more rotors cross, apparently this assumption is no longer valid because now the rotation of any of them will interfere with the others and this will result in a reduction in the total number of possible low-energy conformations (Figure 3). Therefore, simply counting the number of rotors often overestimates the conformational flexibility of certain kinds of molecules, such as oligo-peptides.

In our algorithm, rotor is defined as acyclic sp^3-sp^3 or sp^3-sp^2 single bond between two non-hydrogen atoms. Terminal groups, such as $-CH_3$, $-NH_2$, $-OH$, and $-X$ (X = F, Cl, Br, I), whose rotation does not produce any new conformation of heavy atoms are not counted as rotors. The potential flexibility of cyclic portions of the ligand is ignored. The deformation

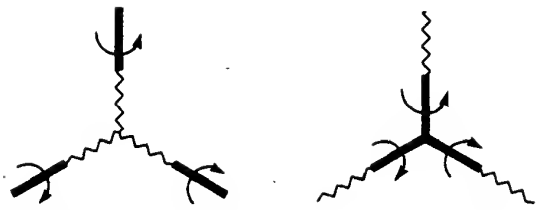

Figure 3. Illustration of 'isolated' (on the left) and 'crossed' rotors (on the right).

effect of the ligand is then expressed as the contribution of all the rotors with proper weight factors. For the convenience of computation, rotors are counted by summing the share of each ligand atom:

$$\mathrm{RT} = \sum_{i}^{ligand} \mathrm{RT}_i, \tag{5}$$

where $\mathrm{RT}_i = 0$ if atom i is not involved in any rotor; $\mathrm{RT}_i = 0.5$ if atom i is involved in one rotor; and $\mathrm{RT}_i = 1.0$ if atom i is involved in two rotors. However, if atom i is involved in more than two rotors, then $\mathrm{RT}_i = 0.5$. Note that, according to the conventional rotor-counting algorithm, RT_i should be 1.5 (in three rotors) or 2.0 (in four rotors) in this case. This reduction in the RT_i value reflects our consideration for offsetting the overestimation of conformational flexibility in the conventional algorithm. Although very crude, we found that our algorithm improves the accuracy of our scoring functions.

In our algorithm, the deformation effect of the protein is neglected. We have attempted to count the number of rotors presented in the side chains of the binding site residues and include it as a term in our scoring functions. However, such attempt did not improve the result. It is not surprising since the side chains of the binding site residues are generally immobilized even in the unbound state due to the stacking of neighboring residues. A more reasonable algorithm needs to be developed to account for the flexibility of the protein.

(5) Hydrophobic effect. Binding of the ligand and the protein is accompanied by the desolvation process that undergoes changes in entropy as well as in enthalpy. One of the results is that non-polar groups tend to favor each other, which is also referred to as 'hydrophobic effect'. This effect is very difficult for accurate characterization since it involves complicated ligand-water, protein-water, and water-water interactions before and after binding. Different algorithms have been used in other empirical scoring functions to calculate this term. We have implemented three representative algorithms in our scoring functions.

(i) Hydrophobic surface algorithm. The hydrophobic effect is assumed to be proportional to the buried hydrophobic surface of the ligand (Equation 6). This algorithm was adopted by Bohm's scoring function [27]. It should be pointed out that technically there are several types of molecular surfaces. Here we choose to use the solvent-accessible surface (SAS).

$$\mathrm{HS} = \sum_{i}^{ligand} \mathrm{SAS}_i. \tag{6}$$

The radius of the solvent probe is set to 1.5 Å. The solvent-accessible surface of the ligand is represented by evenly distributed dots in a spacing of 0.5 Å. Numerical integration is used to calculate the surface area. The surface areas of hydrogen atoms are attributed to their root atoms. Any part of the ligand surface is considered buried if it penetrates into the solvent-accessible surface of the protein. Note that only hydrophobic atoms are considered in Equation 6. The total amount of buried surface area is expressed in square Angstrom.

(ii) Hydrophobic contact algorithm. The hydrophobic effect is calculated by summing up the hydrophobic atom pairs formed between the ligand and the protein. This algorithm was adopted by ChemScore [30]. In our algorithm, it is calculated as:

$$\mathrm{HC} = \sum_{i}^{ligand} \sum_{j}^{protein} f(d_{ij}), \tag{7}$$

where

$$\begin{aligned} f(d) &= 1.0 && d \le d_0 + 0.5\ \text{Å} \\ &= (1/1.5) \times (d_0 + 2.0 - d) && d_0 + 0.5\ \text{Å} < d \\ & && \le d_0 + 2.0\ \text{Å} \\ &= 0.0 && d > d_0 + 2.0\text{Å}. \end{aligned}$$

This distance function reflects the intuition that the strength of 'hydrophobic interaction' will reach the maximum when two hydrophobic atoms form van der Waals contact and diminish gradually with the increase in the inter-atomic distance. We find that this distance function needs to be fairly long-ranged in order to work well.

(iii) Hydrophobic matching algorithm. This algorithm was adopted by SCORE [32]. According to this method, different parts of the ligand sense the protein differently because of the heterogeneous nature of the binding site. If a hydrophobic ligand atom is placed at a hydrophobic site of the protein, then it is

expected to be favorable to the binding process. The overall hydrophobic matching between the ligand and the protein is calculated as:

$$\mathrm{HM} = \sum_{i}^{ligand} \log P_i \times \mathrm{HM}_i. \quad (8)$$

Here HM_i is an indicator variable. It is set to 1 if a hydrophobic atom i is placed in a hydrophobic environment; otherwise it is set to 0. $\mathrm{Log}P_i$ refers to the hydrophobic scale of atom i, which is the contribution of atom i to the n-octanol/water partition coefficient (Log P) of the molecule. In our algorithm, the hydrophobic scales for all kinds of atoms are cited from XLOGP2 [36]. They are introduced as weight factors here to ensure that more hydrophobic atoms contribute more to the hydrophobic effect. The 'environment' of a given ligand atom is defined to consist of all the atoms on the protein which are within 6 Å from the ligand atom. The hydrophobicity of the environment is determined by summing up the hydrophobic scales of all its member atoms. Our investigation of the training set shows that the average hydrophobicity of an environment surrounding a hydrophobic ligand atom is -0.50 log$P$ units. Therefore, in our algorithm an environment is defined as hydrophobic if its hydrophobicity is greater than -0.50 log$P$ units.

Finally, we summarize our scoring functions below. The binding affinity of a given protein-ligand complex, as expressed in pK_d unit, is calculated by summing up all the terms described above. Since three different algorithms for modeling the hydrophobic effect have been implemented, we have three resulting scoring functions:

$$\begin{aligned} pK_{d,1} &= C_{0,1} + C_{\mathrm{VDW},1} \times \mathrm{VDW} \\ &\quad + C_{\mathrm{H-bond},1} \times \mathrm{HB} \\ &\quad + C_{\mathrm{rotor},1} \times \mathrm{RT} \\ &\quad + C_{\mathrm{hydrophobic},1} \times \mathrm{HS}, \end{aligned} \quad (9)$$

$$\begin{aligned} pK_{d,2} &= C_{0,2} + C_{\mathrm{VDW},2} \times \mathrm{VDW} \\ &\quad + C_{\mathrm{H-bond},2} \times \mathrm{HB} \\ &\quad + C_{\mathrm{rotor},2} \times \mathrm{RT} \\ &\quad + C_{\mathrm{hydrophobic},2} \times \mathrm{HC}, \end{aligned} \quad (10)$$

$$\begin{aligned} pK_{d,3} &= C_{0,3} + C_{\mathrm{VDW},3} \times \mathrm{VDW} \\ &\quad + C_{\mathrm{H-bond},3} \times \mathrm{HB} \\ &\quad + C_{\mathrm{rotor},3} \times \mathrm{RT} \\ &\quad + C_{\mathrm{hydrophobic},3} \times \mathrm{HM}. \end{aligned} \quad (11)$$

It should be emphasized that, except for the hydrophobic effect term, all the other terms in these three scoring functions are calculated using identical algorithms. The consensus scoring function, which is named as X-CSCORE, is the arithmetical average of Equations 9–11:

$$\mathrm{X-CSCORE} = \left(pK_{d,1} + pK_{d,2} + pK_{d,3}\right)/3 \quad (12)$$

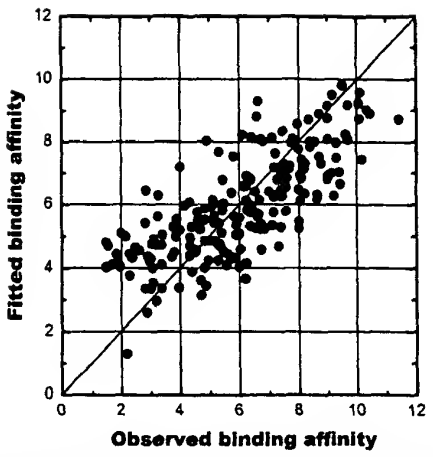

Figure 4. Correlation between the observed binding affinities of the 200 protein-ligand complexes in the training set and the fitted values given by X-CSCORE (in pK_d units).

Regression analyses

Coefficients before each term in Equations 9–11 are derived through standard least-square multivariate regression analyses of the training set. They are listed in Table 1 together with other related information. Correlation coefficients (r^2) and standard deviations (s) obtained from regression are listed in Table 2. The correlation between the observed binding affinities and the fitted values given by X-CSCORE is shown in Figure 4. Leave-one-out cross-validations are performed to judge the quality of the regression models. The resulting q^2 and s_{press} are listed in Table 2. Both the regression and the cross-validation are performed with the QSAR module in SYBYL.

Validation

(1) Test set. An independent test set is usually needed to validate a regression model. When constructing the training set, we deliberately separate all the complexes released by the Protein Data Bank after 1998 from the others. These complexes, 30 in total, are used as a test set in our study. A complete list of the test set can

Table I. Regression models of Equations 9–11

Term	Coefficient[a]	Mean value[b]	Contribution fraction[c]
(Equation 9)			
VDW	-2.01×10^{-3} ($\pm 1.81 \times 10^{-3}$)	-6.00×10^{2}	16.5%
H-Bond	0.307 ($\pm$ 0.137)	4.21	19.8 %
Rotor	−0.159 ($\pm$0.079)	7.28	25.3 %
Hydrophobic surface	7.10×10^{-3} ($\pm 2.50 \times 10^{-3}$)	2.74×10^{2} Å^2	38.4%
Constant	2.69 ($\pm$ 0.66)	–	–
(Equation 10)			
VDW	-0.96×10^{-3} ($\pm 1.91 \times 10^{-3}$)	-6.00×10^{2}	8.6%
H-Bond	0.412 ($\pm$ 0.149)	4.21	29.4%
Rotor	−0.100 ($\pm$ 0.074)	7.28	17.5%
Hydrophobic contact	3.73×10^{-2} ($\pm 1.12 \times 10^{-2}$)	43.1	44.5%
Constant	2.78 ($\pm$ 0.65)	–	–
(Equation 11)			
VDW	-2.14×10^{-3} ($\pm 1.65 \times 10^{-3}$)	-6.00×10^{2}	16.4%
H-Bond	0.311 ($\pm$ 0.131)	4.21	18.8%
Rotor	−0.169 ($\pm$ 0.078)	7.28	25.2%
Hydrophobic matching	0.602 ($\pm$ 0.159)	2.51	39.6%
Constant	3.10 ($\pm$ 0.65)	–	–

[a] All coefficients are presented in pK_d units. They can be converted into binding free energies at 298 K in kcal/mol by multiplying a factor of −1.36. The values in brackets are 95% confidence intervals in regression.
[b] Mean values of each term are calculated over the entire training set.
[c] Contribution fractions are calculated by using the QSAR/PLS module in SYBYL.

Table 2. Statistical results of Equations 9–11 and X-CSCORÉ

	Equation 9	Equation 10	Equation 11	X-CSCORE
R^2	0.504	0.546	0.571	0.591
S[a]	1.58	1.53	1.43	1.47
$F(4, 195)$	49.6	58.7	70.4	–
Q^2	0.480	0.522	0.551	–
S_{press}	1.62	1.57	1.47	–
R^2_{pred}	0.318	0.319	0.249	0.356
S_{pred}	1.51	1.61	1.63	1.58

[a] All the standard deviations, including S, S_{press} and S_{pred}, are presented in pK_d units. They can be converted into binding free energies at 298 K in kcal/mol by multiplying a factor of −1.36.

be found in the *supplementary material* section in this paper.

All the scoring functions, including Equations 9–12, are used to predict the binding affinities of the 30 protein-ligand complexes in the test set. The root-mean-squared deviation (s_{pred}) is used to measure the quality of prediction:

$$s_{\text{pred}} = \sqrt{\sum \left(pK_{d,\text{pred}} - pK_{d,\text{obs}}\right)^2 / (N-1)}. \quad (13)$$

The statistical results are shown in Table 2. The correlation between the experimentally observed binding affinities and the predicted values given by X-CSCORE is shown in Figure 5.

(2) Evolutionary regression. We have adopted an iterative regression procedure to further validate the internal consistency of our scoring functions, which was originally proposed in our previous work SCORE [32]. The central idea of this procedure, called evolutionary regression, is to test a given regression model with training sets of different sizes. In our study, this procedure starts from constructing a subset of 50 complexes which are randomly selected from the training set without duplication. This subset is used to perform multivariate regression and leave-one-out cross-validation for the scoring function under inves-

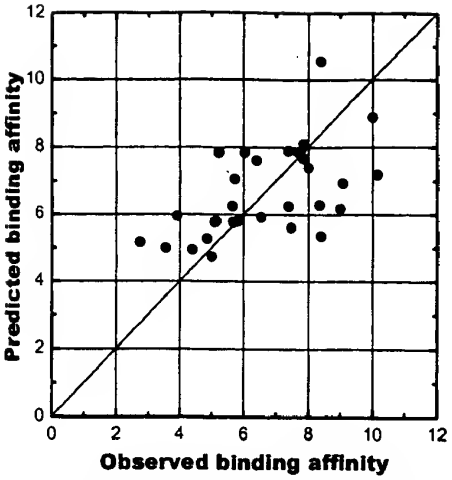

Figure 5. Correlation between the observed binding affinities of the 30 protein-ligand complexes in the test set and the predicted values given by X-CSCORE (in pK_d units).

tigation. All the regression results, including r^2, s, q^2, s_{press}, and the coefficients for each term in the scoring function, are recorded. This regression model is then used to predict the K_d values of the test set. The resulting r^2_{pred} and s_{pred} are also recorded. Since the subset is constructed randomly, the entire procedure, i.e. construction of the subset, multivariate regression, cross-validation, and calculation of the test set, is repeated for 10 times to reduce the noises in all the statistical results. Only the averaged results are used for analysis. At the next step, the size of the subset is increased by 10, and the regression model is re-evaluated with this new subset. This procedure is repeated until the size of the subset reached the full size of the training set. We have performed evolutionary regression for Equations 9–11. The standard deviations observed during the evolutionary regression procedure of Equations 9–11 are shown in Figure 6a–c, respectively.

(3) Molecular docking. We have also tested the performance of X-CSCORE in molecular docking experiments. We select 10 samples from the training set, including the L-arabinose binding protein/L-arabinose complex (PDB code 1ABE), the alcohol dehydrogenase/CNAD complex (PDB code 1ADB), the adenosine deaminase/DAA complex (PDB code 1ADD), the cytidine deaminase/uridine complex (PDB code 1AF2), the maltodextrin binding protein/maltose complex (PDB code 1ANF), the carboxypeptidase A/L-benzylsuccinate complex (PDB code 1CBX), the antibody DB3/progesterone analogue complex

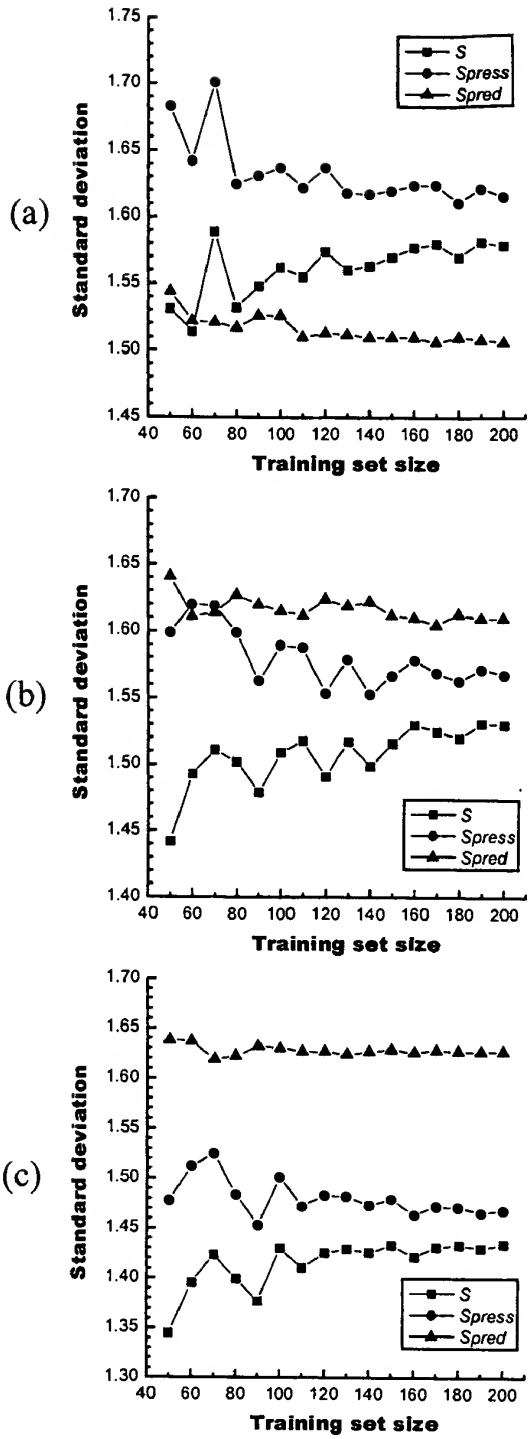

Figure 6. Standard deviations (in pK_d units) observed in the evolutionary regression procedure. (a) Equation 9; (b) Equation 10; (c) Equation 11.

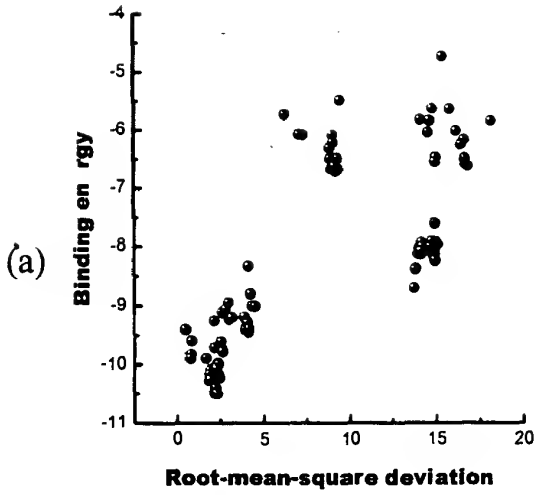

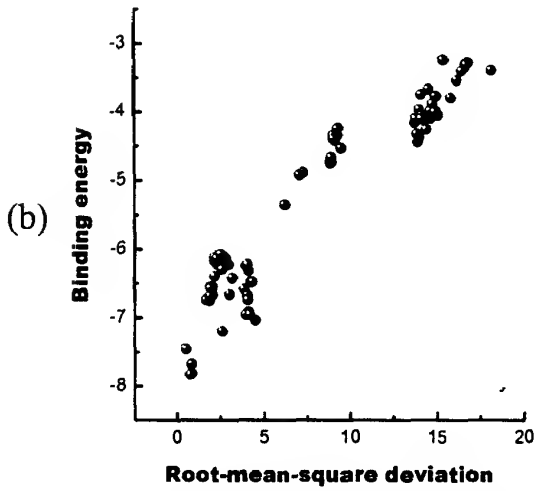

Figure 7. Relationship between the RMSD values (Å) and the binding energies (kcal/mol) of 100 conformations of L-benzylsuccinate in complex with carboxypeptidase A (PDB code 1CBX). (a) Binding energies calculated by AutoDock. (b) Binding energies calculated by X-CSCORE.

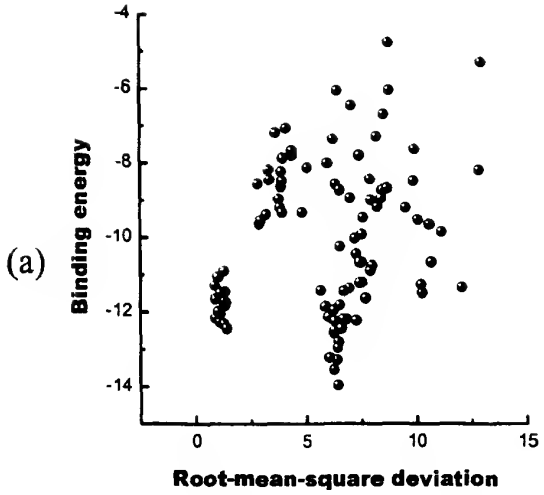

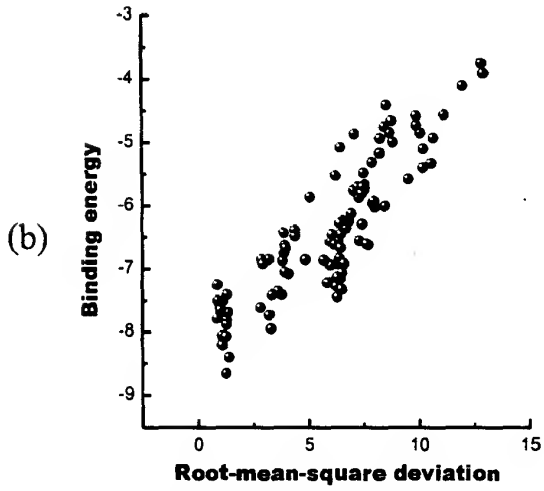

Figure 8. Relationship between the RMSD values (Å) and the binding energies (kcal/mol) of 100 conformations of folate in complex with dihydrofolate reductase (PDB code 1DHF). (a) Binding energies calculated by AutoDock. (b) Binding energies calculated by X-CSCORE.

(PDB code 1DBM), the dihydrofolate reductase/folate complex (PDB code 1DHF), the glutathione S-transferase/glutathione complex (PDB code 1GST), and the HIV-1 protease/VX-478 complex (PDB code 1HPV). The selection of these 10 samples emphasizes the diversity of the ligands and the proteins. For each complex, the AutoDock 3.0 program [8] is employed to perform a molecular docking run. In each case, the experimentally determined complex structure is always used as the starting point. The ligand is treated flexible while the protein is kept rigid. The searching steps in the conformational sampling for translation, quaternion, and torsion are set to 0.5 Å, 15° and 15°, respectively. Fifty thousand genetic algorithm generations are run with a population of 100 conformations. The final 100 best-scored conformations are saved and their root-mean-squared deviations (RMSD), as calculated by using the observed bound conformation as the reference, are recorded. Then the binding

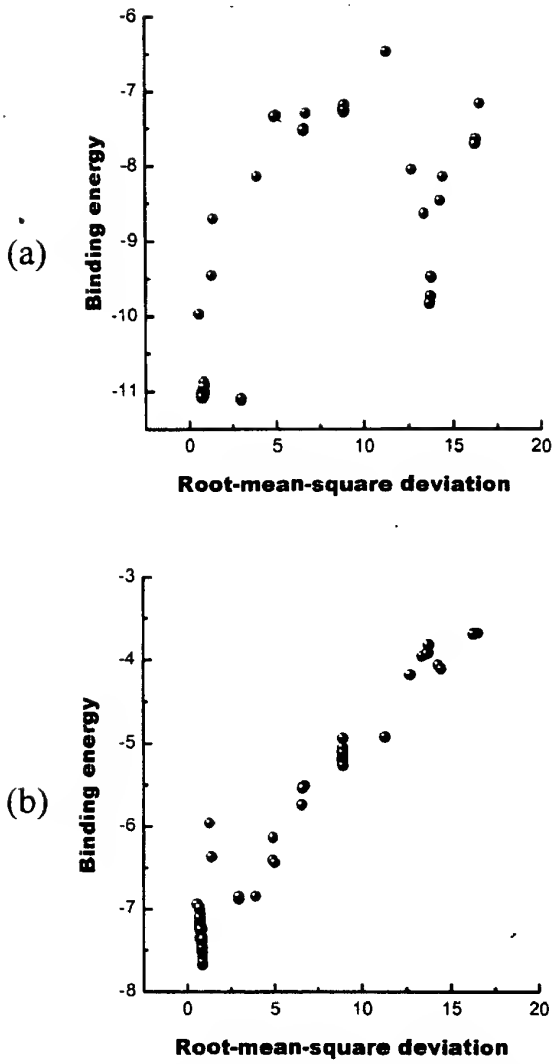

Figure 9. Relationship between the RMSD values (Å) and the binding energies (kcal/mol) of 100 conformations of 1-deaza-adenosine in complex with adenosine deaminase (PDB code 1ADD). (a) Binding energies calculated by AutoDock. (b) Binding energies calculated by X-CSCORE.

energies of these conformations are re-calculated by X-CSCORE. RMSD values of the best-scored conformations, picked by AutoDock and X-CSCORE, of all 10 complexes are summarized in Table 3. For complex 1CBX, 1DHF, and 1ADD, RMSD values of the final 100 conformations are plotted against the binding energies of these conformations in Figures 7–9, respectively.

Program description

We have developed a program, X-CSCORE, to implement the three scoring functions described by Equations 9–11. Here 'CSCORE' means consensus scoring; while the prefix 'X' indicates that it is part of our in-house drug design toolkit X-TOOL. This program is written in ANSI C++ and has been tested on UNIX and LINUX platforms. The required inputs include the three-dimensional structure of the protein in PDB format and the pre-docked ligand molecule(s) in MOL2 format. The user is allowed to enable or disable any of the three scoring functions in computation and the final predicted binding affinities are based on the arithmetic average of all the enabled scoring functions. If all three scoring functions are enabled, typically this program is able to process around 10 000 ligand molecules for a given protein target in an hour on a SGI O2/R5000/180MHz workstation.

Discussion

Accuracy and robustness

As shown in Table 2, Equations 9–11 are able to reproduce the binding affinities of the entire training set with standard deviations (s) of 1.58, 1.53 and 1.43 pK_d units, respectively. Their standard deviations in leave-one-out cross-validation (s_{press}) are at the same level, which are 1.62, 1.57 and 1.47 pK_d units, respectively. More importantly, these scoring functions perform almost equally well for the independent test set: the standard deviations in the predicted binding affinities (s_{pred}) are 1.51, 1.61 and 1.63 pK_d units, respectively. These values correspond to 2.1–2.2 kcal/mol in binding free energy at room temperature. Considering the diversity of the test set, such accuracy in binding affinity prediction is encouraging. Compared to other existing empirical scoring functions, our scoring functions have achieved better or comparable statistical results. If taking the Fisher significant ratio (F) as an objective criterion for comparing different regression models, the values are 32.1, 44.5 and 57.8 for Bohm's scoring function [27], ChemScore [30], and SCORE [32], respectively. In comparison, the F values of our scoring functions are 49.6, 58.7 and 70.4 for Equations 9–11, respectively.

When building a regression model, over-fitting of the regression equation should be avoided because it may fail to give reasonable predictions for samples

Table 3. Results from the molecular docking studies of 10 protein-ligand complexes

PDB code	Resolution (Å)	RMSD (Å)[a]		pK_d	
		AutoDock	X-CSCORE	Exp.[b]	X-CSCORE[c]
1ABE	1.7	0.62	0.73	6.52	5.14 (5.25)
1ADB	2.4	2.74	2.74	8.40	6.71 (8.01)
1ADD	2.4	2.93	0.83	6.74	5.63 (5.36)
1AF2	2.3	0.88	0.88	3.10	5.26 (4.90)
1ANF	1.67	0.60	0.54	5.46	6.16 (6.03)
1CBX	2.0	2.30	0.77	6.35	5.74 (5.74)
1DBM	2.7	1.31	1.13	9.44	6.84 (6.65)
1DHF	2.3	6.44	1.24	7.40	6.34 (5.27)
1GST	2.2	0.74	1.21	4.68	5.92 (5.21)
1HPV	1.9	1.73	1.16	9.22	6.47 (6.28)

[a]RMSD value of the best scored conformation in reference to the observed bound conformation.
[b]Experimentally determined binding affinity.
[c]Calculated binding affinity for the best scored conformation. The values in brackets are the calculated one for the observed bound conformation.

outside the training set. For this reason, only a minimal number of adjustable parameters are included in our scoring functions to achieve maximal N/M ratio in regression analysis. For example, we do not assign additional weighting factors to different types of atoms when calculating the van der Waals interaction. When calculating the hydrogen bonding, we do not differentiate charged and neutral hydrogen bonds. No differentiation in aliphatic and aromatic atoms was made in calculating the hydrophobic effect. Besides the regression constant, there are only four coefficients in each of our scoring functions. As shown in Table 1, they are all significant in regression analysis. Here the van der Waals interaction term in Equation 10 seems to be an exception, which contributes only a relative small fraction. However, it is not surprising since the hydrophobic effect term in Equation 10 is also calculated by counting atom pairs, therefore it overlaps with the van der Waals term partially and 'grabs' some contributions from the van der Waals term.

The N/M ratio issue deserves a little more discussion. It is reasonable to expect that statistically converged results can only be obtained by using a large training set. But how large is large? What is the proper size of the training set for deriving an empirical scoring function like ours? To answer this question, we have adopted the evolutionary regression procedure to look for the answer. The idea of evolutionary regression is to test a given regression model with training sets in different sizes and monitor the quality of the regression model during this procedure. Several trends can be seen in the evolutionary regression experiments of Equations 9–11 (Figure 6). (i) The standard deviation in the whole set fitting (s) gradually increases when the training set grows larger. This can be understood because the scoring function under regression is kept fixed during the whole procedure. A larger training set represents more complexity and thus is more difficult to reconcile. (ii) The predictive ability of the regression model, as indicated by the standard deviations in leave-one-out cross-validation (s_{press}) and test set computation (s_{pred}), is gradually improved when the training set grows larger. This indicates that a larger training set indeed helps our scoring functions achieve better predictive ability. (iii) When the training set is relatively small, the regression model is generally unstable. The final regression model depends very sensitively on the contents of the training set, which may lead to chance correlation in regression and poor predictive ability. When the training set grows larger, the regression model becomes more stable and tends to converge to a certain level. As suggested by our evolutionary regression experiments, a training set containing at least 160 samples is required to derive a stable empirical scoring function with four terms, i.e. a minimal N/M ratio of 40. Unfortunately, the N/M ratios of other existing empirical scoring functions are generally much lower than this, e.g. LUDI (N/M = 45/6 = 9) [27], ChemScore (N/M = 82/4 = 20) [30], and SCORE (N/M = 170/10 = 17) [32]. In our case, the N/M ratio is 200/4 = 50. Therefore, we believe our scoring functions are, if not much more accurate, more

robust in binding affinity prediction for a wider range of protein-ligand complexes.

Consensus scoring

A unique feature of our study is that three different algorithms have been implemented for modeling the hydrophobic effect. As described in the Methods section, hydrophobic effect is calculated either by the buried solvent-accessible molecular surface (Equation 9), or by the number of hydrophobic contacts between the protein and the ligand (Equation 10), or by the hydrophobic matching of the ligand with the binding site (Equation 11). All three algorithms are conceptually acceptable and actually they represent three typical algorithms adopted by empirical scoring functions for modeling the hydrophobic effect. However, it is not a good idea to include all three terms together in *one* scoring function since they account for the same effect and thus are highly correlated to each other. Therefore, they have to be accommodated in three scoring functions. As indicated by our regression results (Table 2), all three scoring functions perform reasonably well and are basically comparable to each other. However, since these three algorithms utilize different geometric features of the given protein-ligand complex structure in computation, their results differ. We have found that, for 40.0% of the samples in the training set, the difference between the lowest and the highest calculated binding affinity by these three scoring functions is less than 0.50 pK_d units; for 40.5% of the samples, the difference is between 0.50 and 1.00 pK_d units; while for the remaining 19.5% of the samples, the difference is larger than 1.00 pK_d units. One can see that such difference is not trivial at all in many cases. Conceivably, if one can predict which scoring function will be the best for a given protein-ligand complex, the accuracy in binding affinity prediction will be improved greatly. Indeed, if the experimental values are correlated to the best fitted values (each of them is chosen from three hits), the standard deviation in the training set fitting will drop by half to about 0.7 pK_d units. We have attempted to find out which scoring function may perform better for certain classes of ligands or families of proteins. Unfortunately this attempt ended without much success.

Based on the fact that there is no reason to bias towards any one of the three scoring functions, we simply combine them together (Equation 12). This practice is consistent with the idea of consensus scoring which has been demonstrated to be an effective way of improving the hit-rates in virtual database screening [33]. As shown in Table 2, the performance of a single scoring function may vary and is not predictable. For example, among the three scoring functions, Equation 9 is the worst one for the training set but the best one for the test set. In contrast, Equation 11 is the best one for the training set but the worst one for the test set. By averaging these scoring functions, i.e. X-CSCORE, the result is not always the closest one to the true value (in fact it is always between the best one and the worst one). However, the advantages are: (i) it provides a clear indication of what level of accuracy these three scoring functions can achieve. Obtaining a converged result in binding affinity prediction is certainly important for structure-based drug design practice; and (ii) large errors in binding affinity prediction can be reduced. Recently we have pointed out that the nature of consensus scoring is multiple sampling [37]. By applying multiple scoring functions in combination, the positive and the negative errors have a chance to cancel each other and that is why consensus scoring generally performs better than any single scoring procedure.

Application to molecular docking

Our scoring function is developed primarily for estimating the binding affinity of a given complex with known structure ('scoring'). We also expect it to be useful for identifying the correct 'pose' of a ligand to its receptor ('docking'). Although some disputes still exist in whether 'docking' or 'scoring' should use the same type of function, we believe that ideally a 'scoring' function should also be able to serve as a 'docking' function. This is very important because in practice 'docking' and 'scoring' are often inseparable, such as in a virtual database screening study.

As described in the *Methods* section, we have investigated the potential application of X-CSCORE in molecular docking with 10 samples. Since we have not implemented this consensus scoring function into any molecular docking program directly, we employ the AutoDock program as a tool to generate possible bound conformations of the given ligand. All the conformations are then re-evaluated by X-CSCORE. RMSD values of the best scored conformations of these 10 protein-ligand complexes are listed in Table 3, where the results of X-CSCORE and the force field calculation in AutoDock are compared side by side. As one can see, if using the force field calculation in AutoDock as the scoring engine, 4 out

of the total 10 samples have RMSD values larger than 2.0 Å; while if using X-CSCORE as the scoring engine, only one sample, i.e. the alcohol dehydrogenase/CNAD complex (PDB code 1ADB), shows a RMSD value larger than 2.0 Å. In this case, we have checked all the 100 conformations generated by AutoDock and we found that the lowest RMSD value is 2.74 Å. This indicates that, with the parameters we were using, AutoDock has not generated any conformation close enough to the observed one. In fact, X-CSCORE predicts a much higher pK_d value of 8.01 for the observed one. The RMSD versus energy relationships observed in our docking tests for the Carboxypeptidase A/L-benzylsuccinate complex (PDB code 1CBX), the Dihydrofolate reductase/folate complex (PDB code 1DHF), and the adenosine deaminase/DAA complex (PDB code 1ADD) are shown in Figures 7–9, respectively. For these three samples, the best RMSD values given by AutoDock are 2.30 Å, 6.44 Å and 2.93 Å; while the corresponding ones given by X-CSCORE are 0.77 Å, 1.24 Å and 0.83 Å. It is very interesting to notice that, in the case of 1DHF, AutoDock has apparently chosen a wrong class of conformations while the correct one is somehow scored about 2 kcal/mol higher. In contrast, X-CSCORE has no problem in identifying the correct conformation.

It is very encouraging that our scoring functions are also applicable to molecular docking. Our scoring functions have all the necessary elements that correspond to the non-covalent interactions in a conventional force field, such as the van der Waals interaction and the electrostatic interaction (replaced by the hydrogen bonding term in our scoring functions). Besides that, our scoring functions also consider the hydrophobic effect and thus provide a better estimation of binding free energies. This is suggested in Figures 7b, 8b and 9b. In these cases, there is always a clear correlation between the RMSD values of the conformations and their binding energies calculated by X-CSCORE. Generally, the smaller is the RMSD value, the lower is the binding energy. The importance of this feature should not be underestimated. Molecular docking is a conformational sampling procedure which is performed on the potential energy surface defined by a certain scoring function. It is important that this potential energy surface does not contain a large number of false minima since such frustration will probably lead to poor convergence or wrong binding modes. The potential energy surface defined by an ideal scoring function should shape like a funnel, on which all the paths finally go down to the right position. As indicated by the RMSD versus energy relationships shown in Figures 7b, 8b and 9b, our consensus scoring function may have such an appealing feature. We expect that if a molecular docking program adopts our consensus scoring function as its scoring engine, its accuracy and efficiency in finding the correct bound structure will be improved considerably.

Considering that in practice our consensus scoring function will be applied in conjunction with molecular docking programs, it is highly desirable that all our scoring functions are able to tolerate at least a small amount of uncertainty in the input structure. For this reason, we have designed our scoring functions in such a way that they are not too sensitive to atomic coordinates. For example, we avoid the explicit use of hydrogen atoms in our algorithms. The reason is that predicting the position of a hydrogen atom precisely could be problematic when the hydrogen atom is bonded to a terminal rotatable group, such as a hydroxyl group. This uncertainty will lead to large deviation if hydrogen atoms have to be included explicitly in the calculation. Secondly, all the terms in our scoring functions are calculated with relatively large tolerances. For example, a 'softer' 8–4 equation is adopted in the van der Waals interaction term; loose criteria for distance and angular dependence are adopted in the hydrogen bonding term; long-distance cutoff is adopted in the hydrophobic effect terms. All these efforts are dedicated to emphasize on the overall fitness of the ligand to the binding site rather than trivial structural details. As shown in Table 3, by applying X-CSCORE, if a conformation is close to the reference conformation, then indeed it will get a score close to the one of the reference conformation.

Strength and weakness

Our scoring functions are developed to provide fast binding affinity estimations for a wide range of proteins and ligands. As demonstrated by the training set and the test set, the average accuracy of our consensus scoring function in calculating absolute binding free energies is approximately 2 kcal/mol. This level of accuracy is acceptable for structure-based lead discovery in which very accurate prediction of binding free energies may not be necessary, such as virtual database screening or *de novo* structure generation. The speed of our consensus scoring function is also perfectly suitable for such approaches.

We have implemented our scoring functions in a user-friendly program and have already applied it to several on-going structure-based drug design projects in our group. In these projects, large chemical databases are screened first by a standard docking program, such as DOCK, to pick out the top 10% compounds. These compounds are then re-evaluated by X-CSCORE. The best compounds selected by X-CSCORE, usually less than 0.1% of the original database, are then tested in biological assays. Very promising compounds have been identified since the application of this approach.

However, the accuracy of our consensus scoring function in binding affinity prediction is still not totally satisfactory: an error of 2 kcal/mol in binding free energy equals to approximately 50 folds in dissociation constant. Several drawbacks in our approach may have contributed to this inaccuracy. Firstly, since our scoring functions are derived from regression, they tend to characterize only the "common" interactions that are exhibited by a large population in the training set. Some other types of interactions, such as cation-π interaction and π-π stacking, are not included in our scoring functions simply because they have rare occurrences and thus do not contribute much to the regression model. It is thus expected that a general-type scoring function like ours could fail to give reasonable predictions when these types of interactions are playing an important role in protein-ligand binding. Secondly, there are also some factors which are common but we do not really have reasonable methods to take them into account. One example is the water molecules existing on the protein-ligand interface. Such water molecules are quite common and in some cases are thought to play an important role in the ligand binding. However, it remains unclear how to consider water molecules explicitly with an empirical scoring function. If water molecules need to be considered explicitly, maybe the entire algorithm for modeling the so-called 'hydrophobic effect' needs be replaced as well.

Our scoring functions also tend to give large positive errors for complexes with very low affinities and large negative errors for complexes with very high affinities (Figure 4). This phenomenon contributes to the significant positive intercept ($\sim 3\ pK_d$ units) observed in all three scoring functions. Given the fact that most of the samples in the training set (80%) have pK_d values between 3.00 and 9.00, our scoring functions are calibrated better for binding affinities at this range. In fact, if only the samples within this affinity range are chosen to derive our scoring functions, the standard deviations in regression will drop to 1.2–1.3 pK_d units ($\sim$ 1.7 kcal/mol in binding free energy).

Another major problem is the quality of the training set. Ideally, each protein-ligand complex in the training set should have a known high-resolution three-dimensional structure together with a reliably measured binding affinity value accessible to the public. Obtaining protein-ligand complex structures is not a problem since the Protein Data Bank provides an excellent resource for such information. However, collecting the binding affinities for these complexes is a tedious job since they all scatter in various literatures. So far, no appreciable database for such information has been established. The training set used in our study is a compilation of the training sets published in others' work plus our own collections from the literature. Containing 200 samples, it is already the largest set published to date in an empirical scoring function approach. As demonstrated in our evolutionary regression test, the size of this training set is sufficient for calibrating our scoring functions. However, the binding affinity data presented in this training set still need careful examination because a large portion of them are cited directly from others' work without further confirmation. Besides, some of the dissociation constants could have been measured under different experimental conditions, such as PH level, temperature, and salt concentration. The uncertainties in the binding affinity data have certainly placed an intrinsic limit on the accuracy of our scoring functions.

It should be mentioned that all the drawbacks we have discussed above are shared by other empirical scoring functions as well. Despite of all these drawbacks, empirical scoring functions remain a valuable and indispensable means for structure-based drug design. Constructing a better training set will not be a problem in the future because more and more structural and binding affinity data are becoming available. We are also optimistic that better algorithms will appear to account for the binding process. All these efforts will lead to a substantial improvement in the performance of future empirical scoring functions.

Conclusion

We have developed a consensus empirical scoring function, X-CSCORE, for estimating the binding affinity of a given protein-ligand complex with a known three-dimensional structure. The framework

of our study is very similar to Böhm's pioneering work. However, we have presented our works on designing better algorithms for the contributing terms and calibrating the scoring functions against a larger training set. As shown in this paper, our consensus scoring function is able to predict the binding free energies with an average accuracy of approximately 2 kcal/mol. Its potential application to molecular docking is demonstrated with a number of protein-ligand complexes. When compared to the conventional force field calculation, X-CSCORE performs considerably better in identifying the correct bound conformations. Considering the reasonable accuracy, the wide applicability, and the respectable speed, we expect that X-CSCORE will become a valuable tool for structure-based drug design.

Supplementary material

Tables of the training set (200 protein-ligand complexes) and the test set (30 protein-ligand complexes). The program, X-CSCORE, is available by contacting the authors.

Acknowledgements

This work is financially supported by the Cap CURE Foundation (2001 Young Investigator Award to Dr Renxiao Wang) and the Department of Defense (Grant No. DOD DAMP17-93-V-3018 to Dr Shaomeng Wang). The authors are grateful to Dr John B. O. Mitchell at University of Cambridge for providing some of the binding affinity data used in this study. The authors are also grateful to Dr Chao-Yie Yang at University of Michigan Medical School for his many thoughtful suggestions.

References

1. Kuntz, I.D., *Science*, 257 (1992) 1078.
2. Greer, J., Erickson, J.W., Baldwin, J.J. and Varney, M.D., J. Med. Chem., 37 (1994) 1035.
3. Verlinde C.L.M.J. and Hol W.G.J., Structure, 2 (1994) 577.
4. Babine, R.E. and Bender, S.L., Chem. Rev., 97 (1997) 1359.
5. Gane, P.J. and Dean, P.M., Curr. Opin. Struct. Biol., 10 (2000) 401.
6. Walters, W.P., Stahl, M.T. and Murcko, M.A., Drug Discovery Today, 3 (1998) 160.
7. Makino, S. and Kuntz, I.D., J. Comp. Chem., 18 (1997) 1812.
8. Morris, G.M., Goodsell, D.S., Halliday, R., Huey, R., Hart, W.E., Belew, R.K. and Olson, A.J., J. Comput. Chem., 19 (1998) 1639.
9. Jones, G., Wilett, P., Glen, R.C., Leach, A.R. and Taylor, R., J. Mol. Biol., 267 (1997) 727.
10. Rarey, M., Kramer, B., Lengauer, T. and Klebe, G., J. Mol. Biol., 261 (1996) 470.
11. Böhm, H.J., Curr. Opin. Biotech., 7 (1996) 433.
12. Miranker, A. and Karplus, M., Proteins, 11 (1991) 29.
13. Böhm, H.J., J. Comput. Aid. Mol. Des., 6 (1992) 61.
14. Gillet, V., Johnson, P. and Mata, P., J. Comput. Aid. Mol. Des., 7 (1993) 127.
15. Clark, D.E., Frenkel, D. and Levy, S.A., J. Comput. Aid. Mol. Des., 5 (1995) 13.
16. Pearlman, D.A. and Murcko, M.A., J. Med. Chem., 39 (1996) 1651.
17. Wang, R., Gao, Y., Lai, L., *J. Mol. Model.*, 6(2000) 498-516.
18. Schneider, G., Lee, M.L., Stahl, M. and Schneider, P., J. Comput. Aid. Mol. Des., 14 (2000) 487.
19. Kollman, P.A., Curr. Opin. Struct. Biol., 4 (1994) 240.
20. Ajay and Murcko, M.A., J. Med. Chem., 38 (1995) 4953.
21. Tame, J.R.H., J. Comput. Aid. Mol. Des., 13 (1999) 99.
22. Goodford, P.J.A., J. Med. Chem., 28 (1985) 849.
23. Massova, I. and Kollman, P., Perspect. Drug Disc. Des., 18 (2000) 113.
24. Kollman, P., Chem. Rev., 7 (1993) 2395.
25. Aqvist, J., Medina, C. and Samuelsson, J.E., Protein Eng., 7 (1994) 385.
26. Carlson, H.A. and Jorgensen, W.L., J. Phys. Chem., 99 (1995) 10667.
27. Böhm, H.J., J. Comput. Aid. Mol. Des., 8 (1994) 243.
28. Jain, A.N., J. Comput. Aid. Mol. Des., 10 (1996) 427.
29. Head, R.D., Smythe, M.L., Oprea, T.I., Waller, C.L., Green, S.M. and Marshall, G.R., J. Am. Chem. Soc., 118 (1996) 3959.
30. Eldridge, M.D., Murray, C.W., Auton, T.R., Paolini, G.V. and Mee, R.P., J. Comput. Aid. Mol. Des., 11 (1997) 425.
31. Böhm, H.J., J. Comput. Aid. Mol. Des., 12 (1998) 309.
32. Wang, R., Gao, Y. and Lai, L., J. Mol. Model., 4 (1998) 379.
33. Charifson, P.S., Corkery, J.J., Murcko, M.A. and Walters, W.P., J. Med. Chem. 42 (1999) 5100.
34. Berman, H.M., Westbrook, J., Feng, Z., Gilliland, G., Bhat, T.N., Weissig, H., Shindyalov, I.N. and Bourne, P.E., Nucleic Acids Res., 28 (2000) 235, http://www.rcsb.org/pdb/.
35. SYBYL v6.2, Tripos Inc. St. Louis, MO, U.S.A. http://www.tripos.com/
36. Wang, R., Gao, Y. and Lai, L., Perspect. Drug Disc. Des., 19 (2000) 47.
37. Wang, R. and Wang, S., J. Chem. Inf. Comput. Sci., 41 (2001) 1422.

Anti-malarial drug development using models of enzyme structure

Zhe Li[1], Xiaowu Chen[1], Eugene Davidson[4], Oren Zwang[4], Chandana Mendis[4], Christine S Ring[1], William R Roush[5], Glenn Fegley[5], Rongshi Li[1], Philip J Rosenthal[3], Garson K Lee[3], George L Kenyon[1], Irwin D Kuntz[1,2], and Fred E Cohen[1,2,3*]

[1]Departments of Pharmaceutical Chemistry, [2]Biochemistry and Biophysics and [3]Medicine, University of California, San Francisco, CA 94143-0446, USA, [4]Department of Biochemistry and Molecular Biology, Georgetown University, Washington DC 20007, USA and [5]Department of Chemistry, Indiana University, Bloomington, IN 47405-8300, USA

Background: The trophozoite stage of the malaria parasite infects red blood cells. During this phase of their lifecycle, the parasites use hemoglobin as their principal source of amino acids, using a cysteine protease to degrade it. We have previously reported a three-dimensional model of this cysteine protease, based on the structures of homologous proteases, and the use of the program DOCK to identify a ligand for the malaria protease.

Results: Here we describe the design of improved ligands starting from this lead. Ligand design was based on the predicted configuration of the lead compound docked to the model three-dimensional structure of the protease. The lead compound has an IC_{50} of 6 μM, and our design/synthesis strategy has resulted in increasingly potent derivatives that block the ability of the parasites to infect and/or mature in red blood cells. The two best derivatives to date have IC_{50}s of 450 nM and 150 nM.

Conclusions: A new class of anti-malarial chemotherapeutics has resulted from a computational search that was based on a model of the target protease. Despite the lack of a detailed experimental structure of the target enzyme or the enzyme–inhibitor complex, we have been able to identify compounds with increased potency. These compounds approach the activity of chloroquine (IC_{50} = 20 nM), but have a distinct mechanism of action. This series of compounds could thus lead to new therapies for chloroquine-resistant malaria.

Chemistry & Biology September 1994, 1:31–37

Key words: docking strategies, homology modeling, novel anti-malarial compounds, structure–activity relationships, trophozoite cysteine protease

Introduction

The World Health Organization estimates that 280 million people are infected with malaria yearly [1]. Although various classes of anti-malarial agents exist, the most valuable are the quinoline-derived compounds, such as chloroquine and mefloquine. Chloroquine has been an especially effective drug in prophylactic and therapeutic settings, and thus the appearance of malaria strains resistant to chloroquine, and more recently, to mefloquine, poses a serious threat to travelers and to people in countries where malaria is endemic. Reports of multi-drug resistant strains of these parasites make the search for novel therapies especially urgent [2].

In this work, a novel target for anti-malarial chemotherapy is pursued. During the erythrocytic stage of their lifecycle, malaria parasites infect circulating red blood cells (RBCs) and use hemoglobin as their principal source of amino acids. Rosenthal and coworkers have identified a cysteine protease from malaria parasites that mediates host hemoglobin degradation [3]. Blocking this enzyme with cysteine protease inhibitors, such as L-*trans*-epoxysuccinylleucyl amido-(4-guanidino)butane (E-64) and peptide fluoromethyl ketones, arrests parasite growth *in vitro* [4] and cures murine malaria (*Plasmodium vinckei*) infection *in vivo* [5]. These results support the therapeutic rationale behind using the protease as a target. Inhibiting this protease may, either by itself or in conjunction with established therapies, offer an alternative treatment for malaria. Most cysteine protease inhibitors, however, are sulfhydryl reagents that covalently modify the enzyme active site, and thus may inactivate some host cysteine proteases. Noncovalent angiotensin-converting enzyme inhibitors have been successful in the treatment of hypertension [6], and the clinical success of these compounds has motivated us to develop a new class of compounds that inhibit the malarial cysteine protease through noncovalent interactions.

Results and discussion

Initial lead discovery

The discovery of a nonpeptidic lead compound, oxalic *bis*((2-hydroxy-1-naphthylmethylene)hydrazide) (ZLI48A), for the malaria cysteine protease has previously been described [7]. Briefly, a model structure for the malaria

*Corresponding author.

Fig. 1. The active site of the malarial protease and putative binding mode of the original lead compound, ZLI48A. The protease is shown in white and the ligand in gray. Oxygen and nitrogen atoms near the active site are colored in red and dark blue, respectively. The S_2, S_1, and S_1' binding subsites are shown in green, yellow, and cyan, respectively.

cysteine protease was proposed using the X-ray structures of papain and actinidin as a basis for modeling. The model structure was then used to search the Fine Chemicals Directory of commercially available small molecules (the Fine Chemicals Directory distributed by Molecular Design is currently known as the Available Chemical Directory) for putative ligands using the docking program, DOCK 3.0 [8]. Thirty-one compounds were finally tested and ZLI48A was identified as the best inhibitor of the protease. The IC_{50} value for enzyme inhibition against the substrate benzyloxycarbonyl-Phe-Arg-(7-amino-4-methylcoumarin) was 6 μM [7]. More importantly, this compound inhibits the growth of parasites in culture, as judged by its ability to block hypoxanthine uptake by malaria parasites, with an apparent IC_{50} value of 7 μM.

Circulating RBCs are a major target for malaria infection, and the magnitude of the infection can be quantified by counting the fraction of infected RBCs on a thick blood smear. This process is sufficiently laborious that it precludes the evaluation of dose-response curves for potential therapeutics in an acceptable time frame. To overcome this problem, we have developed a high-throughput assay that efficiently counts parasitized RBCs. Normally, circulating RBCs are enucleate and hence lack DNA. Parasitized RBCs contain malarial DNA. Thus, RBC staining by the DNA-binding dye propidium iodide can be exploited in an assay that uses a fluorescence-activated cell sorter (FACS) to count the fraction of infected RBCs in a rapid and automated fashion. In this assay, ZLI48A has an IC_{50} value of 4.5 μM.

Berger and Schechter [9] first demonstrated that papain-like cysteine proteases contain active sites that can accommodate up to seven amino acids. For notational convenience, the amino acid residues on the acyl side of the scissile bond are denoted P_1, P_2 . . . P_n and those on the leaving group side are labeled P_1', P_2' . . . P_n'. The corresponding binding sites on the enzyme are S_1, S_2 . . . S_n and S_1', S_2' . . . S_n'. The seven-residue binding pocket of papain-like cysteine proteases involves the S_4 through S_3' subsites. The S_2 and S_1 subsites are those most responsible for the peptide cleavage specificity of this class of enzymes. The most stable conformer of ZLI48A is symmetric about its midpoint, with a second axis of pseudosymmetry about the backbone. Thus, there are essentially two ways to orient the compound in the active site. In both cases, the compound lies across the active site cleft of the malaria cysteine protease with one naphthyl group fitting into the S_2 pocket and with the other stacking with the indole ring of Trp177 in the S_1' pocket. The presumed binding mode is shown in Fig. 1. This orientation was chosen as the working model for the orientation in the complex, because it maximizes the compound's interaction with the enzyme, with each hydroxyl group within hydrogen bonding distance of a suitable residue in the enzyme (Ser160 and Gln19). Alternatively, the compound could be rotated 180 degrees about the horizontal axis of pseudosymmetry. In this orientation, the hydroxyl groups seem to interact with the enzyme less effectively but might interact with solvent water molecules.

Lead optimization

The starting point for lead optimization was the protease–ZLI48A complex generated by the program DOCK 3.0 [10]. Kuntz and colleagues developed the DOCK algorithm to capture the static geometric features of a molecular recognition site. In the malarial protease work, the homology-based model of the enzyme provides the template, and the DOCK algorithm identifies a set of spheres with approximately atom-sized radii to fill the active site cleft. Frequently, many overlapping spheres are used to fill the cleft, and a clustering algorithm is used to reduce the complexity of the sphere representation. Preliminary binding modes for a compound are defined through attempts to match the centers of cleft spheres with the centers of atoms within the compound of interest. Within DOCK 3.0, the quality of a compound's fit to the binding cleft can be evaluated based on its shape complementarity (contact score) or molecular mechanics interaction energy (AMBER force field score). When searching a database of compounds, DOCK 3.0 examines only the best orientation of the small molecule within the binding cleft (DOCK database screening mode). When a single compound is studied, multiple possible binding modes can be examined (DOCK single mode). Of course, the initial orientation of the compound is dictated, in part,

by the irregular lattice of sphere centers identified originally. To overcome some of the scoring distortion that this bias could impart, a rigid body minimization algorithm has been developed to move the ligand modest distances within the binding cleft and optimize the interaction energies. The use of a rigid body minimization algorithm reflects the trade-off between the need for rapid evaluation and the reality that many ligands are flexible. ZLI48A was selected based on its score for shape complementarity. Rigid body minimization was applied to the ligand positioned in a preliminary orientation in the active site cleft so that other contributory factors (van der Waals and electrostatic interactions) required for efficient binding could be reflected in the enzyme–ligand complex (see Fig. 2).

The energetics of the enzyme–ligand assembly depends heavily upon the detailed conformation of the complex. Unfortunately, errors in the precise geometry of the complex are likely given the computational origins of the model. Potential problems could result from the fact that gross conformational changes can occur between the complexed and uncomplexed enzyme structures. In papain, the active site cleft widens upon binding a peptide-like ligand [11]. In the HIV protease, the flaps around the active site close on the substrate with backbone movements as large as 7 Å [12,13]. Ligands are also able to alter their conformations upon binding to the enzyme. For example, the structures of methotrexate alone and complexed to dihydrofolate reductase are dramatically different [14]. Consequently, choosing the relevant conformations of both enzyme and ligand can be critical for successful inhibitor design. Unfortunately, such structural changes are difficult to anticipate *a priori* and so our approach to ligand design is guided by, rather than dependent solely upon, the model of the ligand–enzyme structure.

Despite these uncertainties, a reasonable structure of the enzyme and/or enzyme–ligand complex has proven to be very useful. In this project, the malarial cysteine protease was modeled by homology to the known structures of papain and actinidin. The malarial protease has 33 % sequence identity with both enzymes. The anticipated root mean-square errors average approximately 1.5 Å for the core of the molecule [15]. Fortunately, the errors within the active site should be smaller, as it is the most conserved portion of the structure. The ligand conformation was calculated using CONCORD, an algorithm that relies on heuristic rules for translating chemical connectivities into three-dimensional coordinates [16]. This could create errors in the models of the ligand conformation. Because of the uncertainties inherent in the models of both the enzyme and the ligands, sophisticated energy calculations such as free energy perturbation are not warranted. The interpretation of these results would be difficult at best.

The model of the protease–ZLI48A complex has aryl groups filling the S_1' and S_2' pockets, but the S_1 pocket is only partially filled. In addition, although the conjugated eight-atom backbone of ZLI48A is most likely to be found in the all *anti*-conformation, *syn* isomers are possible that should not fit into the protease active site. We therefore designed analogs of ZLI48A that have a less flexible backbone, fill the S_2 and S_1 or S_2, S_1, and S_1' subsites, and effectively interact with the side chains lining the subsite specificity pockets. Because malaria is endemic principally in developing countries, useful anti-malarial agents must be inexpensive to produce. We thus favored analogs that are easily synthesized from relatively inexpensive starting materials in a small number of steps. The basic strategy for lead optimization is outlined in Fig. 3.

Starting with the rigid-body minimized complex of enzyme–ZLI48A, and using the strategy highlighted above, we explored the S_2, S_1, and S_1' subsites by varying the size of the aromatic rings, the linker lengths, and the substituents of the aromatic rings. A third aromatic ring system was also introduced (tri-aryl compounds) to study the concerted binding of the ligand molecule to the S_2, S_1 and S_1' subsites. Newly synthesized compounds were tested by FACS assay for their potency in inhibiting

Fig. 2. Optimization of the orientation of ZLI48A using rigid body minimization. The initial positioning of the ligand in the active site cleft (red) was estimated to have an interaction energy of 27.7 kcal mol^{-1} using the AMBER force field. After 12 steps of minimization, the ligand (purple) moved 0.74 Å and the energy was lowered to −35.3 kcal mol^{-1}. Although the change in the position of the ligand was small, the difference between the energies of the starting and final conformations is significant. Green, yellow, and cyan colors highlight key residues in the S_2, S_1, and S_1' binding subsites, respectively.

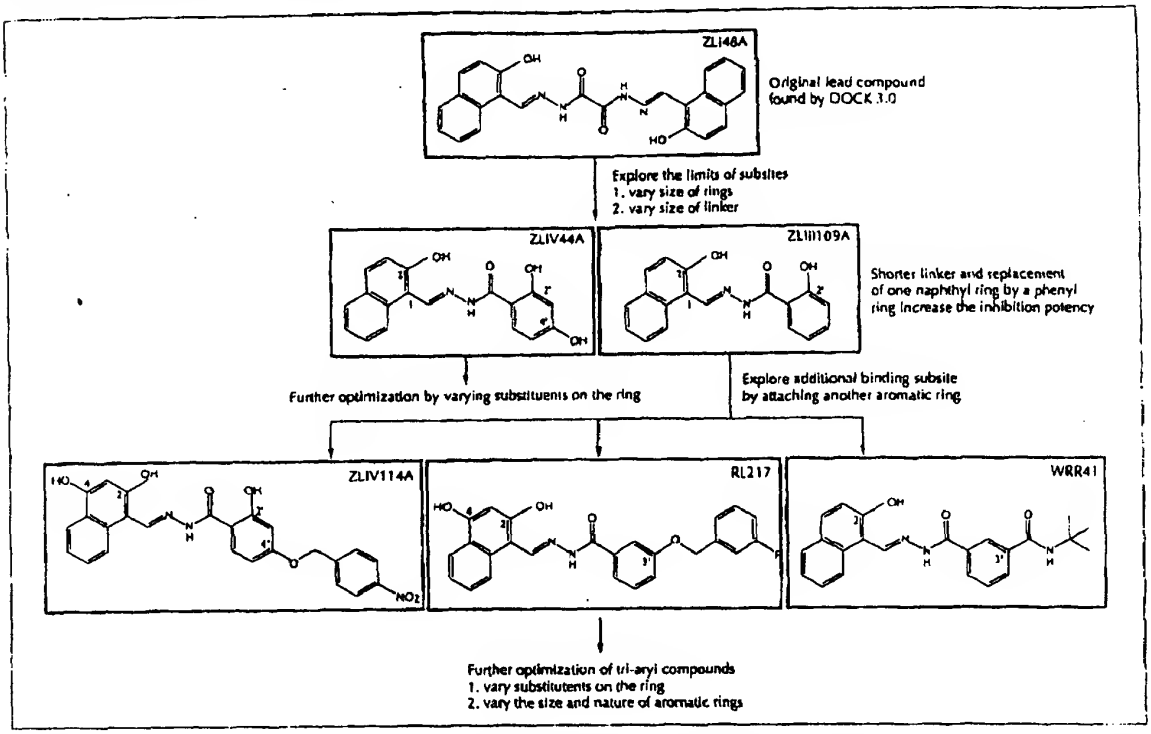

Fig. 3. Strategy for lead optimization. The fit of the compound within the S_2, S_1 and S_1' subsites was explored by varying the size of the aromatic rings and the length of the linker, and further optimized by varying ring substituents. A third aromatic system was also introduced to explore the concerted binding of the ligand to these subsites. Six compounds are shown in this chart to illustrate the strategy.

parasite growth. The assay results of some representative compounds are shown in Fig. 4.

From a study of analogs with varying linker lengths and ring sizes, we found that compounds with half the length of the original linker and a phenyl ring instead of a naphthyl ring (compound ZLIII109A in Fig. 4) seemed to be twice as effective as the original lead, ZLI48A. A series of compounds was also made to test the role of ring substituents on inhibitor potency. It seems that hydroxyl groups at the 2, 2', and 4' positions are required for effective inhibition. The most potent compound (ZLIV44A) has an IC_{50} value of 150 nM. The best tri-aryl inhibitor tested so far, ZLIV114A, has an IC_{50} value of 450 nM. Overall, the four compounds listed in Fig. 4 have absolute IC_{50} values at or below 1 μM. It is clear from Fig. 4 that there is a progressive increase in inhibition potency following the design, synthesis, and testing paradigm.

Modeling of ligand binding

DOCK calculations (in DOCK single mode) of the binding of a series of *bis* aromatic compounds with one naphthyl ring, a short linker, and one smaller aromatic ring reveal some interesting insights. The results indicate that there are essentially two ways to orient an asymmetric ligand. Both binding modes are similar to that for the symmetrical ZLI48A, shown in Fig. 1. In one binding mode (Fig. 5a), the larger naphthyl ring interacts with the deeper, well-defined S_2 specificity subsite, whereas the phenyl ring binds to the more accessible, but less well-defined, S_1' subsite. Alternatively, the ligand molecule can be rotated 180 degrees around the S_1 subsite (Fig. 5b). In this binding mode, the naphthyl ring now interacts with the S_1' subsite, whereas the phenyl ring binds to the S_1 and S_2 subsites. Compounds with three aromatic components seem more likely to adopt the binding mode shown in Fig. 5a. In this orientation, the larger naphthyl ring binds to the well-formed S_2 subsite and the third ring now interacts fully with the more accessible, less well-defined S_1' subsite.

A recent report on the structures of inhibitors bound to the serine protease elastase, with K_is as small as 10 nM, shows that chemically similar inhibitors can adopt different binding modes and interact with different subsites [17]. Several inhibitors were found to bind to the enzyme in an orientation opposite to that of natural substrate and other chemically similar inhibitors. The compounds with two-fold degeneracy that we have designed and tested may also bind to the malarial protease with more than one binding mode. Obviously, this could complicate the development of a structure–activity relationship. Further work is under way to explore the availability of alternative binding modes.

In either binding mode, it seems that polar substituents on either aromatic ring can potentially form hydrogen bonds with a number of side chains lining the binding subsites as well as with backbone oxygen and nitrogen atoms from some loop residues. This observation is consistent with our finding that the 2 and 2' hydroxyl groups are required for effective inhibition. Substitutions at other positions, such as 4 and 4', are also associated with increased potency. For example, calculation of the model of the protease–ZLIII109A complex suggests possible hydrogen bonding interactions between residues Gln19, His67, Cys25, Asn133, His159, Ser160, Trp177 and the ligand oxygen and nitrogen atoms. Presumably, this explains part of the correlation between these ligand hydroxyl groups and compound potency. The modeling studies also provide a basis for the design of other tri-aryl compounds, a group of ligands that could lead to even more potent inhibitors via their extensive interactions with the protease subsites.

Conclusions

We report here the results of a structure-based approach for inhibitor design targeted toward a critical malarial protease. Starting with a lead compound identified by computer screening of a three-dimensional small molecule database, we have designed molecules with significantly increased inhibition potency against malaria parasites. This method provides a practical strategy for future work on structure-based drug design even in the absence of a crystallographic structure of the target enzyme. Our approach not only emphasizes the structural rationale for inhibitor design, but also uses simple chemistry and commercially available starting materials for inhibitor synthesis. This approach permits us to screen a relatively large number of potential inhibitors rapidly and inexpensively.

The potency of this new class of compounds in preventing parasite growth *in vitro* begins to approach that of available traditional quinoline-based drugs. As their target is distinct from that of chloroquine, these compounds should be effective against chloroquine-resistant strains of the malaria parasite. The FACS assay we used in this report provides a practical and relevant method for evaluating inhibitor potency. The combination of structure-based screening and design coupled with simple chemical synthesis and a relevant biological assay has rapidly led to identification of a series of increasingly potent anti-malarial agents. Although therapeutic candidates will need to be active at low nanomolar concentrations, we anticipate that modifications of existing analogs will result in molecules that are suitable for preclinical efficacy and toxicology studies.

Significance

Malaria parasites, usually *Plasmodium falciparum* and *Plasmodium vivax*, infect 280 million people annually [1], and multi-drug resistant *P. falciparum* has become a significant pathogen in areas where the disease is endemic. We have chosen a cysteine protease that is central to the parasite's life cycle but distinct from the target of chloroquine action as a target for a structure-based drug development program. The choice of this target means that the chemotherapeutics that we develop should be active against chloroquine-resistant organisms.

Structure-based drug design usually depends upon the experimental determination of the target structure by X-ray crystallography or NMR spectroscopy. We have circumvented this step and relied exclusively on the sequence homology between the malaria enzyme and other cysteine proteases of known structure. A homology-based

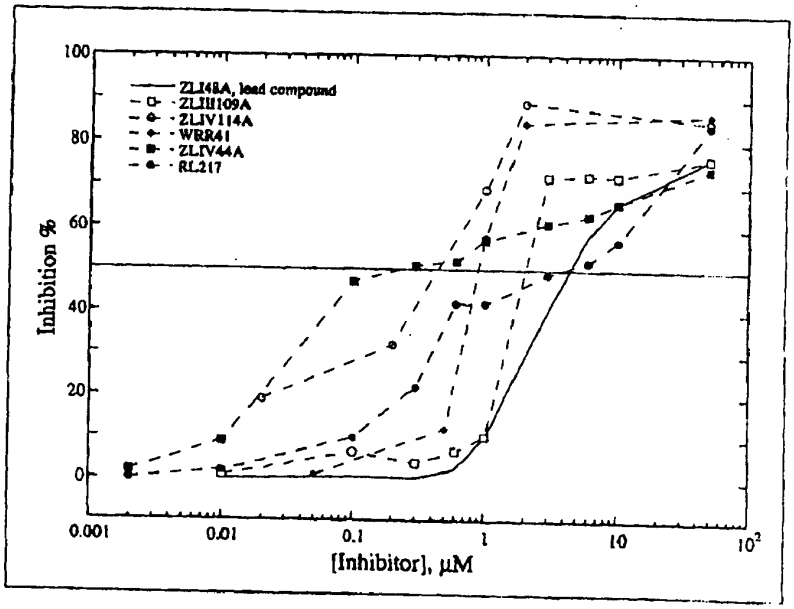

Fig. 4. Inhibition of the growth of malaria parasites in red blood cells by ZLI48A, the initial lead compound, and selected derivatives.

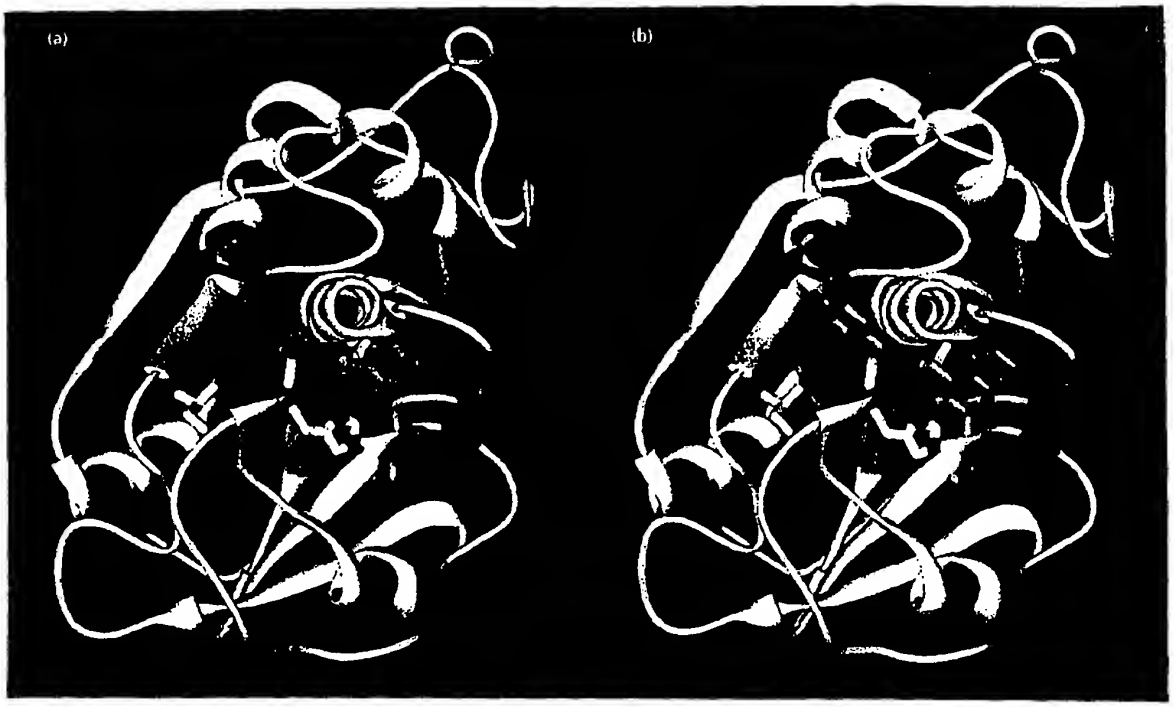

Fig. 5. Two putative binding modes of a representative *bis*-aryl compound ZLIV44A. In (a) the larger naphthyl ring interacts with S_2, whereas in (b) it interacts with the S_1 subsite. The protease is shown in white and the ligand in gray. Oxygen and nitrogen atoms near the active site are colored in red and dark blue, respectively. The S_2, S_1, and S_1' binding subsites are shown in green, yellow, and cyan, respectively.

model of the malaria enzyme was used as the template for a computer-based ligand docking calculation that identified a useful lead compound. Lead optimization was achieved by a combined approach of computational and synthetic analysis. Derivatives of the lead were first optimized for fit using the computer docking program, then synthesized and experimentally tested.

The entire process of lead optimization was completed in eighteen months and resulted in the identification of compounds that are about ten times more effective than the initial lead and are simple and inexpensive to produce. This study shows that it is possible to start with a protein sequence and end with non-peptidic small molecule inhibitors of a medically relevant target enzyme. Thus, there may be many more systems amenable to structure-based drug development efforts than was previously believed.

Materials and Methods

Computer modeling

The three-dimensional structures of potential inhibitors were constructed interactively using the molecular modeling program SYBYL and the CONCORD conversion algorithm (Tripos Associates, St Louis, MO). The Cambridge Crystallographic Database was used to determine probable low-energy conformations of certain ligand groups. Partial charges of ligands were calculated using the Gasteiger–Marsili method. DOCK 3.0 was used in single ligand mode to aid inhibitor design. All plausible binding orientations of a single ligand that meet certain user-defined criteria (contact and force field scores) were obtained by DOCK. Rigid body minimization of DOCK-derived ligand–protease complexes were performed to optimize the interaction energy between the protease and the ligand. This method provides a detailed profile of potential binding orientations of a ligand molecule in the active site of the malarial protease. All computer-assisted modeling and docking studies were carried out using a Silicon Graphics workstation IRIS4D/35 or Indigo2. All color figures were produced using the MidasPlus program from the Computer Graphics Laboratory, University of California, San Francisco (supported by NIH RR-01081) [18,19].

Biological assay

An assay based on FACS analysis was used to evaluate the potency of the compounds reviewed in this paper against parasite growth. Synchronized trophozoite-stage parasites were cultured in human blood at various inhibitor concentrations. The parasites were allowed to mature, lyse the host cell and attempt invasion of fresh red blood cells. Using propidium iodide to stain DNA, the FACS can discriminate between infected and uninfected cells and between stages of intra-erythrocytic parasite development, as only infected red blood cells contain DNA [20].

Because all of the clinical manifestations of malaria are caused by the erythrocytic cycle of lysis and reinfection, this assay is especially relevant for evaluating the efficacy of potential anti-malarial agents. The full dose inhibition curves for oxalic *bis*((2-hydroxy-1-naphthylmethylene)hydrazide) and several of the key derivatives are shown in Fig. 4.

Chemical syntheses

2-Hydroxy-1-naphthaldehyde, oxalic dihydrazide, salicylic hydrazide, methyl 2,4-dihydroxybenzoate and 4-nitrobenzyl bromide were all purchased from Aldrich. 2,4-Dihydroxybenzoic hydrazide was obtained from Trans World Chemicals. 2,4-Dihydroxynaphthaldehyde was prepared from 1,3-dihydroxynaphthalenes (Aldrich) according to published procedures [21].

General procedure for condensation of aldehyde with acylhydrazine: to a solution of the aldehyde (1 mmol) in methanol (20 ml) was added the corresponding acylhydrazine (1 mmol) in one portion. The resulting mixture was heated at reflux for 3 h. In most cases, a precipitate was observed after 10 min. The precipitate was filtered, washed with hot methanol (50 ml) and dried in vacuum (2 mm Hg). If needed, additional purification was performed by recrystallization using appropriate solvents.

For the tri-aryl compounds, the acylhydrazine was made as follows: a mixture of benzyl bromide (10.0 mmol), methyl hydroxybenzoate (10.0 mmol) and cesium carbonate (10.0 mmol) in acetone (80 ml) was heated at 56 °C for 18 h. This mixture was filtered, and the filtrate was concentrated to give the corresponding methyl phenylmethyleneoxybenzoate. This crude methyl ester was then dissolved in EtOH (80 ml) and treated with hydrazine monohydrate (5.01 g, 100.0 mmol). The resulting mixture was stirred overnight at 20 °C and then concentrated to give the corresponding acylhydrazide, which was further purified by recrystallization from EtOH/H_2O (7:3, v/v). The structures of these compounds were confirmed by spectroscopic methods.

Acknowledgements: We thank Dr Elaine Meng and Daniel Gschwend for useful comments on DOCK simulations. This work was supported by grants from the Advanced Research Projects Agency (MDA-972-91-J1013; N00014-90-2032), the National Institutes of Health (GM 39900), and the UNDP/World Bank/WHO Special Program for Research and Training in Tropical Diseases (TDR890499). The MidasPlus program from the Computer Graphics Laboratory, University of California, San Francisco was supported by the National Institutes of Health (RR-01081). Molecular Design Ltd Information Systems and Tripos Associates kindly provided software materials.

References

1. Gibbons, A. (1992). Researchers fret over neglect of 600 million patients. *Science* **256**, 1135.
2. Bruce-Chwatt, L.J. (1985). *Essential Malariology*. (2nd edn), Wiley, New York.
3. Rosenthal, P.J., McKerrow, J.H., Aikawa, M., Nagasawa, H. & Leech, J.H. (1988). A malarial cysteine proteinase is necessary for hemoglobin degradation by *Plasmodium falciparum*. *J. Clin. Invest.* **82**, 1560–1566.
4. Rosenthal, P.J., Wollish, W.S., Palmer, J.T. & Rasnick, D. (1991). Antimalarial effects of peptide inhibitors of a *Plasmodium falciparum* cysteine proteinase. *J. Clin. Invest.* **88**, 1467–1472.
5. Rosenthal, P.J., Lee, G.K. & Smith, R.E. (1993). Inhibition of a *Plasmodium vinckei* cysteine proteinase cures murine malaria. *J. Clin. Invest.* **91**, 1052–1056.
6. Williams, G.H. (1988). Converting-enzyme inhibitors in the treatment of hypertension. *New England J. Med.* **319**, 1517–1525.
7. Ring, C.S., *et al.*, & Cohen, F.E. (1993). Structure-based inhibitor design using model built structures. *Proc. Natl. Acad. Sci. USA* **90**, 3583–3587.
8. Kuntz, I.D. (1992). Structure-based strategies for drug design and discovery. *Science* **257**, 1078–1082.
9. Berger, A. & Schechter, I. (1970). Mapping the active site of papain with the aid of peptide substrates and inhibitors. *Philos. Trans. R. Soc. Lond. (Biol.)* **257**, 149–264.
10. Meng, E.C., Shoichet, B.K. & Kuntz, I.D. (1992). Automated docking with grid-based energy evaluation. *J. Comp. Chem.* **13**, 505–524.
11. Drenth, J., Kalk, K.H. & Swen, H.M. (1976). Binding of chloromethyl ketone substrate analogues to crystalline papain. *Biochemistry* **15**, 3731–3738.
12. Wlodawer, A., Miller, M., Jaskolski, M., Sathyanarayana, B.K., Baldwin, E., Weber, I.T., Selk, L.M., Clawson, L., Schneider, J. & Kent, S.B. (1988). Conserved folding in retroviral proteases: crystal structure of synthetic HIV-1 protease. *Science* **245**, 616–621.
13. Miller, M., Schneider, J., Sathyanarayana, B.K., Toth, M.V., Marshall, G.R. & Clawson, L. (1989). Structure of complex of synthetic HIV-1 protease with a substrate-based inhibitor at 2.3 Å resolution. *Science* **246**, 1149–1152.
14. Bolin, J.T., Filman, D.J., Matthews, D.A., Hamlin, R.C. & Kraut, J. (1982). Crystal structures of *Escherichia coli* and *Lactobacillus casei* dihydrofolate reductase refined at 1.7 Å resolution. I. General features and binding of methotrexate. *J. Biol. Chem.* **257**, 13650–13662.
15. Chothia, C. & Lesk, A. (1986). The relation between the divergence of sequence and structure in proteins. *EMBO J.* **5**, 823–826.
16. Pearlman, R.S. (1991). 3D-searching: an overview of a new technique for computer-assisted molecular design. *Nida Research Monograph* **112**, 62–77.
17. Mattos, C., Rasmussen, B., Ding, X., Petsko, G.A. & Ringe, D. (1994). Analogous inhibitors of elastase do not always bind analogously. *Nature Struct. Biol.* **1**, 55–58.
18. Ferrin, T.E., Huang, C.C., Jarvis, L.E. & Langridge, R. (1988). The Midas display system. *J. Mol. Graph.* **6**, 13–37.
19. Huang, C.C., Pettersen, E.F., Klein, T.E., Ferrin, T.E & Langridge, R. (1991). Conic: A fast renderer for space-filling molecules with shadows. *J. Mol. Graph.* **9**, 230–236.
20. Clark, D.L., Chrisey, L.A., Campbell, F.R. & Davidson, E.A. (1994). Non-sequence specific antimalarial activity of oligodeoxynucleotides. *Molec. Biochem. Parasitol.* **63**, 129–134.
21. Morgan, G.T. & Vining, D.C. (1921). Dihydroxynaphthaldehydes. *J. Chem. Soc.* **119**, 177–187.

Received: **13 Apr 1994**; revisions requested: **29 Apr 1994**; revisions received: **17 Jun 1994**. Accepted: **22 Jun 1994**.

~~Figure 1~~

ATOM	1	CB	GLU	1	55.967	11.986	66.300	1.00 59.11	AAAA C
ATOM	2	CG	GLU	1	56.138	11.012	65.162	1.00 79.17	AAAA C
ATOM	3	CD	GLU	1	57.382	11.319	64.321	1.00 85.10	AAAA C
ATOM	4	OE1	GLU	1	58.404	10.754	64.796	1.00 86.18	AAAA O
ATOM	5	OE2	GLU	1	57.424	12.013	63.270	1.00 78.70	AAAA O
ATOM	6	C	GLU	1	53.508	12.557	66.350	1.00 48.46	AAAA C
ATOM	7	O	GLU	1	52.685	11.863	65.784	1.00 51.27	AAAA O
ATOM	10	N	GLU	1	54.256	10.338	67.159	1.00 61.64	AAAA N
ATOM	12	CA	GLU	1	54.602	11.778	67.081	1.00 54.77	AAAA C
ATOM	13	N	ILE	2	53.608	13.860	66.375	1.00 37.66	AAAA N
ATOM	15	CA	ILE	2	52.769	14.699	65.604	1.00 40.87	AAAA C
ATOM	16	CB	ILE	2	52.925	16.122	66.160	1.00 41.97	AAAA C
ATOM	17	CG2	ILE	2	52.036	17.122	65.484	1.00 38.50	AAAA C
ATOM	18	CG1	ILE	2	52.560	16.006	67.663	1.00 46.58	AAAA C
ATOM	19	CD1	ILE	2	53.150	17.176	68.498	1.00 32.29	AAAA C
ATOM	20	C	ILE	2	53.122	14.711	64.139	1.00 46.47	AAAA C
ATOM	21	O	ILE	2	54.258	15.029	63.852	1.00 51.65	AAAA O
ATOM	22	N	CYS	3	52.235	14.409	63.196	1.00 49.61	AAAA N
ATOM	24	CA	CYS	3	52.435	14.677	61.773	1.00 38.93	AAAA C
ATOM	25	C	CYS	3	51.429	15.708	61.302	1.00 42.06	AAAA C
ATOM	26	O	CYS	3	50.290	15.521	61.690	1.00 42.37	AAAA O
ATOM	27	CB	CYS	3	52.159	13.415	60.999	1.00 35.66	AAAA C
ATOM	28	SG	CYS	3	53.019	12.004	61.674	1.00 36.98	AAAA S
ATOM	29	N	GLY	4	51.851	16.709	60.580	1.00 42.39	AAAA N
ATOM	31	CA	GLY	4	50.973	17.718	60.003	1.00 47.71	AAAA C
ATOM	32	C	GLY	4	51.703	18.407	58.869	1.00 48.23	AAAA C
ATOM	33	O	GLY	4	52.916	18.345	58.884	1.00 55.36	AAAA O
ATOM	34	N	PRO	5	51.056	19.212	58.048	1.00 49.63	AAAA N
ATOM	35	CD	PRO	5	51.637	19.947	56.860	1.00 45.28	AAAA C
ATOM	36	CA	PRO	5	49.605	19.341	58.083	1.00 41.57	AAAA C
ATOM	37	CB	PRO	5	49.397	20.703	57.474	1.00 44.30	AAAA C
ATOM	38	CG	PRO	5	50.632	21.036	56.683	1.00 46.43	AAAA C
ATOM	39	C	PRO	5	48.932	18.217	57.354	1.00 36.40	AAAA C
ATOM	40	O	PRO	5	49.403	17.094	57.396	1.00 43.35	AAAA O
ATOM	41	N	GLY	6	47.787	18.438	56.795	1.00 39.15	AAAA N
ATOM	43	CA	GLY	6	46.896	17.336	56.350	1.00 39.24	AAAA C
ATOM	44	C	GLY	6	47.710	16.365	55.529	1.00 33.68	AAAA C
ATOM	45	O	GLY	6	48.510	16.863	54.753	1.00 36.00	AAAA O
ATOM	46	N	ILE	7	47.586	15.111	55.788	1.00 35.70	AAAA N
ATOM	48	CA	ILE	7	48.307	14.053	55.141	1.00 37.65	AAAA C
ATOM	49	CB	ILE	7	48.556	12.797	55.933	1.00 36.31	AAAA C
ATOM	50	CG2	ILE	7	49.043	11.700	54.988	1.00 34.67	AAAA C
ATOM	51	CG1	ILE	7	49.561	12.857	57.067	1.00 39.34	AAAA C
ATOM	52	CD1	ILE	7	49.678	14.249	57.668	1.00 40.22	AAAA C
ATOM	53	C	ILE	7	47.338	13.762	53.977	1.00 45.00	AAAA C
ATOM	54	O	ILE	7	46.150	13.843	54.195	1.00 51.52	AAAA O
ATOM	55	N	ASP	8	47.767	13.631	52.751	1.00 45.60	AAAA N
ATOM	57	CA	ASP	8	46.938	13.283	51.631	1.00 44.05	AAAA C
ATOM	58	CB	ASP	8	47.003	14.469	50.651	1.00 44.21	AAAA C
ATOM	59	CG	ASP	8	45.909	14.379	49.600	1.00 43.48	AAAA C
ATOM	60	OD1	ASP	8	45.660	13.262	49.096	1.00 51.77	AAAA O
ATOM	61	OD2	ASP	8	45.253	15.374	49.251	1.00 46.84	AAAA O
ATOM	62	C	ASP	8	47.428	12.000	50.992	1.00 42.10	AAAA C
ATOM	63	O	ASP	8	48.423	12.143	50.330	1.00 48.50	AAAA O
ATOM	64	N	ILE	9	47.096	10.817	51.321	1.00 42.76	AAAA N
ATOM	66	CA	ILE	9	47.441	9.505	50.939	1.00 44.05	AAAA C
ATOM	67	CB	ILE	9	47.212	8.483	52.077	1.00 40.82	AAAA C
ATOM	68	CG2	ILE	9	47.669	7.085	51.653	1.00 36.35	AAAA C
ATOM	69	CG1	ILE	9	47.888	8.917	53.364	1.00 41.17	AAAA C
ATOM	70	CD1	ILE	9	49.376	8.947	53.286	1.00 43.78	AAAA C
ATOM	71	C	ILE	9	46.530	9.137	49.794	1.00 51.48	AAAA C
ATOM	72	O	ILE	9	45.338	9.420	49.832	1.00 63.05	AAAA O
ATOM	73	N	ARG	10	47.004	8.417	48.812	1.00 54.87	AAAA N
ATOM	75	CA	ARG	10	46.283	8.089	47.600	1.00 54.17	AAAA C
ATOM	76	CB	ARG	10	45.703	9.358	47.023	1.00 48.54	AAAA C
ATOM	77	CG	ARG	10	46.361	10.169	45.952	1.00 46.55	AAAA C
ATOM	78	CD	ARG	10	46.002	11.635	46.264	1.00 52.63	AAAA C
ATOM	79	NE	ARG	10	45.082	12.226	45.284	1.00 59.27	AAAA N
ATOM	81	CZ	ARG	10	44.269	13.262	45.498	1.00 56.22	AAAA C
ATOM	82	NH1	ARG	10	44.153	13.891	46.666	1.00 55.14	AAAA N
ATOM	85	NH2	ARG	10	43.455	13.803	44.602	1.00 52.29	AAAA N
ATOM	88	C	ARG	10	47.019	7.373	46.492	1.00 57.23	AAAA C
ATOM	89	O	ARG	10	48.240	7.288	46.281	1.00 56.32	AAAA O
ATOM	90	N	ASN	11	46.248	6.654	45.629	1.00 57.23	AAAA N
ATOM	92	CA	ASN	11	46.800	5.917	44.494	1.00 50.73	AAAA C
ATOM	93	CB	ASN	11	47.704	6.798	43.671	1.00 44.65	AAAA C
ATOM	94	CG	ASN	11	46.878	7.732	42.829	1.00 50.72	AAAA C
ATOM	95	OD1	ASN	11	45.749	7.451	42.403	1.00 72.59	AAAA O
ATOM	96	ND2	ASN	11	47.499	8.869	42.587	1.00 54.38	AAAA N
ATOM	99	C	ASN	11	47.635	4.736	44.915	1.00 53.07	AAAA C
ATOM	100	O	ASN	11	47.393	3.701	44.347	1.00 51.95	AAAA O
ATOM	101	N	ASP	12	48.566	4.822	45.878	1.00 50.96	AAAA N
ATOM	103	CA	ASP	12	49.204	3.570	46.263	1.00 55.44	AAAA C

Figure 1

ATOM	194	CB	ASP	12	50.668	3.568	45.758	1.00	66.47	AAAA C
ATOM	195	CG	ASP	12	50.879	4.026	44.314	1.00	68.25	AAAA C
ATOM	196	OD1	ASP	12	50.441	3.185	43.457	1.00	58.31	AAAA O
ATOM	197	OD2	ASP	12	51.391	5.120	43.989	1.00	70.56	AAAA O
ATOM	198	C	ASP	12	49.061	3.322	47.758	1.00	59.23	AAAA C
ATOM	199	O	ASP	12	49.687	3.849	48.711	1.00	59.65	AAAA O
ATOM	110	N	TYR	13	48.411	2.197	48.036	1.00	59.64	AAAA N
ATOM	112	CA	TYR	13	48.328	1.672	49.397	1.00	64.06	AAAA C
ATOM	113	CB	TYR	13	47.968	0.196	49.409	1.00	64.56	AAAA C
ATOM	114	CG	TYR	13	47.467	-0.357	50.721	1.00	69.18	AAAA C
ATOM	115	CD1	TYR	13	46.216	-0.024	51.248	1.00	72.71	AAAA C
ATOM	116	CE1	TYR	13	45.746	-0.541	52.450	1.00	71.51	AAAA C
ATOM	117	CD2	TYR	13	48.233	-1.247	51.457	1.00	70.36	AAAA C
ATOM	118	CE2	TYR	13	47.788	-1.778	52.661	1.00	71.64	AAAA C
ATOM	119	CZ	TYR	13	46.542	-1.420	53.160	1.00	71.31	AAAA C
ATOM	120	OH	TYR	13	46.144	-1.977	54.358	1.00	63.25	AAAA O
ATOM	122	C	TYR	13	49.622	1.839	50.198	1.00	65.99	AAAA C
ATOM	123	O	TYR	13	49.621	2.321	51.354	1.00	65.01	AAAA O
ATOM	124	N	GLN	14	50.786	1.541	49.594	1.00	63.51	AAAA N
ATOM	126	CA	GLN	14	52.078	1.681	50.218	1.00	63.51	AAAA C
ATOM	127	CB	GLN	14	53.174	1.318	49.219	1.00	68.37	AAAA C
ATOM	128	CG	GLN	14	52.963	-0.078	48.686	1.00	84.62	AAAA C
ATOM	129	CD	GLN	14	53.990	-0.515	47.754	1.00	92.28	AAAA C
ATOM	130	OE1	GLN	14	53.945	-0.161	46.573	1.00	94.82	AAAA O
ATOM	131	NE2	GLN	14	54.920	-1.254	48.361	1.00	98.03	AAAA N
ATOM	134	C	GLN	14	52.434	3.058	50.753	1.00	61.62	AAAA C
ATOM	135	O	GLN	14	53.266	3.292	51.644	1.00	62.09	AAAA O
ATOM	136	N	GLN	15	51.628	4.038	50.349	1.00	57.02	AAAA N
ATOM	138	CA	GLN	15	51.724	5.399	50.831	1.00	51.71	AAAA C
ATOM	139	CB	GLN	15	50.861	6.220	49.911	1.00	43.75	AAAA C
ATOM	140	CG	GLN	15	51.566	6.605	48.648	1.00	59.65	AAAA C
ATOM	141	CD	GLN	15	51.554	8.105	48.428	1.00	72.96	AAAA C
ATOM	142	OE1	GLN	15	51.168	9.005	49.184	1.00	80.58	AAAA O
ATOM	143	NE2	GLN	15	52.016	8.378	47.211	1.00	74.17	AAAA N
ATOM	146	C	GLN	15	51.219	5.530	52.258	1.00	50.15	AAAA C
ATOM	147	O	GLN	15	51.576	6.500	52.940	1.00	48.04	AAAA O
ATOM	148	N	LEU	16	50.440	4.535	52.688	1.00	46.22	AAAA N
ATOM	150	CA	LEU	16	49.913	4.449	54.019	1.00	45.52	AAAA C
ATOM	151	CB	LEU	16	48.950	3.295	54.159	1.00	37.73	AAAA C
ATOM	152	CG	LEU	16	47.502	3.425	53.707	1.00	41.40	AAAA C
ATOM	153	CD1	LEU	16	46.857	2.063	53.790	1.00	42.43	AAAA C
ATOM	154	CD2	LEU	16	46.687	4.424	54.545	1.00	35.93	AAAA C
ATOM	155	C	LEU	16	51.042	4.280	55.039	1.00	51.52	AAAA C
ATOM	156	O	LEU	16	50.913	4.601	56.235	1.00	52.53	AAAA O
ATOM	157	N	LYS	17	52.252	3.936	54.560	1.00	51.01	AAAA N
ATOM	159	CA	LYS	17	53.422	3.914	55.404	1.00	50.73	AAAA C
ATOM	160	CB	LYS	17	54.609	3.252	54.737	1.00	56.10	AAAA C
ATOM	161	CG	LYS	17	54.539	1.733	54.831	1.00	62.40	AAAA C
ATOM	162	CD	LYS	17	54.768	1.278	53.387	1.00	63.85	AAAA C
ATOM	163	CE	LYS	17	55.316	-0.141	53.426	1.00	68.40	AAAA C
ATOM	164	NZ	LYS	17	56.537	-0.225	52.554	1.00	73.83	AAAA N
ATOM	168	C	LYS	17	53.944	5.270	55.852	1.00	44.78	AAAA C
ATOM	169	O	LYS	17	54.492	5.262	56.933	1.00	39.39	AAAA O
ATOM	170	N	ARG	18	53.524	6.344	55.201	1.00	41.15	AAAA N
ATOM	172	CA	ARG	18	53.827	7.673	55.676	1.00	43.01	AAAA C
ATOM	173	CB	ARG	18	53.250	8.702	54.704	1.00	43.97	AAAA C
ATOM	174	CG	ARG	18	53.888	8.764	53.333	1.00	53.60	AAAA C
ATOM	175	CD	ARG	18	52.961	9.362	52.269	1.00	60.34	AAAA C
ATOM	176	NE	ARG	18	52.528	10.703	52.650	1.00	50.00	AAAA N
ATOM	178	CZ	ARG	18	51.628	11.444	52.021	1.00	48.86	AAAA C
ATOM	179	NH1	ARG	18	51.068	10.941	50.943	1.00	47.96	AAAA N
ATOM	182	NH2	ARG	18	51.377	12.656	52.555	1.00	43.72	AAAA N
ATOM	185	C	ARG	18	53.268	7.924	57.077	1.00	44.03	AAAA C
ATOM	186	O	ARG	18	53.402	9.010	57.644	1.00	45.53	AAAA O
ATOM	187	N	LEU	19	52.145	7.069	57.632	1.00	46.36	AAAA N
ATOM	189	CA	LEU	19	51.653	7.282	58.794	1.00	50.25	AAAA C
ATOM	190	CB	LEU	19	50.198	6.924	58.674	1.00	50.83	AAAA C
ATOM	191	CG	LEU	19	49.202	7.371	57.608	1.00	46.43	AAAA C
ATOM	192	CD1	LEU	19	47.946	6.743	57.852	1.00	22.57	AAAA C
ATOM	193	CD2	LEU	19	49.018	8.866	57.495	1.00	45.88	AAAA C
ATOM	194	C	LEU	19	52.210	6.428	59.912	1.00	49.87	AAAA C
ATOM	195	O	LEU	19	51.970	6.810	61.030	1.00	51.54	AAAA O
ATOM	196	N	GLU	20	53.270	5.708	59.652	1.00	49.35	AAAA N
ATOM	198	CA	GLU	20	53.819	4.833	60.679	1.00	49.60	AAAA C
ATOM	199	CB	GLU	20	54.876	3.960	59.982	1.00	57.91	AAAA C
ATOM	200	CG	GLU	20	55.893	4.840	59.272	1.00	70.16	AAAA C
ATOM	201	CD	GLU	20	57.095	4.077	58.757	1.00	69.35	AAAA C
ATOM	202	OE1	GLU	20	58.123	4.795	58.722	1.00	71.38	AAAA O
ATOM	203	OE2	GLU	20	56.993	2.885	58.420	1.00	72.84	AAAA O
ATOM	204	C	GLU	20	54.310	5.417	61.989	1.00	43.55	AAAA C
ATOM	205	O	GLU	20	54.301	4.652	62.937	1.00	40.01	AAAA O
ATOM	206	N	ASN	21	54.635	6.659	62.207	1.00	41.06	AAAA N
ATOM	208	CA	ASN	21	55.054	7.204	63.454	1.00	47.12	AAAA C
ATOM	209	C	ASN	21	54.066	8.141	64.108	1.00	49.76	AAAA C
ATOM	210	O	ASN	21	54.228	8.456	65.303	1.00	48.19	AAAA O

Figure 1A-1

ATOM	211	CB	ASN	21	56.379	6.093	63.200	1.00	50.11	AAAA C
ATOM	212	CG	ASN	21	57.413	7.951	62.796	1.00	68.38	AAAA C
ATOM	213	OD1	ASN	21	57.499	8.855	63.122	1.00	58.51	AAAA O
ATOM	214	ND2	ASN	21	58.348	7.469	61.899	1.00	77.00	AAAA N
ATOM	216	N	CYS	22	53.129	8.711	63.351	1.00	47.44	AAAA N
ATOM	218	CA	CYS	22	52.107	9.614	63.879	1.00	42.99	AAAA C
ATOM	219	C	CYS	22	51.215	9.089	65.021	1.00	40.43	AAAA C
ATOM	220	O	CYS	22	50.750	7.923	65.069	1.00	36.07	AAAA O
ATOM	221	CB	CYS	22	51.182	9.921	62.690	1.00	44.82	AAAA C
ATOM	222	SG	CYS	22	52.076	10.328	61.118	1.00	39.51	AAAA S
ATOM	223	N	THR	23	51.287	9.801	66.137	1.00	36.24	AAAA N
ATOM	225	CA	THR	23	50.339	9.482	67.204	1.00	43.51	AAAA C
ATOM	226	CB	THR	23	50.944	9.491	66.593	1.00	41.38	AAAA C
ATOM	227	OG1	THR	23	51.410	10.843	66.822	1.00	51.21	AAAA O
ATOM	229	CG2	THR	23	52.110	8.571	68.838	1.00	33.83	AAAA C
ATOM	230	C	THR	23	49.250	10.599	67.116	1.00	44.55	AAAA C
ATOM	231	O	THR	23	48.085	10.414	67.481	1.00	45.95	AAAA O
ATOM	232	N	VAL	24	49.646	11.797	66.689	1.00	33.03	AAAA N
ATOM	234	CA	VAL	24	48.732	12.855	66.442	1.00	35.29	AAAA C
ATOM	235	CB	VAL	24	48.925	13.979	67.456	1.00	30.60	AAAA C
ATOM	236	CG1	VAL	24	48.056	15.157	67.082	1.00	27.21	AAAA C
ATOM	237	CG2	VAL	24	48.656	13.566	68.886	1.00	25.37	AAAA C
ATOM	238	C	VAL	24	48.895	13.447	65.043	1.00	41.52	AAAA C
ATOM	239	O	VAL	24	49.987	13.963	64.791	1.00	44.40	AAAA O
ATOM	240	N	ILE	25	47.855	13.450	64.203	1.00	40.13	AAAA N
ATOM	242	CA	ILE	25	47.908	14.094	62.882	1.00	32.05	AAAA C
ATOM	243	CB	ILE	25	47.113	13.299	61.853	1.00	25.85	AAAA C
ATOM	244	CG2	ILE	25	47.027	14.039	60.542	1.00	18.73	AAAA C
ATOM	245	CG1	ILE	25	47.677	11.896	61.705	1.00	29.80	AAAA C
ATOM	246	CD1	ILE	25	47.169	11.155	60.471	1.00	27.41	AAAA C
ATOM	247	C	ILE	25	47.397	15.490	62.941	1.00	32.92	AAAA C
ATOM	248	O	ILE	25	46.223	15.776	63.213	1.00	40.91	AAAA O
ATOM	249	N	GLU	26	48.264	16.472	63.042	1.00	36.60	AAAA N
ATOM	251	CA	GLU	26	47.832	17.847	63.226	1.00	29.24	AAAA C
ATOM	252	CB	GLU	26	48.875	18.703	63.856	1.00	29.92	AAAA C
ATOM	253	CG	GLU	26	48.490	20.144	64.116	1.00	38.06	AAAA C
ATOM	254	CD	GLU	26	49.561	20.762	65.013	1.00	37.39	AAAA C
ATOM	255	OE1	GLU	26	50.654	20.937	64.489	1.00	41.56	AAAA O
ATOM	256	OE2	GLU	26	49.571	21.175	66.182	1.00	49.16	AAAA O
ATOM	257	C	GLU	26	47.413	18.376	61.869	1.00	37.79	AAAA C
ATOM	258	O	GLU	26	48.161	19.069	61.181	1.00	39.68	AAAA O
ATOM	259	N	GLY	27	46.117	18.104	61.582	1.00	37.28	AAAA N
ATOM	261	CA	GLY	27	45.498	18.503	60.320	1.00	31.17	AAAA C
ATOM	262	C	GLY	27	44.531	17.400	59.893	1.00	33.72	AAAA C
ATOM	263	O	GLY	27	43.988	16.715	60.775	1.00	33.29	AAAA O
ATOM	264	N	TYR	28	44.304	17.209	58.604	1.00	29.24	AAAA N
ATOM	266	CA	TYR	28	43.318	16.189	58.253	1.00	28.93	AAAA C
ATOM	267	CB	TYR	28	42.403	16.794	57.217	1.00	31.53	AAAA C
ATOM	268	CG	TYR	28	43.058	17.256	55.962	1.00	31.79	AAAA C
ATOM	269	CD1	TYR	28	43.704	16.355	55.116	1.00	36.07	AAAA C
ATOM	270	CE1	TYR	28	44.361	16.706	53.967	1.00	28.91	AAAA C
ATOM	271	CD2	TYR	28	43.130	18.572	55.606	1.00	30.98	AAAA C
ATOM	272	CE2	TYR	28	43.769	18.972	54.428	1.00	28.77	AAAA C
ATOM	273	CZ	TYR	28	44.367	18.021	53.652	1.00	31.53	AAAA C
ATOM	274	OH	TYR	28	44.971	18.425	52.464	1.00	44.74	AAAA O
ATOM	276	C	TYR	28	43.953	14.946	57.697	1.00	29.23	AAAA C
ATOM	277	O	TYR	28	45.119	15.147	57.383	1.00	35.58	AAAA O
ATOM	278	N	LEU	29	43.250	13.900	57.445	1.00	26.63	AAAA N
ATOM	280	CA	LEU	29	43.764	12.730	56.803	1.00	29.83	AAAA C
ATOM	281	CB	LEU	29	43.830	11.611	57.856	1.00	27.09	AAAA C
ATOM	282	CG	LEU	29	44.212	10.258	57.242	1.00	31.90	AAAA C
ATOM	283	CD1	LEU	29	45.538	10.396	56.469	1.00	35.03	AAAA C
ATOM	284	CD2	LEU	29	44.551	9.203	58.290	1.00	25.05	AAAA C
ATOM	285	C	LEU	29	42.897	12.342	55.616	1.00	33.84	AAAA C
ATOM	286	O	LEU	29	41.689	12.165	55.906	1.00	43.29	AAAA O
ATOM	287	N	HIS	30	43.389	12.285	54.395	1.00	35.95	AAAA N
ATOM	289	CA	HIS	30	42.681	11.891	53.197	1.00	34.92	AAAA C
ATOM	290	CB	HIS	30	42.893	12.801	52.027	1.00	32.85	AAAA C
ATOM	291	CG	HIS	30	42.372	14.155	52.046	1.00	25.08	AAAA C
ATOM	292	CD2	HIS	30	41.519	14.753	52.907	1.00	40.88	AAAA C
ATOM	293	ND1	HIS	30	42.713	15.120	51.128	1.00	33.66	AAAA N
ATOM	295	CE1	HIS	30	42.080	16.281	51.444	1.00	31.33	AAAA C
ATOM	296	NE2	HIS	30	41.329	16.093	52.539	1.00	37.27	AAAA N
ATOM	298	C	HIS	30	43.173	10.538	52.714	1.00	37.68	AAAA C
ATOM	299	O	HIS	30	44.357	10.388	52.541	1.00	38.70	AAAA O
ATOM	300	N	ILE	31	42.308	9.542	52.584	1.00	40.02	AAAA N
ATOM	302	CA	ILE	31	42.750	8.271	51.992	1.00	39.47	AAAA C
ATOM	303	CB	ILE	31	42.668	7.204	53.063	1.00	37.95	AAAA C
ATOM	304	CG2	ILE	31	43.161	5.830	52.651	1.00	23.86	AAAA C
ATOM	305	CG1	ILE	31	43.481	7.555	54.335	1.00	41.66	AAAA C
ATOM	306	CD1	ILE	31	43.170	6.575	55.473	1.00	28.22	AAAA C
ATOM	307	C	ILE	31	41.804	8.044	50.759	1.00	46.52	AAAA C
ATOM	308	O	ILE	31	40.753	7.589	50.827	1.00	43.56	AAAA O
ATOM	309	N	LEU	32	42.314	8.489	49.596	1.00	49.89	AAAA N
ATOM	311	CA	LEU	32	41.484	8.235	48.380	1.00	49.77	AAAA C

Figure 1A-2

ATOM	312	CB	LEU	32	41.127	9.515	47.603	1.00 47.49	AAAA C
ATOM	313	CG	LEU	32	42.691	10.688	47.562	1.00 45.33	AAAA C
ATOM	314	CD1	LEU	32	41.517	11.812	46.673	1.00 35.77	AAAA C
ATOM	315	CD2	LEU	32	42.371	11.229	48.969	1.00 49.19	AAAA C
ATOM	316	C	LEU	32	42.136	7.296	47.353	1.00 51.09	AAAA C
ATOM	317	O	LEU	32	43.338	7.370	47.186	1.00 41.36	AAAA O
ATOM	318	N	LEU	33	41.270	6.722	46.497	1.00 50.74	AAAA N
ATOM	320	CA	LEU	33	41.602	6.175	45.197	1.00 49.92	AAAA C
ATOM	321	CB	LEU	33	42.091	7.262	44.192	1.00 34.83	AAAA C
ATOM	322	CG	LEU	33	41.233	8.537	44.164	1.00 33.92	AAAA C
ATOM	323	CD1	LEU	33	41.892	9.587	43.298	1.00 37.49	AAAA C
ATOM	324	CD2	LEU	33	39.823	8.313	43.644	1.00 33.01	AAAA C
ATOM	325	C	LEU	33	42.618	5.073	45.287	1.00 48.35	AAAA C
ATOM	326	O	LEU	33	43.580	5.077	44.538	1.00 54.14	AAAA O
ATOM	327	N	ILE	34	42.543	4.212	46.254	1.00 47.61	AAAA N
ATOM	329	CA	ILE	34	43.523	3.184	46.540	1.00 51.70	AAAA C
ATOM	330	CB	ILE	34	44.101	3.346	47.963	1.00 57.98	AAAA C
ATOM	331	CG2	ILE	34	44.538	2.043	48.600	1.00 48.98	AAAA C
ATOM	332	CG1	ILE	34	45.267	4.371	47.967	1.00 46.70	AAAA C
ATOM	333	CD1	ILE	34	45.561	4.704	49.439	1.00 66.47	AAAA C
ATOM	334	C	ILE	34	42.829	1.844	46.406	1.00 59.85	AAAA C
ATOM	335	O	ILE	34	41.726	1.531	46.856	1.00 60.11	AAAA O
ATOM	336	N	SER	35	43.622	0.833	46.013	1.00 67.79	AAAA N
ATOM	338	CA	SER	35	43.048	-0.511	45.922	1.00 68.80	AAAA C
ATOM	339	CB	SER	35	42.767	-0.882	44.469	1.00 64.16	AAAA C
ATOM	340	OG	SER	35	41.731	-1.846	44.498	1.00 75.76	AAAA O
ATOM	342	C	SER	35	43.929	-1.564	46.537	1.00 70.73	AAAA C
ATOM	343	O	SER	35	44.885	-1.954	45.909	1.00 73.65	AAAA O
ATOM	344	N	LYS	36	43.687	-2.017	47.740	1.00 74.75	AAAA N
ATOM	346	CA	LYS	36	44.465	-3.014	48.421	1.00 76.59	AAAA C
ATOM	347	CB	LYS	36	44.046	-3.131	49.885	1.00 81.22	AAAA C
ATOM	348	CG	LYS	36	45.147	-3.654	50.775	1.00 78.87	AAAA C
ATOM	349	CD	LYS	36	44.693	-4.575	51.887	1.00 81.39	AAAA C
ATOM	350	CE	LYS	36	44.899	-6.025	51.492	1.00 89.38	AAAA C
ATOM	351	NZ	LYS	36	44.371	-6.989	52.506	1.00 91.63	AAAA N
ATOM	355	C	LYS	36	44.252	-4.362	47.753	1.00 81.41	AAAA C
ATOM	356	O	LYS	36	43.145	-4.772	47.451	1.00 78.20	AAAA O
ATOM	357	N	ALA	37	45.371	-5.080	47.615	1.00 88.27	AAAA N
ATOM	359	CA	ALA	37	45.361	-6.396	46.986	1.00 90.10	AAAA C
ATOM	360	CB	ALA	37	46.700	-6.655	46.327	1.00 95.49	AAAA C
ATOM	361	C	ALA	37	45.011	-7.473	47.995	1.00 92.36	AAAA C
ATOM	362	O	ALA	37	45.668	-7.627	49.012	1.00 92.35	AAAA O
ATOM	363	N	SER	38	44.031	-8.301	47.622	1.00 94.31	AAAA N
ATOM	365	CA	SER	38	43.528	-9.352	48.484	1.00 95.70	AAAA C
ATOM	366	CB	SER	38	42.405	-10.164	47.858	1.00 97.44	AAAA C
ATOM	367	OG	SER	38	42.061	-11.176	48.814	1.00103.48	AAAA O
ATOM	369	C	SER	38	44.702	-10.263	48.821	1.00 96.87	AAAA C
ATOM	370	O	SER	38	44.761	-10.778	49.924	1.00 98.06	AAAA O
ATOM	371	N	ASP	39	45.584	-10.415	47.852	1.00 97.99	AAAA N
ATOM	373	CA	ASP	39	46.821	-11.148	47.980	1.00 99.19	AAAA C
ATOM	374	CB	ASP	39	47.579	-11.059	46.652	1.00102.13	AAAA C
ATOM	375	CG	ASP	39	47.696	-12.387	45.948	0.01101.22	AAAA C
ATOM	376	OD1	ASP	39	46.644	-12.978	45.623	0.01101.42	AAAA O
ATOM	377	OD2	ASP	39	48.833	-12.848	45.719	0.01101.41	AAAA O
ATOM	378	C	ASP	39	47.660	-10.564	49.105	1.00 99.40	AAAA C
ATOM	379	O	ASP	39	47.692	-11.056	50.224	1.00 99.15	AAAA O
ATOM	380	N	TYR	40	48.354	-9.479	48.818	1.00100.96	AAAA N
ATOM	382	CA	TYR	40	49.120	-8.706	49.802	1.00101.16	AAAA C
ATOM	383	CB	TYR	40	49.511	-7.393	49.130	1.00103.67	AAAA C
ATOM	384	CG	TYR	40	50.159	-6.281	49.887	1.00107.81	AAAA C
ATOM	385	CD1	TYR	40	50.931	-5.325	49.228	1.00109.56	AAAA C
ATOM	386	CE1	TYR	40	51.540	-4.280	49.910	1.00109.67	AAAA C
ATOM	387	CD2	TYR	40	50.044	-6.115	51.254	1.00109.29	AAAA C
ATOM	388	CE2	TYR	40	50.618	-5.102	51.976	1.00109.83	AAAA C
ATOM	389	CZ	TYR	40	51.372	-4.191	51.276	1.00110.16	AAAA C
ATOM	390	OH	TYR	40	51.999	-3.127	51.993	1.00109.84	AAAA O
ATOM	392	C	TYR	40	48.343	-8.529	51.100	1.00 99.10	AAAA C
ATOM	393	O	TYR	40	47.168	-8.182	51.183	1.00 99.05	AAAA O
ATOM	394	N	LYS	41	49.041	-8.653	52.218	1.00 98.62	AAAA N
ATOM	396	CA	LYS	41	48.443	-9.549	53.546	1.00100.30	AAAA C
ATOM	397	CB	LYS	41	49.385	-9.160	54.599	1.00104.42	AAAA C
ATOM	398	CG	LYS	41	49.218	-10.649	54.814	0.01101.06	AAAA C
ATOM	399	CD	LYS	41	47.776	-11.107	54.919	0.01100.66	AAAA C
ATOM	400	CE	LYS	41	47.205	-10.880	56.308	0.01 99.86	AAAA C
ATOM	401	NZ	LYS	41	47.982	-11.728	57.328	0.01 99.62	AAAA N
ATOM	405	C	LYS	41	48.035	-7.136	53.947	1.00 98.99	AAAA C
ATOM	406	O	LYS	41	47.615	-6.371	53.057	1.00103.33	AAAA O
ATOM	407	N	SER	42	48.198	-6.754	55.221	1.00 91.75	AAAA N
ATOM	409	CA	SER	42	47.829	-5.412	55.604	1.00 85.06	AAAA C
ATOM	410	CB	SER	42	46.385	-5.520	56.147	1.00 95.33	AAAA C
ATOM	411	OG	SER	42	46.547	-6.140	57.426	1.00104.63	AAAA O
ATOM	413	C	SER	42	48.628	-4.715	56.687	1.00 80.78	AAAA C
ATOM	414	O	SER	42	49.326	-5.259	57.538	1.00 81.03	AAAA O
ATOM	415	N	TYR	43	48.495	-3.395	56.675	1.00 73.03	AAAA N
ATOM	417	CA	TYR	43	49.069	-2.489	57.635	1.00 67.25	AAAA C

Figure 1A-3

ATOM	479	CB	TYR	43	49.066	-1.119	56.985	1.00	65.37	AAAA C
ATOM	479	CG	TYR	43	49.953	-1.021	55.727	1.00	63.92	AAAA C
ATOM	480	CD1	TYR	43	50.931	-1.935	55.466	1.00	63.87	AAAA C
ATOM	481	CE1	TYR	43	51.698	-1.781	54.274	1.00	66.09	AAAA C
ATOM	482	CD2	TYR	43	49.770	0.050	54.970	1.00	63.39	AAAA C
ATOM	483	CE2	TYR	43	50.536	0.214	53.728	1.00	67.62	AAAA C
ATOM	484	CZ	TYR	43	51.508	-0.710	53.430	1.00	66.94	AAAA C
ATOM	485	OH	TYR	43	52.262	-0.563	52.305	1.00	65.23	AAAA O
ATOM	487	C	TYR	43	48.248	-2.381	58.925	1.00	64.88	AAAA C
ATOM	488	O	TYR	43	47.088	-2.851	59.036	1.00	62.90	AAAA O
ATOM	489	N	ARG	44	48.782	-1.567	59.825	1.00	57.88	AAAA N
ATOM	491	CA	ARG	44	48.019	-1.285	61.039	1.00	56.45	AAAA C
ATOM	492	CB	ARG	44	47.842	-2.611	61.780	1.00	46.51	AAAA C
ATOM	493	CG	ARG	44	47.815	-2.375	63.244	1.00	54.66	AAAA C
ATOM	494	CD	ARG	44	46.885	-3.327	63.986	1.00	58.54	AAAA C
ATOM	495	NE	ARG	44	47.090	-2.927	65.403	1.00	68.56	AAAA N
ATOM	497	CZ	ARG	44	46.464	-3.536	66.395	1.00	64.82	AAAA C
ATOM	498	NH1	ARG	44	45.644	-4.529	66.132	1.00	61.53	AAAA N
ATOM	501	NH2	ARG	44	46.674	-3.139	67.628	1.00	66.03	AAAA N
ATOM	444	C	ARG	44	48.911	-0.285	61.845	1.00	55.59	AAAA C
ATOM	445	O	ARG	44	49.916	-0.552	62.320	1.00	58.43	AAAA O
ATOM	446	N	PHE	45	48.276	0.866	62.139	1.00	51.13	AAAA N
ATOM	448	CA	PHE	45	48.865	1.944	62.863	1.00	45.94	AAAA C
ATOM	449	CB	PHE	45	48.774	3.249	61.978	1.00	35.89	AAAA C
ATOM	450	CG	PHE	45	49.106	2.937	60.554	1.00	30.29	AAAA C
ATOM	451	CD1	PHE	45	50.373	3.051	59.998	1.00	45.72	AAAA C
ATOM	452	CD2	PHE	45	48.127	2.428	59.728	1.00	35.95	AAAA C
ATOM	453	CE1	PHE	45	50.653	2.715	58.672	1.00	47.76	AAAA C
ATOM	454	CE2	PHE	45	48.358	2.096	58.406	1.00	39.92	AAAA C
ATOM	455	CZ	PHE	45	49.612	2.244	57.847	1.00	46.44	AAAA C
ATOM	456	C	PHE	45	48.181	2.123	64.203	1.00	41.65	AAAA C
ATOM	457	O	PHE	45	47.708	3.223	64.475	1.00	40.99	AAAA O
ATOM	458	N	PRO	46	48.494	1.338	65.212	1.00	43.20	AAAA N
ATOM	459	CD	PRO	46	49.300	0.097	65.132	1.00	47.74	AAAA C
ATOM	460	CA	PRO	46	48.032	1.530	66.560	1.00	43.34	AAAA C
ATOM	461	CB	PRO	46	48.514	0.319	67.380	1.00	44.92	AAAA C
ATOM	462	CG	PRO	46	49.404	-0.464	66.514	1.00	45.48	AAAA C
ATOM	463	C	PRO	46	48.558	2.768	67.233	1.00	41.30	AAAA C
ATOM	464	O	PRO	46	48.329	2.830	68.443	1.00	44.57	AAAA O
ATOM	465	N	LYS	47	49.450	3.533	66.676	1.00	39.33	AAAA N
ATOM	467	CA	LYS	47	49.991	4.679	67.362	1.00	38.10	AAAA C
ATOM	468	CB	LYS	47	51.378	4.981	66.852	1.00	48.07	AAAA C
ATOM	469	CG	LYS	47	52.032	3.995	65.902	1.00	67.95	AAAA C
ATOM	470	CD	LYS	47	53.563	3.976	65.891	1.00	61.33	AAAA C
ATOM	471	CE	LYS	47	54.115	4.648	67.147	1.00	72.19	AAAA C
ATOM	472	NZ	LYS	47	54.024	6.132	66.874	1.00	79.29	AAAA N
ATOM	476	C	LYS	47	49.014	5.848	67.195	1.00	39.76	AAAA C
ATOM	477	O	LYS	47	49.189	6.827	67.952	1.00	35.45	AAAA O
ATOM	478	N	LEU	48	48.300	5.886	66.053	1.00	36.45	AAAA N
ATOM	480	CA	LEU	48	47.370	7.004	65.890	1.00	40.40	AAAA C
ATOM	481	CB	LEU	48	46.823	6.919	64.389	1.00	28.59	AAAA C
ATOM	482	CG	LEU	48	45.947	7.967	63.787	1.00	31.04	AAAA C
ATOM	483	CD1	LEU	48	46.637	9.310	63.879	1.00	36.86	AAAA C
ATOM	484	CD2	LEU	48	45.591	7.738	62.294	1.00	34.49	AAAA C
ATOM	485	C	LEU	48	46.186	7.022	66.867	1.00	42.21	AAAA C
ATOM	486	O	LEU	48	45.271	6.187	66.863	1.00	36.48	AAAA O
ATOM	487	N	THR	49	46.138	8.041	67.673	1.00	38.95	AAAA N
ATOM	489	CA	THR	49	45.045	8.151	68.574	1.00	37.96	AAAA C
ATOM	490	CB	THR	49	45.548	8.207	70.034	1.00	48.69	AAAA C
ATOM	491	OG1	THR	49	46.396	9.340	70.225	1.00	35.99	AAAA O
ATOM	493	CG2	THR	49	48.230	6.957	70.529	1.00	31.99	AAAA C
ATOM	494	C	THR	49	44.230	9.425	68.321	1.00	39.48	AAAA C
ATOM	495	O	THR	49	43.111	9.451	68.837	1.00	34.49	AAAA O
ATOM	496	N	VAL	50	44.735	10.415	67.605	1.00	37.32	AAAA N
ATOM	498	CA	VAL	50	43.995	11.664	67.418	1.00	38.72	AAAA C
ATOM	499	CB	VAL	50	44.293	12.708	68.503	1.00	37.24	AAAA C
ATOM	500	CG1	VAL	50	43.630	14.066	68.208	1.00	29.96	AAAA C
ATOM	501	CG2	VAL	50	43.884	12.311	69.913	1.00	32.52	AAAA C
ATOM	502	C	VAL	50	44.271	12.305	66.048	1.00	37.03	AAAA C
ATOM	503	O	VAL	50	45.195	11.863	65.431	1.00	37.96	AAAA O
ATOM	504	N	ILE	51	43.319	12.939	65.415	1.00	37.49	AAAA N
ATOM	506	CA	ILE	51	43.391	13.575	64.133	1.00	32.48	AAAA C
ATOM	507	CB	ILE	51	42.346	12.864	63.152	1.00	34.51	AAAA C
ATOM	508	CG2	ILE	51	41.995	13.802	61.978	1.00	32.31	AAAA C
ATOM	509	CG1	ILE	51	43.026	11.611	62.671	1.00	30.78	AAAA C
ATOM	510	CD1	ILE	51	42.358	10.559	61.815	1.00	19.69	AAAA C
ATOM	511	C	ILE	51	42.659	14.939	64.431	1.00	34.14	AAAA C
ATOM	512	O	ILE	51	41.546	14.830	64.923	1.00	29.08	AAAA O
ATOM	513	N	THR	52	43.342	16.058	64.238	1.00	33.93	AAAA N
ATOM	515	CA	THR	52	42.806	17.305	64.719	1.00	33.83	AAAA C
ATOM	516	CB	THR	52	43.961	18.338	64.939	1.00	35.39	AAAA C
ATOM	517	OG1	THR	52	44.726	18.567	63.781	1.00	41.28	AAAA O
ATOM	519	CG2	THR	52	44.775	17.926	66.134	1.00	22.01	AAAA C
ATOM	520	C	THR	52	41.741	17.961	63.863	1.00	39.02	AAAA C
ATOM	521	O	THR	52	41.203	19.036	64.243	1.00	38.88	AAAA O

Figure 1A-4

Application No. 09/555,275
Annotated Sheet Showing Changes

ATOM	522	H	GLU	53	41.524	17.477	62.639	1.00	36.93	AAAA H
ATOM	524	CA	GLU	53	40.434	17.053	61.795	1.00	38.38	AAAA C
ATOM	525	CB	GLU	53	41.064	18.512	60.483	1.00	29.76	AAAA C
ATOM	526	CG	GLU	53	42.061	19.552	60.834	1.00	30.48	AAAA C
ATOM	527	CD	GLU	53	42.517	20.396	59.697	1.00	40.82	AAAA C
ATOM	528	OE1	GLU	53	42.638	19.908	58.556	1.00	57.56	AAAA O
ATOM	529	OE2	GLU	53	42.799	21.559	59.931	1.00	35.74	AAAA O
ATOM	530	C	GLU	53	39.506	16.799	61.388	1.00	39.19	AAAA C
ATOM	531	O	GLU	53	38.922	16.311	62.386	1.00	38.95	AAAA O
ATOM	532	H	TYR	54	39.639	16.353	60.102	1.00	30.60	AAAA H
ATOM	534	CA	TYR	54	38.666	15.342	59.713	1.00	35.96	AAAA C
ATOM	535	CB	TYR	54	37.654	15.902	58.636	1.00	30.71	AAAA C
ATOM	536	CG	TYR	54	38.247	16.476	57.388	1.00	21.18	AAAA C
ATOM	537	CD1	TYR	54	38.487	15.733	56.305	1.00	20.22	AAAA C
ATOM	538	CE1	TYR	54	38.980	16.243	55.086	1.00	21.04	AAAA C
ATOM	539	CD2	TYR	54	38.577	17.844	57.307	1.00	33.97	AAAA C
ATOM	540	CE2	TYR	54	39.049	18.384	56.124	1.00	24.69	AAAA C
ATOM	541	CZ	TYR	54	39.263	17.569	55.032	1.00	26.72	AAAA C
ATOM	542	OH	TYR	54	39.763	18.047	53.847	1.00	37.55	AAAA O
ATOM	544	C	TYR	54	39.405	14.115	59.142	1.00	33.87	AAAA C
ATOM	545	O	TYR	54	40.513	14.360	58.678	1.00	30.40	AAAA O
ATOM	546	H	LEU	55	38.683	13.021	59.004	1.00	23.24	AAAA H
ATOM	548	CA	LEU	55	39.111	11.812	58.454	1.00	30.08	AAAA C
ATOM	549	CB	LEU	55	39.011	10.663	59.510	1.00	14.78	AAAA C
ATOM	550	CG	LEU	55	39.349	9.314	58.818	1.00	26.98	AAAA C
ATOM	551	CD1	LEU	55	40.668	9.477	58.040	1.00	26.66	AAAA C
ATOM	552	CD2	LEU	55	39.496	8.093	59.705	1.00	14.45	AAAA C
ATOM	553	C	LEU	55	38.201	11.548	57.238	1.00	37.43	AAAA C
ATOM	554	O	LEU	55	36.995	11.630	57.427	1.00	39.55	AAAA O
ATOM	555	H	LEU	56	38.700	11.348	56.035	1.00	41.83	AAAA H
ATOM	557	CA	LEU	56	37.955	11.201	54.794	1.00	36.98	AAAA C
ATOM	558	CB	LEU	56	37.998	12.446	53.949	1.00	33.29	AAAA C
ATOM	559	CG	LEU	56	37.984	12.514	52.416	1.00	30.35	AAAA C
ATOM	560	CD1	LEU	56	37.076	11.460	51.821	1.00	47.95	AAAA C
ATOM	561	CD2	LEU	56	37.286	13.807	51.985	1.00	33.47	AAAA C
ATOM	562	C	LEU	56	38.595	10.047	54.008	1.00	39.75	AAAA C
ATOM	563	O	LEU	56	39.714	10.205	53.547	1.00	44.38	AAAA O
ATOM	564	H	LEU	57	37.846	9.008	53.800	1.00	36.68	AAAA H
ATOM	566	CA	LEU	57	38.133	7.832	53.034	1.00	41.53	AAAA C
ATOM	567	CB	LEU	57	37.944	6.588	53.916	1.00	37.00	AAAA C
ATOM	568	CG	LEU	57	39.064	6.534	55.026	1.00	36.13	AAAA C
ATOM	569	CD1	LEU	57	38.513	6.890	56.417	1.00	33.26	AAAA C
ATOM	570	CD2	LEU	57	39.630	5.162	55.039	1.00	24.11	AAAA C
ATOM	571	C	LEU	57	37.203	7.825	51.838	1.00	46.03	AAAA C
ATOM	572	O	LEU	57	35.985	7.993	51.969	1.00	44.78	AAAA O
ATOM	573	H	PHE	58	37.792	7.898	50.642	1.00	47.07	AAAA H
ATOM	575	CA	PHE	58	36.895	8.002	49.467	1.00	48.75	AAAA C
ATOM	576	CB	PHE	58	36.704	9.448	49.102	1.00	46.67	AAAA C
ATOM	577	CG	PHE	58	36.447	9.815	47.692	1.00	54.66	AAAA C
ATOM	578	CD1	PHE	58	37.413	9.706	46.697	1.00	55.19	AAAA C
ATOM	579	CD2	PHE	58	35.200	10.301	47.326	1.00	53.86	AAAA C
ATOM	580	CE1	PHE	58	37.124	10.063	45.396	1.00	50.36	AAAA C
ATOM	581	CE2	PHE	58	34.885	10.655	46.011	1.00	41.84	AAAA C
ATOM	582	CZ	PHE	58	35.877	10.521	45.037	1.00	46.50	AAAA C
ATOM	583	C	PHE	58	37.351	7.052	48.379	1.00	49.71	AAAA C
ATOM	584	O	PHE	58	38.487	7.073	47.934	1.00	52.16	AAAA O
ATOM	585	H	ARG	59	36.471	6.118	47.944	1.00	44.26	AAAA H
ATOM	587	CA	ARG	59	36.753	5.281	46.815	1.00	40.80	AAAA C
ATOM	588	CB	ARG	59	36.911	5.993	45.427	1.00	23.79	AAAA C
ATOM	589	CG	ARG	59	35.869	7.020	45.121	1.00	46.53	AAAA C
ATOM	590	CD	ARG	59	35.921	7.562	43.706	1.00	37.64	AAAA C
ATOM	591	NE	ARG	59	35.822	6.422	42.806	1.00	49.23	AAAA H
ATOM	593	CZ	ARG	59	34.950	5.832	42.036	1.00	41.36	AAAA C
ATOM	594	NH1	ARG	59	33.702	6.277	41.931	1.00	47.00	AAAA H
ATOM	597	NH2	ARG	59	35.237	4.729	41.327	1.00	42.58	AAAA H
ATOM	600	C	ARG	59	38.037	4.494	47.049	1.00	42.25	AAAA C
ATOM	601	O	ARG	59	38.981	4.513	46.232	1.00	44.11	AAAA O
ATOM	602	H	VAL	60	38.001	3.625	48.023	1.00	40.84	AAAA H
ATOM	604	CA	VAL	60	39.191	2.743	48.341	1.00	39.14	AAAA C
ATOM	605	CB	VAL	60	39.624	3.066	49.781	1.00	40.12	AAAA C
ATOM	606	CG1	VAL	60	40.407	1.972	50.296	1.00	35.05	AAAA C
ATOM	607	CG2	VAL	60	40.425	4.352	49.803	1.00	28.86	AAAA C
ATOM	608	C	VAL	60	38.539	1.337	48.368	1.00	43.56	AAAA C
ATOM	609	O	VAL	60	37.535	1.224	49.072	1.00	47.66	AAAA O
ATOM	610	H	ALA	61	39.094	0.371	47.659	1.00	41.92	AAAA H
ATOM	612	CA	ALA	61	38.617	-0.992	47.749	1.00	42.05	AAAA C
ATOM	613	CB	ALA	61	38.302	-1.483	46.364	1.00	52.40	AAAA C
ATOM	614	C	ALA	61	39.613	-1.934	48.386	1.00	43.08	AAAA C
ATOM	615	O	ALA	61	40.757	-1.602	48.670	1.00	50.59	AAAA O
ATOM	616	H	GLY	62	39.200	-3.105	48.849	1.00	45.71	AAAA H
ATOM	618	CA	GLY	62	40.136	-4.079	49.385	1.00	45.39	AAAA C
ATOM	619	C	GLY	62	40.262	-3.902	50.872	1.00	48.04	AAAA C
ATOM	620	O	GLY	62	40.587	-4.835	51.604	1.00	52.34	AAAA O
ATOM	621	H	LEU	63	39.985	-2.734	51.383	1.00	46.90	AAAA H
ATOM	623	CA	LEU	63	40.003	-2.443	52.805	1.00	49.11	AAAA C

Figure 1A-5

Application No. 09/555,275
Annotated Sheet Showing Changes

ATOM	624	CB	LEU	63	40.274	-0.953	53.027	1.00	41.41	AAAA C
ATOM	625	CG	LEU	63	40.265	-0.423	54.443	1.00	53.41	AAAA C
ATOM	626	CD1	LEU	63	41.172	-1.164	55.416	1.00	48.27	AAAA C
ATOM	627	CD2	LEU	63	40.637	1.047	54.246	1.00	50.51	AAAA C
ATOM	628	C	LEU	63	38.643	-2.881	53.323	1.00	54.20	AAAA C
ATOM	629	O	LEU	63	37.587	-2.430	52.837	1.00	57.73	AAAA O
ATOM	630	N	GLU	64	38.658	-3.862	54.190	1.00	53.97	AAAA N
ATOM	632	CA	GLU	64	37.462	-4.448	54.749	1.00	56.96	AAAA C
ATOM	633	CB	GLU	64	37.589	-5.956	54.734	1.00	65.33	AAAA C
ATOM	634	CG	GLU	64	37.832	-6.484	53.293	1.00	75.14	AAAA C
ATOM	635	CD	GLU	64	37.104	-7.940	53.128	1.00	78.10	AAAA C
ATOM	636	OE1	GLU	64	37.424	-8.699	54.132	1.00	63.92	AAAA O
ATOM	637	OE2	GLU	64	37.036	-8.320	51.978	1.00	88.77	AAAA O
ATOM	638	C	GLU	64	37.096	-4.007	56.163	1.00	57.12	AAAA C
ATOM	639	O	GLU	64	35.986	-4.332	56.600	1.00	59.82	AAAA O
ATOM	640	N	SER	65	37.766	-3.042	56.761	1.00	50.64	AAAA N
ATOM	642	CA	SER	65	37.539	-2.523	58.069	1.00	47.19	AAAA C
ATOM	643	CB	SER	65	37.743	-3.596	59.139	1.00	49.24	AAAA C
ATOM	644	OG	SER	65	37.501	-2.971	60.429	1.00	50.90	AAAA O
ATOM	646	C	SER	65	38.516	-1.405	58.432	1.00	48.35	AAAA C
ATOM	647	O	SER	65	39.716	-1.692	58.374	1.00	52.75	AAAA O
ATOM	648	N	LEU	66	38.054	-0.289	58.984	1.00	41.03	AAAA N
ATOM	650	CA	LEU	66	38.956	0.758	59.405	1.00	41.94	AAAA C
ATOM	651	CB	LEU	66	38.247	2.085	59.498	1.00	25.25	AAAA C
ATOM	652	CG	LEU	66	37.283	2.476	58.402	1.00	34.49	AAAA C
ATOM	653	CD1	LEU	66	36.974	3.951	58.512	1.00	30.81	AAAA C
ATOM	654	CD2	LEU	66	37.767	2.200	56.994	1.00	34.34	AAAA C
ATOM	655	C	LEU	66	39.646	0.462	60.734	1.00	45.39	AAAA C
ATOM	656	O	LEU	66	40.762	0.947	60.927	1.00	41.05	AAAA O
ATOM	657	N	GLY	67	39.000	-0.346	61.583	1.00	45.21	AAAA N
ATOM	659	CA	GLY	67	39.773	-0.672	62.799	1.00	48.14	AAAA C
ATOM	660	C	GLY	67	40.998	-1.508	62.445	1.00	44.51	AAAA C
ATOM	661	O	GLY	67	41.855	-1.724	63.287	1.00	45.42	AAAA O
ATOM	662	N	ASP	68	41.013	-2.189	61.309	1.00	47.60	AAAA N
ATOM	664	CA	ASP	68	42.194	-2.834	60.738	1.00	50.99	AAAA C
ATOM	665	CB	ASP	68	42.012	-3.417	59.361	1.00	39.43	AAAA C
ATOM	666	CG	ASP	68	41.205	-4.678	59.311	1.00	45.82	AAAA C
ATOM	667	OD1	ASP	68	40.912	-5.341	60.320	1.00	44.69	AAAA O
ATOM	668	OD2	ASP	68	40.819	-5.065	58.187	1.00	47.23	AAAA O
ATOM	669	C	ASP	68	43.363	-1.837	60.596	1.00	45.89	AAAA C
ATOM	670	O	ASP	68	44.436	-2.269	60.903	1.00	44.84	AAAA O
ATOM	671	N	LEU	69	43.145	-0.609	60.247	1.00	42.49	AAAA N
ATOM	673	CA	LEU	69	44.175	0.352	60.048	1.00	45.80	AAAA C
ATOM	674	CB	LEU	69	43.920	1.393	58.945	1.00	45.25	AAAA C
ATOM	675	CG	LEU	69	43.902	0.882	57.494	1.00	54.25	AAAA C
ATOM	676	CD1	LEU	69	43.541	2.037	56.565	1.00	47.26	AAAA C
ATOM	677	CD2	LEU	69	45.211	0.200	57.113	1.00	50.76	AAAA C
ATOM	678	C	LEU	69	44.347	1.107	61.350	1.00	49.50	AAAA C
ATOM	679	O	LEU	69	45.470	1.210	61.851	1.00	54.51	AAAA O
ATOM	680	N	PHE	70	43.296	1.737	61.869	1.00	44.60	AAAA N
ATOM	682	CA	PHE	70	43.423	2.564	63.046	1.00	39.67	AAAA C
ATOM	683	CB	PHE	70	42.987	3.973	62.700	1.00	26.08	AAAA C
ATOM	684	CG	PHE	70	43.465	4.501	61.390	1.00	45.32	AAAA C
ATOM	685	CD1	PHE	70	42.532	4.748	60.384	1.00	47.41	AAAA C
ATOM	686	CD2	PHE	70	44.815	4.767	61.130	1.00	48.77	AAAA C
ATOM	687	CE1	PHE	70	42.945	5.263	59.159	1.00	56.16	AAAA C
ATOM	688	CE2	PHE	70	45.229	5.256	59.895	1.00	47.24	AAAA C
ATOM	689	CZ	PHE	70	44.293	5.506	58.896	1.00	49.54	AAAA C
ATOM	690	C	PHE	70	42.655	1.999	64.219	1.00	40.09	AAAA C
ATOM	691	O	PHE	70	41.874	2.734	64.838	1.00	35.74	AAAA O
ATOM	692	N	PRO	71	43.053	0.852	64.768	1.00	39.19	AAAA N
ATOM	693	CD	PRO	71	44.269	0.058	64.411	1.00	39.94	AAAA C
ATOM	694	CA	PRO	71	42.444	0.237	65.899	1.00	35.30	AAAA C
ATOM	695	CB	PRO	71	43.308	-0.983	66.246	1.00	38.03	AAAA C
ATOM	696	CG	PRO	71	44.669	-0.564	65.717	1.00	38.36	AAAA C
ATOM	697	C	PRO	71	42.453	1.089	67.126	1.00	33.72	AAAA C
ATOM	698	O	PRO	71	42.005	0.630	68.159	1.00	39.32	AAAA O
ATOM	699	N	ASN	72	43.058	2.220	67.231	1.00	36.55	AAAA N
ATOM	701	CA	ASN	72	43.204	3.032	68.401	1.00	32.69	AAAA C
ATOM	702	CB	ASN	72	44.637	2.916	68.962	1.00	36.89	AAAA C
ATOM	703	CG	ASN	72	44.735	1.638	69.761	1.00	47.03	AAAA C
ATOM	704	OD1	ASN	72	44.644	1.619	70.979	1.00	64.42	AAAA O
ATOM	705	ND2	ASN	72	44.880	0.475	69.169	1.00	63.17	AAAA N
ATOM	708	C	ASN	72	42.875	4.477	68.135	1.00	30.11	AAAA C
ATOM	709	O	ASN	72	43.099	5.201	69.104	1.00	36.53	AAAA O
ATOM	710	N	LEU	73	42.309	4.809	66.978	1.00	27.62	AAAA N
ATOM	712	CA	LEU	73	41.940	6.207	66.730	1.00	34.07	AAAA C
ATOM	713	CB	LEU	73	41.476	6.373	65.292	1.00	28.37	AAAA C
ATOM	714	CG	LEU	73	40.819	7.713	64.882	1.00	29.33	AAAA C
ATOM	715	CD1	LEU	73	41.918	8.721	64.963	1.00	31.86	AAAA C
ATOM	716	CD2	LEU	73	40.202	7.518	63.470	1.00	32.07	AAAA C
ATOM	717	C	LEU	73	40.929	6.569	67.817	1.00	32.14	AAAA C
ATOM	718	O	LEU	73	40.073	5.737	68.081	1.00	35.62	AAAA O
ATOM	719	N	THR	74	41.081	7.585	68.582	1.00	29.47	AAAA N
ATOM	721	CA	THR	74	40.150	7.826	69.683	1.00	34.86	AAAA C

Figure 1A-6

ATOM	722	CB	THR	74	41.028	7.744	70.952	1.00	46.09	AAAA C
ATOM	723	OG1	THR	74	41.729	6.485	70.880	1.00	46.30	AAAA O
ATOM	725	CG2	THR	74	40.262	7.831	72.253	1.00	39.45	AAAA C
ATOM	726	C	THR	74	39.424	9.155	69.602	1.00	35.48	AAAA C
ATOM	727	O	THR	74	38.270	9.322	70.077	1.00	35.32	AAAA O
ATOM	728	N	VAL	75	40.047	10.199	69.073	1.00	29.80	AAAA N
ATOM	730	CA	VAL	75	39.351	11.474	68.892	1.00	34.91	AAAA C
ATOM	731	CB	VAL	75	39.856	12.445	69.955	1.00	26.03	AAAA C
ATOM	732	CG1	VAL	75	39.173	13.801	69.934	1.00	24.51	AAAA C
ATOM	733	CG2	VAL	75	39.675	11.910	71.366	1.00	19.87	AAAA C
ATOM	734	C	VAL	75	39.613	12.045	67.494	1.00	37.57	AAAA C
ATOM	735	O	VAL	75	40.724	11.908	67.022	1.00	35.99	AAAA O
ATOM	736	N	ILE	76	38.600	12.555	66.796	1.00	35.91	AAAA N
ATOM	738	CA	ILE	76	38.696	13.340	65.592	1.00	31.48	AAAA C
ATOM	739	CB	ILE	76	37.931	12.769	64.492	1.00	29.60	AAAA C
ATOM	740	CG2	ILE	76	37.856	13.630	63.209	1.00	19.54	AAAA C
ATOM	741	CG1	ILE	76	38.222	11.314	64.227	1.00	29.52	AAAA C
ATOM	742	CD1	ILE	76	37.149	10.556	63.478	1.00	28.85	AAAA C
ATOM	743	C	ILE	76	38.157	14.718	66.000	1.00	33.84	AAAA C
ATOM	744	O	ILE	76	36.987	14.777	66.274	1.00	38.84	AAAA O
ATOM	745	N	ARG	77	38.906	15.733	66.230	1.00	30.32	AAAA N
ATOM	747	CA	ARG	77	38.605	16.901	67.021	1.00	30.82	AAAA C
ATOM	748	CB	ARG	77	39.961	17.475	67.461	1.00	25.62	AAAA C
ATOM	749	CG	ARG	77	39.993	18.836	68.058	1.00	52.42	AAAA C
ATOM	750	CD	ARG	77	41.290	18.957	68.908	1.00	49.10	AAAA C
ATOM	751	NE	ARG	77	41.411	17.817	69.773	1.00	39.23	AAAA N
ATOM	753	CZ	ARG	77	40.977	18.016	71.064	1.00	48.79	AAAA C
ATOM	754	NH1	ARG	77	40.440	19.104	71.610	1.00	30.34	AAAA N
ATOM	757	NH2	ARG	77	41.061	17.012	71.941	1.00	40.38	AAAA N
ATOM	760	C	ARG	77	37.643	17.733	66.225	1.00	31.75	AAAA C
ATOM	761	O	ARG	77	36.944	18.637	66.664	1.00	31.40	AAAA O
ATOM	762	N	GLY	78	37.688	17.661	64.884	1.00	32.87	AAAA N
ATOM	764	CA	GLY	78	36.982	18.409	63.950	1.00	16.23	AAAA C
ATOM	765	C	GLY	78	37.199	19.880	64.063	1.00	31.58	AAAA C
ATOM	766	O	GLY	78	36.363	20.775	63.674	1.00	34.03	AAAA O
ATOM	767	N	TRP	79	38.439	20.321	64.304	1.00	31.21	AAAA N
ATOM	769	CA	TRP	79	38.757	21.740	64.337	1.00	30.80	AAAA C
ATOM	770	CB	TRP	79	40.177	21.943	64.845	1.00	39.07	AAAA C
ATOM	771	CG	TRP	79	40.626	23.343	65.164	1.00	36.64	AAAA C
ATOM	772	CD2	TRP	79	41.691	24.001	64.433	1.00	28.52	AAAA C
ATOM	773	CE2	TRP	79	41.826	25.288	65.002	1.00	36.49	AAAA C
ATOM	774	CE3	TRP	79	42.473	23.625	63.370	1.00	37.96	AAAA C
ATOM	775	CD1	TRP	79	40.199	24.235	66.113	1.00	29.59	AAAA C
ATOM	776	NE1	TRP	79	40.917	25.413	66.054	1.00	27.67	AAAA N
ATOM	778	CZ2	TRP	79	42.770	26.213	64.543	1.00	31.83	AAAA C
ATOM	779	CZ3	TRP	79	43.389	24.548	62.876	1.00	46.24	AAAA C
ATOM	780	CH2	TRP	79	43.525	25.794	63.470	1.00	35.31	AAAA C
ATOM	781	C	TRP	79	38.606	22.418	62.986	1.00	28.75	AAAA C
ATOM	782	O	TRP	79	38.585	23.624	62.961	1.00	23.61	AAAA O
ATOM	783	N	LYS	80	38.659	21.684	61.895	1.00	31.84	AAAA N
ATOM	785	CA	LYS	80	38.305	22.153	60.573	1.00	32.78	AAAA C
ATOM	786	CB	LYS	80	39.463	22.498	59.689	1.00	41.17	AAAA C
ATOM	787	CG	LYS	80	39.838	23.911	59.470	1.00	34.68	AAAA C
ATOM	788	CD	LYS	80	41.025	24.350	60.306	1.00	44.77	AAAA C
ATOM	789	CE	LYS	80	41.276	25.811	59.898	1.00	50.41	AAAA C
ATOM	790	NZ	LYS	80	42.530	25.752	59.092	1.00	67.26	AAAA N
ATOM	791	C	LYS	80	37.585	20.960	59.917	1.00	34.52	AAAA C
ATOM	792	O	LYS	80	37.950	19.843	60.237	1.00	37.62	AAAA O
ATOM	793	N	LEU	81	36.477	21.267	59.207	1.00	31.77	AAAA N
ATOM	795	CA	LEU	81	35.742	20.157	58.600	1.00	31.02	AAAA C
ATOM	796	CB	LEU	81	34.290	20.315	59.092	1.00	31.20	AAAA C
ATOM	797	CG	LEU	81	34.115	20.319	60.632	1.00	36.97	AAAA C
ATOM	798	CD1	LEU	81	32.832	21.080	60.954	1.00	27.98	AAAA C
ATOM	799	CD2	LEU	81	34.089	18.955	61.097	1.00	28.77	AAAA C
ATOM	800	C	LEU	81	35.733	20.023	57.104	1.00	29.86	AAAA C
ATOM	801	O	LEU	81	36.082	20.947	56.368	1.00	29.34	AAAA O
ATOM	802	N	PHE	82	35.430	18.813	56.594	1.00	27.78	AAAA N
ATOM	804	CA	PHE	82	35.176	16.653	55.182	1.00	28.68	AAAA C
ATOM	805	CB	PHE	82	35.513	17.236	54.795	1.00	32.78	AAAA C
ATOM	806	CG	PHE	82	35.348	16.901	53.357	1.00	30.48	AAAA C
ATOM	807	CD1	PHE	82	36.378	17.130	52.447	1.00	32.86	AAAA C
ATOM	809	CD2	PHE	82	34.142	16.361	52.914	1.00	30.93	AAAA C
ATOM	809	CE1	PHE	82	36.217	16.769	51.104	1.00	43.27	AAAA C
ATOM	810	CE2	PHE	82	33.963	16.061	51.538	1.00	26.30	AAAA C
ATOM	811	CZ	PHE	82	35.005	16.238	50.672	1.00	37.73	AAAA C
ATOM	812	C	PHE	82	33.670	18.911	54.993	1.00	30.06	AAAA C
ATOM	813	O	PHE	82	32.830	18.045	55.278	1.00	27.36	AAAA O
ATOM	814	N	TYR	83	33.301	20.148	54.770	1.00	31.68	AAAA N
ATOM	815	CA	TYR	83	31.911	20.605	54.633	1.00	40.76	AAAA C
ATOM	816	C	TYR	83	31.043	19.977	55.726	1.00	44.00	AAAA C
ATOM	817	O	TYR	83	30.075	19.210	55.487	1.00	50.47	AAAA O
ATOM	818	CB	TYR	83	31.359	20.199	53.269	1.00	31.55	AAAA C
ATOM	819	CG	TYR	83	32.196	20.742	52.117	0.01	20.00	AAAA C
ATOM	820	CD1	TYR	83	33.254	19.982	51.609	0.01	20.00	AAAA C
ATOM	821	CD2	TYR	83	31.906	21.998	51.575	0.01	20.00	AAAA C

Figure 1A-7

ATOM	822	CE1	TYR	83	34.827	20.480	50.556	1.00	20.00	AAAA C
ATOM	823	CE2	TYR	83	32.679	22.496	50.521	1.00	20.00	AAAA C
ATOM	824	CZ	TYR	83	33.749	21.737	50.012	1.00	20.00	AAAA C
ATOM	825	OH	TYR	83	34.492	22.222	48.989	1.00	20.00	AAAA O
ATOM	826	N	ASN	84	31.043	20.461	56.924	1.00	40.91	AAAA N
ATOM	827	CA	ASN	84	30.250	20.057	58.056	1.00	36.54	AAAA C
ATOM	828	CB	ASN	84	28.763	20.046	57.700	1.00	47.84	AAAA C
ATOM	829	CG	ASN	84	28.274	21.164	56.797	1.00	60.75	AAAA C
ATOM	830	OD1	ASN	84	28.319	22.343	57.119	1.00	45.55	AAAA O
ATOM	831	ND2	ASN	84	27.839	20.876	55.552	1.00	65.98	AAAA N
ATOM	832	C	ASN	84	30.686	18.679	58.556	1.00	36.33	AAAA C
ATOM	833	O	ASN	84	30.137	18.206	59.580	1.00	38.24	AAAA O
ATOM	834	N	TYR	85	31.455	17.900	57.800	1.00	32.78	AAAA N
ATOM	836	CA	TYR	85	31.617	16.504	58.222	1.00	35.45	AAAA C
ATOM	837	CB	TYR	85	31.473	15.579	57.000	1.00	35.54	AAAA C
ATOM	838	CG	TYR	85	30.078	15.733	56.453	1.00	41.35	AAAA C
ATOM	839	CD1	TYR	85	29.968	16.291	55.199	1.00	38.22	AAAA C
ATOM	840	CE1	TYR	85	28.611	16.445	54.704	1.00	40.83	AAAA C
ATOM	841	CD2	TYR	85	28.954	15.371	57.200	1.00	47.42	AAAA C
ATOM	842	CE2	TYR	85	27.661	15.533	56.705	1.00	45.91	AAAA C
ATOM	843	CZ	TYR	85	27.497	16.072	55.445	1.00	46.06	AAAA C
ATOM	844	OH	TYR	85	26.258	16.315	54.886	1.00	46.05	AAAA O
ATOM	846	C	TYR	85	32.977	16.367	58.891	1.00	32.08	AAAA C
ATOM	847	O	TYR	85	33.943	16.977	58.405	1.00	37.44	AAAA O
ATOM	848	N	ALA	86	33.027	15.691	59.979	1.00	30.21	AAAA N
ATOM	850	CA	ALA	86	34.257	15.325	60.670	1.00	34.10	AAAA C
ATOM	851	CB	ALA	86	33.999	15.370	62.157	1.00	25.48	AAAA C
ATOM	852	C	ALA	86	34.729	13.962	60.216	1.00	32.67	AAAA C
ATOM	853	O	ALA	86	35.795	13.481	60.577	1.00	35.10	AAAA O
ATOM	854	N	LEU	87	33.832	13.173	59.597	1.00	28.56	AAAA N
ATOM	856	CA	LEU	87	34.188	11.805	59.323	1.00	29.26	AAAA C
ATOM	857	CB	LEU	87	33.798	10.860	60.471	1.00	13.64	AAAA C
ATOM	858	CG	LEU	87	33.801	9.363	60.188	1.00	25.77	AAAA C
ATOM	859	CD1	LEU	87	35.140	8.915	59.571	1.00	27.21	AAAA C
ATOM	860	CD2	LEU	87	33.637	8.432	61.393	1.00	23.52	AAAA C
ATOM	861	C	LEU	87	33.530	11.429	58.021	1.00	35.60	AAAA C
ATOM	862	O	LEU	87	32.320	11.421	58.001	1.00	38.97	AAAA O
ATOM	863	N	VAL	88	34.174	11.300	56.875	1.00	37.86	AAAA N
ATOM	865	CA	VAL	88	33.438	11.032	55.628	1.00	33.32	AAAA C
ATOM	866	CB	VAL	88	33.666	12.085	54.553	1.00	22.38	AAAA C
ATOM	867	CG1	VAL	88	32.974	11.675	53.261	1.00	19.24	AAAA C
ATOM	868	CG2	VAL	88	33.165	13.402	55.042	1.00	13.27	AAAA C
ATOM	869	C	VAL	88	33.898	9.684	55.114	1.00	31.79	AAAA C
ATOM	870	O	VAL	88	35.069	9.407	55.117	1.00	33.57	AAAA O
ATOM	871	N	ILE	89	33.078	8.728	54.822	1.00	31.08	AAAA N
ATOM	873	CA	ILE	89	33.361	7.433	54.280	1.00	30.45	AAAA C
ATOM	874	CB	ILE	89	32.941	6.384	55.296	1.00	30.17	AAAA C
ATOM	875	CG2	ILE	89	32.898	4.954	54.821	1.00	37.24	AAAA C
ATOM	876	CG1	ILE	89	33.893	6.420	56.500	1.00	24.92	AAAA C
ATOM	877	CD1	ILE	89	33.424	5.613	57.675	1.00	23.96	AAAA C
ATOM	878	C	ILE	89	32.509	7.206	53.027	1.00	40.64	AAAA C
ATOM	879	O	ILE	89	31.330	6.881	53.205	1.00	38.69	AAAA O
ATOM	880	N	PHE	90	33.082	7.464	51.845	1.00	41.45	AAAA N
ATOM	882	CA	PHE	90	32.346	7.371	50.591	1.00	37.67	AAAA C
ATOM	883	CB	PHE	90	32.347	8.776	50.110	1.00	32.17	AAAA C
ATOM	884	CG	PHE	90	31.591	9.081	48.865	1.00	39.77	AAAA C
ATOM	885	CD1	PHE	90	30.387	9.772	49.025	1.00	32.02	AAAA C
ATOM	886	CD2	PHE	90	32.052	8.721	47.620	1.00	29.28	AAAA C
ATOM	887	CE1	PHE	90	29.611	10.111	47.938	1.00	33.30	AAAA C
ATOM	888	CE2	PHE	90	31.290	9.086	46.534	1.00	43.09	AAAA C
ATOM	889	CZ	PHE	90	30.083	9.764	46.687	1.00	50.24	AAAA C
ATOM	890	C	PHE	90	32.856	6.384	49.557	1.00	40.72	AAAA C
ATOM	891	O	PHE	90	34.027	6.296	49.203	1.00	46.15	AAAA O
ATOM	892	N	GLU	91	32.024	5.519	49.001	1.00	39.16	AAAA N
ATOM	894	CA	GLU	91	32.248	4.691	47.954	1.00	42.45	AAAA C
ATOM	895	CB	GLU	91	32.479	5.231	46.583	1.00	38.08	AAAA C
ATOM	896	CG	GLU	91	31.136	5.865	46.250	1.00	58.86	AAAA C
ATOM	897	CD	GLU	91	30.855	5.776	44.757	1.00	63.55	AAAA C
ATOM	898	OE1	GLU	91	31.473	6.651	44.082	1.00	64.10	AAAA O
ATOM	899	OE2	GLU	91	30.068	4.813	44.573	1.00	63.04	AAAA O
ATOM	900	C	GLU	91	33.422	3.734	48.313	1.00	42.06	AAAA C
ATOM	901	O	GLU	91	34.298	3.411	47.587	1.00	44.71	AAAA O
ATOM	902	N	MET	92	33.350	3.209	49.482	1.00	46.52	AAAA N
ATOM	904	CA	MET	92	34.409	2.401	50.088	1.00	42.26	AAAA C
ATOM	905	CB	MET	92	34.299	2.659	51.584	1.00	38.37	AAAA C
ATOM	906	CG	MET	92	35.412	2.156	52.420	1.00	59.29	AAAA C
ATOM	907	SD	MET	92	36.802	3.306	52.401	1.00	57.67	AAAA S
ATOM	908	CE	MET	92	36.349	4.405	51.109	1.00	38.36	AAAA C
ATOM	909	C	MET	92	34.012	1.005	49.745	1.00	43.37	AAAA C
ATOM	910	O	MET	92	33.335	0.298	50.523	1.00	45.58	AAAA O
ATOM	911	N	THR	93	34.449	0.518	48.602	1.00	47.09	AAAA N
ATOM	913	CA	THR	93	34.175	-0.900	48.273	1.00	47.32	AAAA C
ATOM	914	CB	THR	93	34.666	-1.281	46.868	1.00	55.29	AAAA C
ATOM	915	OG1	THR	93	34.913	-0.480	45.892	1.00	57.81	AAAA O
ATOM	917	CG2	THR	93	34.332	-2.715	46.516	1.00	44.71	AAAA C

Figure 1A-8

ATOM	918	C	THR	93	34.985	-1.874	49.196	1.00	51.93	AAAA C
ATOM	919	O	THR	93	36.115	-1.777	49.361	1.00	57.91	AAAA O
ATOM	920	N	ASN	94	34.237	-2.983	49.493	1.00	49.85	AAAA N
ATOM	922	CA	ASN	94	34.747	-4.069	50.285	1.00	45.64	AAAA C
ATOM	923	CB	ASN	94	36.241	-4.315	50.001	1.00	59.01	AAAA C
ATOM	924	CG	ASN	94	36.494	-4.849	48.599	1.00	75.44	AAAA C
ATOM	925	OD1	ASN	94	36.847	-4.081	47.688	1.00	77.49	AAAA O
ATOM	926	ND2	ASN	94	36.308	-6.153	48.408	1.00	79.63	AAAA N
ATOM	929	C	ASN	94	34.522	-3.938	51.763	1.00	42.58	AAAA C
ATOM	930	O	ASN	94	34.752	-4.814	52.591	1.00	46.36	AAAA O
ATOM	931	N	LEU	95	34.308	-2.609	52.132	1.00	37.28	AAAA N
ATOM	933	CA	LEU	95	34.324	-2.277	53.621	1.00	39.96	AAAA C
ATOM	934	CB	LEU	95	34.185	-0.786	53.851	1.00	34.05	AAAA C
ATOM	935	CG	LEU	95	34.323	-0.296	55.269	1.00	35.91	AAAA C
ATOM	936	CD1	LEU	95	35.785	-0.537	55.598	1.00	35.48	AAAA C
ATOM	937	CD2	LEU	95	33.847	1.177	55.344	1.00	25.46	AAAA C
ATOM	938	C	LEU	95	33.163	-2.986	54.275	1.00	43.75	AAAA C
ATOM	939	O	LEU	95	32.048	-2.936	53.772	1.00	44.04	AAAA O
ATOM	940	N	LYS	96	33.451	-3.863	55.213	1.00	46.50	AAAA N
ATOM	942	CA	LYS	96	32.364	-4.648	55.779	1.00	42.76	AAAA C
ATOM	943	CB	LYS	96	32.801	-6.075	55.995	1.00	41.41	AAAA C
ATOM	944	CG	LYS	96	32.760	-6.976	54.788	1.00	49.78	AAAA C
ATOM	945	CD	LYS	96	32.984	-8.446	55.127	1.00	58.09	AAAA C
ATOM	946	CE	LYS	96	33.772	-9.160	54.027	1.00	73.43	AAAA C
ATOM	947	NZ	LYS	96	34.098	-10.556	54.489	1.00	79.13	AAAA N
ATOM	951	C	LYS	96	31.970	-4.055	57.122	1.00	45.29	AAAA C
ATOM	952	O	LYS	96	30.978	-4.502	57.691	1.00	46.23	AAAA O
ATOM	953	N	ASP	97	32.685	-3.071	57.645	1.00	45.15	AAAA N
ATOM	955	CA	ASP	97	32.299	-2.384	58.961	1.00	42.15	AAAA C
ATOM	956	CB	ASP	97	32.294	-3.292	60.059	1.00	45.39	AAAA C
ATOM	957	CG	ASP	97	33.662	-3.562	60.624	1.00	56.95	AAAA C
ATOM	958	OD1	ASP	97	34.579	-2.825	61.012	1.00	59.88	AAAA O
ATOM	959	OD2	ASP	97	33.931	-4.782	60.714	1.00	56.01	AAAA O
ATOM	960	C	ASP	97	33.209	-1.224	59.201	1.00	41.25	AAAA C
ATOM	961	O	ASP	97	34.160	-1.074	58.437	1.00	47.03	AAAA O
ATOM	962	N	ILE	98	32.822	-0.366	60.139	1.00	40.41	AAAA N
ATOM	964	CA	ILE	98	33.675	0.820	60.340	1.00	37.83	AAAA C
ATOM	965	CB	ILE	98	32.983	2.006	61.006	1.00	38.99	AAAA C
ATOM	966	CG2	ILE	98	34.007	3.133	61.207	1.00	38.95	AAAA C
ATOM	967	CG1	ILE	98	31.835	2.488	60.092	1.00	34.84	AAAA C
ATOM	968	CD1	ILE	98	31.629	3.958	59.948	1.00	39.29	AAAA C
ATOM	969	C	ILE	98	34.854	0.322	61.114	1.00	35.11	AAAA C
ATOM	970	O	ILE	98	35.970	0.669	60.841	1.00	43.05	AAAA O
ATOM	971	N	GLY	99	34.618	-0.393	62.192	1.00	34.22	AAAA N
ATOM	973	CA	GLY	99	35.477	-0.972	63.121	1.00	33.74	AAAA C
ATOM	974	C	GLY	99	36.279	-0.084	64.024	1.00	35.90	AAAA C
ATOM	975	O	GLY	99	37.023	-0.572	64.899	1.00	38.21	AAAA O
ATOM	976	N	LEU	100	36.190	1.221	63.913	1.00	33.35	AAAA N
ATOM	978	CA	LEU	100	36.763	2.215	64.771	1.00	31.65	AAAA C
ATOM	979	CB	LEU	100	36.496	3.636	64.294	1.00	29.87	AAAA C
ATOM	980	CG	LEU	100	36.943	3.980	62.835	1.00	32.13	AAAA C
ATOM	981	CD1	LEU	100	36.710	5.479	62.610	1.00	21.38	AAAA C
ATOM	982	CD2	LEU	100	38.412	3.599	62.644	1.00	37.68	AAAA C
ATOM	983	C	LEU	100	36.312	1.976	66.194	1.00	31.94	AAAA C
ATOM	984	O	LEU	100	35.950	2.863	66.979	1.00	31.95	AAAA O
ATOM	985	N	TYR	101	36.704	0.851	66.779	1.00	31.87	AAAA N
ATOM	987	CA	TYR	101	36.329	0.395	68.071	1.00	33.33	AAAA C
ATOM	988	CB	TYR	101	36.491	-1.104	68.264	1.00	41.03	AAAA C
ATOM	989	CG	TYR	101	37.919	-1.559	68.369	1.00	46.66	AAAA C
ATOM	990	CD1	TYR	101	38.571	-1.380	69.587	1.00	51.20	AAAA C
ATOM	991	CE1	TYR	101	39.901	-1.743	69.749	1.00	49.44	AAAA C
ATOM	992	CD2	TYR	101	38.615	-2.112	67.322	1.00	45.15	AAAA C
ATOM	993	CE2	TYR	101	39.927	-2.505	67.479	1.00	47.09	AAAA C
ATOM	994	CZ	TYR	101	40.548	-2.321	68.688	1.00	49.43	AAAA C
ATOM	995	OH	TYR	101	41.834	-2.662	68.997	1.00	55.82	AAAA O
ATOM	997	C	TYR	101	36.989	1.059	69.214	1.00	33.46	AAAA C
ATOM	998	O	TYR	101	36.630	0.813	70.375	1.00	43.00	AAAA O
ATOM	999	N	ASN	102	37.752	2.091	69.068	1.00	38.12	AAAA N
ATOM	1001	CA	ASN	102	38.093	2.979	70.223	1.00	30.79	AAAA C
ATOM	1002	CB	ASN	102	39.603	2.911	70.363	1.00	48.63	AAAA C
ATOM	1003	CG	ASN	102	40.112	1.804	71.268	1.00	54.01	AAAA C
ATOM	1004	OD1	ASN	102	39.738	1.864	72.454	1.00	47.22	AAAA O
ATOM	1005	ND2	ASN	102	40.864	0.845	70.767	1.00	43.08	AAAA N
ATOM	1008	C	ASN	102	37.673	4.385	69.947	1.00	33.82	AAAA C
ATOM	1009	O	ASN	102	38.047	5.364	70.592	1.00	39.84	AAAA O
ATOM	1010	N	LEU	103	36.845	4.640	68.882	1.00	35.28	AAAA N
ATOM	1012	CA	LEU	103	36.473	6.040	68.621	1.00	36.57	AAAA C
ATOM	1013	CB	LEU	103	35.948	6.140	67.213	1.00	34.77	AAAA C
ATOM	1014	CG	LEU	103	35.525	7.482	66.612	1.00	30.32	AAAA C
ATOM	1015	CD1	LEU	103	36.606	8.513	66.646	1.00	23.20	AAAA C
ATOM	1016	CD2	LEU	103	35.199	7.169	65.146	1.00	37.10	AAAA C
ATOM	1017	C	LEU	103	35.484	6.508	69.691	1.00	37.31	AAAA C
ATOM	1019	O	LEU	103	34.449	5.874	69.837	1.00	34.24	AAAA O
ATOM	1019	N	ARG	104	35.810	7.456	70.563	1.00	33.31	AAAA N
ATOM	1021	CA	ARG	104	34.920	7.841	71.605	1.00	29.68	AAAA C

Figure 1A-9

ATOM	1022	CB	ARG	104	35.568	7.657	73.019	1.00	38.17	AAAA C
ATOM	1023	CG	ARG	104	36.356	6.375	73.165	1.00	48.37	AAAA C
ATOM	1024	CD	ARG	104	35.425	5.193	73.248	1.00	50.71	AAAA C
ATOM	1025	NE	ARG	104	34.582	5.320	74.413	1.00	52.38	AAAA N
ATOM	1027	CZ	ARG	104	34.900	4.847	75.621	1.00	72.73	AAAA C
ATOM	1028	NH1	ARG	104	36.047	4.214	75.809	1.00	81.87	AAAA N
ATOM	1031	NH2	ARG	104	33.990	5.070	76.577	1.00	78.27	AAAA N
ATOM	1034	C	ARG	104	34.466	9.273	71.540	1.00	32.58	AAAA C
ATOM	1035	O	ARG	104	33.553	9.743	72.223	1.00	39.89	AAAA O
ATOM	1036	N	ASN	105	34.992	10.065	70.637	1.00	33.47	AAAA N
ATOM	1038	CA	ASN	105	34.549	11.450	70.590	1.00	30.97	AAAA C
ATOM	1044	C	ASN	105	34.907	12.149	69.310	1.00	31.00	AAAA C
ATOM	1045	O	ASN	105	36.086	12.067	69.050	1.00	37.79	AAAA O
ATOM	1039	CB	ASN	105	35.203	12.199	71.721	1.00	42.28	AAAA C
ATOM	1040	CG	ASN	105	34.786	13.568	71.756	1.00	24.93	AAAA C
ATOM	1041	OD1	ASN	105	35.125	14.549	71.127	1.00	38.14	AAAA O
ATOM	1042	ND2	ASN	105	33.828	13.985	72.649	1.00	35.96	AAAA N
ATOM	1016	N	ILE	106	33.969	12.669	68.576	1.00	31.90	AAAA N
ATOM	1048	CA	ILE	106	34.129	13.551	67.469	1.00	23.39	AAAA C
ATOM	1049	CB	ILE	106	33.239	13.185	66.307	1.00	16.54	AAAA C
ATOM	1050	CG2	ILE	106	33.132	14.408	65.374	1.00	20.38	AAAA C
ATOM	1051	CG1	ILE	106	33.928	12.034	65.558	1.00	18.30	AAAA C
ATOM	1052	CD1	ILE	106	33.055	11.293	64.643	1.00	25.48	AAAA C
ATOM	1053	C	ILE	106	33.803	14.909	68.009	1.00	27.40	AAAA C
ATOM	1054	O	ILE	106	32.628	15.106	68.243	1.00	32.86	AAAA O
ATOM	1055	N	THR	107	34.719	15.789	68.350	1.00	30.43	AAAA N
ATOM	1057	CA	THR	107	34.532	16.983	69.145	1.00	28.27	AAAA C
ATOM	1058	CB	THR	107	35.902	17.607	69.570	1.00	35.78	AAAA C
ATOM	1059	OG1	THR	107	36.819	16.503	69.738	1.00	40.26	AAAA O
ATOM	1061	CG2	THR	107	35.954	18.411	70.855	1.00	28.13	AAAA C
ATOM	1062	C	THR	107	33.728	17.950	69.332	1.00	27.95	AAAA C
ATOM	1063	O	THR	107	33.392	19.060	68.831	1.00	32.99	AAAA O
ATOM	1064	N	ARG	108	33.669	17.777	67.019	1.00	30.28	AAAA N
ATOM	1066	CA	ARG	108	33.046	18.809	66.180	1.00	31.25	AAAA C
ATOM	1067	CB	ARG	108	33.965	20.011	65.951	1.00	25.13	AAAA C
ATOM	1068	CG	ARG	108	33.105	21.174	65.543	1.00	30.68	AAAA C
ATOM	1069	CD	ARG	108	33.917	22.444	65.529	1.00	17.12	AAAA C
ATOM	1070	NE	ARG	108	33.511	23.376	64.451	1.00	33.40	AAAA N
ATOM	1072	CZ	ARG	108	34.045	23.608	63.266	1.00	46.41	AAAA C
ATOM	1073	NH1	ARG	108	35.162	22.929	62.868	1.00	40.30	AAAA N
ATOM	1076	NH2	ARG	108	33.454	24.543	62.494	1.00	39.82	AAAA N
ATOM	1079	C	ARG	108	32.701	18.328	64.784	1.00	31.50	AAAA C
ATOM	1080	O	ARG	108	33.379	17.381	64.430	1.00	32.67	AAAA O
ATOM	1081	N	GLY	109	31.567	18.809	64.284	1.00	32.60	AAAA N
ATOM	1083	CA	GLY	109	31.082	18.385	62.983	1.00	28.87	AAAA C
ATOM	1084	C	GLY	109	30.470	17.008	63.001	1.00	32.32	AAAA C
ATOM	1085	O	GLY	109	30.471	16.306	64.006	1.00	38.03	AAAA O
ATOM	1086	N	ALA	110	29.920	16.560	61.894	1.00	34.11	AAAA N
ATOM	1088	CA	ALA	110	29.086	15.371	61.833	1.00	36.77	AAAA C
ATOM	1089	CB	ALA	110	27.708	15.721	61.223	1.00	15.32	AAAA C
ATOM	1090	C	ALA	110	29.745	14.335	60.957	1.00	32.10	AAAA C
ATOM	1091	O	ALA	110	30.921	14.332	60.687	1.00	34.11	AAAA O
ATOM	1092	N	ILE	111	29.030	13.337	60.557	1.00	26.55	AAAA N
ATOM	1094	CA	ILE	111	29.569	12.273	59.771	1.00	32.90	AAAA C
ATOM	1095	CB	ILE	111	29.669	10.967	60.591	1.00	38.07	AAAA C
ATOM	1096	CG2	ILE	111	30.091	11.140	62.036	1.00	34.05	AAAA C
ATOM	1097	CG1	ILE	111	28.345	10.237	60.684	1.00	26.54	AAAA C
ATOM	1098	CD1	ILE	111	28.437	8.872	61.407	1.00	27.11	AAAA C
ATOM	1099	C	ILE	111	28.738	11.928	58.521	1.00	33.98	AAAA C
ATOM	1100	O	ILE	111	27.533	12.179	58.532	1.00	32.15	AAAA O
ATOM	1101	N	ARG	112	29.432	11.423	57.501	1.00	30.54	AAAA N
ATOM	1103	CA	ARG	112	28.773	11.107	56.247	1.00	27.48	AAAA C
ATOM	1104	CB	ARG	112	29.186	12.085	55.169	1.00	26.35	AAAA C
ATOM	1105	CG	ARG	112	28.548	11.653	53.816	1.00	25.83	AAAA C
ATOM	1106	CD	ARG	112	28.659	12.912	52.992	1.00	32.92	AAAA C
ATOM	1107	NE	ARG	112	27.950	12.726	51.770	1.00	50.34	AAAA N
ATOM	1109	CZ	ARG	112	27.778	13.503	50.720	1.00	47.61	AAAA C
ATOM	1110	NH1	ARG	112	28.334	14.695	50.696	1.00	44.92	AAAA N
ATOM	1113	NH2	ARG	112	27.012	12.925	49.789	1.00	46.00	AAAA N
ATOM	1116	C	ARG	112	29.200	9.738	55.791	1.00	29.74	AAAA C
ATOM	1117	O	ARG	112	30.343	9.611	55.406	1.00	36.52	AAAA O
ATOM	1118	N	ILE	113	28.326	8.754	55.886	1.00	33.99	AAAA N
ATOM	1120	CA	ILE	113	28.612	7.376	55.555	1.00	36.26	AAAA C
ATOM	1121	CB	ILE	113	28.457	6.461	56.760	1.00	33.27	AAAA C
ATOM	1122	CG2	ILE	113	28.850	5.021	56.449	1.00	15.85	AAAA C
ATOM	1123	CG1	ILE	113	29.374	7.012	57.874	1.00	31.92	AAAA C
ATOM	1124	CD1	ILE	113	29.324	6.250	59.176	1.00	42.34	AAAA C
ATOM	1125	C	ILE	113	27.729	6.959	54.398	1.00	39.26	AAAA C
ATOM	1126	O	ILE	113	26.637	6.482	54.664	1.00	50.72	AAAA O
ATOM	1127	N	GLU	114	28.175	7.199	53.190	1.00	35.86	AAAA N
ATOM	1129	CA	GLU	114	27.491	7.103	51.935	1.00	38.76	AAAA C
ATOM	1130	CB	GLU	114	27.471	8.443	51.216	1.00	25.58	AAAA C
ATOM	1131	CG	GLU	114	26.567	8.402	49.969	1.00	27.97	AAAA C
ATOM	1132	CD	GLU	114	26.349	9.810	49.578	1.00	36.85	AAAA C
ATOM	1133	OE1	GLU	114	26.763	10.662	50.414	1.00	45.57	AAAA O

Figure 1A-10

ATOM	1134	OE2	GLU	114	25.787	10.106	49.488	1.00	35.53	AAAA O
ATOM	1135	C	GLU	114	28.039	6.072	50.944	1.00	44.17	AAAA C
ATOM	1136	O	GLU	114	29.120	5.538	51.090	1.00	49.97	AAAA O
ATOM	1137	N	LYS	115	27.191	5.556	50.096	1.00	40.55	AAAA N
ATOM	1139	CA	LYS	115	27.219	4.440	49.242	1.00	41.16	AAAA C
ATOM	1140	CB	LYS	115	27.275	4.764	47.719	1.00	23.62	AAAA C
ATOM	1141	CG	LYS	115	27.019	6.194	47.411	1.00	18.39	AAAA C
ATOM	1142	CD	LYS	115	26.537	6.355	45.982	1.00	24.74	AAAA C
ATOM	1143	CE	LYS	115	26.751	7.804	45.622	1.00	41.86	AAAA C
ATOM	1144	NZ	LYS	115	27.165	8.045	44.196	1.00	60.91	AAAA N
ATOM	1148	C	LYS	115	28.287	3.421	49.611	1.00	42.39	AAAA C
ATOM	1149	O	LYS	115	29.102	3.103	48.749	1.00	46.68	AAAA O
ATOM	1150	N	ASN	116	28.137	2.677	50.665	1.00	40.99	AAAA N
ATOM	1152	CA	ASN	116	29.022	1.570	50.976	1.00	37.33	AAAA C
ATOM	1153	CB	ASN	116	29.534	1.868	52.381	1.00	46.12	AAAA C
ATOM	1154	CG	ASN	116	30.372	3.193	52.315	1.00	49.90	AAAA C
ATOM	1155	OD1	ASN	116	31.337	3.016	51.583	1.00	38.59	AAAA O
ATOM	1156	ND2	ASN	116	29.927	4.174	53.056	1.00	37.35	AAAA N
ATOM	1159	C	ASN	116	28.275	0.277	50.974	1.00	42.82	AAAA C
ATOM	1160	O	ASN	116	28.067	-0.361	52.033	1.00	48.24	AAAA O
ATOM	1161	N	ALA	117	27.989	-0.188	49.772	1.00	40.94	AAAA N
ATOM	1163	CA	ALA	117	27.195	-1.376	49.542	1.00	43.35	AAAA C
ATOM	1164	CB	ALA	117	27.494	-1.884	48.156	1.00	47.63	AAAA C
ATOM	1165	C	ALA	117	27.294	-2.504	50.529	1.00	46.55	AAAA C
ATOM	1166	O	ALA	117	26.211	-2.998	50.890	1.00	51.24	AAAA O
ATOM	1167	N	ASP	118	28.484	-2.823	51.005	1.00	47.43	AAAA N
ATOM	1169	CA	ASP	118	28.559	-3.980	51.920	1.00	45.74	AAAA C
ATOM	1170	CB	ASP	118	29.659	-4.945	51.477	1.00	55.39	AAAA C
ATOM	1171	CG	ASP	118	29.684	-5.119	49.958	1.00	59.40	AAAA C
ATOM	1172	OD1	ASP	118	28.870	-5.976	49.608	1.00	64.40	AAAA O
ATOM	1173	OD2	ASP	118	30.449	-4.447	49.207	1.00	66.73	AAAA O
ATOM	1174	C	ASP	118	28.818	-3.586	53.353	1.00	37.29	AAAA C
ATOM	1175	O	ASP	118	29.127	-4.536	54.026	1.00	42.89	AAAA O
ATOM	1176	N	LEU	119	28.670	-2.327	53.685	1.00	36.46	AAAA N
ATOM	1178	CA	LEU	119	28.986	-1.885	55.047	1.00	40.58	AAAA C
ATOM	1179	CB	LEU	119	29.159	-0.389	55.145	1.00	34.31	AAAA C
ATOM	1180	CG	LEU	119	29.640	0.331	56.378	1.00	36.58	AAAA C
ATOM	1181	CD1	LEU	119	30.950	-0.101	56.948	1.00	35.77	AAAA C
ATOM	1182	CD2	LEU	119	29.791	1.830	56.104	1.00	29.68	AAAA C
ATOM	1183	C	LEU	119	27.927	-2.376	56.007	1.00	43.67	AAAA C
ATOM	1184	O	LEU	119	26.748	-2.248	55.743	1.00	45.32	AAAA O
ATOM	1185	N	CYS	120	28.361	-2.967	57.110	1.00	43.53	AAAA N
ATOM	1187	CA	CYS	120	27.378	-3.407	58.089	1.00	38.93	AAAA C
ATOM	1188	C	CYS	120	27.881	-2.921	59.426	1.00	41.91	AAAA C
ATOM	1189	O	CYS	120	28.660	-1.960	59.446	1.00	43.66	AAAA O
ATOM	1190	CB	CYS	120	27.285	-4.907	58.100	1.00	37.59	AAAA C
ATOM	1191	SG	CYS	120	26.568	-5.622	56.639	1.00	58.32	AAAA S
ATOM	1192	N	TYR	121	27.328	-3.456	60.509	1.00	38.05	AAAA N
ATOM	1194	CA	TYR	121	27.795	-3.010	61.827	1.00	39.68	AAAA C
ATOM	1195	CB	TYR	121	29.189	-3.572	62.130	1.00	34.61	AAAA C
ATOM	1196	CG	TYR	121	28.950	-5.032	62.519	1.00	36.52	AAAA C
ATOM	1197	CD1	TYR	121	29.087	-6.045	61.582	1.00	33.58	AAAA C
ATOM	1198	CE1	TYR	121	28.952	-7.350	61.980	1.00	41.21	AAAA C
ATOM	1199	CD2	TYR	121	28.560	-5.337	63.817	1.00	36.31	AAAA C
ATOM	1200	CE2	TYR	121	28.257	-6.630	64.201	1.00	39.48	AAAA C
ATOM	1201	CZ	TYR	121	28.432	-7.641	63.270	1.00	46.07	AAAA C
ATOM	1202	OH	TYR	121	28.161	-8.924	63.730	1.00	49.20	AAAA O
ATOM	1204	C	TYR	121	27.674	-1.523	61.789	1.00	38.83	AAAA C
ATOM	1205	O	TYR	121	28.445	-0.778	62.369	1.00	43.22	AAAA O
ATOM	1206	N	LEU	122	26.587	-1.045	61.180	1.00	39.58	AAAA N
ATOM	1208	CA	LEU	122	26.361	0.405	61.090	1.00	44.82	AAAA C
ATOM	1209	CB	LEU	122	25.990	0.715	59.634	1.00	46.48	AAAA C
ATOM	1210	CG	LEU	122	26.497	2.014	59.108	1.00	44.44	AAAA C
ATOM	1211	CD1	LEU	122	25.778	2.448	57.859	1.00	32.19	AAAA C
ATOM	1212	CD2	LEU	122	26.136	3.057	60.170	1.00	47.76	AAAA C
ATOM	1213	C	LEU	122	25.212	0.910	61.935	1.00	44.85	AAAA C
ATOM	1214	O	LEU	122	25.269	1.759	62.839	1.00	47.66	AAAA O
ATOM	1215	N	SER	123	24.194	0.137	61.843	1.00	40.12	AAAA N
ATOM	1217	CA	SER	123	22.949	0.435	62.703	1.00	33.98	AAAA C
ATOM	1218	CB	SER	123	21.754	-0.330	62.239	1.00	19.26	AAAA C
ATOM	1219	OG	SER	123	21.964	-1.762	62.402	1.00	34.35	AAAA O
ATOM	1221	C	SER	123	23.165	0.060	64.159	1.00	37.43	AAAA C
ATOM	1222	O	SER	123	22.326	0.280	65.025	1.00	35.33	AAAA O
ATOM	1223	N	THR	124	24.242	-0.698	64.432	1.00	39.03	AAAA N
ATOM	1225	CA	THR	124	24.554	-1.165	65.753	1.00	37.79	AAAA C
ATOM	1226	CB	THR	124	25.368	-2.461	65.719	1.00	42.39	AAAA C
ATOM	1227	OG1	THR	124	26.502	-2.020	64.924	1.00	47.70	AAAA O
ATOM	1229	CG2	THR	124	24.677	-3.622	65.006	1.00	40.93	AAAA C
ATOM	1230	C	THR	124	25.522	-0.206	66.445	1.00	39.29	AAAA C
ATOM	1231	O	THR	124	25.948	-0.642	67.499	1.00	41.41	AAAA O
ATOM	1232	N	VAL	125	25.737	1.001	65.985	1.00	37.80	AAAA N
ATOM	1234	CA	VAL	125	26.594	1.964	66.661	1.00	41.06	AAAA C
ATOM	1235	CB	VAL	125	27.683	2.542	65.711	1.00	39.50	AAAA C
ATOM	1236	CG1	VAL	125	28.570	3.599	66.352	1.00	28.36	AAAA C
ATOM	1237	CG2	VAL	125	28.693	1.565	65.110	1.00	33.07	AAAA C

Figure 1A-11

ATOM	1239	C	VAL	125	25.750	3.127	67.173	1.00 41.17	AAAA C
ATOM	1239	O	VAL	125	24.941	3.750	66.531	1.00 41.22	AAAA O
ATOM	1240	N	ASP	126	26.672	3.636	68.367	1.00 44.54	AAAA N
ATOM	1242	CA	ASP	126	25.310	1.734	68.967	1.00 37.44	AAAA C
ATOM	1243	CB	ASP	126	24.862	1.335	70.342	1.00 34.73	AAAA C
ATOM	1244	CG	ASP	126	23.879	5.303	70.993	1.00 45.53	AAAA C
ATOM	1245	OD1	ASP	126	23.699	6.520	70.685	1.00 27.71	AAAA O
ATOM	1246	OD2	ASP	126	23.220	4.865	71.964	1.00 52.32	AAAA O
ATOM	1247	C	ASP	126	26.146	5.985	68.872	1.00 40.83	AAAA C
ATOM	1248	O	ASP	126	26.740	6.400	69.888	1.00 42.78	AAAA O
ATOM	1249	N	TRP	127	26.029	6.649	67.704	1.00 35.42	AAAA N
ATOM	1251	CA	TRP	127	26.777	7.856	67.410	1.00 33.02	AAAA C
ATOM	1252	CB	TRP	127	26.568	9.296	65.930	1.00 24.89	AAAA C
ATOM	1253	CG	TRP	127	27.195	7.372	64.907	1.00 34.36	AAAA C
ATOM	1254	CD2	TRP	127	28.587	7.208	64.518	1.00 28.69	AAAA C
ATOM	1255	CE2	TRP	127	28.631	6.186	63.579	1.00 29.06	AAAA C
ATOM	1256	CE3	TRP	127	29.778	7.845	64.873	1.00 35.51	AAAA C
ATOM	1257	CD1	TRP	127	26.465	6.450	64.188	1.00 18.67	AAAA C
ATOM	1258	NE1	TRP	127	27.311	5.712	63.391	1.00 42.87	AAAA N
ATOM	1260	CZ2	TRP	127	29.792	5.783	62.954	1.00 32.53	AAAA C
ATOM	1261	CZ3	TRP	127	30.972	7.445	64.285	1.00 31.51	AAAA C
ATOM	1262	CH2	TRP	127	30.937	6.405	63.336	1.00 37.86	AAAA C
ATOM	1263	C	TRP	127	26.558	9.010	68.367	1.00 36.09	AAAA C
ATOM	1264	O	TRP	127	27.382	9.977	68.497	1.00 40.87	AAAA O
ATOM	1265	N	SER	128	25.493	8.931	69.171	1.00 31.24	AAAA N
ATOM	1267	CA	SER	128	25.201	10.041	70.081	1.00 34.04	AAAA C
ATOM	1268	CB	SER	128	23.757	10.042	70.603	1.00 36.87	AAAA C
ATOM	1269	OG	SER	128	23.433	8.917	71.424	1.00 28.96	AAAA O
ATOM	1271	C	SER	128	26.133	9.975	71.292	1.00 32.39	AAAA C
ATOM	1272	O	SER	128	26.212	10.957	72.134	1.00 30.91	AAAA O
ATOM	1273	N	LEU	129	26.662	8.792	71.549	1.00 27.18	AAAA N
ATOM	1275	CA	LEU	129	27.701	8.607	72.526	1.00 36.73	AAAA C
ATOM	1276	CB	LEU	129	27.920	7.132	72.741	1.00 32.53	AAAA C
ATOM	1277	CG	LEU	129	26.795	6.324	73.371	1.00 39.28	AAAA C
ATOM	1278	CD1	LEU	129	27.292	5.024	73.975	1.00 32.54	AAAA C
ATOM	1279	CD2	LEU	129	26.237	7.117	74.560	1.00 32.12	AAAA C
ATOM	1280	C	LEU	129	29.054	9.226	72.113	1.00 38.04	AAAA C
ATOM	1281	O	LEU	129	29.645	10.001	72.874	1.00 34.50	AAAA O
ATOM	1282	N	ILE	130	29.316	9.217	70.807	1.00 42.09	AAAA N
ATOM	1284	CA	ILE	130	30.480	9.743	70.144	1.00 41.35	AAAA C
ATOM	1285	CB	ILE	130	30.793	8.886	68.901	1.00 41.73	AAAA C
ATOM	1286	CG2	ILE	130	31.992	9.434	68.176	1.00 31.95	AAAA C
ATOM	1287	CG1	ILE	130	30.969	7.413	69.347	1.00 26.64	AAAA C
ATOM	1288	CD1	ILE	130	31.053	6.457	68.165	1.00 42.65	AAAA C
ATOM	1289	C	ILE	130	30.305	11.178	69.679	1.00 46.48	AAAA C
ATOM	1290	O	ILE	130	31.224	11.985	69.966	1.00 38.46	AAAA O
ATOM	1291	N	LEU	131	29.089	11.495	69.193	1.00 45.14	AAAA N
ATOM	1293	CA	LEU	131	28.895	12.865	68.651	1.00 41.45	AAAA C
ATOM	1294	CB	LEU	131	28.499	12.616	67.259	1.00 46.81	AAAA C
ATOM	1295	CG	LEU	131	28.823	13.805	66.378	1.00 36.79	AAAA C
ATOM	1296	CD1	LEU	131	29.128	11.405	66.324	1.00 30.15	AAAA C
ATOM	1297	CD2	LEU	131	27.625	13.581	65.334	1.00 19.92	AAAA C
ATOM	1298	C	LEU	131	27.661	13.525	69.285	1.00 39.28	AAAA C
ATOM	1299	O	LEU	131	26.599	12.867	69.311	1.00 37.75	AAAA O
ATOM	1300	N	ASP	132	27.742	14.811	69.518	1.00 33.72	AAAA N
ATOM	1302	CA	ASP	132	26.610	15.542	70.003	1.00 38.20	AAAA C
ATOM	1303	CB	ASP	132	27.017	16.944	70.381	1.00 43.17	AAAA C
ATOM	1304	CG	ASP	132	27.349	17.137	71.834	1.00 43.29	AAAA C
ATOM	1305	OD1	ASP	132	27.536	16.122	72.521	1.00 47.12	AAAA O
ATOM	1306	OD2	ASP	132	27.413	18.331	72.208	1.00 60.58	AAAA O
ATOM	1307	C	ASP	132	25.520	15.659	68.946	1.00 43.46	AAAA C
ATOM	1308	O	ASP	132	24.481	15.032	68.939	1.00 49.32	AAAA O
ATOM	1309	N	ALA	133	25.754	16.398	67.900	1.00 45.03	AAAA N
ATOM	1311	CA	ALA	133	24.947	16.776	66.773	1.00 38.62	AAAA C
ATOM	1312	CB	ALA	133	25.620	17.987	66.092	1.00 33.82	AAAA C
ATOM	1313	C	ALA	133	24.694	15.669	65.775	1.00 33.33	AAAA C
ATOM	1314	O	ALA	133	24.777	15.791	64.517	1.00 33.71	AAAA O
ATOM	1315	N	VAL	134	24.115	14.565	66.219	1.00 27.88	AAAA N
ATOM	1317	CA	VAL	134	23.813	13.440	65.377	1.00 29.90	AAAA C
ATOM	1318	CB	VAL	134	23.202	12.241	66.120	1.00 40.63	AAAA C
ATOM	1319	CG1	VAL	134	24.265	11.441	66.855	1.00 35.20	AAAA C
ATOM	1320	CG2	VAL	134	22.095	12.701	67.068	1.00 30.84	AAAA C
ATOM	1321	C	VAL	134	22.735	13.732	64.353	1.00 36.98	AAAA C
ATOM	1322	O	VAL	134	22.616	13.106	63.292	1.00 32.95	AAAA O
ATOM	1323	N	SER	135	21.920	14.777	64.626	1.00 39.65	AAAA N
ATOM	1325	CA	SER	135	20.886	15.139	63.692	1.00 43.12	AAAA C
ATOM	1326	CB	SER	135	20.093	16.277	64.305	1.00 45.19	AAAA C
ATOM	1327	OG	SER	135	20.882	17.369	64.684	1.00 39.25	AAAA O
ATOM	1329	C	SER	135	21.396	15.516	62.309	1.00 41.15	AAAA C
ATOM	1330	O	SER	135	20.615	15.642	61.359	1.00 43.81	AAAA O
ATOM	1331	N	ASN	136	22.615	15.911	62.165	1.00 41.11	AAAA N
ATOM	1333	CA	ASN	136	23.298	16.353	60.978	1.00 37.21	AAAA C
ATOM	1334	CB	ASN	136	24.324	17.372	61.399	1.00 39.66	AAAA C
ATOM	1335	CG	ASN	136	23.724	18.709	61.717	1.00 36.59	AAAA C
ATOM	1336	OD1	ASN	136	22.695	19.079	61.149	1.00 50.81	AAAA O

Figure 1A-12

ATOM	1337	HD2	ASN	136	24.579	19.441	62.585	1.00	47.85	AAAA H
ATOM	1340	C	ASN	136	21.931	15.230	60.259	1.00	35.31	AAAA C
ATOM	1341	O	ASN	136	24.535	15.484	59.194	1.00	38.70	AAAA O
ATOM	1342	N	ASN	137	24.057	14.035	60.793	1.00	29.11	AAAA N
ATOM	1344	CA	ASN	137	24.721	12.959	60.126	1.00	32.98	AAAA C
ATOM	1345	CB	ASN	137	24.737	11.703	61.033	1.00	24.45	AAAA C
ATOM	1346	CG	ASN	137	25.631	11.965	62.217	1.00	26.63	AAAA C
ATOM	1347	OD1	ASN	137	26.070	13.121	62.369	1.00	30.22	AAAA O
ATOM	1348	ND2	ASN	137	25.830	10.923	63.000	1.00	18.90	AAAA N
ATOM	1351	C	ASN	137	23.959	12.749	58.817	1.00	35.89	AAAA C
ATOM	1352	O	ASN	137	22.716	12.755	58.855	1.00	38.57	AAAA O
ATOM	1353	N	TYR	138	24.592	12.251	57.785	1.00	32.86	AAAA N
ATOM	1355	CA	TYR	138	24.093	11.983	56.489	1.00	30.25	AAAA C
ATOM	1356	CB	TYR	138	24.682	12.861	55.421	1.00	27.10	AAAA C
ATOM	1357	CG	TYR	138	24.918	12.741	54.079	1.00	37.89	AAAA C
ATOM	1358	CD1	TYR	138	23.893	13.671	53.648	1.00	39.22	AAAA C
ATOM	1359	CE1	TYR	138	22.910	13.579	52.392	1.00	37.65	AAAA C
ATOM	1360	CD2	TYR	138	24.357	11.717	53.195	1.00	44.28	AAAA C
ATOM	1361	CE2	TYR	138	23.901	11.615	51.951	1.00	41.97	AAAA C
ATOM	1362	CZ	TYR	138	22.868	12.562	51.584	1.00	39.42	AAAA C
ATOM	1363	OH	TYR	138	22.296	12.504	50.318	1.00	45.48	AAAA O
ATOM	1365	C	TYR	138	24.373	10.579	56.051	1.00	31.33	AAAA C
ATOM	1366	O	TYR	138	25.505	10.317	55.797	1.00	37.76	AAAA O
ATOM	1367	N	ILE	139	23.461	9.660	56.116	1.00	35.40	AAAA N
ATOM	1369	CA	ILE	139	23.637	8.249	55.935	1.00	34.04	AAAA C
ATOM	1370	CB	ILE	139	23.234	7.450	57.171	1.00	28.66	AAAA C
ATOM	1371	CG2	ILE	139	23.640	5.984	57.093	1.00	21.99	AAAA C
ATOM	1372	CG1	ILE	139	23.711	8.057	58.469	1.00	42.81	AAAA C
ATOM	1373	CD1	ILE	139	24.455	7.100	59.389	1.00	52.23	AAAA C
ATOM	1374	C	ILE	139	22.729	7.708	54.830	1.00	35.73	AAAA C
ATOM	1375	O	ILE	139	21.538	7.890	54.757	1.00	42.61	AAAA O
ATOM	1376	N	VAL	140	23.286	6.997	53.873	1.00	35.29	AAAA N
ATOM	1378	CA	VAL	140	22.533	6.481	52.765	1.00	32.39	AAAA C
ATOM	1379	CB	VAL	140	21.967	7.627	51.881	1.00	36.05	AAAA C
ATOM	1380	CG1	VAL	140	22.800	8.375	50.881	1.00	25.88	AAAA C
ATOM	1381	CG2	VAL	140	20.807	7.034	51.047	1.00	34.96	AAAA C
ATOM	1382	C	VAL	140	23.422	5.670	51.874	1.00	41.96	AAAA C
ATOM	1383	O	VAL	140	24.537	6.172	51.637	1.00	44.03	AAAA O
ATOM	1384	N	GLY	141	22.899	4.562	51.402	1.00	42.66	AAAA N
ATOM	1386	CA	GLY	141	23.381	3.805	50.278	1.00	30.94	AAAA C
ATOM	1387	C	GLY	141	24.265	2.696	50.835	1.00	38.98	AAAA C
ATOM	1388	O	GLY	141	25.132	2.003	50.176	1.00	35.87	AAAA O
ATOM	1389	N	ASN	142	23.985	2.418	52.116	1.00	38.90	AAAA N
ATOM	1391	CA	ASN	142	24.858	1.390	52.746	1.00	44.32	AAAA C
ATOM	1392	CB	ASN	142	25.257	1.774	54.187	1.00	43.12	AAAA C
ATOM	1393	CG	ASN	142	26.131	3.022	54.152	1.00	42.00	AAAA C
ATOM	1394	OD1	ASN	142	26.984	3.077	53.269	1.00	40.47	AAAA O
ATOM	1395	ND2	ASN	142	25.945	4.022	55.019	1.00	41.98	AAAA N
ATOM	1398	C	ASN	142	24.153	0.066	52.687	1.00	45.84	AAAA C
ATOM	1399	O	ASN	142	23.113	-0.015	52.055	1.00	49.65	AAAA O
ATOM	1400	N	LYS	143	24.574	-0.990	53.272	1.00	45.23	AAAA N
ATOM	1402	CA	LYS	143	24.073	-2.299	53.195	1.00	49.14	AAAA C
ATOM	1403	CB	LYS	143	25.166	-3.328	53.433	1.00	41.49	AAAA C
ATOM	1404	CG	LYS	143	24.750	-4.686	53.832	1.00	44.96	AAAA C
ATOM	1405	CD	LYS	143	25.512	-5.743	53.100	1.00	48.66	AAAA C
ATOM	1406	CE	LYS	143	25.043	-7.131	53.558	1.00	38.35	AAAA C
ATOM	1407	NZ	LYS	143	26.080	-8.093	53.040	1.00	53.83	AAAA N
ATOM	1411	C	LYS	143	22.902	-2.431	54.169	1.00	52.85	AAAA C
ATOM	1412	O	LYS	143	22.960	-2.099	55.360	1.00	55.21	AAAA O
ATOM	1413	N	PRO	144	21.806	-3.047	53.731	1.00	52.39	AAAA N
ATOM	1414	CD	PRO	144	21.617	-3.469	52.315	1.00	52.58	AAAA C
ATOM	1415	CA	PRO	144	20.559	-3.118	54.489	1.00	48.30	AAAA C
ATOM	1416	CB	PRO	144	19.549	-3.602	53.455	1.00	51.41	AAAA C
ATOM	1417	CG	PRO	144	20.134	-3.299	52.099	1.00	50.41	AAAA C
ATOM	1418	C	PRO	144	20.621	-4.050	55.659	1.00	44.65	AAAA C
ATOM	1419	O	PRO	144	20.904	-5.236	55.501	1.00	36.84	AAAA O
ATOM	1420	N	PRO	145	20.319	-3.533	56.859	1.00	45.12	AAAA N
ATOM	1421	CD	PRO	145	20.123	-2.054	57.094	1.00	38.17	AAAA C
ATOM	1422	CA	PRO	145	20.448	-4.233	58.128	1.00	40.19	AAAA C
ATOM	1423	CB	PRO	145	19.704	-3.288	59.099	1.00	37.08	AAAA C
ATOM	1424	CG	PRO	145	20.040	-1.910	58.602	1.00	33.65	AAAA C
ATOM	1425	C	PRO	145	19.993	-5.655	58.155	1.00	47.17	AAAA C
ATOM	1426	O	PRO	145	20.556	-6.592	58.768	1.00	48.05	AAAA O
ATOM	1427	N	LYS	146	18.979	-5.924	57.489	1.00	53.72	AAAA N
ATOM	1429	CA	LYS	146	18.268	-7.229	57.295	1.00	56.94	AAAA C
ATOM	1430	CB	LYS	146	16.994	-7.050	56.647	1.00	65.44	AAAA C
ATOM	1431	CG	LYS	146	16.220	-8.232	55.982	1.00	64.32	AAAA C
ATOM	1432	CD	LYS	146	14.797	-8.422	56.451	0.01	62.75	AAAA C
ATOM	1433	CE	LYS	146	14.194	-9.717	55.934	0.01	62.14	AAAA C
ATOM	1434	NZ	LYS	146	12.720	-9.610	55.753	0.01	61.38	AAAA N
ATOM	1436	C	LYS	146	19.138	-8.138	56.446	1.00	61.40	AAAA C
ATOM	1439	O	LYS	146	19.237	-9.346	56.732	1.00	66.22	AAAA O
ATOM	1440	N	GLU	147	19.779	-7.649	55.399	1.00	62.92	AAAA N
ATOM	1442	CA	GLU	147	20.927	-8.446	54.742	1.00	67.00	AAAA C
ATOM	1443	CB	GLU	147	21.191	-8.070	53.294	1.00	62.32	AAAA C

Figure 1A-13

ATOM	1444	CG	GLU	147	19.967	-7.579	52.567	1.00 73.15	AAAA C
ATOM	1445	CD	GLU	147	20.164	-7.413	51.093	1.00 85.90	AAAA C
ATOM	1446	OE1	GLU	147	21.339	-7.636	50.701	1.00 95.25	AAAA O
ATOM	1447	OE2	GLU	147	19.201	-7.053	50.376	1.00 87.47	AAAA O
ATOM	1448	C	GLU	147	22.136	-8.470	55.541	1.00 69.40	AAAA C
ATOM	1449	O	GLU	147	22.883	-9.437	55.361	1.00 72.86	AAAA O
ATOM	1450	N	CYS	148	22.506	-7.484	56.355	1.00 66.76	AAAA N
ATOM	1452	CA	CYS	148	23.693	-7.588	57.183	1.00 64.65	AAAA C
ATOM	1453	C	CYS	148	23.598	-8.702	58.196	1.00 65.56	AAAA C
ATOM	1454	O	CYS	148	24.473	-9.524	58.414	1.00 65.89	AAAA O
ATOM	1455	CB	CYS	148	23.952	-6.301	58.001	1.00 57.29	AAAA C
ATOM	1456	SG	CYS	148	24.565	-5.091	56.808	1.00 59.22	AAAA S
ATOM	1457	N	GLY	149	22.514	-8.743	58.977	1.00 67.88	AAAA N
ATOM	1459	CA	GLY	149	22.387	-9.744	60.029	1.00 62.15	AAAA C
ATOM	1460	C	GLY	149	23.443	-9.627	61.120	1.00 59.18	AAAA C
ATOM	1461	O	GLY	149	23.925	-10.603	61.699	1.00 61.11	AAAA O
ATOM	1462	N	ASP	150	23.717	-8.426	61.596	1.00 54.88	AAAA N
ATOM	1464	CA	ASP	150	24.794	-8.198	62.533	1.00 55.79	AAAA C
ATOM	1465	CB	ASP	150	25.941	-6.703	62.750	1.00 48.10	AAAA C
ATOM	1466	CG	ASP	150	25.320	-6.034	61.419	1.00 58.50	AAAA C
ATOM	1467	OD1	ASP	150	25.726	-6.796	60.480	1.00 57.73	AAAA O
ATOM	1468	OD2	ASP	150	25.102	-4.819	61.363	1.00 49.69	AAAA O
ATOM	1469	C	ASP	150	24.519	-8.854	63.855	1.00 59.36	AAAA C
ATOM	1470	O	ASP	150	23.392	-8.820	64.377	1.00 67.48	AAAA O
ATOM	1471	N	LEU	151	25.532	-9.369	64.524	1.00 54.39	AAAA N
ATOM	1473	CA	LEU	151	25.314	-9.908	65.853	1.00 52.79	AAAA C
ATOM	1474	CB	LEU	151	25.209	-11.409	65.806	1.00 58.55	AAAA C
ATOM	1475	CG	LEU	151	24.063	-12.101	65.092	1.00 69.45	AAAA C
ATOM	1476	CD1	LEU	151	24.515	-13.421	64.489	1.00 65.26	AAAA C
ATOM	1477	CD2	LEU	151	22.837	-12.372	65.951	1.00 65.43	AAAA C
ATOM	1478	C	LEU	151	26.469	-9.454	66.805	1.00 51.93	AAAA C
ATOM	1479	O	LEU	151	27.598	-9.734	66.634	1.00 55.59	AAAA O
ATOM	1480	N	CYS	152	26.024	-8.773	67.849	1.00 48.62	AAAA N
ATOM	1482	CA	CYS	152	26.992	-8.189	68.740	1.00 56.73	AAAA C
ATOM	1483	C	CYS	152	27.650	-9.325	69.493	1.00 63.58	AAAA C
ATOM	1484	O	CYS	152	27.074	-10.405	69.575	1.00 62.40	AAAA O
ATOM	1485	CB	CYS	152	26.358	-7.144	69.657	1.00 41.99	AAAA C
ATOM	1486	SG	CYS	152	25.985	-5.635	68.703	1.00 55.83	AAAA S
ATOM	1487	N	PRO	153	28.826	-9.072	70.059	1.00 68.05	AAAA N
ATOM	1488	CD	PRO	153	29.618	-7.838	69.903	1.00 66.66	AAAA C
ATOM	1489	CA	PRO	153	29.497	-10.094	70.851	1.00 70.60	AAAA C
ATOM	1490	CB	PRO	153	30.601	-9.323	71.557	1.00 69.98	AAAA C
ATOM	1491	CG	PRO	153	30.861	-8.159	70.690	1.00 70.58	AAAA C
ATOM	1492	C	PRO	153	28.543	-10.734	71.850	1.00 69.64	AAAA C
ATOM	1493	O	PRO	153	27.859	-10.075	72.615	1.00 69.58	AAAA O
ATOM	1494	N	GLY	154	28.444	-12.049	71.843	1.00 71.23	AAAA N
ATOM	1496	CA	GLY	154	27.610	-12.804	72.745	1.00 78.07	AAAA C
ATOM	1497	C	GLY	154	26.245	-13.230	72.223	1.00 81.75	AAAA C
ATOM	1498	O	GLY	154	25.786	-14.318	72.547	1.00 80.26	AAAA O
ATOM	1499	N	THR	155	25.549	-12.468	71.314	1.00 84.54	AAAA N
ATOM	1501	CA	THR	155	24.314	-12.683	70.828	1.00 89.38	AAAA C
ATOM	1502	CB	THR	155	24.016	-11.661	69.705	1.00 86.07	AAAA C
ATOM	1503	OG1	THR	155	24.963	-10.417	70.420	1.00 84.51	AAAA O
ATOM	1505	CG2	THR	155	22.686	-11.995	69.092	1.00 82.27	AAAA C
ATOM	1506	C	THR	155	24.060	-14.094	70.353	1.00 93.69	AAAA C
ATOM	1507	O	THR	155	23.005	-14.664	70.617	1.00 95.92	AAAA O
ATOM	1508	N	MET	156	25.003	-14.655	69.617	1.00 97.23	AAAA N
ATOM	1510	CA	MET	156	24.884	-15.973	69.024	1.00 99.05	AAAA C
ATOM	1511	CB	MET	156	25.907	-16.190	67.896	1.00100.46	AAAA C
ATOM	1512	CG	MET	156	25.456	-15.675	66.542	0.01 99.75	AAAA C
ATOM	1513	SD	MET	156	23.687	-15.857	66.255	0.01 99.72	AAAA S
ATOM	1514	CE	MET	156	23.664	-17.214	65.087	0.01 99.59	AAAA C
ATOM	1515	C	MET	156	25.027	-17.106	70.032	1.00100.57	AAAA C
ATOM	1516	O	MET	156	24.353	-18.122	69.835	1.00101.64	AAAA O
ATOM	1517	N	ALA	157	25.974	-17.057	70.967	1.00100.53	AAAA N
ATOM	1519	CA	ALA	157	26.022	-18.102	71.986	1.00101.00	AAAA C
ATOM	1520	CB	ALA	157	27.317	-18.158	72.766	1.00103.42	AAAA C
ATOM	1521	C	ALA	157	24.856	-17.890	72.959	1.00101.16	AAAA C
ATOM	1522	O	ALA	157	23.993	-18.654	72.921	1.00104.59	AAAA O
ATOM	1523	N	GLU	158	24.984	-16.906	73.841	1.00 98.39	AAAA N
ATOM	1525	CA	GLU	158	23.935	-16.629	74.781	1.00 97.43	AAAA C
ATOM	1526	CB	GLU	158	23.128	-17.865	75.208	1.00105.93	AAAA C
ATOM	1527	CG	GLU	158	21.687	-17.546	75.560	1.00113.87	AAAA C
ATOM	1528	CD	GLU	158	21.347	-16.081	75.302	1.00119.34	AAAA C
ATOM	1529	OE1	GLU	158	21.284	-15.733	74.096	1.00126.27	AAAA O
ATOM	1530	OE2	GLU	158	21.199	-15.317	76.282	1.00117.79	AAAA O
ATOM	1531	C	GLU	158	24.434	-15.915	76.025	1.00 95.00	AAAA C
ATOM	1532	O	GLU	158	23.988	-16.117	77.145	1.00 95.89	AAAA O
ATOM	1533	N	SER	159	25.276	-14.942	75.769	1.00 93.30	AAAA N
ATOM	1535	CA	SER	159	25.810	-14.119	76.848	1.00 92.28	AAAA C
ATOM	1536	CB	SER	159	26.989	-14.805	77.517	1.00 97.37	AAAA C
ATOM	1537	OG	SER	159	26.072	-14.427	78.886	1.00 98.09	AAAA O
ATOM	1539	C	SER	159	26.228	-12.793	76.226	1.00 91.47	AAAA C
ATOM	1540	O	SER	159	27.368	-12.592	75.810	1.00 92.75	AAAA O
ATOM	1541	N	PRO	160	25.196	-12.003	75.932	1.00 88.65	AAAA N

Figure 1A-14

ATOM	1642	CD	PRO	160	23.789	-12.122	76.395	1.00	86.67	AAAA C
ATOM	1643	CA	PRO	160	25.463	-10.701	75.361	1.00	84.74	AAAA C
ATOM	1644	CB	PRO	160	24.125	-9.978	75.456	1.00	84.79	AAAA C
ATOM	1645	CG	PRO	160	23.370	-10.671	76.515	1.00	84.62	AAAA C
ATOM	1646	C	PRO	160	26.503	-10.025	76.236	1.00	79.60	AAAA C
ATOM	1647	O	PRO	160	26.319	-9.934	77.456	1.00	79.70	AAAA O
ATOM	1648	N	MET	161	27.563	-9.522	75.596	1.00	74.45	AAAA N
ATOM	1650	CA	MET	161	28.530	-8.735	76.378	1.00	67.04	AAAA C
ATOM	1651	CB	MET	161	29.924	-9.178	76.038	1.00	69.93	AAAA C
ATOM	1652	CG	MET	161	30.118	-10.630	75.706	1.00	71.43	AAAA C
ATOM	1653	SD	MET	161	30.716	-11.621	77.094	1.00	85.25	AAAA S
ATOM	1654	CE	MET	161	29.841	-10.905	78.471	1.00	69.31	AAAA C
ATOM	1655	C	MET	161	28.358	-7.234	76.189	1.00	61.76	AAAA C
ATOM	1656	O	MET	161	28.788	-6.443	77.034	1.00	58.60	AAAA O
ATOM	1657	N	CYS	162	27.681	-6.819	75.095	1.00	54.81	AAAA N
ATOM	1659	CA	CYS	162	27.493	-5.381	74.938	1.00	49.76	AAAA C
ATOM	1660	C	CYS	162	26.306	-4.777	75.670	1.00	51.52	AAAA C
ATOM	1661	O	CYS	162	25.224	-5.324	75.928	1.00	53.89	AAAA O
ATOM	1662	CB	CYS	162	27.422	-5.099	73.459	1.00	48.31	AAAA C
ATOM	1663	SG	CYS	162	28.523	-6.064	72.432	1.00	54.02	AAAA S
ATOM	1664	N	GLU	163	26.409	-3.522	76.031	1.00	46.31	AAAA N
ATOM	1666	CA	GLU	163	25.355	-2.675	76.538	1.00	47.19	AAAA C
ATOM	1667	CB	GLU	163	26.051	-1.412	77.027	1.00	49.95	AAAA C
ATOM	1668	CG	GLU	163	26.476	-1.364	78.465	1.00	62.30	AAAA C
ATOM	1669	CD	GLU	163	25.917	-0.135	79.116	1.00	81.67	AAAA C
ATOM	1670	OE1	GLU	163	26.470	0.473	80.016	1.00	73.22	AAAA O
ATOM	1671	OE2	GLU	163	24.646	0.208	78.721	1.00	80.93	AAAA O
ATOM	1672	C	GLU	163	24.299	-2.340	75.472	1.00	49.05	AAAA C
ATOM	1673	O	GLU	163	24.488	-2.423	74.234	1.00	45.90	AAAA O
ATOM	1674	N	LYS	164	23.142	-1.815	75.880	1.00	47.43	AAAA N
ATOM	1676	CA	LYS	164	22.011	-1.499	75.081	1.00	43.92	AAAA C
ATOM	1677	CB	LYS	164	20.714	-2.244	75.450	1.00	44.48	AAAA C
ATOM	1678	CG	LYS	164	20.560	-3.639	74.870	1.00	48.65	AAAA C
ATOM	1679	CD	LYS	164	19.480	-4.432	75.622	1.00	49.04	AAAA C
ATOM	1680	CE	LYS	164	18.409	-5.012	74.720	1.00	49.21	AAAA C
ATOM	1681	NZ	LYS	164	17.951	-6.372	75.134	1.00	37.67	AAAA N
ATOM	1685	C	LYS	164	21.615	-0.040	75.204	1.00	45.01	AAAA C
ATOM	1686	O	LYS	164	21.466	0.484	76.282	1.00	45.69	AAAA O
ATOM	1687	N	THR	165	21.333	0.570	74.034	1.00	44.94	AAAA N
ATOM	1689	CA	THR	165	20.775	1.943	74.077	1.00	43.13	AAAA C
ATOM	1690	CB	THR	165	21.831	2.952	73.553	1.00	47.81	AAAA C
ATOM	1691	OG1	THR	165	22.053	2.689	72.127	1.00	39.13	AAAA O
ATOM	1693	CG2	THR	165	23.119	2.842	74.362	1.00	40.40	AAAA C
ATOM	1694	C	THR	165	19.532	1.881	73.189	1.00	40.92	AAAA C
ATOM	1695	O	THR	165	19.346	0.897	72.414	1.00	35.91	AAAA O
ATOM	1696	N	THR	166	18.781	2.985	73.173	1.00	39.18	AAAA N
ATOM	1698	CA	THR	166	17.689	2.991	72.182	1.00	42.97	AAAA C
ATOM	1699	CB	THR	166	16.297	3.096	72.833	1.00	55.99	AAAA C
ATOM	1700	OG1	THR	166	15.662	4.385	72.819	1.00	41.42	AAAA O
ATOM	1702	CG2	THR	166	16.157	2.940	74.313	1.00	42.83	AAAA C
ATOM	1703	C	THR	166	17.983	4.051	71.137	1.00	40.17	AAAA C
ATOM	1704	O	THR	166	18.219	5.206	71.509	1.00	35.72	AAAA O
ATOM	1705	N	ILE	167	17.912	3.725	69.866	1.00	42.21	AAAA N
ATOM	1707	CA	ILE	167	18.182	4.672	68.777	1.00	41.05	AAAA C
ATOM	1708	CB	ILE	167	19.437	4.335	67.904	1.00	39.50	AAAA C
ATOM	1709	CG2	ILE	167	19.589	5.346	66.716	1.00	15.26	AAAA C
ATOM	1710	CG1	ILE	167	20.722	4.305	68.724	1.00	36.20	AAAA C
ATOM	1711	CD1	ILE	167	21.899	3.665	67.966	1.00	35.70	AAAA C
ATOM	1712	C	ILE	167	16.937	4.524	67.882	1.00	40.94	AAAA C
ATOM	1713	O	ILE	167	16.655	3.435	67.394	1.00	35.51	AAAA O
ATOM	1714	N	ASN	168	16.318	5.635	67.537	1.00	42.29	AAAA N
ATOM	1716	CA	ASN	168	15.112	5.633	66.713	1.00	45.22	AAAA C
ATOM	1717	CB	ASN	168	15.526	5.253	65.292	1.00	45.69	AAAA C
ATOM	1718	CG	ASN	168	14.497	5.696	64.244	1.00	51.19	AAAA C
ATOM	1719	OD1	ASN	168	14.344	5.112	63.150	1.00	41.75	AAAA O
ATOM	1720	ND2	ASN	168	13.749	6.763	64.522	1.00	48.89	AAAA N
ATOM	1723	C	ASN	168	13.954	4.739	67.141	1.00	46.55	AAAA C
ATOM	1724	O	ASN	168	13.544	3.879	66.326	1.00	45.95	AAAA O
ATOM	1725	N	ASN	169	13.644	4.728	68.433	1.00	45.12	AAAA N
ATOM	1727	CA	ASN	169	12.717	3.759	69.007	1.00	43.67	AAAA C
ATOM	1728	CB	ASN	169	11.315	4.106	68.540	1.00	36.84	AAAA C
ATOM	1729	CG	ASN	169	10.943	5.487	69.093	1.00	42.75	AAAA C
ATOM	1730	OD1	ASN	169	10.917	5.779	70.289	1.00	36.67	AAAA O
ATOM	1731	ND2	ASN	169	10.658	6.448	68.213	1.00	40.74	AAAA N
ATOM	1734	C	ASN	169	13.003	2.306	68.719	1.00	44.69	AAAA C
ATOM	1735	O	ASN	169	12.100	1.544	68.383	1.00	45.72	AAAA O
ATOM	1736	N	GLU	170	14.226	1.907	68.862	1.00	41.64	AAAA N
ATOM	1738	CA	GLU	170	14.655	0.513	68.850	1.00	45.88	AAAA C
ATOM	1739	CB	GLU	170	15.283	0.278	67.524	1.00	55.92	AAAA C
ATOM	1740	CG	GLU	170	15.028	-0.953	66.702	1.00	67.08	AAAA C
ATOM	1741	CD	GLU	170	14.517	-0.605	65.294	1.00	74.56	AAAA C
ATOM	1742	OE1	GLU	170	13.969	0.466	65.049	1.00	77.75	AAAA O
ATOM	1743	OE2	GLU	170	14.763	-1.437	64.389	1.00	70.71	AAAA O
ATOM	1744	C	GLU	170	15.647	0.379	70.010	1.00	47.16	AAAA C
ATOM	1745	O	GLU	170	16.582	1.172	70.213	1.00	49.92	AAAA O

Figure 1A-15

ATOM	1646	N	TYR	171	15.344	-0.462	70.952	1.00	49.19	AAAA N
ATOM	1648	CA	TYR	171	16.231	-0.689	72.097	1.00	51.91	AAAA C
ATOM	1649	CB	TYR	171	15.434	-0.861	73.359	1.00	49.94	AAAA C
ATOM	1650	CG	TYR	171	16.175	-1.168	74.620	1.00	48.90	AAAA C
ATOM	1651	CD1	TYR	171	16.980	-0.210	75.237	1.00	46.46	AAAA C
ATOM	1652	CE1	TYR	171	17.634	-0.469	76.467	1.00	41.17	AAAA C
ATOM	1653	CD2	TYR	171	16.065	-2.429	75.194	1.00	43.62	AAAA C
ATOM	1654	CE2	TYR	171	16.734	-2.675	76.366	1.00	44.44	AAAA C
ATOM	1655	CZ	TYR	171	17.516	-1.718	76.973	1.00	43.58	AAAA C
ATOM	1656	OH	TYR	171	18.174	-2.017	78.146	1.00	40.16	AAAA O
ATOM	1658	C	TYR	171	17.058	-1.938	71.832	1.00	51.41	AAAA C
ATOM	1659	O	TYR	171	16.519	-3.024	72.089	1.00	52.59	AAAA O
ATOM	1660	N	ASN	172	18.331	-1.752	71.493	1.00	53.70	AAAA N
ATOM	1662	CA	ASN	172	19.203	-2.898	71.193	1.00	52.36	AAAA C
ATOM	1663	CB	ASN	172	19.985	-3.278	69.769	1.00	55.43	AAAA C
ATOM	1664	CG	ASN	172	18.939	-4.766	69.498	1.00	61.75	AAAA C
ATOM	1665	OD1	ASN	172	19.233	-5.646	70.304	1.00	61.61	AAAA O
ATOM	1666	ND2	ASN	172	18.449	-5.048	68.295	1.00	57.97	AAAA N
ATOM	1669	C	ASN	172	20.665	-2.712	71.560	1.00	43.81	AAAA C
ATOM	1670	O	ASN	172	21.163	-1.760	72.213	1.00	39.38	AAAA O
ATOM	1671	N	TYR	173	21.375	-3.796	71.393	1.00	43.20	AAAA N
ATOM	1673	CA	TYR	173	22.794	-3.929	71.699	1.00	44.76	AAAA C
ATOM	1674	CB	TYR	173	23.223	-5.374	71.514	1.00	41.66	AAAA C
ATOM	1675	CG	TYR	173	22.759	-6.274	72.630	1.00	45.18	AAAA C
ATOM	1676	CD1	TYR	173	21.931	-7.316	72.237	1.00	46.48	AAAA C
ATOM	1677	CE1	TYR	173	21.438	-8.181	73.193	1.00	51.36	AAAA C
ATOM	1678	CD2	TYR	173	23.081	-6.132	73.978	1.00	44.86	AAAA C
ATOM	1679	CE2	TYR	173	22.583	-7.016	74.916	1.00	46.92	AAAA C
ATOM	1680	CZ	TYR	173	21.757	-8.038	74.535	1.00	50.33	AAAA C
ATOM	1681	OH	TYR	173	21.171	-9.006	75.329	1.00	50.64	AAAA O
ATOM	1683	C	TYR	173	23.673	-3.099	70.762	1.00	46.94	AAAA C
ATOM	1684	O	TYR	173	23.389	-2.983	69.567	1.00	49.76	AAAA O
ATOM	1685	N	ARG	174	24.579	-2.318	71.366	1.00	47.79	AAAA N
ATOM	1687	CA	ARG	174	25.517	-1.496	70.577	1.00	49.13	AAAA C
ATOM	1688	CB	ARG	174	25.537	-0.132	71.233	1.00	44.32	AAAA C
ATOM	1689	CG	ARG	174	24.219	0.623	71.234	1.00	48.14	AAAA C
ATOM	1690	CD	ARG	174	23.372	0.344	70.003	1.00	51.47	AAAA C
ATOM	1691	NE	ARG	174	21.974	0.760	70.039	1.00	48.35	AAAA N
ATOM	1693	CZ	ARG	174	21.144	0.570	69.017	1.00	48.23	AAAA C
ATOM	1694	NH1	ARG	174	21.477	0.022	67.864	1.00	38.96	AAAA N
ATOM	1697	NH2	ARG	174	19.909	1.022	69.197	1.00	54.65	AAAA N
ATOM	1700	C	ARG	174	26.921	-2.094	70.461	1.00	45.98	AAAA C
ATOM	1701	O	ARG	174	27.548	-2.557	71.406	1.00	44.97	AAAA O
ATOM	1702	N	CYS	175	27.493	-2.183	69.294	1.00	46.21	AAAA N
ATOM	1704	CA	CYS	175	28.787	-2.758	68.997	1.00	45.60	AAAA C
ATOM	1705	C	CYS	175	29.407	-2.395	67.665	1.00	46.23	AAAA C
ATOM	1706	O	CYS	175	28.755	-2.018	66.665	1.00	44.78	AAAA O
ATOM	1707	CB	CYS	175	28.576	-4.253	69.167	1.00	35.62	AAAA C
ATOM	1708	SG	CYS	175	27.812	-5.181	67.827	1.00	51.92	AAAA S
ATOM	1709	N	TRP	176	30.764	-2.517	67.583	1.00	48.16	AAAA N
ATOM	1711	CA	TRP	176	31.430	-2.091	66.325	1.00	42.48	AAAA C
ATOM	1712	CB	TRP	176	32.769	-1.409	66.564	1.00	36.38	AAAA C
ATOM	1713	CG	TRP	176	32.689	-0.069	67.203	1.00	25.56	AAAA C
ATOM	1714	CD2	TRP	176	32.588	1.186	66.489	1.00	23.71	AAAA C
ATOM	1715	CE2	TRP	176	32.559	2.217	67.422	1.00	30.40	AAAA C
ATOM	1716	CE3	TRP	176	32.535	1.520	65.141	1.00	24.31	AAAA C
ATOM	1717	CD1	TRP	176	32.730	0.257	68.523	1.00	28.37	AAAA C
ATOM	1718	NE1	TRP	176	32.636	1.636	68.679	1.00	37.21	AAAA N
ATOM	1720	CZ2	TRP	176	32.441	3.565	67.088	1.00	28.51	AAAA C
ATOM	1721	CZ3	TRP	176	32.447	2.822	64.789	1.00	22.23	AAAA C
ATOM	1722	CH2	TRP	176	32.406	3.817	65.745	1.00	29.51	AAAA C
ATOM	1723	C	TRP	176	31.631	-3.268	65.109	1.00	39.30	AAAA C
ATOM	1724	O	TRP	176	31.703	-3.121	64.199	1.00	39.15	AAAA O
ATOM	1725	N	THR	177	31.682	-4.460	66.005	1.00	41.33	AAAA N
ATOM	1727	CA	THR	177	31.964	-5.644	65.161	1.00	49.28	AAAA C
ATOM	1728	CB	THR	177	33.480	-6.062	65.162	1.00	43.66	AAAA C
ATOM	1729	OG1	THR	177	34.309	-5.025	64.615	1.00	47.85	AAAA O
ATOM	1731	CG2	THR	177	33.676	-7.271	64.283	1.00	58.51	AAAA C
ATOM	1732	C	THR	177	31.290	-6.814	65.859	1.00	48.76	AAAA C
ATOM	1733	O	THR	177	30.982	-6.539	67.661	1.00	51.53	AAAA O
ATOM	1734	N	THR	178	31.269	-8.000	65.331	1.00	51.96	AAAA N
ATOM	1736	CA	THR	178	30.921	-9.236	65.948	1.00	58.95	AAAA C
ATOM	1737	CB	THR	178	31.253	-10.500	65.092	1.00	66.55	AAAA C
ATOM	1738	OG1	THR	178	31.505	-10.066	63.734	1.00	75.70	AAAA O
ATOM	1740	CG2	THR	178	30.104	-11.489	65.148	1.00	74.23	AAAA C
ATOM	1741	C	THR	178	31.714	-9.539	67.213	1.00	60.29	AAAA C
ATOM	1742	O	THR	178	31.204	-10.202	68.135	1.00	66.05	AAAA O
ATOM	1743	N	ASN	179	32.977	-9.130	67.253	1.00	57.56	AAAA N
ATOM	1745	CA	ASN	179	33.793	-9.392	68.443	1.00	53.39	AAAA C
ATOM	1746	CB	ASN	179	35.130	-10.024	68.068	1.00	48.46	AAAA C
ATOM	1747	CG	ASN	179	34.997	-11.218	67.126	1.00	56.25	AAAA C
ATOM	1748	OD1	ASN	179	34.412	-12.291	67.559	1.00	51.38	AAAA O
ATOM	1749	ND2	ASN	179	35.229	-11.063	65.969	1.00	48.10	AAAA N
ATOM	1752	C	ASN	179	34.096	-8.109	69.295	1.00	50.79	AAAA C
ATOM	1753	O	ASN	179	34.556	-8.377	70.429	1.00	57.97	AAAA O

Figure 1A-16

Application No. 09/555,275
Annotated Sheet Showing Changes

ATOM	1754	N	ARG	180	33.626	-7.022	68.913	1.00 47.06	AAAA N
ATOM	1756	CA	ARG	180	33.908	-5.820	69.691	1.00 48.25	AAAA C
ATOM	1757	CB	ARG	180	34.925	-4.962	69.074	1.00 49.72	AAAA C
ATOM	1758	CG	ARG	180	36.324	-5.501	69.285	1.00 60.92	AAAA C
ATOM	1759	CD	ARG	180	37.288	-4.948	68.279	1.00 70.83	AAAA C
ATOM	1760	NE	ARG	180	38.569	-5.605	68.203	1.00 76.18	AAAA N
ATOM	1762	CZ	ARG	180	39.298	-5.995	69.276	1.00 76.59	AAAA C
ATOM	1763	NH1	ARG	180	38.877	-5.608	70.498	1.00 80.82	AAAA N
ATOM	1766	NH2	ARG	180	40.474	-6.478	69.180	1.00 79.33	AAAA N
ATOM	1769	C	ARG	180	32.530	-4.977	69.821	1.00 48.10	AAAA C
ATOM	1770	O	ARG	180	31.862	-4.476	68.905	1.00 46.99	AAAA O
ATOM	1771	N	CYS	181	32.230	-4.728	71.063	1.00 44.80	AAAA N
ATOM	1773	CA	CYS	181	31.199	-3.924	71.619	1.00 45.20	AAAA C
ATOM	1774	C	CYS	181	31.646	-2.463	71.692	1.00 44.50	AAAA C
ATOM	1775	O	CYS	181	32.835	-2.227	71.724	1.00 47.09	AAAA O
ATOM	1776	CB	CYS	181	30.940	-4.282	73.110	1.00 43.88	AAAA C
ATOM	1777	SG	CYS	181	30.363	-5.944	73.316	1.00 56.08	AAAA S
ATOM	1778	N	GLN	182	30.659	-1.600	71.690	1.00 39.30	AAAA N
ATOM	1780	CA	GLN	182	30.948	-0.177	71.690	1.00 43.43	AAAA C
ATOM	1781	CB	GLN	182	29.749	0.619	71.196	1.00 23.99	AAAA C
ATOM	1782	CG	GLN	182	29.809	2.085	71.435	1.00 28.57	AAAA C
ATOM	1783	CD	GLN	182	28.757	2.867	70.733	1.00 29.35	AAAA C
ATOM	1784	OE1	GLN	182	27.898	2.304	70.033	1.00 30.55	AAAA O
ATOM	1785	NE2	GLN	182	28.857	4.164	70.912	1.00 28.14	AAAA N
ATOM	1788	C	GLN	182	31.218	0.089	73.162	1.00 46.07	AAAA C
ATOM	1789	O	GLN	182	30.458	-0.327	74.041	1.00 47.01	AAAA O
ATOM	1790	N	LYS	183	32.213	0.866	73.524	1.00 46.98	AAAA N
ATOM	1792	CA	LYS	183	32.479	1.064	74.934	1.00 45.26	AAAA C
ATOM	1793	CB	LYS	183	33.966	1.275	75.185	1.00 48.68	AAAA C
ATOM	1794	CG	LYS	183	34.865	0.267	74.482	1.00 47.95	AAAA C
ATOM	1795	CD	LYS	183	36.337	0.734	74.523	1.00 48.06	AAAA C
ATOM	1796	CE	LYS	183	37.278	-0.208	73.684	1.00 46.78	AAAA C
ATOM	1797	NZ	LYS	183	38.499	-0.654	74.158	1.00 44.00	AAAA N
ATOM	1801	C	LYS	183	31.659	2.205	75.477	1.00 48.13	AAAA C
ATOM	1802	O	LYS	183	31.679	3.305	74.946	1.00 48.84	AAAA O
ATOM	1803	N	MET	184	31.165	2.014	76.698	1.00 52.59	AAAA N
ATOM	1805	CA	MET	184	30.388	3.041	77.413	1.00 53.22	AAAA C
ATOM	1806	CB	MET	184	28.927	2.613	77.537	1.00 54.27	AAAA C
ATOM	1807	CG	MET	184	27.855	2.955	76.536	1.00 56.16	AAAA C
ATOM	1808	SD	MET	184	26.911	1.601	75.912	1.00 57.56	AAAA S
ATOM	1809	CE	MET	184	26.738	1.855	74.171	1.00 46.57	AAAA C
ATOM	1810	C	MET	184	31.051	3.200	78.770	1.00 50.55	AAAA C
ATOM	1811	O	MET	184	31.770	2.292	79.116	1.00 48.82	AAAA O
ATOM	1812	N	CYS	185	30.796	4.195	79.565	1.00 53.97	AAAA N
ATOM	1814	CA	CYS	185	31.342	4.365	80.892	1.00 58.63	AAAA C
ATOM	1815	C	CYS	185	30.297	4.320	81.989	1.00 65.16	AAAA C
ATOM	1816	O	CYS	185	29.133	4.649	81.761	1.00 65.87	AAAA O
ATOM	1817	CB	CYS	185	31.965	5.772	81.000	1.00 60.37	AAAA C
ATOM	1818	SG	CYS	185	33.623	5.771	80.312	1.00 60.09	AAAA S
ATOM	1819	N	PRO	186	30.688	3.978	83.206	1.00 69.41	AAAA N
ATOM	1820	CD	PRO	186	32.066	3.777	83.702	1.00 71.11	AAAA C
ATOM	1821	CA	PRO	186	29.717	3.933	84.304	1.00 69.11	AAAA C
ATOM	1822	CB	PRO	186	30.523	3.487	85.503	1.00 68.03	AAAA C
ATOM	1823	CG	PRO	186	31.910	3.920	85.198	1.00 71.02	AAAA C
ATOM	1824	C	PRO	186	29.129	5.320	84.431	1.00 69.47	AAAA C
ATOM	1825	O	PRO	186	29.820	6.345	84.507	1.00 65.93	AAAA O
ATOM	1826	N	SER	187	27.801	5.367	84.546	1.00 68.78	AAAA N
ATOM	1828	CA	SER	187	27.050	6.592	84.750	1.00 69.29	AAAA C
ATOM	1829	CB	SER	187	25.594	6.287	85.129	1.00 78.29	AAAA C
ATOM	1830	OG	SER	187	25.474	4.935	85.566	1.00 91.78	AAAA O
ATOM	1832	C	SER	187	27.630	7.476	85.836	1.00 67.19	AAAA C
ATOM	1833	O	SER	187	27.606	8.708	85.803	1.00 63.98	AAAA O
ATOM	1834	N	THR	188	28.108	6.853	86.908	1.00 68.20	AAAA N
ATOM	1836	CA	THR	188	28.870	7.507	87.963	1.00 68.39	AAAA C
ATOM	1837	CB	THR	188	29.805	6.459	88.618	1.00 73.84	AAAA C
ATOM	1838	OG1	THR	188	28.943	5.365	89.016	1.00 89.33	AAAA O
ATOM	1840	CG2	THR	188	30.605	7.048	89.750	1.00 73.71	AAAA C
ATOM	1841	C	THR	188	29.802	8.583	87.429	1.00 67.52	AAAA C
ATOM	1842	O	THR	188	29.843	9.739	87.834	1.00 68.30	AAAA O
ATOM	1843	N	CYS	189	30.643	8.247	86.446	1.00 63.89	AAAA N
ATOM	1845	CA	CYS	189	31.583	9.116	85.817	1.00 57.29	AAAA C
ATOM	1846	C	CYS	189	30.951	10.331	85.195	1.00 57.70	AAAA C
ATOM	1847	O	CYS	189	31.648	11.327	85.017	1.00 57.56	AAAA O
ATOM	1848	CB	CYS	189	32.416	8.372	84.769	1.00 58.67	AAAA C
ATOM	1849	SG	CYS	189	33.347	7.001	85.535	1.00 53.46	AAAA S
ATOM	1850	N	GLY	190	29.689	10.322	84.806	1.00 56.91	AAAA N
ATOM	1852	CA	GLY	190	29.038	11.521	84.323	1.00 57.28	AAAA C
ATOM	1853	C	GLY	190	29.444	11.834	82.886	1.00 59.62	AAAA C
ATOM	1854	O	GLY	190	29.609	10.932	82.082	1.00 57.91	AAAA O
ATOM	1855	N	LYS	191	29.842	13.052	82.624	1.00 62.78	AAAA N
ATOM	1857	CA	LYS	191	30.359	13.520	81.364	1.00 67.72	AAAA C
ATOM	1858	CB	LYS	191	30.058	15.035	81.214	1.00 72.76	AAAA C
ATOM	1859	CG	LYS	191	28.568	15.288	81.002	1.00 84.69	AAAA C
ATOM	1860	CD	LYS	191	28.207	16.733	80.723	1.00 90.15	AAAA C
ATOM	1861	CE	LYS	191	26.713	16.806	80.471	1.00 91.85	AAAA C

Figure 1A-17

Application No. 09/555,275
Annotated Sheet Showing Changes

ATOM	1962	HG	CYS	191	26.368	16.182	79.152	1.00	97.62	AAAA H
ATOM	1966	C	CYS	191	31.868	13.299	81.270	1.00	70.13	AAAA C
ATOM	1967	O	CYS	191	32.486	13.935	80.415	1.00	71.76	AAAA O
ATOM	1968	N	ARG	192	32.408	12.441	82.079	1.00	66.29	AAAA N
ATOM	1970	CA	ARG	192	33.885	12.171	82.044	1.00	59.95	AAAA C
ATOM	1971	CB	ARG	192	34.505	12.070	83.432	1.00	66.58	AAAA C
ATOM	1972	CG	ARG	192	34.670	13.400	84.131	1.00	71.59	AAAA C
ATOM	1973	CD	ARG	192	34.385	13.330	85.625	1.00	73.91	AAAA C
ATOM	1974	NE	ARG	192	35.522	13.280	86.377	1.00	85.74	AAAA N
ATOM	1976	CZ	ARG	192	35.968	12.407	87.330	1.00	90.67	AAAA C
ATOM	1977	NH1	ARG	192	35.026	11.486	87.600	1.00	88.49	AAAA N
ATOM	1980	NH2	ARG	192	37.162	12.463	87.950	1.00	72.95	AAAA N
ATOM	1983	C	ARG	192	34.221	10.851	81.337	1.00	58.83	AAAA C
ATOM	1984	O	ARG	192	33.336	10.007	81.176	1.00	55.13	AAAA O
ATOM	1985	N	ALA	193	35.521	10.795	80.968	1.00	50.19	AAAA N
ATOM	1987	CA	ALA	193	35.962	9.557	80.355	1.00	46.24	AAAA C
ATOM	1988	CB	ALA	193	37.167	9.921	79.541	1.00	45.15	AAAA C
ATOM	1989	C	ALA	193	36.221	8.525	81.451	1.00	48.97	AAAA C
ATOM	1990	O	ALA	193	36.220	8.908	82.616	1.00	44.80	AAAA O
ATOM	1991	N	CYS	194	36.544	7.304	81.065	1.00	50.30	AAAA N
ATOM	1993	CA	CYS	194	36.836	6.302	82.043	1.00	57.50	AAAA C
ATOM	1994	C	CYS	194	37.834	5.304	81.448	1.00	61.25	AAAA C
ATOM	1995	O	CYS	194	37.952	5.291	80.216	1.00	61.52	AAAA O
ATOM	1996	CB	CYS	194	35.510	5.741	82.504	1.00	57.96	AAAA C
ATOM	1997	SG	CYS	194	34.785	4.524	81.402	1.00	54.49	AAAA S
ATOM	1998	N	THR	195	38.422	4.499	82.311	1.00	58.51	AAAA N
ATOM	1900	CA	THR	195	39.462	3.584	81.913	1.00	57.42	AAAA C
ATOM	1901	CB	THR	195	40.237	3.142	83.188	1.00	65.73	AAAA C
ATOM	1902	OG1	THR	195	40.288	4.248	84.091	1.00	70.15	AAAA O
ATOM	1904	CG2	THR	195	41.684	2.864	82.745	1.00	77.91	AAAA C
ATOM	1905	C	THR	195	38.857	2.404	81.226	1.00	54.59	AAAA C
ATOM	1906	O	THR	195	37.633	2.315	81.319	1.00	58.75	AAAA O
ATOM	1907	N	GLU	196	39.610	1.408	80.882	1.00	55.95	AAAA N
ATOM	1909	CA	GLU	196	39.139	0.145	80.364	1.00	60.07	AAAA C
ATOM	1910	CB	GLU	196	40.395	-0.612	79.914	1.00	68.06	AAAA C
ATOM	1911	CG	GLU	196	40.479	-1.146	78.526	1.00	73.96	AAAA C
ATOM	1912	CD	GLU	196	39.235	-0.983	77.670	1.00	83.08	AAAA C
ATOM	1913	OE1	GLU	196	38.356	-1.884	77.687	1.00	81.19	AAAA O
ATOM	1914	OE2	GLU	196	39.060	0.041	76.939	1.00	82.10	AAAA O
ATOM	1915	C	GLU	196	38.382	-0.579	81.467	1.00	63.91	AAAA C
ATOM	1916	O	GLU	196	37.690	-1.537	81.159	1.00	63.51	AAAA O
ATOM	1917	N	ASN	197	38.666	-0.312	82.739	1.00	67.40	AAAA N
ATOM	1919	CA	ASN	197	38.025	-0.947	83.886	1.00	69.21	AAAA C
ATOM	1920	CB	ASN	197	39.021	-1.394	84.966	1.00	68.49	AAAA C
ATOM	1921	CG	ASN	197	39.722	-2.692	84.672	0.01	69.09	AAAA C
ATOM	1922	OD1	ASN	197	40.364	-3.273	85.551	0.01	69.04	AAAA O
ATOM	1923	ND2	ASN	197	39.622	-3.183	83.443	0.01	68.97	AAAA N
ATOM	1926	C	ASN	197	37.033	0.043	84.486	1.00	69.01	AAAA C
ATOM	1927	O	ASN	197	36.845	0.281	85.664	1.00	68.24	AAAA O
ATOM	1928	N	ASN	198	36.384	0.795	83.607	1.00	69.91	AAAA N
ATOM	1930	CA	ASN	198	35.356	1.734	84.048	1.00	68.48	AAAA C
ATOM	1931	CB	ASN	198	34.120	0.880	84.373	1.00	60.12	AAAA C
ATOM	1932	CG	ASN	198	33.806	0.095	83.102	1.00	69.29	AAAA C
ATOM	1933	OD1	ASN	198	33.475	0.654	82.054	1.00	73.20	AAAA O
ATOM	1934	ND2	ASN	198	33.980	-1.206	83.268	1.00	65.34	AAAA N
ATOM	1937	C	ASN	198	35.784	2.563	85.228	1.00	64.01	AAAA C
ATOM	1938	O	ASN	198	34.992	2.827	86.117	1.00	64.20	AAAA O
ATOM	1939	N	GLU	199	36.955	3.164	85.157	1.00	64.75	AAAA N
ATOM	1941	CA	GLU	199	37.342	4.054	86.255	1.00	64.61	AAAA C
ATOM	1942	CB	GLU	199	38.702	3.624	86.744	1.00	66.11	AAAA C
ATOM	1943	CG	GLU	199	38.846	3.717	88.233	1.00	77.15	AAAA C
ATOM	1944	CD	GLU	199	39.579	2.532	88.832	1.00	80.24	AAAA C
ATOM	1945	OE1	GLU	199	39.385	2.406	90.066	1.00	81.65	AAAA O
ATOM	1946	OE2	GLU	199	40.282	1.821	88.079	1.00	77.94	AAAA O
ATOM	1947	C	GLU	199	37.314	5.463	85.690	1.00	62.92	AAAA C
ATOM	1948	O	GLU	199	37.922	5.676	84.632	1.00	63.62	AAAA O
ATOM	1949	N	CYS	200	36.605	6.393	86.313	1.00	56.16	AAAA N
ATOM	1951	CA	CYS	200	36.600	7.721	85.740	1.00	55.11	AAAA C
ATOM	1952	C	CYS	200	37.978	8.315	85.521	1.00	57.77	AAAA C
ATOM	1953	O	CYS	200	38.884	8.058	86.300	1.00	63.79	AAAA O
ATOM	1954	CB	CYS	200	35.824	8.664	86.648	1.00	52.70	AAAA C
ATOM	1955	SG	CYS	200	34.196	8.100	87.098	1.00	55.85	AAAA S
ATOM	1956	N	CYS	201	38.124	9.192	84.540	1.00	54.50	AAAA N
ATOM	1958	CA	CYS	201	39.338	9.889	84.202	1.00	48.19	AAAA C
ATOM	1959	C	CYS	201	39.236	11.287	84.786	1.00	42.34	AAAA C
ATOM	1960	O	CYS	201	38.165	11.704	85.166	1.00	54.32	AAAA O
ATOM	1961	CB	CYS	201	39.590	10.070	82.695	1.00	40.90	AAAA C
ATOM	1962	SG	CYS	201	39.644	8.597	81.747	1.00	51.42	AAAA S
ATOM	1963	N	HIS	202	40.254	12.075	84.675	1.00	39.12	AAAA N
ATOM	1965	CA	HIS	202	40.290	13.461	85.128	1.00	41.55	AAAA C
ATOM	1966	C	HIS	202	39.284	14.184	84.289	1.00	46.59	AAAA C
ATOM	1967	O	HIS	202	39.176	13.851	83.103	1.00	51.64	AAAA O
ATOM	1968	CB	HIS	202	41.712	13.952	84.814	1.00	45.20	AAAA C
ATOM	1969	CG	HIS	202	41.996	15.330	85.287	1.00	38.71	AAAA C
ATOM	1970	ND1	HIS	202	42.501	16.404	84.559	1.00	51.32	AAAA N

Figure 1A-18

ATOM	1971	CE1	HIS	202	41.887	17.528	85.179	1.00	47.62	AAAA C
ATOM	1972	CD2	HIS	202	42.665	15.813	86.340	1.00	39.59	AAAA C
ATOM	1973	NE2	HIS	202	42.563	17.207	86.258	1.00	43.48	AAAA N
ATOM	1975	N	PRO	203	38.738	15.293	84.711	1.00	47.74	AAAA N
ATOM	1976	CD	PRO	203	38.758	15.840	86.082	1.00	46.97	AAAA C
ATOM	1977	CA	PRO	203	37.780	15.987	83.879	1.00	46.44	AAAA C
ATOM	1978	CB	PRO	203	37.248	17.107	84.742	1.00	39.47	AAAA C
ATOM	1979	CG	PRO	203	38.131	17.210	85.910	1.00	43.37	AAAA C
ATOM	1980	C	PRO	203	38.440	16.519	82.607	1.00	53.27	AAAA C
ATOM	1981	O	PRO	203	37.698	17.045	81.731	1.00	53.16	AAAA O
ATOM	1982	N	GLU	204	39.792	16.535	82.561	1.00	50.34	AAAA N
ATOM	1984	CA	GLU	204	40.439	17.139	81.381	1.00	50.52	AAAA C
ATOM	1985	CB	GLU	204	41.727	17.891	81.804	1.00	48.58	AAAA C
ATOM	1986	CG	GLU	204	41.397	19.251	82.397	1.00	43.74	AAAA C
ATOM	1987	CD	GLU	204	40.778	20.282	81.501	1.00	55.26	AAAA C
ATOM	1988	OE1	GLU	204	40.766	20.344	80.248	1.00	64.04	AAAA O
ATOM	1989	OE2	GLU	204	40.226	21.198	82.141	1.00	57.66	AAAA O
ATOM	1990	C	GLU	204	40.718	16.084	80.319	1.00	45.71	AAAA C
ATOM	1991	O	GLU	204	41.238	16.405	79.251	1.00	46.56	AAAA O
ATOM	1992	N	CYS	205	40.612	14.830	80.735	1.00	42.05	AAAA N
ATOM	1994	CA	CYS	205	40.997	13.764	79.838	1.00	45.81	AAAA C
ATOM	1995	C	CYS	205	39.892	13.628	78.819	1.00	49.20	AAAA C
ATOM	1996	O	CYS	205	38.746	13.920	79.133	1.00	50.34	AAAA O
ATOM	1997	CB	CYS	205	41.288	12.491	80.572	1.00	51.55	AAAA C
ATOM	1998	SG	CYS	205	42.923	12.246	81.251	1.00	52.89	AAAA S
ATOM	1999	N	LEU	206	40.232	13.579	77.520	1.00	49.68	AAAA N
ATOM	2001	CA	LEU	206	39.169	13.446	76.533	1.00	41.49	AAAA C
ATOM	2002	CB	LEU	206	39.266	14.505	75.462	1.00	48.66	AAAA C
ATOM	2003	CG	LEU	206	38.274	14.365	74.305	1.00	47.45	AAAA C
ATOM	2004	CD1	LEU	206	36.879	14.243	74.895	1.00	45.79	AAAA C
ATOM	2005	CD2	LEU	206	38.331	15.599	73.420	1.00	50.71	AAAA C
ATOM	2006	C	LEU	206	39.310	12.109	75.912	1.00	38.44	AAAA C
ATOM	2007	O	LEU	206	40.400	11.568	75.813	1.00	36.59	AAAA O
ATOM	2008	N	GLY	207	38.264	11.359	75.681	1.00	42.41	AAAA N
ATOM	2010	CA	GLY	207	38.403	10.098	74.978	1.00	40.57	AAAA C
ATOM	2011	C	GLY	207	38.466	9.061	76.058	1.00	47.15	AAAA C
ATOM	2012	O	GLY	207	37.668	8.102	76.057	1.00	45.04	AAAA O
ATOM	2013	N	SER	208	39.622	9.079	76.760	1.00	50.36	AAAA N
ATOM	2015	CA	SER	208	39.832	7.898	77.660	1.00	48.27	AAAA C
ATOM	2016	CB	SER	208	39.909	6.631	76.787	1.00	35.77	AAAA C
ATOM	2017	OG	SER	208	40.600	5.597	77.461	1.00	61.34	AAAA O
ATOM	2019	C	SER	208	41.144	8.068	78.377	1.00	49.17	AAAA C
ATOM	2020	O	SER	208	41.781	9.084	78.163	1.00	48.24	AAAA O
ATOM	2021	N	CYS	209	41.599	7.123	79.189	1.00	52.04	AAAA N
ATOM	2023	CA	CYS	209	42.824	7.307	79.964	1.00	55.98	AAAA C
ATOM	2024	C	CYS	209	43.453	6.035	80.484	1.00	57.41	AAAA C
ATOM	2025	O	CYS	209	42.862	4.963	80.423	1.00	58.33	AAAA O
ATOM	2026	CB	CYS	209	42.629	8.258	81.146	1.00	52.51	AAAA C
ATOM	2027	SG	CYS	209	41.380	7.602	82.261	1.00	58.22	AAAA S
ATOM	2028	N	SER	210	44.734	6.145	80.883	1.00	59.37	AAAA N
ATOM	2030	CA	SER	210	45.506	4.950	81.318	1.00	58.10	AAAA C
ATOM	2031	CB	SER	210	47.022	5.083	81.105	1.00	55.07	AAAA C
ATOM	2032	OG	SER	210	47.546	6.204	81.819	1.00	64.49	AAAA O
ATOM	2034	C	SER	210	45.331	4.713	82.826	1.00	56.34	AAAA C
ATOM	2035	O	SER	210	45.529	3.614	83.326	1.00	54.42	AAAA O
ATOM	2036	N	ALA	211	45.105	5.806	83.548	1.00	52.79	AAAA N
ATOM	2038	CA	ALA	211	44.980	5.684	85.001	1.00	56.60	AAAA C
ATOM	2039	CB	ALA	211	46.333	5.926	85.649	1.00	63.41	AAAA C
ATOM	2040	C	ALA	211	43.962	6.747	85.395	1.00	56.58	AAAA C
ATOM	2041	O	ALA	211	43.957	7.792	84.711	1.00	50.78	AAAA O
ATOM	2042	N	PRO	212	43.117	6.416	86.359	1.00	55.93	AAAA N
ATOM	2043	CD	PRO	212	43.042	5.166	87.115	1.00	55.86	AAAA C
ATOM	2044	CA	PRO	212	41.951	7.257	86.575	1.00	55.50	AAAA C
ATOM	2045	CB	PRO	212	41.104	6.470	87.556	1.00	59.65	AAAA C
ATOM	2046	CG	PRO	212	42.021	5.483	88.175	1.00	51.56	AAAA C
ATOM	2047	C	PRO	212	42.409	8.535	87.177	1.00	53.64	AAAA C
ATOM	2048	O	PRO	212	43.611	8.725	87.393	1.00	57.46	AAAA O
ATOM	2049	N	ALA	213	41.537	9.492	87.347	1.00	53.87	AAAA N
ATOM	2051	CA	ALA	213	41.912	10.710	88.057	1.00	59.41	AAAA C
ATOM	2052	CB	ALA	213	41.783	10.255	89.541	1.00	66.40	AAAA C
ATOM	2053	C	ALA	213	43.289	11.300	87.907	1.00	61.40	AAAA C
ATOM	2054	O	ALA	213	43.729	12.202	88.652	1.00	60.03	AAAA O
ATOM	2055	N	ASN	214	44.068	10.999	86.899	1.00	64.80	AAAA N
ATOM	2057	CA	ASN	214	45.366	11.551	86.596	1.00	63.36	AAAA C
ATOM	2063	C	ASN	214	45.300	12.284	85.251	1.00	61.56	AAAA C
ATOM	2064	O	ASN	214	45.198	11.794	84.117	1.00	58.38	AAAA O
ATOM	2058	CB	ASN	214	46.336	10.379	86.608	1.00	67.32	AAAA C
ATOM	2059	CG	ASN	214	47.697	10.896	86.362	1.00	75.48	AAAA C
ATOM	2060	OD1	ASN	214	48.254	11.105	85.302	1.00	83.64	AAAA O
ATOM	2061	ND2	ASN	214	48.513	11.170	87.427	1.00	90.05	AAAA N
ATOM	2065	N	ASP	215	45.666	13.565	85.305	1.00	59.78	AAAA N
ATOM	2067	CA	ASP	215	45.618	14.432	84.143	1.00	56.47	AAAA C
ATOM	2068	CB	ASP	215	45.430	15.926	84.446	1.00	40.19	AAAA C
ATOM	2069	CG	ASP	215	46.671	16.543	84.986	1.00	56.36	AAAA C
ATOM	2070	OD1	ASP	215	46.590	17.699	85.473	1.00	56.17	AAAA O

Figure 1A-19

ATOM	2071	OD2	ASP	215	47.766	15.026	84.941	1.00	60.11	AAAA O
ATOM	2072	C	ASP	215	46.819	14.315	83.221	1.00	53.78	AAAA C
ATOM	2073	O	ASP	215	46.998	15.148	82.322	1.00	53.58	AAAA O
ATOM	2074	N	THR	216	47.719	13.425	83.511	1.00	50.87	AAAA N
ATOM	2076	CA	THR	216	48.883	13.114	82.734	1.00	45.76	AAAA C
ATOM	2077	CB	THR	216	50.201	13.176	83.529	1.00	53.46	AAAA C
ATOM	2078	OG1	THR	216	50.403	11.977	84.335	1.00	45.14	AAAA O
ATOM	2080	CG2	THR	216	50.436	14.314	84.518	1.00	41.38	AAAA C
ATOM	2081	C	THR	216	48.681	11.712	82.159	1.00	48.34	AAAA C
ATOM	2082	O	THR	216	49.596	11.282	81.444	1.00	47.49	AAAA O
ATOM	2083	N	ALA	217	47.559	11.057	82.476	1.00	49.65	AAAA N
ATOM	2085	CA	ALA	217	47.259	9.760	81.945	1.00	51.83	AAAA C
ATOM	2086	CB	ALA	217	46.908	9.775	82.943	1.00	52.62	AAAA C
ATOM	2087	C	ALA	217	46.207	9.547	80.709	1.00	50.60	AAAA C
ATOM	2088	O	ALA	217	45.775	8.632	80.335	1.00	49.13	AAAA O
ATOM	2089	N	CYS	218	45.744	10.905	80.226	1.00	43.56	AAAA N
ATOM	2091	CA	CYS	218	44.802	11.030	79.157	1.00	48.09	AAAA C
ATOM	2092	C	CYS	218	45.168	10.331	78.869	1.00	47.06	AAAA C
ATOM	2093	O	CYS	218	46.300	9.907	77.642	1.00	55.57	AAAA O
ATOM	2094	CB	CYS	218	44.536	12.501	78.775	1.00	51.54	AAAA C
ATOM	2095	SG	CYS	218	44.256	13.494	80.302	1.00	56.99	AAAA S
ATOM	2096	N	VAL	219	44.226	10.085	76.970	1.00	43.40	AAAA N
ATOM	2098	CA	VAL	219	44.575	9.547	75.654	1.00	35.22	AAAA C
ATOM	2099	CB	VAL	219	43.693	8.427	75.242	1.00	32.26	AAAA C
ATOM	2100	CG1	VAL	219	43.952	7.873	73.886	1.00	36.19	AAAA C
ATOM	2101	CG2	VAL	219	43.811	7.144	76.071	1.00	45.51	AAAA C
ATOM	2102	C	VAL	219	44.453	10.750	74.735	1.00	32.06	AAAA C
ATOM	2103	O	VAL	219	45.303	10.897	73.874	1.00	42.27	AAAA O
ATOM	2104	N	ALA	220	43.729	11.759	75.187	1.00	24.24	AAAA N
ATOM	2106	CA	ALA	220	43.638	12.985	74.385	1.00	27.09	AAAA C
ATOM	2107	CB	ALA	220	42.536	12.919	73.331	1.00	28.42	AAAA C
ATOM	2108	C	ALA	220	43.292	14.071	75.390	1.00	29.21	AAAA C
ATOM	2109	O	ALA	220	42.846	13.604	76.455	1.00	37.88	AAAA O
ATOM	2110	N	CYS	221	43.285	15.334	75.058	1.00	30.27	AAAA N
ATOM	2112	CA	CYS	221	42.753	16.382	75.875	1.00	35.55	AAAA C
ATOM	2113	C	CYS	221	41.460	17.055	75.452	1.00	47.06	AAAA C
ATOM	2114	O	CYS	221	41.265	17.598	74.368	1.00	49.57	AAAA O
ATOM	2115	CB	CYS	221	43.804	17.478	76.063	1.00	47.45	AAAA C
ATOM	2116	SG	CYS	221	45.494	16.935	76.538	1.00	47.06	AAAA S
ATOM	2117	N	ARG	222	40.503	17.133	76.396	1.00	51.47	AAAA N
ATOM	2119	CA	ARG	222	39.231	17.906	76.339	1.00	51.86	AAAA C
ATOM	2120	CB	ARG	222	38.647	18.074	77.712	1.00	54.53	AAAA C
ATOM	2121	CG	ARG	222	37.314	18.687	77.854	1.00	45.56	AAAA C
ATOM	2122	CD	ARG	222	36.538	18.338	79.087	1.00	54.45	AAAA C
ATOM	2123	NE	ARG	222	36.272	16.947	79.269	1.00	65.53	AAAA N
ATOM	2125	CZ	ARG	222	35.534	16.080	78.617	1.00	67.60	AAAA C
ATOM	2126	NH1	ARG	222	34.925	16.599	77.533	1.00	70.26	AAAA N
ATOM	2129	NH2	ARG	222	35.342	14.780	78.901	1.00	54.11	AAAA N
ATOM	2132	C	ARG	222	39.562	19.286	75.740	1.00	50.56	AAAA C
ATOM	2133	O	ARG	222	38.737	19.845	75.009	1.00	58.34	AAAA O
ATOM	2134	N	HIS	223	40.556	19.981	76.120	1.00	45.68	AAAA N
ATOM	2136	CA	HIS	223	40.988	21.291	75.921	1.00	46.93	AAAA C
ATOM	2137	CB	HIS	223	41.067	22.251	77.021	1.00	49.51	AAAA C
ATOM	2138	CG	HIS	223	39.710	22.344	77.617	1.00	56.83	AAAA C
ATOM	2139	CD2	HIS	223	38.820	23.360	77.556	1.00	61.08	AAAA C
ATOM	2140	ND1	HIS	223	39.082	21.380	78.425	1.00	63.28	AAAA N
ATOM	2142	CE1	HIS	223	37.881	21.815	78.759	1.00	56.01	AAAA C
ATOM	2143	NE2	HIS	223	37.681	23.019	78.230	1.00	48.56	AAAA N
ATOM	2145	C	HIS	223	42.363	21.260	75.122	1.00	50.78	AAAA C
ATOM	2146	O	HIS	223	42.506	20.755	74.003	1.00	47.45	AAAA O
ATOM	2147	N	TYR	224	43.359	21.847	75.769	1.00	49.20	AAAA N
ATOM	2149	CA	TYR	224	44.712	21.992	75.259	1.00	48.17	AAAA C
ATOM	2150	CB	TYR	224	45.144	23.430	75.426	1.00	44.07	AAAA C
ATOM	2151	CG	TYR	224	44.318	24.234	74.417	1.00	51.77	AAAA C
ATOM	2152	CD1	TYR	224	43.193	24.869	74.904	1.00	48.94	AAAA C
ATOM	2153	CE1	TYR	224	42.401	25.633	74.089	1.00	48.41	AAAA C
ATOM	2154	CD2	TYR	224	44.623	24.358	73.065	1.00	54.82	AAAA C
ATOM	2155	CE2	TYR	224	43.847	25.131	72.233	1.00	56.09	AAAA C
ATOM	2156	CZ	TYR	224	42.739	25.745	72.766	1.00	54.23	AAAA C
ATOM	2157	OH	TYR	224	41.915	26.522	72.017	1.00	61.70	AAAA O
ATOM	2159	C	TYR	224	45.725	21.095	75.892	1.00	48.19	AAAA C
ATOM	2160	O	TYR	224	45.776	20.913	77.111	1.00	55.75	AAAA O
ATOM	2161	N	TYR	225	46.524	20.514	75.077	1.00	48.79	AAAA N
ATOM	2163	CA	TYR	225	47.655	19.653	75.555	1.00	43.02	AAAA C
ATOM	2164	CB	TYR	225	48.020	18.639	74.548	1.00	42.30	AAAA C
ATOM	2165	CG	TYR	225	49.286	17.926	74.954	1.00	46.95	AAAA C
ATOM	2166	CD1	TYR	225	49.299	16.858	75.817	1.00	43.57	AAAA C
ATOM	2167	CE1	TYR	225	50.450	16.221	76.173	1.00	47.26	AAAA C
ATOM	2168	CD2	TYR	225	50.487	18.407	74.421	1.00	52.82	AAAA C
ATOM	2169	CE2	TYR	225	51.656	17.791	74.781	1.00	53.94	AAAA C
ATOM	2170	CZ	TYR	225	51.639	16.707	75.644	1.00	52.31	AAAA C
ATOM	2171	OH	TYR	225	52.806	16.186	75.995	1.00	50.71	AAAA O
ATOM	2173	C	TYR	225	48.870	20.507	75.793	1.00	47.13	AAAA C
ATOM	2174	O	TYR	225	49.089	21.514	75.150	1.00	53.97	AAAA O
ATOM	2175	N	TYR	226	49.634	20.253	76.821	1.00	56.84	AAAA N

Figure 1A-20

ATOM	2177	CA	TYR	226	50.811	21.691	77.172	1.00	56.83	AAAA C
ATOM	2178	CB	TYR	226	50.455	22.343	77.785	1.00	59.51	AAAA C
ATOM	2179	CG	TYR	226	51.741	23.126	77.941	1.00	65.45	AAAA C
ATOM	2180	CD1	TYR	226	52.121	23.557	79.197	1.00	69.12	AAAA C
ATOM	2181	CE1	TYR	226	53.289	24.275	79.400	1.00	70.77	AAAA C
ATOM	2182	CD2	TYR	226	52.580	23.409	76.864	1.00	69.38	AAAA C
ATOM	2183	CE2	TYR	226	53.758	24.118	77.020	1.00	70.94	AAAA C
ATOM	2184	CZ	TYR	226	54.099	24.549	78.301	1.00	72.96	AAAA C
ATOM	2185	OH	TYR	226	55.267	25.254	78.435	1.00	70.84	AAAA O
ATOM	2187	C	TYR	226	51.784	20.356	78.165	1.00	57.55	AAAA C
ATOM	2188	O	TYR	226	51.492	20.133	79.359	1.00	56.90	AAAA O
ATOM	2189	N	ALA	227	52.978	20.080	77.642	1.00	53.82	AAAA N
ATOM	2191	CA	ALA	227	54.061	19.557	78.440	1.00	51.82	AAAA C
ATOM	2192	CB	ALA	227	54.528	20.620	79.428	1.00	55.81	AAAA C
ATOM	2193	C	ALA	227	53.600	18.309	79.170	1.00	53.56	AAAA C
ATOM	2194	O	ALA	227	53.663	18.218	80.413	1.00	49.63	AAAA O
ATOM	2195	N	GLY	228	53.076	17.360	78.393	1.00	50.68	AAAA N
ATOM	2197	CA	GLY	228	52.585	16.135	79.028	1.00	49.02	AAAA C
ATOM	2198	C	GLY	228	51.312	16.330	79.861	1.00	51.61	AAAA C
ATOM	2199	O	GLY	228	51.028	15.538	80.776	1.00	51.10	AAAA O
ATOM	2200	N	VAL	229	50.643	17.495	79.791	1.00	47.09	AAAA N
ATOM	2202	CA	VAL	229	49.489	17.671	80.635	1.00	51.11	AAAA C
ATOM	2203	CB	VAL	229	49.908	18.610	81.774	1.00	56.52	AAAA C
ATOM	2204	CG1	VAL	229	48.627	18.896	82.566	1.00	38.39	AAAA C
ATOM	2205	CG2	VAL	229	51.002	18.035	82.682	1.00	50.16	AAAA C
ATOM	2206	C	VAL	229	48.255	18.173	79.873	1.00	51.37	AAAA C
ATOM	2207	O	VAL	229	48.344	19.279	79.309	1.00	53.71	AAAA O
ATOM	2208	N	CYS	230	47.100	17.518	80.036	1.00	42.21	AAAA N
ATOM	2210	CA	CYS	230	45.981	18.117	79.471	1.00	40.32	AAAA C
ATOM	2211	C	CYS	230	45.456	19.350	80.229	1.00	38.42	AAAA C
ATOM	2212	O	CYS	230	44.964	19.248	81.321	1.00	41.62	AAAA O
ATOM	2213	CB	CYS	230	44.746	17.132	79.370	1.00	31.54	AAAA C
ATOM	2214	SG	CYS	230	45.149	15.753	78.266	1.00	43.61	AAAA S
ATOM	2215	N	VAL	231	45.637	20.534	79.731	1.00	39.83	AAAA N
ATOM	2217	CA	VAL	231	45.445	21.769	80.462	1.00	46.57	AAAA C
ATOM	2218	CB	VAL	231	46.518	22.736	80.088	1.00	50.99	AAAA C
ATOM	2219	CG1	VAL	231	46.798	23.878	81.053	1.00	50.41	AAAA C
ATOM	2220	CG2	VAL	231	47.838	21.913	80.506	1.00	44.95	AAAA C
ATOM	2221	C	VAL	231	44.111	22.321	80.057	1.00	52.59	AAAA C
ATOM	2222	O	VAL	231	43.599	22.183	78.936	1.00	55.30	AAAA O
ATOM	2223	N	PRO	232	43.482	23.105	80.913	1.00	54.28	AAAA N
ATOM	2224	CD	PRO	232	43.830	23.385	82.320	1.00	54.25	AAAA C
ATOM	2225	CA	PRO	232	42.153	23.625	80.575	1.00	54.39	AAAA C
ATOM	2226	CB	PRO	232	41.537	23.877	81.928	1.00	53.73	AAAA C
ATOM	2227	CG	PRO	232	42.683	24.287	82.765	1.00	55.00	AAAA C
ATOM	2228	C	PRO	232	42.361	24.913	79.795	1.00	56.37	AAAA C
ATOM	2229	O	PRO	232	41.498	25.482	79.137	1.00	55.79	AAAA O
ATOM	2230	N	ALA	233	43.615	25.400	79.901	1.00	54.76	AAAA N
ATOM	2232	CA	ALA	233	43.998	26.569	79.124	1.00	49.93	AAAA C
ATOM	2233	CB	ALA	233	43.440	27.807	79.746	1.00	35.43	AAAA C
ATOM	2234	C	ALA	233	45.502	26.662	78.974	1.00	49.79	AAAA C
ATOM	2235	O	ALA	233	46.195	25.879	79.616	1.00	51.41	AAAA O
ATOM	2236	N	CYS	234	45.984	27.508	78.072	1.00	45.07	AAAA N
ATOM	2238	CA	CYS	234	47.430	27.518	77.967	1.00	48.63	AAAA C
ATOM	2239	C	CYS	234	48.001	28.340	79.076	1.00	50.93	AAAA C
ATOM	2240	O	CYS	234	47.650	29.513	79.250	1.00	47.57	AAAA O
ATOM	2241	CB	CYS	234	47.816	28.034	76.511	1.00	43.10	AAAA C
ATOM	2242	SG	CYS	234	47.608	26.789	75.226	1.00	43.04	AAAA S
ATOM	2243	N	PRO	235	49.127	27.853	79.599	1.00	49.55	AAAA N
ATOM	2244	CD	PRO	235	49.692	26.557	79.207	1.00	48.75	AAAA C
ATOM	2245	CA	PRO	235	49.911	28.569	80.599	1.00	51.69	AAAA C
ATOM	2246	CB	PRO	235	50.984	27.581	80.975	1.00	50.80	AAAA C
ATOM	2247	CG	PRO	235	50.912	26.417	80.077	1.00	50.06	AAAA C
ATOM	2248	C	PRO	235	50.487	29.852	80.050	1.00	57.11	AAAA C
ATOM	2249	O	PRO	235	50.848	29.957	78.870	1.00	59.60	AAAA O
ATOM	2250	N	PRO	236	50.676	30.875	80.887	1.00	59.85	AAAA N
ATOM	2251	CD	PRO	236	50.405	30.822	82.363	1.00	55.85	AAAA C
ATOM	2252	CA	PRO	236	51.323	32.143	80.493	1.00	52.27	AAAA C
ATOM	2253	CB	PRO	236	51.695	32.814	81.826	1.00	53.62	AAAA C
ATOM	2254	CG	PRO	236	50.652	32.277	82.754	1.00	56.73	AAAA C
ATOM	2255	C	PRO	236	52.545	31.886	79.671	1.00	44.21	AAAA C
ATOM	2256	O	PRO	236	53.219	30.892	79.928	1.00	43.40	AAAA O
ATOM	2257	N	ASN	237	52.837	32.757	78.716	1.00	46.54	AAAA N
ATOM	2259	CA	ASN	237	53.895	32.623	77.716	1.00	45.94	AAAA C
ATOM	2260	CB	ASN	237	55.259	32.653	78.456	1.00	58.65	AAAA C
ATOM	2261	CG	ASN	237	55.357	33.855	79.371	1.00	58.51	AAAA C
ATOM	2262	OD1	ASN	237	56.044	33.783	80.379	1.00	72.25	AAAA O
ATOM	2263	ND2	ASN	237	54.631	34.910	79.051	1.00	62.99	AAAA N
ATOM	2266	C	ASN	237	53.897	31.425	76.788	1.00	46.87	AAAA C
ATOM	2267	O	ASN	237	54.960	30.935	76.326	1.00	54.50	AAAA O
ATOM	2268	N	THR	238	52.617	30.657	76.692	1.00	42.91	AAAA N
ATOM	2270	CA	THR	238	52.617	29.567	75.790	1.00	40.20	AAAA C
ATOM	2271	CB	THR	238	52.461	28.248	76.466	1.00	42.62	AAAA C
ATOM	2272	OG1	THR	238	51.227	28.343	77.243	1.00	50.88	AAAA O
ATOM	2274	CG2	THR	238	53.552	27.886	77.424	1.00	34.84	AAAA C

Figure 1A-21

```
ATOM  2275  C   THR  238      51.270   29.875   75.978  1.00 42.59      AAAA C
ATOM  2276  O   THR  238      50.669   30.864   75.509  1.00 42.51      AAAA O
ATOM  2277  N   TYR  239      51.051   28.488   73.832  1.00 42.62      AAAA N
ATOM  2278  CA  TYR  239      49.949   28.959   73.024  1.00 41.97      AAAA C
ATOM  2279  CB  TYR  239      50.457   30.907   71.931  1.00 44.86      AAAA C
ATOM  2280  CG  TYR  239      51.099   32.125   72.564  1.00 42.05      AAAA C
ATOM  2281  CD1 TYR  239      52.467   32.086   72.815  1.00 39.41      AAAA C
ATOM  2282  CE1 TYR  239      53.092   33.152   73.415  1.00 43.27      AAAA C
ATOM  2283  CD2 TYR  239      50.376   33.230   72.923  1.00 44.15      AAAA C
ATOM  2284  CE2 TYR  239      50.972   34.310   73.536  1.00 46.22      AAAA C
ATOM  2285  CZ  TYR  239      52.339   34.243   70.779  1.00 50.42      AAAA C
ATOM  2286  OH  TYR  239      53.013   35.289   74.387  1.00 55.47      AAAA O
ATOM  2287  C   TYR  239      49.232   28.813   72.315  1.00 45.54      AAAA C
ATOM  2288  O   TYR  239      49.922   27.810   72.021  1.00 46.66      AAAA O
ATOM  2289  N   ARG  240      47.895   28.990   72.126  1.00 40.62      AAAA N
ATOM  2290  CA  ARG  240      47.177   27.892   71.426  1.00 38.78      AAAA C
ATOM  2291  CB  ARG  240      45.675   28.127   71.452  1.00 39.77      AAAA C
ATOM  2292  CG  ARG  240      45.116   28.944   72.589  1.00 43.37      AAAA C
ATOM  2293  CD  ARG  240      43.573   28.957   72.683  1.00 38.60      AAAA C
ATOM  2294  NE  ARG  240      43.114   29.693   71.455  1.00 53.05      AAAA N
ATOM  2295  CZ  ARG  240      43.123   31.015   71.530  1.00 48.07      AAAA C
ATOM  2296  NH1 ARG  240      43.513   31.562   72.668  1.00 47.65      AAAA N
ATOM  2297  NH2 ARG  240      42.788   31.778   70.533  1.00 51.03      AAAA N
ATOM  2298  C   ARG  240      47.627   27.737   69.979  1.00 31.72      AAAA C
ATOM  2299  O   ARG  240      47.937   28.730   69.302  1.00 32.37      AAAA O
ATOM  2300  N   PHE  241      47.779   26.542   69.549  1.00 27.95      AAAA N
ATOM  2301  CA  PHE  241      48.182   26.269   68.183  1.00 30.41      AAAA C
ATOM  2302  CB  PHE  241      49.678   25.940   68.151  1.00 34.83      AAAA C
ATOM  2303  CG  PHE  241      50.235   25.653   66.773  1.00 26.84      AAAA C
ATOM  2304  CD1 PHE  241      50.165   26.567   65.753  1.00 25.31      AAAA C
ATOM  2305  CD2 PHE  241      50.785   24.417   66.573  1.00 27.38      AAAA C
ATOM  2306  CE1 PHE  241      50.676   26.232   64.509  1.00 37.24      AAAA C
ATOM  2307  CE2 PHE  241      51.294   24.101   65.320  1.00 38.45      AAAA C
ATOM  2308  CZ  PHE  241      51.281   25.010   64.281  1.00 21.17      AAAA C
ATOM  2309  C   PHE  241      47.382   25.089   67.621  1.00 35.77      AAAA C
ATOM  2310  O   PHE  241      47.543   24.013   68.186  1.00 36.77      AAAA O
ATOM  2311  N   GLU  242      46.738   25.301   66.468  1.00 32.30      AAAA N
ATOM  2312  CA  GLU  242      45.964   24.269   65.805  1.00 35.43      AAAA C
ATOM  2313  CB  GLU  242      46.953   23.144   65.472  1.00 37.98      AAAA C
ATOM  2314  CG  GLU  242      47.867   23.415   64.314  1.00 38.63      AAAA C
ATOM  2315  CD  GLU  242      47.207   23.965   63.075  1.00 39.27      AAAA C
ATOM  2316  OE1 GLU  242      46.380   23.205   62.517  1.00 42.79      AAAA O
ATOM  2317  OE2 GLU  242      47.354   25.109   62.626  1.00 36.36      AAAA O
ATOM  2318  C   GLU  242      44.752   23.771   66.600  1.00 34.36      AAAA C
ATOM  2319  O   GLU  242      44.390   22.611   66.511  1.00 28.53      AAAA O
ATOM  2320  N   GLY  243      44.135   24.589   67.449  1.00 36.94      AAAA N
ATOM  2321  CA  GLY  243      43.048   24.154   68.303  1.00 34.57      AAAA C
ATOM  2322  C   GLY  243      43.428   23.107   69.319  1.00 37.76      AAAA C
ATOM  2323  O   GLY  243      42.474   22.473   69.746  1.00 43.00      AAAA O
ATOM  2324  N   TRP  244      44.637   22.636   69.611  1.00 39.53      AAAA N
ATOM  2325  CA  TRP  244      44.797   21.536   70.566  1.00 40.85      AAAA C
ATOM  2326  CB  TRP  244      44.774   20.271   69.764  1.00 26.76      AAAA C
ATOM  2327  CG  TRP  244      46.012   19.885   69.029  1.00 43.19      AAAA C
ATOM  2328  CD2 TRP  244      47.019   18.983   69.498  1.00 39.55      AAAA C
ATOM  2329  CE2 TRP  244      47.998   18.906   68.489  1.00 36.50      AAAA C
ATOM  2330  CE3 TRP  244      47.186   18.254   70.692  1.00 32.18      AAAA C
ATOM  2331  CD1 TRP  244      46.424   20.308   67.779  1.00 43.37      AAAA C
ATOM  2332  NE1 TRP  244      47.595   19.727   67.469  1.00 38.89      AAAA N
ATOM  2333  CZ2 TRP  244      49.150   18.128   68.620  1.00 39.01      AAAA C
ATOM  2334  CZ3 TRP  244      48.336   17.478   70.815  1.00 43.98      AAAA C
ATOM  2335  CH2 TRP  244      49.322   17.425   69.784  1.00 42.50      AAAA C
ATOM  2336  C   TRP  244      45.998   21.517   71.509  1.00 42.98      AAAA C
ATOM  2337  O   TRP  244      46.253   20.501   72.146  1.00 42.70      AAAA O
ATOM  2338  N   ARG  245      46.888   22.495   71.435  1.00 44.16      AAAA N
ATOM  2339  CA  ARG  245      48.168   22.472   72.095  1.00 46.47      AAAA C
ATOM  2340  CB  ARG  245      49.203   21.602   71.367  1.00 47.30      AAAA C
ATOM  2341  CG  ARG  245      49.985   22.309   70.203  1.00 48.97      AAAA C
ATOM  2342  CD  ARG  245      51.129   21.552   69.819  1.00 39.28      AAAA C
ATOM  2343  NE  ARG  245      51.586   21.665   68.444  1.00 50.86      AAAA N
ATOM  2344  CZ  ARG  245      52.629   21.044   67.895  1.00 46.73      AAAA C
ATOM  2345  NH1 ARG  245      53.344   20.236   68.653  1.00 50.15      AAAA N
ATOM  2346  NH2 ARG  245      53.072   21.126   66.638  1.00 41.69      AAAA N
ATOM  2347  C   ARG  245      48.771   23.863   72.271  1.00 46.01      AAAA C
ATOM  2348  O   ARG  245      48.394   24.793   71.541  1.00 47.44      AAAA O
ATOM  2349  N   CYS  246      49.625   23.881   73.317  1.00 42.08      AAAA N
ATOM  2350  CA  CYS  246      50.246   25.199   73.628  1.00 43.48      AAAA C
ATOM  2351  C   CYS  246      51.695   25.217   73.183  1.00 43.38      AAAA C
ATOM  2352  O   CYS  246      52.476   24.239   73.320  1.00 42.51      AAAA O
ATOM  2353  CB  CYS  246      50.102   25.392   75.138  1.00 48.91      AAAA C
ATOM  2354  SG  CYS  246      48.386   25.049   75.797  1.00 43.68      AAAA S
ATOM  2355  N   VAL  247      52.121   26.288   72.564  1.00 41.21      AAAA N
ATOM  2356  CA  VAL  247      53.417   26.468   71.982  1.00 36.51      AAAA C
ATOM  2357  CB  VAL  247      53.569   25.357   70.444  1.00 36.87      AAAA C
ATOM  2358  CG1 VAL  247      53.089   24.988   70.024  1.00 32.71      AAAA C
ATOM  2359  CG2 VAL  247      53.129   27.602   69.729  1.00 28.20      AAAA C
```

Figure 1A-22

ATOM	2381	C	VAL	247	53.969	27.812	72.179	1.00	39.39	AAAA C
ATOM	2382	O	VAL	247	53.230	28.770	72.549	1.00	38.80	AAAA O
ATOM	2383	N	ASP	248	55.291	27.820	72.211	1.00	45.21	AAAA N
ATOM	2385	CA	ASP	248	55.895	29.115	73.099	1.00	40.19	AAAA C
ATOM	2386	CB	ASP	248	57.091	28.946	73.953	1.00	42.63	AAAA C
ATOM	2387	CG	ASP	248	58.126	27.997	73.394	1.00	58.81	AAAA C
ATOM	2388	OD1	ASP	248	59.067	27.795	74.187	1.00	53.06	AAAA O
ATOM	2389	OD2	ASP	248	58.167	27.395	72.313	1.00	69.51	AAAA O
ATOM	2390	C	ASP	248	56.315	29.883	71.839	1.00	36.99	AAAA C
ATOM	2391	O	ASP	248	56.292	29.288	70.772	1.00	39.70	AAAA O
ATOM	2392	N	ARG	249	56.545	31.163	71.918	1.00	30.72	AAAA N
ATOM	2394	CA	ARG	249	56.950	32.057	70.906	1.00	36.17	AAAA C
ATOM	2395	CB	ARG	249	57.223	33.495	71.491	1.00	21.29	AAAA C
ATOM	2396	CG	ARG	249	57.594	34.424	70.326	1.00	24.96	AAAA C
ATOM	2397	CD	ARG	249	57.814	35.811	70.843	1.00	21.23	AAAA C
ATOM	2398	NE	ARG	249	56.658	36.150	71.669	1.00	39.75	AAAA N
ATOM	2400	CZ	ARG	249	55.632	36.923	71.101	1.00	39.35	AAAA C
ATOM	2401	NH1	ARG	249	55.642	37.118	69.801	1.00	25.41	AAAA N
ATOM	2404	NH2	ARG	249	54.641	37.118	71.946	1.00	44.04	AAAA N
ATOM	2407	C	ARG	249	58.134	31.685	70.010	1.00	40.63	AAAA C
ATOM	2408	O	ARG	249	58.086	31.923	68.797	1.00	44.79	AAAA O
ATOM	2409	N	ASP	250	59.149	30.974	70.468	1.00	41.87	AAAA N
ATOM	2411	CA	ASP	250	60.287	30.739	69.606	1.00	46.90	AAAA C
ATOM	2412	CB	ASP	250	61.740	30.726	70.154	1.00	53.11	AAAA C
ATOM	2413	CG	ASP	250	62.421	32.122	70.081	1.00	71.49	AAAA C
ATOM	2414	OD1	ASP	250	63.124	32.682	69.176	1.00	58.53	AAAA O
ATOM	2415	OD2	ASP	250	62.272	32.928	71.071	1.00	70.30	AAAA O
ATOM	2416	C	ASP	250	59.881	29.536	68.771	1.00	41.22	AAAA C
ATOM	2417	O	ASP	250	60.291	29.443	67.616	1.00	39.06	AAAA O
ATOM	2418	N	PHE	251	59.116	28.609	69.209	1.00	36.13	AAAA N
ATOM	2420	CA	PHE	251	58.457	27.601	68.389	1.00	34.88	AAAA C
ATOM	2421	CB	PHE	251	57.468	26.746	69.256	1.00	29.82	AAAA C
ATOM	2422	CG	PHE	251	56.701	25.801	68.385	1.00	41.59	AAAA C
ATOM	2423	CD1	PHE	251	57.101	24.479	68.263	1.00	30.66	AAAA C
ATOM	2424	CD2	PHE	251	55.559	26.213	67.686	1.00	37.78	AAAA C
ATOM	2425	CE1	PHE	251	56.414	23.597	67.424	1.00	29.30	AAAA C
ATOM	2426	CE2	PHE	251	54.847	25.372	66.856	1.00	36.09	AAAA C
ATOM	2427	CZ	PHE	251	55.294	24.070	66.715	1.00	36.21	AAAA C
ATOM	2428	C	PHE	251	57.624	28.290	67.338	1.00	39.28	AAAA C
ATOM	2429	O	PHE	251	57.811	28.010	66.144	1.00	30.27	AAAA O
ATOM	2430	N	CYS	252	56.734	29.225	67.713	1.00	35.13	AAAA N
ATOM	2432	CA	CYS	252	55.895	29.870	66.728	1.00	38.80	AAAA C
ATOM	2433	C	CYS	252	56.827	30.598	65.747	1.00	44.73	AAAA C
ATOM	2434	O	CYS	252	56.552	30.534	64.536	1.00	43.20	AAAA O
ATOM	2435	CB	CYS	252	54.903	30.778	67.379	1.00	35.65	AAAA C
ATOM	2436	SG	CYS	252	53.562	31.544	66.459	1.00	39.03	AAAA S
ATOM	2437	N	ALA	253	57.872	31.256	66.285	1.00	41.53	AAAA N
ATOM	2439	CA	ALA	253	58.687	32.071	65.415	1.00	40.39	AAAA C
ATOM	2440	CB	ALA	253	59.539	33.088	66.172	1.00	36.07	AAAA C
ATOM	2441	C	ALA	253	59.551	31.167	64.539	1.00	42.88	AAAA C
ATOM	2442	O	ALA	253	60.147	31.735	63.640	1.00	47.42	AAAA O
ATOM	2443	N	ASN	254	59.657	29.859	64.709	1.00	38.75	AAAA N
ATOM	2445	CA	ASN	254	60.546	29.073	63.929	1.00	42.94	AAAA C
ATOM	2446	CB	ASN	254	61.667	28.497	64.847	1.00	48.09	AAAA C
ATOM	2447	CG	ASN	254	62.696	29.635	65.031	1.00	49.94	AAAA C
ATOM	2448	OD1	ASN	254	63.468	29.840	64.081	1.00	61.36	AAAA O
ATOM	2449	ND2	ASN	254	62.607	30.321	66.144	1.00	48.38	AAAA N
ATOM	2452	C	ASN	254	59.907	27.959	63.135	1.00	53.72	AAAA C
ATOM	2453	O	ASN	254	60.552	26.965	62.804	1.00	51.19	AAAA O
ATOM	2454	N	ILE	255	58.612	28.136	62.766	1.00	57.77	AAAA N
ATOM	2456	CA	ILE	255	57.828	27.107	62.134	1.00	53.29	AAAA C
ATOM	2457	CB	ILE	255	56.329	27.322	62.304	1.00	50.41	AAAA C
ATOM	2458	CG2	ILE	255	55.477	26.595	61.246	1.00	51.95	AAAA C
ATOM	2459	CG1	ILE	255	55.778	26.675	63.553	1.00	49.59	AAAA C
ATOM	2460	CD1	ILE	255	54.479	27.317	64.006	1.00	38.97	AAAA C
ATOM	2461	C	ILE	255	58.127	26.886	60.651	1.00	52.62	AAAA C
ATOM	2462	O	ILE	255	58.196	25.709	60.252	1.00	53.96	AAAA O
ATOM	2463	N	LEU	256	58.290	27.960	59.910	1.00	49.96	AAAA N
ATOM	2465	CA	LEU	256	58.680	27.764	58.516	1.00	63.68	AAAA C
ATOM	2466	CB	LEU	256	58.175	29.012	57.799	1.00	56.80	AAAA C
ATOM	2467	CG	LEU	256	56.671	29.196	57.864	1.00	59.11	AAAA C
ATOM	2468	CD1	LEU	256	56.310	30.654	57.645	1.00	43.31	AAAA C
ATOM	2469	CD2	LEU	256	55.965	29.222	56.928	1.00	55.88	AAAA C
ATOM	2470	C	LEU	256	60.193	27.622	58.355	1.00	66.23	AAAA C
ATOM	2471	O	LEU	256	60.691	27.511	57.245	1.00	70.29	AAAA O
ATOM	2472	N	SER	257	60.942	27.559	59.430	1.00	64.61	AAAA N
ATOM	2474	CA	SER	257	62.352	27.529	59.534	1.00	69.23	AAAA C
ATOM	2475	CB	SER	257	62.924	27.318	60.955	1.00	62.45	AAAA C
ATOM	2476	OG	SER	257	63.381	25.990	61.074	1.00	56.18	AAAA O
ATOM	2478	C	SER	257	62.973	26.497	58.610	1.00	70.72	AAAA C
ATOM	2479	O	SER	257	64.127	26.731	58.248	1.00	72.50	AAAA O
ATOM	2480	N	ALA	258	62.322	25.399	58.329	1.00	74.61	AAAA N
ATOM	2482	CA	ALA	258	62.933	24.488	57.313	1.00	76.34	AAAA C
ATOM	2483	CB	ALA	258	62.570	23.039	57.584	1.00	80.82	AAAA C
ATOM	2484	C	ALA	258	62.663	24.964	55.921	1.00	78.21	AAAA C

Figure 1A-23

ATOM	2485	N	ALA	258	62.980	24.130	55.028	1.00	79.60	AAAA N
ATOM	2486	H	GLU	259	62.069	26.109	55.651	1.00	79.05	AAAA H
ATOM	2488	CA	GLU	259	61.742	26.621	54.849	1.00	83.84	AAAA C
ATOM	2489	CB	GLU	259	60.259	26.457	54.135	1.00	86.99	AAAA C
ATOM	2490	CG	GLU	259	59.687	25.049	54.314	1.00	99.38	AAAA C
ATOM	2491	CD	GLU	259	58.364	25.032	55.057	1.00	97.77	AAAA C
ATOM	2492	OE1	GLU	259	58.080	24.088	55.839	1.00	101.45	AAAA O
ATOM	2493	OE2	GLU	259	57.598	26.002	54.837	1.00	94.58	AAAA O
ATOM	2494	C	GLU	259	62.117	28.078	54.983	1.00	85.43	AAAA C
ATOM	2495	O	GLU	259	62.059	29.009	54.903	1.00	88.01	AAAA O
ATOM	2496	N	SER	260	62.298	28.338	52.799	1.00	84.66	AAAA N
ATOM	2498	CA	SER	260	62.725	29.625	52.254	1.00	84.03	AAAA C
ATOM	2499	CB	SER	260	63.753	29.269	51.173	1.00	87.24	AAAA C
ATOM	2500	OG	SER	260	63.306	29.419	49.835	1.00	93.65	AAAA O
ATOM	2502	C	SER	260	61.558	30.466	51.799	1.00	80.84	AAAA C
ATOM	2503	O	SER	260	61.496	30.889	50.635	1.00	81.31	AAAA O
ATOM	2504	N	SER	261	60.617	30.705	52.685	1.00	78.56	AAAA N
ATOM	2506	CA	SER	261	59.423	31.540	52.308	1.00	72.13	AAAA C
ATOM	2507	CB	SER	261	58.179	31.287	53.170	1.00	67.30	AAAA C
ATOM	2508	OG	SER	261	57.436	30.334	52.451	1.00	74.74	AAAA O
ATOM	2510	C	SER	261	59.683	33.032	52.318	1.00	66.90	AAAA C
ATOM	2511	O	SER	261	60.048	33.588	53.334	1.00	63.24	AAAA O
ATOM	2512	N	ASP	262	59.364	33.659	51.284	1.00	65.30	AAAA N
ATOM	2514	CA	ASP	262	59.358	35.071	50.915	1.00	58.55	AAAA C
ATOM	2515	CB	ASP	262	59.268	35.285	49.400	1.00	64.85	AAAA C
ATOM	2516	CG	ASP	262	59.389	36.713	48.931	1.00	76.42	AAAA C
ATOM	2517	OD1	ASP	262	59.473	37.708	49.701	1.00	79.81	AAAA O
ATOM	2518	OD2	ASP	262	59.404	36.873	47.671	1.00	80.46	AAAA O
ATOM	2519	C	ASP	262	58.121	35.706	51.529	1.00	56.88	AAAA C
ATOM	2520	O	ASP	262	57.851	36.919	51.515	1.00	52.48	AAAA O
ATOM	2521	N	SER	263	57.259	34.849	52.219	1.00	53.43	AAAA N
ATOM	2523	CA	SER	263	56.047	35.352	52.734	1.00	52.84	AAAA C
ATOM	2524	CB	SER	263	55.020	34.245	52.885	1.00	46.60	AAAA C
ATOM	2525	OG	SER	263	55.149	33.348	51.791	1.00	66.80	AAAA O
ATOM	2527	C	SER	263	56.310	35.965	54.117	1.00	49.52	AAAA C
ATOM	2528	O	SER	263	57.396	35.737	54.709	1.00	42.33	AAAA O
ATOM	2529	N	GLU	264	55.320	36.783	54.540	1.00	38.93	AAAA N
ATOM	2531	CA	GLU	264	55.362	37.222	55.921	1.00	36.70	AAAA C
ATOM	2532	CB	GLU	264	54.359	38.337	56.208	1.00	43.71	AAAA C
ATOM	2533	CG	GLU	264	54.575	39.482	55.218	1.00	37.74	AAAA C
ATOM	2534	CD	GLU	264	55.374	40.632	55.793	1.00	34.36	AAAA C
ATOM	2535	OE1	GLU	264	55.493	40.600	57.034	1.00	41.55	AAAA O
ATOM	2536	OE2	GLU	264	55.832	41.576	55.146	1.00	39.60	AAAA O
ATOM	2537	C	GLU	264	55.098	36.056	56.827	1.00	35.84	AAAA C
ATOM	2538	O	GLU	264	54.368	35.151	56.355	1.00	39.60	AAAA O
ATOM	2539	N	GLY	265	55.861	35.938	57.962	1.00	35.64	AAAA N
ATOM	2541	CA	GLY	265	55.671	34.690	58.727	1.00	40.30	AAAA C
ATOM	2542	C	GLY	265	54.622	34.716	59.829	1.00	39.51	AAAA C
ATOM	2543	O	GLY	265	53.951	35.699	60.135	1.00	37.20	AAAA O
ATOM	2544	N	PHE	266	54.537	33.569	60.516	1.00	35.75	AAAA N
ATOM	2546	CA	PHE	266	53.637	33.434	61.625	1.00	33.70	AAAA C
ATOM	2547	CB	PHE	266	53.924	32.155	62.396	1.00	28.20	AAAA C
ATOM	2548	CG	PHE	266	53.356	30.958	61.671	1.00	37.07	AAAA C
ATOM	2549	CD1	PHE	266	53.760	30.618	60.377	1.00	34.72	AAAA C
ATOM	2550	CD2	PHE	266	52.383	30.195	62.313	1.00	25.65	AAAA C
ATOM	2551	CE1	PHE	266	53.225	29.506	59.760	1.00	37.72	AAAA C
ATOM	2552	CE2	PHE	266	51.879	29.094	61.672	1.00	24.63	AAAA C
ATOM	2553	CZ	PHE	266	52.260	28.708	60.402	1.00	23.58	AAAA C
ATOM	2554	C	PHE	266	53.571	34.570	62.608	1.00	35.82	AAAA C
ATOM	2555	O	PHE	266	54.446	35.372	62.979	1.00	39.23	AAAA O
ATOM	2556	N	VAL	267	52.360	34.763	63.161	1.00	37.10	AAAA N
ATOM	2558	CA	VAL	267	52.118	35.812	64.113	1.00	36.09	AAAA C
ATOM	2559	CB	VAL	267	51.315	36.974	63.567	1.00	39.01	AAAA C
ATOM	2560	CG1	VAL	267	51.626	37.601	62.239	1.00	31.10	AAAA C
ATOM	2561	CG2	VAL	267	49.490	36.490	63.679	1.00	36.88	AAAA C
ATOM	2562	C	VAL	267	51.506	35.260	65.409	1.00	33.55	AAAA C
ATOM	2563	O	VAL	267	51.202	34.098	65.519	1.00	32.41	AAAA O
ATOM	2564	N	ILE	268	51.539	36.088	66.477	1.00	35.98	AAAA N
ATOM	2566	CA	ILE	268	50.867	35.573	67.691	1.00	39.79	AAAA C
ATOM	2567	CB	ILE	268	51.791	35.232	68.849	1.00	31.17	AAAA C
ATOM	2568	CG2	ILE	268	50.922	35.253	70.150	1.00	32.66	AAAA C
ATOM	2569	CG1	ILE	268	52.403	33.866	68.724	1.00	23.56	AAAA C
ATOM	2570	CD1	ILE	268	53.421	33.546	69.806	1.00	25.93	AAAA C
ATOM	2571	C	ILE	268	49.806	36.608	68.060	1.00	42.44	AAAA C
ATOM	2572	O	ILE	268	50.116	37.767	68.327	1.00	39.99	AAAA O
ATOM	2573	N	HIS	269	48.528	36.292	67.864	1.00	44.26	AAAA N
ATOM	2575	CA	HIS	269	47.491	37.320	68.173	1.00	44.28	AAAA C
ATOM	2576	CB	HIS	269	46.885	37.876	66.901	1.00	45.48	AAAA C
ATOM	2577	CG	HIS	269	45.915	38.986	67.079	1.00	54.33	AAAA C
ATOM	2578	CD2	HIS	269	44.551	39.014	67.096	1.00	46.61	AAAA C
ATOM	2579	ND1	HIS	269	46.356	40.290	67.307	1.00	51.86	AAAA N
ATOM	2581	CE1	HIS	269	45.282	41.057	67.437	1.00	55.17	AAAA C
ATOM	2582	NE2	HIS	269	44.175	40.324	67.309	1.00	46.97	AAAA N
ATOM	2584	C	HIS	269	46.423	36.740	69.054	1.00	45.54	AAAA C
ATOM	2585	O	HIS	269	46.076	35.582	69.127	1.00	42.94	AAAA O

Figure 1A-24

ATOM	2596	N	ASP	270	45.952	37.526	70.959	1.00	49.92	AAAA N
ATOM	2588	CA	ASP	270	44.918	37.025	71.001	1.00	48.03	AAAA C
ATOM	2589	CB	ASP	270	43.573	37.014	70.339	1.00	63.63	AAAA C
ATOM	2590	CG	ASP	270	42.919	38.393	70.294	1.00	80.82	AAAA C
ATOM	2591	OD1	ASP	270	41.737	38.379	69.835	1.00	90.92	AAAA O
ATOM	2592	OD2	ASP	270	43.407	39.494	70.652	1.00	86.49	AAAA O
ATOM	2593	C	ASP	270	45.226	35.667	71.594	1.00	44.66	AAAA C
ATOM	2594	O	ASP	270	44.357	34.782	71.576	1.00	45.54	AAAA O
ATOM	2595	N	GLY	271	46.477	35.379	71.924	1.00	41.63	AAAA N
ATOM	2597	CA	GLY	271	46.839	34.117	72.506	1.00	37.20	AAAA C
ATOM	2598	C	GLY	271	46.819	32.998	71.537	1.00	39.15	AAAA C
ATOM	2599	O	GLY	271	46.775	31.865	72.039	1.00	46.56	AAAA O
ATOM	2600	N	GLU	272	47.015	33.292	70.251	1.00	41.49	AAAA N
ATOM	2602	CA	GLU	272	47.169	32.092	69.371	1.00	43.56	AAAA C
ATOM	2603	CB	GLU	272	45.752	31.737	68.876	1.00	37.58	AAAA C
ATOM	2604	CG	GLU	272	45.779	30.600	67.839	1.00	45.30	AAAA C
ATOM	2605	CD	GLU	272	44.413	30.528	67.149	1.00	36.92	AAAA C
ATOM	2606	OE1	GLU	272	43.515	31.345	67.533	1.00	48.41	AAAA O
ATOM	2607	OE2	GLU	272	44.223	29.696	66.286	1.00	44.10	AAAA O
ATOM	2608	C	GLU	272	48.211	32.324	68.335	1.00	40.32	AAAA C
ATOM	2609	O	GLU	272	48.445	33.447	67.896	1.00	37.04	AAAA O
ATOM	2610	N	CYS	273	48.942	31.237	68.138	1.00	38.83	AAAA N
ATOM	2612	CA	CYS	273	50.046	31.187	67.188	1.00	40.27	AAAA C
ATOM	2613	C	CYS	273	49.321	30.810	65.883	1.00	42.16	AAAA C
ATOM	2614	O	CYS	273	48.713	29.712	65.831	1.00	40.86	AAAA O
ATOM	2615	CB	CYS	273	51.098	30.148	67.529	1.00	40.21	AAAA C
ATOM	2616	SG	CYS	273	52.337	29.825	66.260	1.00	39.79	AAAA S
ATOM	2617	N	MET	274	49.373	31.749	64.933	1.00	33.70	AAAA N
ATOM	2619	CA	MET	274	48.586	31.351	63.720	1.00	36.68	AAAA C
ATOM	2620	CB	MET	274	47.136	31.861	63.847	1.00	29.11	AAAA C
ATOM	2621	CG	MET	274	46.923	33.379	63.691	1.00	36.51	AAAA C
ATOM	2622	SD	MET	274	45.477	33.921	64.677	1.00	40.09	AAAA S
ATOM	2623	CE	MET	274	45.650	35.658	64.754	1.00	22.47	AAAA C
ATOM	2624	C	MET	274	49.426	31.900	62.608	1.00	39.35	AAAA C
ATOM	2625	O	MET	274	50.167	32.880	62.672	1.00	41.00	AAAA O
ATOM	2626	N	GLN	275	49.378	31.353	61.428	1.00	42.55	AAAA N
ATOM	2628	CA	GLN	275	50.041	31.834	60.232	1.00	37.69	AAAA C
ATOM	2629	CB	GLN	275	49.618	30.765	59.242	1.00	34.01	AAAA C
ATOM	2630	CG	GLN	275	49.329	31.274	57.864	1.00	56.40	AAAA C
ATOM	2631	CD	GLN	275	49.275	30.190	56.812	1.00	66.46	AAAA C
ATOM	2632	OE1	GLN	275	49.941	29.151	56.910	1.00	67.24	AAAA O
ATOM	2633	NE2	GLN	275	48.451	30.436	55.799	1.00	78.29	AAAA N
ATOM	2636	C	GLN	275	49.721	33.195	59.720	1.00	35.41	AAAA C
ATOM	2637	O	GLN	275	50.526	33.831	59.064	1.00	35.95	AAAA O
ATOM	2638	N	GLU	276	48.566	33.754	60.056	1.00	41.70	AAAA N
ATOM	2640	CA	GLU	276	48.222	35.080	59.571	1.00	43.96	AAAA C
ATOM	2641	CB	GLU	276	47.387	34.884	58.245	1.00	42.40	AAAA C
ATOM	2642	CG	GLU	276	47.154	36.269	57.650	1.00	53.84	AAAA C
ATOM	2643	CD	GLU	276	48.359	37.198	57.460	1.00	61.37	AAAA C
ATOM	2644	OE1	GLU	276	49.356	36.595	56.943	1.00	67.32	AAAA O
ATOM	2645	OE2	GLU	276	48.242	38.411	57.811	1.00	45.16	AAAA O
ATOM	2646	C	GLU	276	47.444	35.935	60.540	1.00	39.74	AAAA C
ATOM	2647	O	GLU	276	46.769	35.449	61.444	1.00	45.06	AAAA O
ATOM	2648	N	CYS	277	47.495	37.235	60.500	1.00	38.69	AAAA N
ATOM	2650	CA	CYS	277	46.718	38.089	61.332	1.00	46.11	AAAA C
ATOM	2651	C	CYS	277	45.205	37.938	60.994	1.00	52.76	AAAA C
ATOM	2652	O	CYS	277	44.760	37.511	59.936	1.00	49.43	AAAA O
ATOM	2653	CB	CYS	277	47.039	39.537	61.111	1.00	45.56	AAAA C
ATOM	2654	SG	CYS	277	48.629	40.083	61.645	1.00	52.86	AAAA S
ATOM	2655	N	PRO	278	44.380	38.261	61.993	1.00	54.65	AAAA N
ATOM	2656	CD	PRO	278	44.921	38.778	63.311	1.00	57.20	AAAA C
ATOM	2657	CA	PRO	278	42.946	38.185	61.899	1.00	55.82	AAAA C
ATOM	2658	CB	PRO	278	42.445	38.635	63.267	1.00	55.61	AAAA C
ATOM	2659	CG	PRO	278	43.605	38.670	64.153	1.00	55.58	AAAA C
ATOM	2660	C	PRO	278	42.487	39.116	60.781	1.00	52.55	AAAA C
ATOM	2661	O	PRO	278	43.003	40.195	60.631	1.00	48.76	AAAA O
ATOM	2662	N	SER	279	41.370	38.845	60.143	1.00	49.35	AAAA N
ATOM	2664	CA	SER	279	40.915	39.720	59.140	1.00	52.03	AAAA C
ATOM	2665	CB	SER	279	39.280	39.572	58.975	1.00	47.62	AAAA C
ATOM	2666	OG	SER	279	39.320	38.778	57.785	1.00	68.16	AAAA O
ATOM	2668	C	SER	279	41.003	41.209	59.173	1.00	55.40	AAAA C
ATOM	2669	O	SER	279	41.220	41.740	58.059	1.00	55.49	AAAA O
ATOM	2670	N	GLY	280	40.779	41.962	60.247	1.00	55.32	AAAA N
ATOM	2672	CA	GLY	280	40.968	43.406	59.868	1.00	48.58	AAAA C
ATOM	2673	C	GLY	280	42.248	43.890	60.479	1.00	55.08	AAAA C
ATOM	2674	O	GLY	280	42.249	45.097	60.772	1.00	56.00	AAAA O
ATOM	2675	N	PHE	281	43.213	42.983	60.742	1.00	55.42	AAAA N
ATOM	2677	CA	PHE	281	44.506	43.411	61.262	1.00	52.94	AAAA C
ATOM	2678	CB	PHE	281	44.938	42.644	62.523	1.00	61.20	AAAA C
ATOM	2679	CG	PHE	281	43.958	42.792	63.637	1.00	53.66	AAAA C
ATOM	2680	CD1	PHE	281	44.142	43.702	64.630	1.00	60.47	AAAA C
ATOM	2681	CD2	PHE	281	42.939	41.992	63.712	1.00	60.09	AAAA C
ATOM	2682	CE1	PHE	281	43.272	43.901	65.678	1.00	64.71	AAAA C
ATOM	2683	CE2	PHE	281	41.931	42.162	64.756	1.00	63.19	AAAA C
ATOM	2684	CZ	PHE	281	42.141	43.115	65.744	1.00	58.80	AAAA C

Figure 1A-25

ATOM	2685	N	PHE	281	45.630	43.217	60.249	1.00	48.00	AAAA N
ATOM	2686	O	PHE	281	45.738	42.395	59.327	1.00	38.84	AAAA O
ATOM	2687	H	ILE	282	46.670	43.990	60.557	1.00	49.55	AAAA H
ATOM	2689	CA	ILE	282	47.937	43.984	59.748	1.00	45.00	AAAA C
ATOM	2690	CB	ILE	282	47.945	45.188	58.799	1.00	39.25	AAAA C
ATOM	2691	CG2	ILE	282	48.041	46.494	59.507	1.00	24.60	AAAA C
ATOM	2692	CG1	ILE	282	49.092	45.022	57.795	1.00	38.71	AAAA C
ATOM	2693	CD1	ILE	282	49.194	46.043	56.669	1.00	33.38	AAAA C
ATOM	2694	C	ILE	282	49.081	43.889	60.673	1.00	44.30	AAAA C
ATOM	2695	O	ILE	282	49.079	44.447	61.759	1.00	48.49	AAAA O
ATOM	2696	N	ARG	283	50.126	43.153	60.298	1.00	48.68	AAAA N
ATOM	2698	CA	ARG	283	51.396	43.094	61.048	1.00	39.30	AAAA C
ATOM	2699	CB	ARG	283	52.300	42.200	60.296	1.00	41.10	AAAA C
ATOM	2700	CG	ARG	283	52.295	40.696	60.515	1.00	29.19	AAAA C
ATOM	2701	CD	ARG	283	53.078	39.986	59.451	1.00	29.85	AAAA C
ATOM	2702	NE	ARG	283	52.823	38.545	59.404	1.00	29.39	AAAA N
ATOM	2704	CZ	ARG	283	51.862	38.024	58.646	1.00	37.61	AAAA C
ATOM	2705	NH1	ARG	283	51.065	38.846	57.944	1.00	31.41	AAAA N
ATOM	2708	NH2	ARG	283	51.651	36.722	58.696	1.00	31.97	AAAA N
ATOM	2711	C	ARG	283	51.945	44.498	61.190	1.00	42.27	AAAA C
ATOM	2712	O	ARG	283	51.931	45.228	60.173	1.00	43.42	AAAA O
ATOM	2713	N	ASN	284	52.362	44.886	62.422	1.00	39.49	AAAA N
ATOM	2715	CA	ASN	284	52.733	46.311	62.574	1.00	42.07	AAAA C
ATOM	2721	C	ASN	284	54.078	46.656	61.929	1.00	41.64	AAAA C
ATOM	2722	O	ASN	284	54.431	47.798	61.742	1.00	39.01	AAAA O
ATOM	2716	CB	ASN	284	52.734	46.760	64.032	1.00	37.33	AAAA C
ATOM	2717	CG	ASN	284	53.917	46.028	64.611	1.00	50.21	AAAA C
ATOM	2718	OD1	ASN	284	54.609	45.104	64.192	1.00	44.30	AAAA O
ATOM	2719	ND2	ASN	284	54.323	46.432	65.842	1.00	42.46	AAAA N
ATOM	2723	N	GLY	285	54.931	45.699	61.562	1.00	40.10	AAAA N
ATOM	2725	CA	GLY	285	55.971	45.815	60.593	1.00	26.91	AAAA C
ATOM	2726	C	GLY	285	56.091	44.468	59.848	1.00	33.12	AAAA C
ATOM	2727	O	GLY	285	55.584	43.331	60.187	1.00	29.51	AAAA O
ATOM	2728	N	SER	286	56.915	44.619	58.766	1.00	26.53	AAAA N
ATOM	2730	CA	SER	286	57.109	43.385	57.975	1.00	32.67	AAAA C
ATOM	2731	CB	SER	286	57.944	43.681	56.757	1.00	33.19	AAAA C
ATOM	2732	OG	SER	286	58.283	42.480	56.014	1.00	31.95	AAAA O
ATOM	2734	C	SER	286	57.750	42.310	58.836	1.00	34.57	AAAA C
ATOM	2735	O	SER	286	58.700	42.495	59.607	1.00	44.29	AAAA O
ATOM	2736	N	GLN	287	57.227	41.148	58.940	1.00	34.45	AAAA N
ATOM	2738	CA	GLN	287	57.738	40.005	59.634	1.00	35.25	AAAA C
ATOM	2739	CB	GLN	287	59.139	39.610	59.083	1.00	27.97	AAAA C
ATOM	2740	CG	GLN	287	59.037	39.234	57.664	1.00	26.61	AAAA C
ATOM	2741	CD	GLN	287	58.539	37.963	57.130	1.00	21.25	AAAA C
ATOM	2742	OE1	GLN	287	58.192	37.023	57.845	1.00	28.18	AAAA O
ATOM	2743	NE2	GLN	287	58.492	37.838	55.782	1.00	27.55	AAAA N
ATOM	2746	C	GLN	287	57.773	40.286	61.111	1.00	30.25	AAAA C
ATOM	2747	O	GLN	287	58.163	39.415	61.908	1.00	32.78	AAAA O
ATOM	2748	N	SER	288	57.021	41.217	61.624	1.00	32.49	AAAA N
ATOM	2750	CA	SER	288	56.696	41.322	63.043	1.00	28.98	AAAA C
ATOM	2751	CB	SER	288	56.024	42.675	63.313	1.00	35.79	AAAA C
ATOM	2752	OG	SER	288	55.639	42.612	64.701	1.00	36.61	AAAA O
ATOM	2754	C	SER	288	55.665	40.285	63.442	1.00	28.96	AAAA C
ATOM	2755	O	SER	288	54.993	39.776	62.553	1.00	31.16	AAAA O
ATOM	2756	N	MET	289	55.774	39.720	64.621	1.00	32.51	AAAA N
ATOM	2758	CA	MET	289	54.875	38.697	65.105	1.00	34.53	AAAA C
ATOM	2759	CB	MET	289	55.507	37.823	66.153	1.00	30.31	AAAA C
ATOM	2760	CG	MET	289	56.571	36.872	65.680	1.00	40.50	AAAA C
ATOM	2761	SD	MET	289	56.977	35.623	66.881	1.00	31.65	AAAA S
ATOM	2762	CE	MET	289	55.745	34.315	66.508	1.00	30.47	AAAA C
ATOM	2763	C	MET	289	53.557	39.286	65.703	1.00	35.55	AAAA C
ATOM	2764	O	MET	289	52.630	38.512	66.014	1.00	38.37	AAAA O
ATOM	2765	N	TYR	290	53.380	40.565	65.742	1.00	29.54	AAAA N
ATOM	2767	CA	TYR	290	52.363	41.358	66.297	1.00	38.81	AAAA C
ATOM	2768	CB	TYR	290	52.947	42.589	67.042	1.00	36.72	AAAA C
ATOM	2769	CG	TYR	290	53.570	42.184	68.351	1.00	41.94	AAAA C
ATOM	2770	CD1	TYR	290	54.932	41.780	68.350	1.00	37.79	AAAA C
ATOM	2771	CE1	TYR	290	55.548	41.368	69.503	1.00	32.60	AAAA C
ATOM	2772	CD2	TYR	290	52.987	42.157	69.570	1.00	39.93	AAAA C
ATOM	2773	CE2	TYR	290	53.501	41.750	70.748	1.00	36.16	AAAA C
ATOM	2774	CZ	TYR	290	54.922	41.356	70.693	1.00	38.85	AAAA C
ATOM	2775	OH	TYR	290	55.581	40.923	71.751	1.00	43.41	AAAA O
ATOM	2777	C	TYR	290	51.361	41.955	65.270	1.00	45.54	AAAA C
ATOM	2778	O	TYR	290	51.733	42.529	64.227	1.00	47.10	AAAA O
ATOM	2779	N	CYS	291	50.071	41.698	65.537	1.00	44.68	AAAA N
ATOM	2781	CA	CYS	291	49.017	42.205	64.685	1.00	47.20	AAAA C
ATOM	2782	C	CYS	291	48.295	43.434	65.194	1.00	46.06	AAAA C
ATOM	2783	O	CYS	291	47.992	43.550	66.343	1.00	49.45	AAAA O
ATOM	2784	CB	CYS	291	47.973	41.103	64.483	1.00	43.44	AAAA C
ATOM	2785	SG	CYS	291	48.766	39.715	63.683	1.00	45.49	AAAA S
ATOM	2786	N	ILE	292	48.136	44.453	64.365	1.00	46.82	AAAA N
ATOM	2788	CA	ILE	292	47.399	45.651	64.755	1.00	50.64	AAAA C
ATOM	2789	CB	ILE	292	48.267	46.932	64.779	1.00	39.19	AAAA C
ATOM	2790	CG2	ILE	292	49.291	46.885	65.861	1.00	44.39	AAAA C
ATOM	2791	CG1	ILE	292	48.929	47.095	63.402	1.00	44.25	AAAA C

Figure 1A-26

ATOM	2792	CD1	ILE	292	49.234	48.564	63.184	1.00	32.89	AAAA C
ATOM	2793	C	ILE	292	46.240	46.003	63.906	1.00	50.01	AAAA C
ATOM	2794	O	ILE	292	46.165	45.526	62.670	1.00	46.64	AAAA O
ATOM	2795	N	PRO	293	45.150	46.507	64.385	1.00	51.86	AAAA N
ATOM	2796	CD	PRO	293	45.009	46.804	65.839	1.00	51.05	AAAA C
ATOM	2797	CA	PRO	293	43.958	46.930	63.675	1.00	51.40	AAAA C
ATOM	2798	CB	PRO	293	43.176	47.784	64.681	1.00	49.00	AAAA C
ATOM	2799	CG	PRO	293	43.533	47.112	65.951	1.00	53.73	AAAA C
ATOM	2800	C	PRO	293	44.253	47.870	62.525	1.00	51.68	AAAA C
ATOM	2801	O	PRO	293	45.053	48.780	62.737	1.00	51.92	AAAA O
ATOM	2802	N	CYS	294	43.607	47.621	61.408	1.00	50.66	AAAA N
ATOM	2804	CA	CYS	294	43.811	48.464	60.254	1.00	57.90	AAAA C
ATOM	2805	C	CYS	294	43.219	49.848	60.345	1.00	59.59	AAAA C
ATOM	2806	O	CYS	294	43.744	50.814	59.785	1.00	60.87	AAAA O
ATOM	2807	CB	CYS	294	43.229	47.686	59.046	1.00	57.59	AAAA C
ATOM	2808	SG	CYS	294	44.498	46.460	58.563	1.00	51.12	AAAA S
ATOM	2809	N	ALA	295	42.009	50.031	60.954	1.00	65.87	AAAA N
ATOM	2811	CA	ALA	295	41.391	51.386	60.804	1.00	71.19	AAAA C
ATOM	2812	CB	ALA	295	42.311	52.459	61.393	1.00	63.82	AAAA C
ATOM	2813	C	ALA	295	40.971	51.770	59.379	1.00	69.17	AAAA C
ATOM	2814	O	ALA	295	41.421	52.717	58.760	1.00	64.79	AAAA O
ATOM	2815	N	GLY	296	40.153	50.920	58.775	1.00	71.30	AAAA N
ATOM	2817	CA	GLY	296	39.640	51.049	57.416	1.00	72.66	AAAA C
ATOM	2818	C	GLY	296	39.895	49.686	56.769	1.00	74.20	AAAA C
ATOM	2819	O	GLY	296	40.408	48.819	57.490	1.00	75.04	AAAA O
ATOM	2820	N	PRO	297	39.561	49.540	55.497	1.00	71.98	AAAA N
ATOM	2821	CD	PRO	297	38.928	50.561	54.637	1.00	72.15	AAAA C
ATOM	2822	CA	PRO	297	39.958	48.344	54.777	1.00	68.23	AAAA C
ATOM	2823	CB	PRO	297	39.488	48.603	53.369	1.00	72.57	AAAA C
ATOM	2824	CG	PRO	297	38.470	49.697	53.490	1.00	74.01	AAAA C
ATOM	2825	C	PRO	297	41.480	48.306	54.860	1.00	65.79	AAAA C
ATOM	2826	O	PRO	297	42.147	49.323	54.997	1.00	62.72	AAAA O
ATOM	2827	N	CYS	298	42.039	47.135	55.073	1.00	63.85	AAAA N
ATOM	2829	CA	CYS	298	43.464	46.953	55.248	1.00	54.47	AAAA C
ATOM	2830	C	CYS	298	44.109	47.303	53.908	1.00	54.56	AAAA C
ATOM	2831	O	CYS	298	43.621	47.030	52.820	1.00	54.83	AAAA O
ATOM	2932	CB	CYS	298	43.665	45.544	55.669	1.00	47.65	AAAA C
ATOM	2833	SG	CYS	298	43.501	45.115	57.371	1.00	46.12	AAAA S
ATOM	2834	N	PRO	299	45.310	47.876	53.967	1.00	49.83	AAAA N
ATOM	2835	CD	PRO	299	46.087	48.168	55.194	1.00	48.14	AAAA C
ATOM	2836	CA	PRO	299	46.055	48.212	52.787	1.00	43.67	AAAA C
ATOM	2837	CB	PRO	299	47.267	48.965	53.281	1.00	44.08	AAAA C
ATOM	2838	CG	PRO	299	47.454	48.361	54.628	1.00	51.38	AAAA C
ATOM	2839	C	PRO	299	46.341	46.969	52.010	1.00	38.86	AAAA C
ATOM	2840	O	PRO	299	46.372	45.874	52.546	1.00	42.85	AAAA O
ATOM	2841	N	LYS	300	46.310	47.073	50.712	1.00	38.30	AAAA N
ATOM	2843	CA	LYS	300	46.484	45.958	49.812	1.00	42.62	AAAA C
ATOM	2844	CB	LYS	300	45.176	45.226	49.595	1.00	34.28	AAAA C
ATOM	2845	CG	LYS	300	45.346	43.901	48.920	1.00	41.45	AAAA C
ATOM	2846	CD	LYS	300	44.013	45.413	49.378	1.00	48.31	AAAA C
ATOM	2847	CE	LYS	300	44.388	42.027	47.797	1.00	48.57	AAAA C
ATOM	2848	NZ	LYS	300	43.662	42.031	46.478	1.00	63.79	AAAA N
ATOM	2852	C	LYS	300	46.964	46.479	48.432	1.00	48.72	AAAA C
ATOM	2853	O	LYS	300	46.413	47.383	47.776	1.00	46.09	AAAA O
ATOM	2854	N	VAL	301	48.150	45.984	48.054	1.00	48.15	AAAA N
ATOM	2856	CA	VAL	301	48.802	46.462	46.871	1.00	44.52	AAAA C
ATOM	2857	CB	VAL	301	50.292	46.729	47.074	1.00	51.52	AAAA C
ATOM	2858	CG1	VAL	301	51.008	47.200	45.796	1.00	43.07	AAAA C
ATOM	2859	CG2	VAL	301	50.495	47.794	45.141	1.00	49.50	AAAA C
ATOM	2860	C	VAL	301	48.526	45.410	45.837	1.00	44.59	AAAA C
ATOM	2861	O	VAL	301	48.913	44.291	46.060	1.00	43.70	AAAA O
ATOM	2862	N	CYS	302	47.919	45.816	44.718	1.00	47.98	AAAA N
ATOM	2864	CA	CYS	302	47.645	44.735	43.739	1.00	55.19	AAAA C
ATOM	2865	C	CYS	302	48.594	44.968	42.583	1.00	57.64	AAAA C
ATOM	2866	O	CYS	302	48.852	46.152	42.313	1.00	60.23	AAAA O
ATOM	2867	CB	CYS	302	46.156	44.630	43.330	1.00	68.30	AAAA C
ATOM	2868	SG	CYS	302	45.070	44.360	44.751	1.00	70.31	AAAA S
ATOM	2869	N	GLU	303	49.184	43.921	42.075	1.00	58.15	AAAA N
ATOM	2871	CA	GLU	303	50.174	43.932	41.034	1.00	62.85	AAAA C
ATOM	2872	CB	GLU	303	51.603	44.006	41.595	1.00	67.85	AAAA C
ATOM	2873	CG	GLU	303	51.760	43.487	43.014	0.01	67.46	AAAA C
ATOM	2874	CD	GLU	303	51.999	41.992	43.097	0.01	67.91	AAAA C
ATOM	2875	OE1	GLU	303	53.011	41.514	42.561	0.01	67.67	AAAA O
ATOM	2876	OE2	GLU	303	51.147	41.290	43.697	0.01	67.65	AAAA O
ATOM	2877	C	GLU	303	50.096	42.662	40.194	1.00	64.12	AAAA C
ATOM	2878	O	GLU	303	50.162	41.562	40.708	1.00	65.08	AAAA O
ATOM	2879	N	GLU	304	49.867	42.794	38.904	1.00	67.37	AAAA N
ATOM	2881	CA	GLU	304	49.672	41.583	38.094	1.00	74.63	AAAA C
ATOM	2882	CB	GLU	304	48.295	41.596	37.458	1.00	71.71	AAAA C
ATOM	2883	CG	GLU	304	47.339	42.663	38.031	1.00	84.54	AAAA C
ATOM	2884	CD	GLU	304	45.930	42.152	38.195	1.00	87.56	AAAA C
ATOM	2885	OE1	GLU	304	45.438	41.571	37.179	1.00	89.13	AAAA O
ATOM	2886	OE2	GLU	304	45.249	42.269	39.233	1.00	93.19	AAAA O
ATOM	2887	C	GLU	304	50.966	41.307	37.139	1.00	76.19	AAAA C
ATOM	2888	O	GLU	304	51.911	41.962	37.217	1.00	74.78	AAAA O

Figure 1A-27

ATOM	2989	N	GLU	305	50.899	40.126	36.546	1.00	77.31	AAAA N
ATOM	2991	CA	GLU	305	51.932	39.656	35.674	1.00	75.99	AAAA C
ATOM	2992	CB	GLU	305	51.467	38.380	34.979	1.00	79.95	AAAA C
ATOM	2993	CG	GLU	305	52.307	37.937	33.807	1.00	87.28	AAAA C
ATOM	2994	CD	GLU	305	51.758	36.801	32.986	0.01	85.39	AAAA C
ATOM	2995	OE1	GLU	305	50.762	36.234	33.252	0.01	83.66	AAAA O
ATOM	2996	OE2	GLU	305	52.319	36.700	31.789	0.01	83.73	AAAA O
ATOM	2997	C	GLU	305	52.276	40.737	34.666	1.00	75.97	AAAA C
ATOM	2998	O	GLU	305	53.381	41.268	34.613	1.00	76.54	AAAA O
ATOM	2999	N	LYS	306	51.291	41.191	33.885	1.00	78.22	AAAA N
ATOM	3001	CA	LYS	306	51.479	42.329	33.004	1.00	75.99	AAAA C
ATOM	3002	CB	LYS	306	50.467	42.253	31.855	1.00	79.78	AAAA C
ATOM	3003	CG	LYS	306	51.208	42.227	30.527	1.00	94.52	AAAA C
ATOM	3004	CD	LYS	306	50.313	42.191	29.314	1.00	92.78	AAAA C
ATOM	3005	CE	LYS	306	50.740	43.227	28.261	1.00	97.10	AAAA C
ATOM	3006	NZ	LYS	306	50.938	44.554	28.929	1.00	84.97	AAAA N
ATOM	3010	C	LYS	306	51.381	43.669	33.703	1.00	73.85	AAAA C
ATOM	3011	O	LYS	306	50.703	43.862	34.710	1.00	76.08	AAAA O
ATOM	3012	N	LYS	307	52.000	44.700	33.180	1.00	71.15	AAAA N
ATOM	3014	CA	LYS	307	51.934	46.053	33.692	1.00	69.45	AAAA C
ATOM	3015	CB	LYS	307	53.022	46.993	33.008	1.00	79.64	AAAA C
ATOM	3016	CG	LYS	307	54.419	46.837	33.564	1.00	78.88	AAAA C
ATOM	3017	CD	LYS	307	55.257	48.084	33.374	1.00	85.84	AAAA C
ATOM	3018	CE	LYS	307	55.708	48.215	31.924	1.00	97.07	AAAA C
ATOM	3019	NZ	LYS	307	54.649	48.840	31.067	1.00	97.80	AAAA N
ATOM	3023	C	LYS	307	50.562	46.716	33.525	1.00	67.97	AAAA C
ATOM	3024	O	LYS	307	50.019	47.369	34.431	1.00	64.46	AAAA O
ATOM	3025	N	THR	308	49.979	46.661	32.323	1.00	65.84	AAAA N
ATOM	3027	CA	THR	308	48.709	47.319	32.091	1.00	64.56	AAAA C
ATOM	3028	CB	THR	308	48.714	47.977	30.711	1.00	59.91	AAAA C
ATOM	3029	OG1	THR	308	49.834	48.843	30.577	1.00	61.97	AAAA O
ATOM	3031	CG2	THR	308	47.392	48.742	30.561	1.00	63.64	AAAA C
ATOM	3032	C	THR	308	47.514	46.379	32.234	1.00	61.82	AAAA C
ATOM	3033	O	THR	308	47.412	45.415	31.477	1.00	62.05	AAAA O
ATOM	3034	N	LYS	309	46.675	46.719	33.211	1.00	55.66	AAAA N
ATOM	3036	CA	LYS	309	45.456	45.926	33.445	1.00	54.67	AAAA C
ATOM	3037	CB	LYS	309	45.043	45.880	34.904	1.00	56.82	AAAA C
ATOM	3038	CG	LYS	309	43.601	45.541	35.223	1.00	57.50	AAAA C
ATOM	3039	CD	LYS	309	43.390	44.039	35.086	1.00	59.50	AAAA C
ATOM	3040	CE	LYS	309	42.703	43.448	36.324	1.00	57.31	AAAA C
ATOM	3041	NZ	LYS	309	42.758	41.954	36.236	1.00	57.22	AAAA N
ATOM	3045	C	LYS	309	44.391	46.570	32.548	1.00	51.21	AAAA C
ATOM	3046	O	LYS	309	44.074	47.763	32.680	1.00	47.23	AAAA O
ATOM	3047	N	THR	310	43.895	45.772	31.610	1.00	47.67	AAAA N
ATOM	3049	CA	THR	310	42.862	46.328	30.733	1.00	51.89	AAAA C
ATOM	3050	CB	THR	310	43.161	46.015	29.266	1.00	54.81	AAAA C
ATOM	3051	OG1	THR	310	41.909	45.710	28.635	1.00	66.29	AAAA O
ATOM	3053	CG2	THR	310	44.032	44.791	29.139	1.00	55.18	AAAA C
ATOM	3054	C	THR	310	41.468	45.841	31.117	1.00	51.15	AAAA C
ATOM	3055	O	THR	310	41.162	44.680	30.991	1.00	49.27	AAAA O
ATOM	3056	N	ILE	311	40.684	46.706	31.732	1.00	50.18	AAAA N
ATOM	3058	CA	ILE	311	39.363	46.453	32.276	1.00	48.67	AAAA C
ATOM	3059	CB	ILE	311	39.120	47.396	33.462	1.00	49.27	AAAA C
ATOM	3060	CG2	ILE	311	37.655	47.596	33.799	1.00	50.72	AAAA C
ATOM	3061	CG1	ILE	311	39.896	46.930	34.699	1.00	41.34	AAAA C
ATOM	3062	CD1	ILE	311	39.847	48.073	35.739	1.00	52.22	AAAA C
ATOM	3063	C	ILE	311	38.334	46.729	31.186	1.00	45.37	AAAA C
ATOM	3064	O	ILE	311	38.132	47.875	30.758	1.00	37.14	AAAA O
ATOM	3065	N	ASP	312	37.871	45.678	30.524	1.00	50.10	AAAA N
ATOM	3067	CA	ASP	312	36.991	45.842	29.377	1.00	56.35	AAAA C
ATOM	3068	CB	ASP	312	37.546	45.152	28.128	1.00	59.45	AAAA C
ATOM	3069	CG	ASP	312	37.761	43.671	28.382	1.00	65.64	AAAA C
ATOM	3070	OD1	ASP	312	38.525	43.034	27.636	1.00	72.60	AAAA O
ATOM	3071	OD2	ASP	312	37.154	43.176	29.348	1.00	66.86	AAAA O
ATOM	3072	C	ASP	312	35.589	45.337	29.693	1.00	59.39	AAAA C
ATOM	3073	O	ASP	312	34.729	45.607	28.867	1.00	61.00	AAAA O
ATOM	3074	N	SER	313	35.278	45.290	30.976	1.00	61.17	AAAA N
ATOM	3076	CA	SER	313	34.053	44.683	31.459	1.00	55.73	AAAA C
ATOM	3077	CB	SER	313	34.121	45.201	31.093	1.00	48.22	AAAA C
ATOM	3078	OG	SER	313	34.373	42.514	32.282	1.00	57.89	AAAA O
ATOM	3080	C	SER	313	33.998	44.818	32.911	1.00	57.87	AAAA C
ATOM	3081	O	SER	313	34.892	45.506	33.537	1.00	66.17	AAAA O
ATOM	3082	N	VAL	314	33.001	44.205	33.545	1.00	64.35	AAAA N
ATOM	3084	CA	VAL	314	32.849	44.305	35.016	1.00	64.39	AAAA C
ATOM	3085	CB	VAL	314	31.360	44.340	35.343	1.00	69.57	AAAA C
ATOM	3086	CG1	VAL	314	31.024	43.693	36.681	1.00	65.60	AAAA C
ATOM	3087	CG2	VAL	314	30.927	45.823	35.319	1.00	65.27	AAAA C
ATOM	3088	C	VAL	314	33.492	43.088	35.638	1.00	62.65	AAAA C
ATOM	3089	O	VAL	314	34.029	43.141	36.704	1.00	63.92	AAAA O
ATOM	3090	N	THR	315	33.468	42.011	34.878	1.00	61.82	AAAA N
ATOM	3092	CA	THR	315	34.029	40.752	35.284	1.00	63.44	AAAA C
ATOM	3093	CB	THR	315	33.618	39.628	34.314	1.00	65.54	AAAA C
ATOM	3094	OG1	THR	315	32.403	40.004	33.634	1.00	74.05	AAAA O
ATOM	3096	CG2	THR	315	33.339	38.366	35.104	1.00	64.86	AAAA C
ATOM	3097	C	THR	315	35.541	40.871	35.325	1.00	65.62	AAAA C

Figure 1A-28

ATOM	2998	O	THR	315	36.217	40.339	36.206	1.00	66.41	AAAA O
ATOM	2999	N	SER	316	36.971	41.593	34.332	1.00	63.28	AAAA N
ATOM	3001	CA	SER	316	37.500	41.793	34.215	1.00	58.72	AAAA C
ATOM	3002	CB	SER	316	37.795	42.537	32.900	1.00	52.20	AAAA C
ATOM	3003	OG	SER	316	37.298	43.859	32.933	1.00	48.04	AAAA O
ATOM	3005	C	SER	316	38.077	42.573	35.387	1.00	58.91	AAAA C
ATOM	3006	O	SER	316	39.293	42.522	35.529	1.00	59.86	AAAA O
ATOM	3007	N	ALA	317	37.310	43.362	36.111	1.00	55.86	AAAA N
ATOM	3009	CA	ALA	317	37.750	44.184	37.191	1.00	57.17	AAAA C
ATOM	3010	CB	ALA	317	36.853	45.409	37.269	1.00	54.23	AAAA C
ATOM	3011	C	ALA	317	37.689	43.487	38.539	1.00	62.05	AAAA C
ATOM	3012	O	ALA	317	37.702	44.128	39.599	1.00	60.30	AAAA O
ATOM	3013	N	GLN	318	37.361	42.205	38.523	1.00	67.91	AAAA N
ATOM	3015	CA	GLN	318	37.185	41.380	39.713	1.00	70.72	AAAA C
ATOM	3016	CB	GLN	318	36.857	39.956	39.293	1.00	74.48	AAAA C
ATOM	3017	CG	GLN	318	36.624	38.947	40.383	1.00	89.82	AAAA C
ATOM	3018	CD	GLN	318	35.265	39.080	41.048	1.00	92.69	AAAA C
ATOM	3019	OE1	GLN	318	34.256	38.867	40.391	1.00	98.57	AAAA O
ATOM	3020	NE2	GLN	318	35.356	39.509	42.308	1.00	92.51	AAAA N
ATOM	3023	C	GLN	318	38.380	41.413	40.653	1.00	72.63	AAAA C
ATOM	3024	O	GLN	318	38.294	41.855	41.804	1.00	68.92	AAAA O
ATOM	3025	N	MET	319	39.562	41.062	40.153	1.00	75.18	AAAA N
ATOM	3027	CA	MET	319	40.846	41.175	40.826	1.00	71.85	AAAA C
ATOM	3028	CB	MET	319	41.950	40.960	39.772	1.00	82.00	AAAA C
ATOM	3029	CG	MET	319	41.740	39.644	39.050	1.00	91.16	AAAA C
ATOM	3030	SD	MET	319	43.123	38.482	39.185	1.00	106.72	AAAA S
ATOM	3031	CE	MET	319	42.486	37.105	38.231	1.00	97.56	AAAA C
ATOM	3032	C	MET	319	41.118	42.509	41.471	1.00	67.68	AAAA C
ATOM	3033	O	MET	319	41.507	42.541	42.612	1.00	69.73	AAAA O
ATOM	3034	N	LEU	320	40.749	43.639	40.887	1.00	62.95	AAAA N
ATOM	3036	CA	LEU	320	40.997	44.938	41.531	1.00	62.31	AAAA C
ATOM	3037	CB	LEU	320	40.440	46.085	40.623	1.00	54.93	AAAA C
ATOM	3038	CG	LEU	320	41.091	46.163	39.238	1.00	53.48	AAAA C
ATOM	3039	CD1	LEU	320	41.005	47.552	38.692	1.00	51.31	AAAA C
ATOM	3040	CD2	LEU	320	42.557	45.709	39.403	1.00	58.43	AAAA C
ATOM	3041	C	LEU	320	40.209	45.008	42.881	1.00	60.30	AAAA C
ATOM	3042	O	LEU	320	40.344	45.969	43.661	1.00	58.72	AAAA O
ATOM	3043	N	GLN	321	39.267	44.106	43.112	1.00	59.62	AAAA N
ATOM	3045	CA	GLN	321	38.482	44.128	44.343	1.00	63.50	AAAA C
ATOM	3046	CB	GLN	321	37.373	43.089	44.250	1.00	62.52	AAAA C
ATOM	3047	CG	GLN	321	36.611	42.854	45.522	1.00	56.83	AAAA C
ATOM	3048	CD	GLN	321	35.337	42.064	45.291	1.00	68.77	AAAA C
ATOM	3049	OE1	GLN	321	35.362	40.969	44.718	1.00	70.37	AAAA O
ATOM	3050	NE2	GLN	321	34.218	42.632	45.764	1.00	63.77	AAAA N
ATOM	3053	C	GLN	321	39.367	44.030	45.594	1.00	60.97	AAAA C
ATOM	3054	O	GLN	321	40.262	43.196	45.782	1.00	57.29	AAAA O
ATOM	3055	N	GLY	322	39.092	44.928	46.546	1.00	57.62	AAAA N
ATOM	3057	CA	GLY	322	39.855	44.928	47.790	1.00	60.63	AAAA C
ATOM	3058	C	GLY	322	41.126	45.773	47.812	1.00	61.78	AAAA C
ATOM	3059	O	GLY	322	41.584	46.198	48.889	1.00	60.16	AAAA O
ATOM	3060	N	CYS	323	41.719	46.224	46.676	1.00	60.03	AAAA N
ATOM	3062	CA	CYS	323	42.938	46.845	46.528	1.00	54.20	AAAA C
ATOM	3063	C	CYS	323	42.924	48.307	46.910	1.00	53.48	AAAA C
ATOM	3064	O	CYS	323	42.105	49.148	46.503	1.00	56.43	AAAA O
ATOM	3065	CB	CYS	323	43.458	46.822	45.096	1.00	53.33	AAAA C
ATOM	3066	SG	CYS	323	43.325	45.222	44.249	1.00	66.22	AAAA S
ATOM	3067	N	THR	324	43.994	48.718	47.580	1.00	49.83	AAAA N
ATOM	3069	CA	THR	324	44.164	50.161	47.811	1.00	52.29	AAAA C
ATOM	3070	CB	THR	324	44.623	50.324	49.264	1.00	52.84	AAAA C
ATOM	3071	OG1	THR	324	45.245	49.087	49.634	1.00	59.82	AAAA O
ATOM	3073	CG2	THR	324	43.430	50.517	50.193	1.00	60.00	AAAA C
ATOM	3074	C	THR	324	45.151	50.802	46.844	1.00	48.91	AAAA C
ATOM	3075	O	THR	324	45.277	52.016	46.719	1.00	46.90	AAAA O
ATOM	3076	N	ILE	325	46.021	49.963	46.254	1.00	46.87	AAAA N
ATOM	3078	CA	ILE	325	47.114	50.511	45.445	1.00	45.10	AAAA C
ATOM	3079	CB	ILE	325	48.473	50.577	46.183	1.00	43.60	AAAA C
ATOM	3080	CG2	ILE	325	49.586	50.905	45.163	1.00	47.47	AAAA C
ATOM	3081	CG1	ILE	325	48.394	51.623	47.294	1.00	34.03	AAAA C
ATOM	3082	CD1	ILE	325	49.595	52.010	48.028	1.00	41.94	AAAA C
ATOM	3083	C	ILE	325	47.265	49.642	44.223	1.00	42.88	AAAA C
ATOM	3084	O	ILE	325	47.406	48.429	44.469	1.00	42.99	AAAA O
ATOM	3085	N	PHE	326	47.170	50.239	43.042	1.00	41.19	AAAA N
ATOM	3087	CA	PHE	326	47.312	49.334	41.880	1.00	42.98	AAAA C
ATOM	3088	CB	PHE	326	46.166	49.437	40.877	1.00	39.15	AAAA C
ATOM	3089	CG	PHE	326	46.403	48.474	39.739	1.00	38.03	AAAA C
ATOM	3090	CD1	PHE	326	46.186	47.125	39.951	1.00	39.68	AAAA C
ATOM	3091	CD2	PHE	326	46.917	48.892	38.525	1.00	37.31	AAAA C
ATOM	3092	CE1	PHE	326	46.447	46.139	39.023	1.00	36.52	AAAA C
ATOM	3093	CE2	PHE	326	47.136	47.919	37.551	1.00	45.74	AAAA C
ATOM	3094	CZ	PHE	326	46.924	46.570	37.787	1.00	39.92	AAAA C
ATOM	3095	C	PHE	326	48.682	49.673	41.280	1.00	48.78	AAAA C
ATOM	3096	O	PHE	326	49.024	50.826	40.966	1.00	51.39	AAAA O
ATOM	3097	N	LYS	327	49.623	48.751	41.379	1.00	50.22	AAAA N
ATOM	3099	CA	LYS	327	50.964	49.963	40.831	1.00	51.49	AAAA C
ATOM	3100	CB	LYS	327	52.050	48.091	41.519	1.00	58.64	AAAA C

Figure 1A-29

ATOM	3101	CG	LYS	327	53.254	48.997	41.991	1.00	59.15	AAAA C
ATOM	3102	CD	LYS	327	54.528	48.257	41.617	1.00	63.49	AAAA C
ATOM	3103	CE	LYS	327	55.400	48.951	40.592	1.00	68.12	AAAA C
ATOM	3104	NZ	LYS	327	56.260	47.889	39.938	1.00	71.97	AAAA N
ATOM	3108	C	LYS	327	50.895	48.464	39.391	1.00	45.70	AAAA C
ATOM	3109	O	LYS	327	50.901	47.245	39.127	1.00	49.55	AAAA O
ATOM	3110	N	GLY	328	50.760	49.397	38.502	1.00	39.68	AAAA N
ATOM	3112	CA	GLY	328	50.647	49.038	37.080	1.00	39.44	AAAA C
ATOM	3113	C	GLY	328	49.845	50.161	36.427	1.00	39.49	AAAA C
ATOM	3114	O	GLY	328	49.858	51.307	36.881	1.00	31.92	AAAA O
ATOM	3115	N	ASN	329	49.286	49.813	35.289	1.00	41.47	AAAA N
ATOM	3117	CA	ASN	329	48.467	50.750	34.543	1.00	45.72	AAAA C
ATOM	3118	CB	ASN	329	49.185	50.942	33.211	1.00	42.50	AAAA C
ATOM	3119	CG	ASN	329	50.624	51.426	33.357	1.00	42.26	AAAA C
ATOM	3120	OD1	ASN	329	50.954	52.331	34.156	1.00	34.77	AAAA O
ATOM	3121	ND2	ASN	329	51.425	50.769	32.530	1.00	30.62	AAAA N
ATOM	3124	C	ASN	329	47.038	50.207	34.357	1.00	50.37	AAAA C
ATOM	3125	O	ASN	329	46.736	49.015	34.119	1.00	50.17	AAAA O
ATOM	3126	N	LEU	330	46.090	51.143	34.413	1.00	47.13	AAAA N
ATOM	3128	CA	LEU	330	44.691	50.860	34.151	1.00	42.53	AAAA C
ATOM	3129	CB	LEU	330	43.751	51.530	35.153	1.00	42.84	AAAA C
ATOM	3130	CG	LEU	330	43.768	50.995	36.598	1.00	38.65	AAAA C
ATOM	3131	CD1	LEU	330	42.864	51.924	37.417	1.00	38.12	AAAA C
ATOM	3132	CD2	LEU	330	43.283	49.565	36.669	1.00	38.74	AAAA C
ATOM	3133	C	LEU	330	44.352	51.377	32.758	1.00	39.10	AAAA C
ATOM	3134	O	LEU	330	44.509	52.545	32.460	1.00	40.71	AAAA O
ATOM	3135	N	LEU	331	43.933	50.516	31.904	1.00	36.10	AAAA N
ATOM	3137	CA	LEU	331	43.367	50.869	30.625	1.00	43.10	AAAA C
ATOM	3138	CB	LEU	331	43.959	49.894	29.585	1.00	42.29	AAAA C
ATOM	3139	CG	LEU	331	43.301	49.960	28.221	1.00	40.89	AAAA C
ATOM	3140	CD1	LEU	331	43.501	51.319	27.627	1.00	46.64	AAAA C
ATOM	3141	CD2	LEU	331	43.844	48.834	27.367	1.00	48.76	AAAA C
ATOM	3142	C	LEU	331	41.872	50.568	30.705	1.00	41.12	AAAA C
ATOM	3143	O	LEU	331	41.562	49.365	30.779	1.00	40.08	AAAA O
ATOM	3144	N	ILE	332	41.029	51.566	30.862	1.00	41.13	AAAA N
ATOM	3146	CA	ILE	332	39.606	51.241	31.044	1.00	36.90	AAAA C
ATOM	3147	CB	ILE	332	38.885	52.085	32.076	1.00	34.77	AAAA C
ATOM	3148	CG2	ILE	332	37.413	51.612	32.195	1.00	34.66	AAAA C
ATOM	3149	CG1	ILE	332	39.550	51.895	33.452	1.00	33.64	AAAA C
ATOM	3150	CD1	ILE	332	39.479	53.152	34.337	1.00	48.21	AAAA C
ATOM	3151	C	ILE	332	38.959	51.367	29.688	1.00	34.03	AAAA C
ATOM	3152	O	ILE	332	38.867	52.489	29.200	1.00	35.89	AAAA O
ATOM	3153	N	ASN	333	38.569	50.273	29.094	1.00	35.25	AAAA N
ATOM	3155	CA	ASN	333	38.014	50.283	27.737	1.00	40.34	AAAA C
ATOM	3156	CB	ASN	333	38.960	49.499	26.797	1.00	50.50	AAAA C
ATOM	3157	CG	ASN	333	38.668	49.493	25.310	1.00	59.29	AAAA C
ATOM	3158	OD1	ASN	333	37.845	48.711	24.784	1.00	64.54	AAAA O
ATOM	3159	ND2	ASN	333	39.290	50.350	24.467	1.00	45.83	AAAA N
ATOM	3162	C	ASN	333	36.666	49.581	27.755	1.00	47.63	AAAA C
ATOM	3163	O	ASN	333	36.462	48.409	27.398	1.00	44.40	AAAA O
ATOM	3164	N	ILE	334	35.644	50.213	28.315	1.00	54.13	AAAA N
ATOM	3166	CA	ILE	334	34.332	49.537	28.460	1.00	59.07	AAAA C
ATOM	3167	CB	ILE	334	33.788	49.826	29.876	1.00	61.98	AAAA C
ATOM	3168	CG2	ILE	334	32.362	49.355	30.047	1.00	54.04	AAAA C
ATOM	3169	CG1	ILE	334	34.737	49.224	30.915	1.00	60.43	AAAA C
ATOM	3170	CD1	ILE	334	34.346	49.687	32.317	1.00	68.57	AAAA C
ATOM	3171	C	ILE	334	33.271	50.032	27.476	1.00	59.45	AAAA C
ATOM	3172	O	ILE	334	32.726	51.136	27.635	1.00	56.22	AAAA O
ATOM	3173	N	ARG	335	32.919	49.181	26.550	1.00	59.69	AAAA N
ATOM	3175	CA	ARG	335	31.910	49.567	25.573	1.00	73.93	AAAA C
ATOM	3176	CB	ARG	335	32.262	48.903	24.240	1.00	74.44	AAAA C
ATOM	3177	CG	ARG	335	33.729	48.932	23.918	1.00	82.97	AAAA C
ATOM	3178	CD	ARG	335	34.102	49.289	22.500	1.00	86.49	AAAA C
ATOM	3179	NE	ARG	335	34.361	48.040	21.777	1.00	89.93	AAAA N
ATOM	3181	CZ	ARG	335	34.011	47.838	20.496	1.00	93.67	AAAA C
ATOM	3182	NH1	ARG	335	33.409	48.852	19.843	1.00	87.24	AAAA N
ATOM	3185	NH2	ARG	335	34.256	46.674	19.877	1.00	75.31	AAAA N
ATOM	3188	C	ARG	335	30.492	49.233	26.021	1.00	81.52	AAAA C
ATOM	3189	O	ARG	335	29.664	50.115	26.239	1.00	84.11	AAAA O
ATOM	3190	N	ALA	336	30.208	47.953	26.234	1.00	87.51	AAAA N
ATOM	3192	CA	ALA	336	28.878	47.484	26.601	1.00	92.40	AAAA C
ATOM	3193	CB	ALA	336	28.835	45.980	26.633	1.00	94.03	AAAA C
ATOM	3194	C	ALA	336	28.479	48.058	27.953	1.00	96.61	AAAA C
ATOM	3195	O	ALA	336	29.316	48.019	28.855	1.00	96.96	AAAA O
ATOM	3196	N	GLY	337	27.298	48.685	28.039	1.00	99.74	AAAA N
ATOM	3198	CA	GLY	337	26.986	49.385	29.272	1.00	103.11	AAAA C
ATOM	3199	C	GLY	337	25.568	49.303	29.763	1.00	105.51	AAAA C
ATOM	3200	O	GLY	337	24.801	50.267	29.596	1.00	106.64	AAAA O
ATOM	3201	N	ASN	338	25.243	48.146	30.346	1.00	105.41	AAAA N
ATOM	3203	CA	ASN	338	23.886	48.017	30.908	1.00	106.92	AAAA C
ATOM	3204	CB	ASN	338	23.714	46.689	31.624	1.00	109.14	AAAA C
ATOM	3205	CG	ASN	338	24.403	45.544	30.928	1.00	112.30	AAAA C
ATOM	3206	OD1	ASN	338	25.598	45.595	30.625	1.00	117.94	AAAA O
ATOM	3207	ND2	ASN	338	23.604	44.508	30.683	1.00	113.72	AAAA N
ATOM	3210	C	ASN	338	23.790	49.160	31.931	1.00	105.84	AAAA C

Figure 1A-30

ATOM	3211	O	ASN	338	29.544	50.345	31.739	1.00	103.97	AAAA O
ATOM	3212	N	ASN	339	24.290	48.762	33.092	1.00	105.47	AAAA N
ATOM	3214	CA	ASN	339	24.529	49.740	34.159	1.00	107.19	AAAA C
ATOM	3215	CB	ASN	339	23.282	49.915	34.945	1.00	109.15	AAAA C
ATOM	3216	CG	ASN	339	22.737	51.351	35.003	1.00	107.52	AAAA C
ATOM	3217	OD1	ASN	339	22.715	51.931	36.089	1.00	107.49	AAAA O
ATOM	3218	ND2	ASN	339	22.441	51.932	33.859	1.00	107.46	AAAA N
ATOM	3221	C	ASN	339	25.697	49.237	35.007	1.00	106.33	AAAA C
ATOM	3222	O	ASN	339	25.520	48.399	35.886	1.00	108.82	AAAA O
ATOM	3223	N	ILE	340	26.897	49.527	34.510	1.00	101.36	AAAA N
ATOM	3225	CA	ILE	340	28.136	49.101	35.138	1.00	97.43	AAAA C
ATOM	3226	CB	ILE	340	29.040	48.354	34.151	1.00	93.63	AAAA C
ATOM	3227	CG2	ILE	340	28.194	47.252	33.499	1.00	99.38	AAAA C
ATOM	3228	CG1	ILE	340	29.726	49.158	33.070	1.00	85.50	AAAA C
ATOM	3229	CD1	ILE	340	28.897	49.634	31.915	1.00	92.53	AAAA C
ATOM	3230	C	ILE	340	28.783	50.357	35.706	1.00	95.32	AAAA C
ATOM	3231	O	ILE	340	29.472	51.099	34.997	1.00	97.86	AAAA O
ATOM	3232	N	ALA	341	28.409	50.739	36.915	1.00	89.89	AAAA N
ATOM	3234	CA	ALA	341	28.892	52.008	37.450	1.00	88.45	AAAA C
ATOM	3235	CB	ALA	341	28.068	53.201	37.006	1.00	84.56	AAAA C
ATOM	3236	C	ALA	341	28.786	51.968	38.970	1.00	85.37	AAAA C
ATOM	3237	O	ALA	341	28.910	52.935	39.690	1.00	86.09	AAAA O
ATOM	3238	N	SER	342	28.204	50.877	39.386	1.00	84.24	AAAA N
ATOM	3240	CA	SER	342	27.910	50.601	40.780	1.00	82.05	AAAA C
ATOM	3241	CB	SER	342	26.426	50.667	41.112	1.00	85.51	AAAA C
ATOM	3242	OG	SER	342	26.145	51.271	42.361	1.00	86.02	AAAA O
ATOM	3244	C	SER	342	28.487	49.196	40.965	1.00	76.62	AAAA C
ATOM	3245	O	SER	342	29.119	48.966	41.964	1.00	71.76	AAAA O
ATOM	3246	N	GLU	343	28.373	48.409	39.905	1.00	76.23	AAAA N
ATOM	3248	CA	GLU	343	29.301	47.109	39.829	1.00	74.59	AAAA C
ATOM	3249	CB	GLU	343	28.595	46.300	38.616	1.00	78.62	AAAA C
ATOM	3250	CG	GLU	343	27.118	46.105	38.316	1.00	85.33	AAAA C
ATOM	3251	CD	GLU	343	26.898	45.121	37.169	1.00	92.76	AAAA C
ATOM	3252	OE1	GLU	343	27.209	43.911	37.310	1.00	96.41	AAAA O
ATOM	3253	OE2	GLU	343	26.423	45.517	36.082	1.00	98.55	AAAA O
ATOM	3254	C	GLU	343	30.525	47.319	39.804	1.00	77.75	AAAA C
ATOM	3255	O	GLU	343	31.273	46.787	40.637	1.00	75.73	AAAA O
ATOM	3256	N	LEU	344	31.022	48.237	38.966	1.00	75.65	AAAA N
ATOM	3258	CA	LEU	344	32.415	48.596	38.839	1.00	72.36	AAAA C
ATOM	3259	CB	LEU	344	32.760	49.697	37.808	1.00	64.33	AAAA C
ATOM	3260	CG	LEU	344	32.687	49.397	36.311	1.00	50.12	AAAA C
ATOM	3261	CD1	LEU	344	33.224	50.577	35.519	1.00	57.00	AAAA C
ATOM	3262	CD2	LEU	344	33.401	48.127	35.905	1.00	51.62	AAAA C
ATOM	3263	C	LEU	344	32.963	49.130	40.174	1.00	69.74	AAAA C
ATOM	3264	O	LEU	344	34.079	48.739	40.551	1.00	69.12	AAAA O
ATOM	3265	N	GLU	345	32.166	49.959	40.822	1.00	63.10	AAAA N
ATOM	3267	CA	GLU	345	32.555	50.591	42.061	1.00	65.42	AAAA C
ATOM	3268	CB	GLU	345	31.592	51.714	42.478	1.00	55.59	AAAA C
ATOM	3269	CG	GLU	345	32.267	52.607	43.486	1.00	68.78	AAAA C
ATOM	3270	CD	GLU	345	31.324	53.374	44.376	1.00	81.31	AAAA C
ATOM	3271	OE1	GLU	345	30.614	54.320	43.976	1.00	85.60	AAAA O
ATOM	3272	OE2	GLU	345	31.237	53.078	45.595	1.00	88.79	AAAA O
ATOM	3273	C	GLU	345	32.706	49.652	43.255	1.00	63.31	AAAA C
ATOM	3274	O	GLU	345	33.501	49.913	44.134	1.00	60.08	AAAA O
ATOM	3275	N	ASN	346	32.151	48.462	43.202	1.00	62.25	AAAA N
ATOM	3277	CA	ASN	346	32.285	47.403	44.173	1.00	63.92	AAAA C
ATOM	3278	CB	ASN	346	31.024	46.498	44.095	1.00	61.66	AAAA C
ATOM	3279	CG	ASN	346	31.110	45.292	45.006	1.00	58.73	AAAA C
ATOM	3280	OD1	ASN	346	31.188	45.352	46.224	1.00	69.11	AAAA O
ATOM	3281	ND2	ASN	346	31.155	44.092	44.444	1.00	51.10	AAAA N
ATOM	3284	C	ASN	346	33.532	46.580	43.870	1.00	63.71	AAAA C
ATOM	3285	O	ASN	346	33.636	45.336	43.905	1.00	65.65	AAAA O
ATOM	3286	N	PHE	347	34.419	47.173	43.066	1.00	63.23	AAAA N
ATOM	3288	CA	PHE	347	35.540	46.411	42.506	1.00	61.39	AAAA C
ATOM	3289	CB	PHE	347	35.123	45.854	41.170	1.00	61.38	AAAA C
ATOM	3290	CG	PHE	347	34.457	44.534	41.142	1.00	65.57	AAAA C
ATOM	3291	CD1	PHE	347	33.090	44.438	40.982	1.00	75.25	AAAA C
ATOM	3292	CD2	PHE	347	35.148	43.351	41.267	1.00	77.15	AAAA C
ATOM	3293	CE1	PHE	347	32.425	43.224	40.951	1.00	75.55	AAAA C
ATOM	3294	CE2	PHE	347	34.512	42.130	41.249	1.00	72.86	AAAA C
ATOM	3295	CZ	PHE	347	33.152	42.051	41.095	1.00	72.74	AAAA C
ATOM	3296	C	PHE	347	36.712	47.375	42.440	1.00	57.70	AAAA C
ATOM	3297	O	PHE	347	37.770	46.820	42.354	1.00	59.92	AAAA O
ATOM	3298	N	MET	348	36.482	48.676	42.319	1.00	50.56	AAAA N
ATOM	3300	CA	MET	348	37.500	49.630	41.964	1.00	42.86	AAAA C
ATOM	3301	CB	MET	348	37.402	50.096	40.493	1.00	31.72	AAAA C
ATOM	3302	CG	MET	348	37.426	48.933	39.471	1.00	33.42	AAAA C
ATOM	3303	SD	MET	348	37.566	49.448	37.732	1.00	44.79	AAAA S
ATOM	3304	CE	MET	348	38.408	50.999	37.791	1.00	59.57	AAAA C
ATOM	3305	C	MET	348	37.368	50.831	42.867	1.00	45.88	AAAA C
ATOM	3306	O	MET	348	38.210	51.772	42.901	1.00	43.33	AAAA O
ATOM	3307	N	GLY	349	36.296	50.793	43.683	1.00	45.30	AAAA N
ATOM	3309	CA	GLY	349	35.990	51.965	44.504	1.00	49.19	AAAA C
ATOM	3310	C	GLY	349	36.980	52.189	45.620	1.00	52.77	AAAA C
ATOM	3311	O	GLY	349	37.933	53.299	46.156	1.00	53.43	AAAA O

Figure 1A-31

ATOM	3312	N	LEU	350	37.791	51.159	45.925	1.00	56.17	AAAA N
ATOM	3314	CA	LEU	350	39.735	51.256	47.621	1.00	58.04	AAAA C
ATOM	3315	CB	LEU	350	38.873	49.949	47.834	1.00	49.00	AAAA C
ATOM	3316	CG	LEU	350	37.971	50.020	49.031	1.00	50.79	AAAA C
ATOM	3317	CD1	LEU	350	37.705	48.680	49.700	1.00	52.92	AAAA C
ATOM	3318	CD2	LEU	350	38.247	51.106	50.038	1.00	56.11	AAAA C
ATOM	3319	C	LEU	350	40.144	51.727	46.685	1.00	61.34	AAAA C
ATOM	3320	O	LEU	350	40.931	51.962	47.619	1.00	63.52	AAAA O
ATOM	3321	N	ILE	351	40.446	51.677	45.372	1.00	57.89	AAAA N
ATOM	3323	CA	ILE	351	41.729	52.098	44.873	1.00	48.69	AAAA C
ATOM	3324	CB	ILE	351	41.914	51.912	43.352	1.00	48.19	AAAA C
ATOM	3325	CG2	ILE	351	43.121	52.416	42.757	1.00	49.01	AAAA C
ATOM	3326	CG1	ILE	351	41.535	50.418	43.059	1.00	36.87	AAAA C
ATOM	3327	CD1	ILE	351	41.172	50.351	41.581	1.00	35.46	AAAA C
ATOM	3328	C	ILE	351	42.031	53.533	45.178	1.00	46.80	AAAA C
ATOM	3329	O	ILE	351	41.367	54.358	44.626	1.00	42.87	AAAA O
ATOM	3330	N	GLU	352	45.002	53.866	46.019	1.00	50.61	AAAA N
ATOM	3332	CA	GLU	352	43.381	55.241	46.248	1.00	51.20	AAAA C
ATOM	3333	CB	GLU	352	43.907	55.353	47.678	1.00	52.12	AAAA C
ATOM	3334	CG	GLU	352	42.912	55.769	48.735	1.00	65.55	AAAA C
ATOM	3335	CD	GLU	352	43.034	54.834	49.947	1.00	71.49	AAAA C
ATOM	3336	OE1	GLU	352	43.881	55.244	50.765	1.00	66.09	AAAA O
ATOM	3337	OE2	GLU	352	42.330	53.799	50.009	1.00	76.07	AAAA O
ATOM	3338	C	GLU	352	44.502	55.751	45.314	1.00	47.43	AAAA C
ATOM	3339	O	GLU	352	44.798	56.951	45.182	1.00	40.38	AAAA O
ATOM	3340	N	VAL	353	45.342	54.838	44.852	1.00	43.54	AAAA N
ATOM	3342	CA	VAL	353	46.512	55.236	44.078	1.00	43.72	AAAA C
ATOM	3343	CB	VAL	353	47.759	55.540	44.911	1.00	45.01	AAAA C
ATOM	3344	CG1	VAL	353	47.766	55.261	46.387	1.00	30.84	AAAA C
ATOM	3345	CG2	VAL	353	48.988	54.844	44.319	1.00	42.55	AAAA C
ATOM	3346	C	VAL	353	46.823	54.233	42.957	1.00	41.41	AAAA C
ATOM	3347	O	VAL	353	46.843	53.003	43.172	1.00	39.19	AAAA O
ATOM	3348	N	VAL	354	47.074	54.855	41.816	1.00	36.31	AAAA N
ATOM	3350	CA	VAL	354	47.586	54.092	40.651	1.00	43.97	AAAA C
ATOM	3351	CB	VAL	354	46.725	54.390	39.407	1.00	40.86	AAAA C
ATOM	3352	CG1	VAL	354	47.347	53.896	38.125	1.00	36.72	AAAA C
ATOM	3353	CG2	VAL	354	45.293	53.849	39.679	1.00	35.35	AAAA C
ATOM	3354	C	VAL	354	49.043	54.510	40.388	1.00	44.56	AAAA C
ATOM	3355	O	VAL	354	49.366	55.718	40.288	1.00	43.32	AAAA O
ATOM	3356	N	THR	355	49.972	53.561	40.431	1.00	43.83	AAAA N
ATOM	3358	CA	THR	355	51.392	53.914	40.284	1.00	44.85	AAAA C
ATOM	3359	CB	THR	355	52.374	52.799	40.653	1.00	42.40	AAAA C
ATOM	3360	OG1	THR	355	52.273	51.744	39.695	1.00	45.30	AAAA O
ATOM	3362	CG2	THR	355	52.210	52.194	42.039	1.00	38.13	AAAA C
ATOM	3363	C	THR	355	51.746	54.339	38.851	1.00	43.84	AAAA C
ATOM	3364	O	THR	355	52.463	55.334	38.697	1.00	44.26	AAAA O
ATOM	3365	N	GLY	356	51.127	53.704	37.870	1.00	41.16	AAAA N
ATOM	3367	CA	GLY	356	51.358	54.073	36.470	1.00	37.91	AAAA C
ATOM	3368	C	GLY	356	50.505	55.204	35.955	1.00	38.07	AAAA C
ATOM	3369	O	GLY	356	50.364	56.261	36.615	1.00	34.65	AAAA O
ATOM	3370	N	TYR	357	49.910	55.004	34.806	1.00	38.47	AAAA N
ATOM	3372	CA	TYR	357	48.982	55.973	34.205	1.00	38.03	AAAA C
ATOM	3373	CB	TYR	357	49.567	56.343	32.806	1.00	31.44	AAAA C
ATOM	3374	CG	TYR	357	49.473	55.219	31.812	1.00	33.04	AAAA C
ATOM	3375	CD1	TYR	357	48.333	54.842	31.077	1.00	32.86	AAAA C
ATOM	3376	CE1	TYR	357	48.352	53.779	30.175	1.00	32.83	AAAA C
ATOM	3377	CD2	TYR	357	50.639	54.465	31.606	1.00	34.28	AAAA C
ATOM	3378	CE2	TYR	357	50.706	53.402	30.720	1.00	32.51	AAAA C
ATOM	3379	CZ	TYR	357	49.552	53.068	30.007	1.00	37.26	AAAA C
ATOM	3380	OH	TYR	357	49.726	51.997	29.166	1.00	35.85	AAAA O
ATOM	3382	C	TYR	357	47.582	55.368	34.150	1.00	38.55	AAAA C
ATOM	3383	O	TYR	357	47.458	54.127	34.088	1.00	36.11	AAAA O
ATOM	3384	N	VAL	358	46.593	56.216	33.814	1.00	40.98	AAAA N
ATOM	3386	CA	VAL	358	45.197	55.798	33.639	1.00	38.90	AAAA C
ATOM	3387	CB	VAL	358	44.211	56.502	34.610	1.00	49.15	AAAA C
ATOM	3388	CG1	VAL	358	42.815	55.883	34.484	1.00	33.12	AAAA C
ATOM	3389	CG2	VAL	358	44.748	56.437	36.043	1.00	29.20	AAAA C
ATOM	3390	C	VAL	358	44.760	56.194	32.234	1.00	35.64	AAAA C
ATOM	3391	O	VAL	358	44.792	57.358	31.885	1.00	34.58	AAAA O
ATOM	3392	N	LYS	359	44.387	55.188	31.461	1.00	36.00	AAAA N
ATOM	3394	CA	LYS	359	43.899	55.419	30.117	1.00	41.27	AAAA C
ATOM	3395	CB	LYS	359	44.945	54.707	29.174	1.00	37.40	AAAA C
ATOM	3396	CG	LYS	359	44.340	54.473	27.770	1.00	45.19	AAAA C
ATOM	3397	CD	LYS	359	45.040	55.317	26.750	1.00	43.40	AAAA C
ATOM	3399	CE	LYS	359	45.958	54.402	25.986	1.00	43.50	AAAA C
ATOM	3399	NZ	LYS	359	45.416	53.937	24.680	1.00	47.98	AAAA N
ATOM	3403	C	LYS	359	42.423	54.979	29.939	1.00	42.14	AAAA C
ATOM	3404	O	LYS	359	42.056	53.791	30.006	1.00	40.40	AAAA O
ATOM	3405	N	ILE	360	41.602	55.974	29.573	1.00	37.16	AAAA N
ATOM	3407	CA	ILE	360	40.164	55.742	29.336	1.00	40.02	AAAA C
ATOM	3408	CB	ILE	360	39.297	56.804	30.046	1.00	38.19	AAAA C
ATOM	3409	CG2	ILE	360	37.887	56.277	29.932	1.00	39.42	AAAA C
ATOM	3410	CG1	ILE	360	39.769	57.211	31.481	1.00	28.54	AAAA C
ATOM	3411	CD1	ILE	360	39.423	56.037	32.491	1.00	33.16	AAAA C
ATOM	3412	C	ILE	360	39.880	55.857	27.831	1.00	39.49	AAAA C

Figure 1A-32

ATOM	3413	O	ILE	360	40.011	56.942	27.235	1.00	37.32	AAAA O
ATOM	3414	N	ARG	361	39.567	54.721	27.221	1.00	31.31	AAAA N
ATOM	3416	CA	ARG	361	39.472	54.782	25.744	1.00	41.24	AAAA C
ATOM	3417	CB	ARG	361	40.783	54.213	25.148	1.00	47.92	AAAA C
ATOM	3418	CG	ARG	361	40.805	54.203	23.646	1.00	50.39	AAAA C
ATOM	3419	CD	ARG	361	41.943	53.357	23.116	1.00	51.36	AAAA C
ATOM	3420	NE	ARG	361	41.473	52.974	23.263	1.00	50.97	AAAA N
ATOM	3422	CZ	ARG	361	42.297	50.962	23.490	1.00	55.79	AAAA C
ATOM	3423	NH1	ARG	361	43.512	51.074	23.616	1.00	51.63	AAAA N
ATOM	3426	NH2	ARG	361	41.834	49.719	23.631	1.00	54.52	AAAA N
ATOM	3429	C	ARG	361	38.382	53.866	25.246	1.00	42.06	AAAA C
ATOM	3430	O	ARG	361	38.536	52.661	25.499	1.00	38.93	AAAA O
ATOM	3431	N	HIS	362	37.514	54.342	24.373	1.00	46.19	AAAA N
ATOM	3433	CA	HIS	362	36.372	53.555	23.885	1.00	49.34	AAAA C
ATOM	3434	CB	HIS	362	37.000	52.300	23.266	1.00	49.94	AAAA C
ATOM	3435	CG	HIS	362	37.849	52.610	22.084	1.00	42.78	AAAA C
ATOM	3436	CD2	HIS	362	38.049	53.765	21.411	1.00	48.32	AAAA C
ATOM	3437	ND1	HIS	362	38.628	51.676	21.469	1.00	43.59	AAAA N
ATOM	3439	CE1	HIS	362	39.256	52.247	20.465	1.00	46.01	AAAA C
ATOM	3440	NE2	HIS	362	38.923	53.515	20.408	1.00	49.22	AAAA N
ATOM	3442	C	HIS	362	35.295	53.113	24.913	1.00	50.32	AAAA C
ATOM	3443	O	HIS	362	34.686	52.030	24.795	1.00	41.31	AAAA O
ATOM	3444	N	SER	363	35.222	53.875	26.013	1.00	46.96	AAAA N
ATOM	3446	CA	SER	363	34.402	53.456	27.139	1.00	52.19	AAAA C
ATOM	3447	CB	SER	363	35.231	53.837	28.400	1.00	53.73	AAAA C
ATOM	3448	OG	SER	363	35.713	52.558	28.816	1.00	41.72	AAAA O
ATOM	3450	C	SER	363	33.005	54.072	27.046	1.00	49.08	AAAA C
ATOM	3451	O	SER	363	32.653	55.040	27.694	1.00	37.49	AAAA O
ATOM	3452	N	HIS	364	32.243	53.577	26.058	1.00	52.25	AAAA N
ATOM	3454	CA	HIS	364	30.954	54.173	25.737	1.00	53.66	AAAA C
ATOM	3455	C	HIS	364	29.879	53.937	26.760	1.00	46.77	AAAA C
ATOM	3456	O	HIS	364	29.287	54.899	27.280	1.00	51.44	AAAA O
ATOM	3457	CB	HIS	364	30.485	53.699	24.348	1.00	49.83	AAAA C
ATOM	3458	CG	HIS	364	31.493	54.182	23.338	1.00	51.51	AAAA C
ATOM	3459	ND1	HIS	364	31.870	55.502	23.156	1.00	44.83	AAAA N
ATOM	3460	CE1	HIS	364	32.708	55.533	22.214	1.00	28.57	AAAA C
ATOM	3461	CD2	HIS	364	32.194	53.393	22.472	1.00	38.62	AAAA C
ATOM	3462	NE2	HIS	364	32.992	54.274	21.810	1.00	41.44	AAAA N
ATOM	3464	N	ALA	365	29.949	52.819	27.427	1.00	47.53	AAAA N
ATOM	3466	CA	ALA	365	29.211	52.488	28.621	1.00	44.41	AAAA C
ATOM	3467	CB	ALA	365	29.678	51.133	29.150	1.00	40.28	AAAA C
ATOM	3468	C	ALA	365	29.318	53.473	29.768	1.00	44.70	AAAA C
ATOM	3469	O	ALA	365	28.576	53.206	30.726	1.00	45.28	AAAA O
ATOM	3470	N	LEU	366	30.158	54.517	29.762	1.00	40.80	AAAA N
ATOM	3472	CA	LEU	366	30.415	55.243	30.968	1.00	42.21	AAAA C
ATOM	3473	CB	LEU	366	31.885	55.241	31.350	1.00	43.78	AAAA C
ATOM	3474	CG	LEU	366	32.740	54.037	31.667	1.00	51.52	AAAA C
ATOM	3475	CD1	LEU	366	34.192	54.373	32.043	1.00	51.77	AAAA C
ATOM	3476	CD2	LEU	366	32.118	53.305	32.834	1.00	51.17	AAAA C
ATOM	3477	C	LEU	366	29.974	56.687	30.896	1.00	46.36	AAAA C
ATOM	3478	O	LEU	366	30.305	57.248	29.849	1.00	48.40	AAAA O
ATOM	3479	N	VAL	367	29.521	57.275	32.015	1.00	43.68	AAAA N
ATOM	3481	CA	VAL	367	29.072	58.675	31.940	1.00	44.18	AAAA C
ATOM	3482	CB	VAL	367	27.557	58.727	32.376	1.00	48.80	AAAA C
ATOM	3483	CG1	VAL	367	26.923	60.073	32.571	1.00	41.69	AAAA C
ATOM	3484	CG2	VAL	367	26.697	57.949	31.365	1.00	34.00	AAAA C
ATOM	3485	C	VAL	367	29.923	59.518	32.845	1.00	44.90	AAAA C
ATOM	3486	O	VAL	367	29.965	60.751	32.720	1.00	44.75	AAAA O
ATOM	3487	N	SER	368	30.591	58.818	33.757	1.00	48.72	AAAA N
ATOM	3489	CA	SER	368	31.487	59.465	34.742	1.00	52.70	AAAA C
ATOM	3490	CB	SER	368	30.658	59.706	36.000	1.00	55.32	AAAA C
ATOM	3491	OG	SER	368	31.300	60.298	37.091	1.00	64.86	AAAA O
ATOM	3493	C	SER	368	32.590	58.497	35.179	1.00	52.76	AAAA C
ATOM	3494	O	SER	368	32.352	57.299	34.976	1.00	48.99	AAAA O
ATOM	3495	N	LEU	369	33.631	59.012	35.831	1.00	53.86	AAAA N
ATOM	3497	CA	LEU	369	34.716	58.129	36.274	1.00	60.15	AAAA C
ATOM	3498	CB	LEU	369	36.073	58.630	35.784	1.00	55.91	AAAA C
ATOM	3499	CG	LEU	369	36.325	58.736	34.271	1.00	45.96	AAAA C
ATOM	3500	CD1	LEU	369	37.669	59.428	34.154	1.00	53.97	AAAA C
ATOM	3501	CD2	LEU	369	36.207	57.384	33.619	1.00	38.77	AAAA C
ATOM	3502	C	LEU	369	34.645	58.036	37.811	1.00	62.52	AAAA C
ATOM	3503	O	LEU	369	35.569	57.700	38.595	1.00	59.33	AAAA O
ATOM	3504	N	SER	370	33.437	58.401	38.285	1.00	56.26	AAAA N
ATOM	3506	CA	SER	370	33.089	58.431	39.690	1.00	53.88	AAAA C
ATOM	3507	CB	SER	370	31.673	59.052	39.816	1.00	57.56	AAAA C
ATOM	3508	OG	SER	370	30.771	58.061	39.261	1.00	69.12	AAAA O
ATOM	3510	C	SER	370	33.060	57.085	40.412	1.00	47.97	AAAA C
ATOM	3511	O	SER	370	33.228	56.943	41.596	1.00	41.93	AAAA O
ATOM	3512	N	PHE	371	32.967	55.936	39.792	1.00	45.48	AAAA N
ATOM	3514	CA	PHE	371	33.223	54.643	40.356	1.00	46.29	AAAA C
ATOM	3515	CB	PHE	371	32.952	53.596	39.287	1.00	43.53	AAAA C
ATOM	3516	CG	PHE	371	33.724	53.629	38.012	1.00	56.45	AAAA C
ATOM	3517	CD1	PHE	371	34.895	52.807	37.764	1.00	58.95	AAAA C
ATOM	3518	CD2	PHE	371	33.371	54.515	37.004	1.00	53.92	AAAA C
ATOM	3519	CE1	PHE	371	35.498	52.842	36.570	1.00	59.50	AAAA C

Figure 1A-33

ATOM	3520	CE2	PHE	371	34.048	54.546	35.917	1.00	56.49	AAAA C
ATOM	3521	CZ	PHE	371	35.119	53.716	35.579	1.00	56.39	AAAA C
ATOM	3522	C	PHE	371	34.684	54.467	40.895	1.00	54.84	AAAA C
ATOM	3523	O	PHE	371	35.005	53.592	41.728	1.00	52.23	AAAA O
ATOM	3524	N	LEU	372	35.633	55.305	40.519	1.00	50.17	AAAA N
ATOM	3526	CA	LEU	372	36.928	55.395	41.109	1.00	46.25	AAAA C
ATOM	3527	CB	LEU	372	38.171	55.812	40.276	1.00	44.82	AAAA C
ATOM	3528	CG	LEU	372	38.411	54.800	39.114	1.00	36.78	AAAA C
ATOM	3529	CD1	LEU	372	38.853	55.643	37.934	1.00	45.04	AAAA C
ATOM	3530	CD2	LEU	372	39.260	53.657	39.565	1.00	35.55	AAAA C
ATOM	3531	C	LEU	372	36.715	56.392	42.213	1.00	42.26	AAAA C
ATOM	3532	O	LEU	372	37.224	57.507	42.364	1.00	38.37	AAAA O
ATOM	3533	N	LYS	373	35.970	55.862	43.102	1.00	47.06	AAAA N
ATOM	3535	CA	LYS	373	35.527	56.509	44.415	1.00	50.19	AAAA C
ATOM	3536	CB	LYS	373	34.546	55.521	45.077	1.00	56.74	AAAA C
ATOM	3537	CG	LYS	373	33.645	56.162	46.119	1.00	59.64	AAAA C
ATOM	3538	CD	LYS	373	32.529	56.956	45.441	0.01	60.17	AAAA C
ATOM	3539	CE	LYS	373	31.674	57.687	46.460	0.01	60.45	AAAA C
ATOM	3540	NZ	LYS	373	31.083	58.933	45.899	0.01	60.30	AAAA N
ATOM	3544	C	LYS	373	36.646	56.863	45.366	1.00	49.72	AAAA C
ATOM	3545	O	LYS	373	36.636	57.960	45.907	1.00	42.42	AAAA O
ATOM	3546	N	ASN	374	37.657	55.986	45.513	1.00	54.43	AAAA N
ATOM	3548	CA	ASN	374	38.765	56.352	46.410	1.00	59.92	AAAA C
ATOM	3549	CB	ASN	374	39.080	55.154	47.314	1.00	63.16	AAAA C
ATOM	3550	CG	ASN	374	38.009	54.978	48.396	1.00	64.53	AAAA C
ATOM	3551	OD1	ASN	374	37.892	53.972	49.096	1.00	66.40	AAAA O
ATOM	3552	ND2	ASN	374	37.160	55.965	48.578	1.00	52.88	AAAA N
ATOM	3555	C	ASN	374	40.043	56.892	45.786	1.00	62.35	AAAA C
ATOM	3556	O	ASN	374	41.031	57.223	46.479	1.00	63.08	AAAA O
ATOM	3557	N	LEU	375	40.091	56.893	44.439	1.00	58.34	AAAA N
ATOM	3559	CA	LEU	375	41.305	57.374	43.795	1.00	54.73	AAAA C
ATOM	3560	CB	LEU	375	41.099	57.359	42.288	1.00	56.41	AAAA C
ATOM	3561	CG	LEU	375	42.396	57.422	41.459	1.00	54.12	AAAA C
ATOM	3562	CD1	LEU	375	43.135	56.112	41.689	1.00	37.88	AAAA C
ATOM	3563	CD2	LEU	375	42.030	57.796	40.041	1.00	40.97	AAAA C
ATOM	3564	C	LEU	375	41.712	58.754	44.245	1.00	52.37	AAAA C
ATOM	3565	O	LEU	375	41.151	59.777	43.877	1.00	52.11	AAAA O
ATOM	3566	N	ARG	376	42.801	58.874	44.982	1.00	55.16	AAAA N
ATOM	3568	CA	ARG	376	43.320	60.155	45.434	1.00	55.45	AAAA C
ATOM	3569	CB	ARG	376	43.706	60.222	46.928	1.00	58.68	AAAA C
ATOM	3570	CG	ARG	376	44.288	58.907	47.415	1.00	69.10	AAAA C
ATOM	3571	CD	ARG	376	44.286	58.817	48.944	1.00	81.17	AAAA C
ATOM	3572	NE	ARG	376	45.377	57.926	49.410	1.00	84.46	AAAA N
ATOM	3574	CZ	ARG	376	46.618	58.380	49.598	1.00	85.64	AAAA C
ATOM	3575	NH1	ARG	376	46.966	59.645	49.383	1.00	81.84	AAAA N
ATOM	3578	NH2	ARG	376	47.571	57.548	50.012	1.00	94.15	AAAA N
ATOM	3581	C	ARG	376	44.556	60.544	44.633	1.00	50.16	AAAA C
ATOM	3582	O	ARG	376	44.746	61.728	44.465	1.00	44.25	AAAA O
ATOM	3583	N	LEU	377	45.375	59.578	44.219	1.00	50.99	AAAA N
ATOM	3585	CA	LEU	377	46.526	59.942	43.379	1.00	49.40	AAAA C
ATOM	3586	CB	LEU	377	47.595	60.411	44.329	1.00	64.72	AAAA C
ATOM	3587	CG	LEU	377	48.806	59.577	44.667	1.00	70.76	AAAA C
ATOM	3588	CD1	LEU	377	50.031	60.157	43.954	1.00	63.32	AAAA C
ATOM	3589	CD2	LEU	377	49.010	59.696	46.179	1.00	68.60	AAAA C
ATOM	3590	C	LEU	377	47.043	59.022	42.311	1.00	46.33	AAAA C
ATOM	3591	O	LEU	377	46.868	57.788	42.286	1.00	45.17	AAAA O
ATOM	3592	N	ILE	378	47.448	59.675	41.199	1.00	45.12	AAAA N
ATOM	3594	CA	ILE	378	48.042	58.976	40.042	1.00	49.10	AAAA C
ATOM	3595	CB	ILE	378	47.342	59.303	38.724	1.00	46.36	AAAA C
ATOM	3596	CG2	ILE	378	48.115	58.696	37.574	1.00	34.36	AAAA C
ATOM	3597	CG1	ILE	378	45.871	58.862	38.829	1.00	38.59	AAAA C
ATOM	3598	CD1	ILE	378	44.999	59.515	37.765	1.00	37.18	AAAA C
ATOM	3599	C	ILE	378	49.524	59.381	40.003	1.00	49.87	AAAA C
ATOM	3600	O	ILE	378	49.801	60.595	40.040	1.00	44.72	AAAA O
ATOM	3601	N	LEU	379	50.454	58.423	40.067	1.00	49.97	AAAA N
ATOM	3603	CA	LEU	379	51.866	58.712	40.341	1.00	48.48	AAAA C
ATOM	3604	CB	LEU	379	52.575	57.531	41.054	1.00	48.44	AAAA C
ATOM	3605	CG	LEU	379	52.234	57.363	42.554	1.00	50.28	AAAA C
ATOM	3606	CD1	LEU	379	52.826	56.187	43.217	1.00	39.89	AAAA C
ATOM	3607	CD2	LEU	379	52.616	58.625	43.300	1.00	42.89	AAAA C
ATOM	3608	C	LEU	379	52.699	59.019	39.080	1.00	50.94	AAAA C
ATOM	3609	O	LEU	379	53.576	59.788	39.139	1.00	54.23	AAAA O
ATOM	3610	N	GLY	380	52.175	58.423	37.972	1.00	48.67	AAAA N
ATOM	3612	CA	GLY	380	52.931	58.715	36.702	1.00	49.94	AAAA C
ATOM	3613	C	GLY	380	54.249	58.155	36.624	1.00	52.70	AAAA C
ATOM	3614	O	GLY	380	55.026	58.657	35.803	1.00	49.94	AAAA O
ATOM	3615	N	GLU	381	54.549	57.033	37.272	1.00	52.51	AAAA N
ATOM	3617	CA	GLU	381	55.849	56.386	37.243	1.00	52.33	AAAA C
ATOM	3618	CB	GLU	381	56.055	55.310	38.323	1.00	45.22	AAAA C
ATOM	3619	CG	GLU	381	55.402	55.779	39.636	1.00	52.91	AAAA C
ATOM	3620	CD	GLU	381	56.050	55.192	40.873	1.00	42.11	AAAA C
ATOM	3621	OE1	GLU	381	56.160	53.966	40.890	1.00	40.26	AAAA O
ATOM	3622	OE2	GLU	381	56.379	56.014	41.754	1.00	51.32	AAAA O
ATOM	3623	C	GLU	381	56.970	55.704	39.059	1.00	55.86	AAAA C
ATOM	3624	O	GLU	381	57.216	55.652	35.344	1.00	54.61	AAAA O

Figure 1A-34

Application No. 09/555,275
Annotated Sheet Showing Changes

ATOM	3625	N	GLU	382	54.980	55.449	35.157	1.00	53.56	AAAA N
ATOM	3627	CA	GLU	382	55.691	55.018	33.766	1.00	48.15	AAAA C
ATOM	3628	CB	GLU	382	55.051	53.550	33.532	1.00	35.27	AAAA C
ATOM	3629	CG	GLU	382	54.739	53.225	32.051	1.00	49.69	AAAA C
ATOM	3630	CD	GLU	382	54.676	51.719	31.807	1.00	56.45	AAAA C
ATOM	3631	OE1	GLU	382	55.062	50.924	32.705	1.00	61.66	AAAA O
ATOM	3632	OE2	GLU	382	54.264	51.201	30.745	1.00	57.69	AAAA O
ATOM	3633	C	GLU	382	54.006	55.732	32.973	1.00	50.84	AAAA C
ATOM	3634	O	GLU	382	53.097	56.282	33.598	1.00	49.44	AAAA O
ATOM	3635	N	GLN	383	54.347	56.256	31.780	1.00	52.25	AAAA N
ATOM	3637	CA	GLN	383	53.498	57.153	31.016	1.00	40.15	AAAA C
ATOM	3638	CB	GLN	383	53.914	58.609	31.155	1.00	38.50	AAAA C
ATOM	3639	CG	GLN	383	54.489	58.909	32.542	1.00	31.10	AAAA C
ATOM	3640	CD	GLN	383	54.950	60.301	32.752	1.00	33.19	AAAA C
ATOM	3641	OE1	GLN	383	55.186	60.840	31.683	1.00	40.34	AAAA O
ATOM	3642	NE2	GLN	383	55.043	60.943	33.934	1.00	36.30	AAAA N
ATOM	3645	C	GLN	383	53.426	56.744	29.563	1.00	40.15	AAAA C
ATOM	3646	O	GLN	383	54.131	55.858	29.139	1.00	43.45	AAAA O
ATOM	3647	N	LEU	384	52.375	57.195	28.860	1.00	42.54	AAAA N
ATOM	3649	CA	LEU	384	52.257	56.889	27.443	1.00	43.24	AAAA C
ATOM	3650	CB	LEU	384	50.814	57.011	26.949	1.00	43.79	AAAA C
ATOM	3651	CG	LEU	384	49.818	56.235	27.861	1.00	41.21	AAAA C
ATOM	3652	CD1	LEU	384	48.611	57.095	28.221	1.00	33.99	AAAA C
ATOM	3653	CD2	LEU	384	49.405	54.968	27.149	1.00	33.20	AAAA C
ATOM	3654	C	LEU	384	53.204	57.809	26.672	1.00	40.51	AAAA C
ATOM	3655	O	LEU	384	53.582	58.872	27.177	1.00	29.66	AAAA O
ATOM	3656	N	GLU	385	53.659	57.319	25.531	1.00	45.22	AAAA N
ATOM	3658	CA	GLU	385	54.410	58.116	24.570	1.00	49.98	AAAA C
ATOM	3659	CB	GLU	385	54.424	57.475	23.174	1.00	60.50	AAAA C
ATOM	3660	CG	GLU	385	55.045	56.095	23.106	1.00	68.76	AAAA C
ATOM	3661	CD	GLU	385	54.195	54.951	23.592	1.00	72.02	AAAA C
ATOM	3662	OE1	GLU	385	53.150	55.213	24.244	1.00	81.88	AAAA O
ATOM	3663	OE2	GLU	385	54.565	53.786	23.301	1.00	73.13	AAAA O
ATOM	3664	C	GLU	385	53.828	59.515	24.450	1.00	47.41	AAAA C
ATOM	3665	O	GLU	385	52.635	59.706	24.184	1.00	54.43	AAAA O
ATOM	3666	N	GLY	386	54.614	60.470	24.902	1.00	43.69	AAAA N
ATOM	3668	CA	GLY	386	54.181	61.870	24.897	1.00	40.34	AAAA C
ATOM	3669	C	GLY	386	54.286	62.449	26.308	1.00	40.65	AAAA C
ATOM	3670	O	GLY	386	53.930	63.615	26.491	1.00	39.75	AAAA O
ATOM	3671	N	ASN	387	54.441	61.537	27.272	1.00	40.75	AAAA N
ATOM	3673	CA	ASN	387	54.479	61.912	28.675	1.00	49.18	AAAA C
ATOM	3674	CB	ASN	387	55.500	63.084	28.874	1.00	44.41	AAAA C
ATOM	3675	CG	ASN	387	56.925	62.541	28.722	1.00	61.51	AAAA C
ATOM	3676	OD1	ASN	387	57.199	61.313	28.677	1.00	57.85	AAAA O
ATOM	3677	ND2	ASN	387	58.063	63.251	28.592	1.00	61.96	AAAA N
ATOM	3680	C	ASN	387	53.095	62.100	29.299	1.00	48.46	AAAA C
ATOM	3681	O	ASN	387	52.836	62.891	30.218	1.00	48.99	AAAA O
ATOM	3682	N	TYR	388	52.214	61.116	29.058	1.00	46.29	AAAA N
ATOM	3684	CA	TYR	388	50.846	61.199	29.540	1.00	45.09	AAAA C
ATOM	3685	CB	TYR	388	49.823	60.957	28.399	1.00	40.70	AAAA C
ATOM	3686	CG	TYR	388	49.925	62.056	27.373	1.00	42.24	AAAA C
ATOM	3687	CD1	TYR	388	50.345	61.854	26.064	1.00	44.38	AAAA C
ATOM	3688	CE1	TYR	388	50.401	62.885	25.157	1.00	35.51	AAAA C
ATOM	3689	CD2	TYR	388	49.625	63.356	27.709	1.00	44.67	AAAA C
ATOM	3690	CE2	TYR	388	49.699	64.428	26.830	1.00	38.14	AAAA C
ATOM	3691	CZ	TYR	388	50.087	64.148	25.555	1.00	41.27	AAAA C
ATOM	3692	OH	TYR	388	50.151	65.181	24.604	1.00	50.18	AAAA O
ATOM	3694	C	TYR	388	50.563	60.288	30.714	1.00	41.88	AAAA C
ATOM	3695	O	TYR	388	50.727	59.092	30.511	1.00	32.99	AAAA O
ATOM	3696	N	SER	389	50.020	60.917	31.753	1.00	45.42	AAAA N
ATOM	3698	CA	SER	389	49.591	60.131	32.931	1.00	50.13	AAAA C
ATOM	3699	CB	SER	389	49.798	60.894	34.261	1.00	45.57	AAAA C
ATOM	3700	OG	SER	389	51.185	60.899	34.504	1.00	51.11	AAAA O
ATOM	3702	C	SER	389	48.097	59.813	32.804	1.00	48.11	AAAA C
ATOM	3703	O	SER	389	47.686	58.792	33.336	1.00	49.25	AAAA O
ATOM	3704	N	PHE	390	47.321	60.685	32.196	1.00	42.56	AAAA N
ATOM	3706	CA	PHE	390	45.867	60.595	32.146	1.00	40.76	AAAA C
ATOM	3707	CB	PHE	390	45.241	61.581	33.139	1.00	44.80	AAAA C
ATOM	3708	CG	PHE	390	43.764	61.358	33.328	1.00	40.53	AAAA C
ATOM	3709	CD1	PHE	390	43.406	60.273	34.089	1.00	40.80	AAAA C
ATOM	3710	CD2	PHE	390	42.769	62.157	32.748	1.00	35.59	AAAA C
ATOM	3711	CE1	PHE	390	42.050	59.985	34.312	1.00	47.09	AAAA C
ATOM	3712	CE2	PHE	390	41.454	61.824	32.965	1.00	44.50	AAAA C
ATOM	3713	CZ	PHE	390	41.063	60.745	33.739	1.00	34.54	AAAA C
ATOM	3714	C	PHE	390	45.372	60.829	30.720	1.00	38.54	AAAA C
ATOM	3715	O	PHE	390	45.542	61.918	30.126	1.00	40.29	AAAA O
ATOM	3716	N	TYR	391	44.819	59.818	30.096	1.00	33.48	AAAA N
ATOM	3718	CA	TYR	391	44.596	59.782	28.663	1.00	38.58	AAAA C
ATOM	3719	CB	TYR	391	45.579	58.871	27.972	1.00	38.95	AAAA C
ATOM	3720	CG	TYR	391	45.760	59.006	26.503	1.00	44.54	AAAA C
ATOM	3721	CD1	TYR	391	46.822	59.815	26.052	1.00	47.14	AAAA C
ATOM	3722	CE1	TYR	391	47.057	59.993	24.722	1.00	46.03	AAAA C
ATOM	3723	CD2	TYR	391	44.927	58.390	25.584	1.00	46.94	AAAA C
ATOM	3724	CE2	TYR	391	45.157	58.569	24.242	1.00	47.45	AAAA C
ATOM	3725	CZ	TYR	391	46.207	59.356	23.830	1.00	45.84	AAAA C

Figure 1A-35

ATOM	3726	OH	TYR	391	46.374	59.492	22.191	1.00 44.78	AAAA O
ATOM	3728	C	TYR	391	43.194	59.232	29.349	1.00 39.74	AAAA C
ATOM	3729	O	TYR	391	42.841	58.103	29.736	1.00 38.49	AAAA O
ATOM	3730	N	VAL	392	42.417	60.158	27.779	1.00 37.07	AAAA N
ATOM	3732	CA	VAL	392	40.958	59.874	27.603	1.00 39.52	AAAA C
ATOM	3733	CB	VAL	392	40.075	60.880	28.440	1.00 41.12	AAAA C
ATOM	3734	CG1	VAL	392	38.612	60.464	28.472	1.00 37.96	AAAA C
ATOM	3735	CG2	VAL	392	40.666	61.041	29.841	1.00 33.19	AAAA C
ATOM	3736	C	VAL	392	40.531	60.092	26.182	1.00 31.08	AAAA C
ATOM	3737	O	VAL	392	40.508	61.227	25.904	1.00 34.71	AAAA O
ATOM	3738	N	LEU	393	40.299	59.113	25.383	1.00 34.62	AAAA N
ATOM	3740	CA	LEU	393	39.948	59.259	23.977	1.00 38.12	AAAA C
ATOM	3741	CB	LEU	393	41.200	59.036	23.096	1.00 42.49	AAAA C
ATOM	3742	CG	LEU	393	41.023	58.649	21.585	1.00 26.48	AAAA C
ATOM	3743	CD1	LEU	393	41.128	59.879	20.753	1.00 26.57	AAAA C
ATOM	3744	CD2	LEU	393	42.078	57.589	21.244	1.00 29.99	AAAA C
ATOM	3745	C	LEU	393	38.821	58.375	23.492	1.00 39.15	AAAA C
ATOM	3746	O	LEU	393	38.760	57.173	23.799	1.00 37.90	AAAA O
ATOM	3747	N	ASP	394	38.015	58.973	22.565	1.00 43.38	AAAA N
ATOM	3749	CA	ASP	394	36.988	59.215	21.575	1.00 44.77	AAAA C
ATOM	3750	CB	ASP	394	37.445	57.073	21.129	1.00 44.80	AAAA C
ATOM	3751	CG	ASP	394	36.466	56.477	20.155	1.00 47.14	AAAA C
ATOM	3752	OD1	ASP	394	36.750	55.577	19.333	1.00 52.91	AAAA O
ATOM	3753	OD2	ASP	394	35.311	56.948	20.180	1.00 49.27	AAAA O
ATOM	3754	C	ASP	394	35.936	57.619	23.021	1.00 43.17	AAAA C
ATOM	3755	O	ASP	394	35.831	56.385	23.212	1.00 43.51	AAAA O
ATOM	3756	N	ASN	395	35.299	58.495	23.746	1.00 39.90	AAAA N
ATOM	3758	CA	ASN	395	34.305	58.158	24.776	1.00 46.32	AAAA C
ATOM	3759	CB	ASN	395	34.804	59.512	26.212	1.00 42.96	AAAA C
ATOM	3760	CG	ASN	395	35.992	57.619	26.579	1.00 36.92	AAAA C
ATOM	3761	OD1	ASN	395	36.013	56.394	26.796	1.00 21.65	AAAA O
ATOM	3762	ND2	ASN	395	37.075	58.409	26.859	1.00 27.87	AAAA N
ATOM	3765	C	ASN	395	32.932	58.816	24.541	1.00 40.44	AAAA C
ATOM	3766	O	ASN	395	32.749	59.982	24.882	1.00 37.06	AAAA O
ATOM	3767	N	GLN	396	32.073	58.055	23.877	1.00 46.74	AAAA N
ATOM	3769	CA	GLN	396	30.771	58.582	23.421	1.00 52.93	AAAA C
ATOM	3770	CB	GLN	396	29.848	57.567	22.744	1.00 52.29	AAAA C
ATOM	3771	CG	GLN	396	30.173	57.405	21.257	1.00 46.42	AAAA C
ATOM	3772	CD	GLN	396	29.817	55.991	20.840	1.00 55.21	AAAA C
ATOM	3773	OE1	GLN	396	28.835	55.421	21.312	1.00 61.17	AAAA O
ATOM	3774	NE2	GLN	396	30.628	55.411	19.971	1.00 55.79	AAAA N
ATOM	3777	C	GLN	396	29.874	59.224	24.458	1.00 48.64	AAAA C
ATOM	3778	O	GLN	396	29.407	60.287	24.113	1.00 51.63	AAAA O
ATOM	3779	N	ASN	397	29.717	58.681	25.633	1.00 48.95	AAAA N
ATOM	3781	CA	ASN	397	28.783	59.196	26.632	1.00 51.72	AAAA C
ATOM	3782	CB	ASN	397	27.969	57.959	27.093	1.00 35.94	AAAA C
ATOM	3783	CG	ASN	397	27.231	57.430	25.860	1.00 49.09	AAAA C
ATOM	3784	OD1	ASN	397	26.591	58.304	25.229	1.00 49.32	AAAA O
ATOM	3785	ND2	ASN	397	27.258	56.175	25.431	1.00 43.31	AAAA N
ATOM	3788	C	ASN	397	29.367	59.945	27.800	1.00 52.98	AAAA C
ATOM	3789	O	ASN	397	28.586	60.344	28.627	1.00 53.33	AAAA O
ATOM	3790	N	LEU	398	30.682	59.990	28.001	1.00 55.73	AAAA N
ATOM	3792	CA	LEU	398	31.312	60.550	29.179	1.00 52.12	AAAA C
ATOM	3793	CB	LEU	398	32.927	60.389	29.149	1.00 48.47	AAAA C
ATOM	3794	CG	LEU	398	33.606	60.283	30.460	1.00 41.81	AAAA C
ATOM	3795	CD1	LEU	398	33.417	58.939	31.136	1.00 40.35	AAAA C
ATOM	3796	CD2	LEU	398	35.070	60.608	30.092	1.00 39.03	AAAA C
ATOM	3797	C	LEU	398	30.923	61.995	29.353	1.00 52.35	AAAA C
ATOM	3798	O	LEU	398	31.422	62.909	28.681	1.00 49.91	AAAA O
ATOM	3799	N	GLN	399	30.241	62.225	30.469	1.00 58.76	AAAA N
ATOM	3801	CA	GLN	399	29.688	63.558	30.796	1.00 60.03	AAAA C
ATOM	3802	CB	GLN	399	28.236	63.331	31.262	1.00 59.55	AAAA C
ATOM	3803	CG	GLN	399	27.235	63.962	30.316	1.00 73.07	AAAA C
ATOM	3804	CD	GLN	399	25.944	63.146	30.340	1.00 78.39	AAAA C
ATOM	3805	OE1	GLN	399	25.097	63.455	31.194	1.00 71.79	AAAA O
ATOM	3806	NE2	GLN	399	25.856	62.158	29.440	1.00 69.88	AAAA N
ATOM	3809	C	GLN	399	30.490	64.252	31.989	1.00 54.49	AAAA C
ATOM	3810	O	GLN	399	30.528	65.477	32.068	1.00 51.96	AAAA O
ATOM	3811	N	GLN	400	31.058	63.389	32.734	1.00 50.44	AAAA N
ATOM	3813	CA	GLN	400	31.938	63.948	33.756	1.00 53.83	AAAA C
ATOM	3814	CB	GLN	400	31.215	64.314	35.049	1.00 54.97	AAAA C
ATOM	3815	CG	GLN	400	30.717	63.150	35.897	1.00 58.99	AAAA C
ATOM	3816	CD	GLN	400	30.678	63.430	37.389	1.00 65.82	AAAA C
ATOM	3817	OE1	GLN	400	30.906	64.502	37.962	1.00 68.10	AAAA O
ATOM	3818	NE2	GLN	400	30.341	62.444	38.222	1.00 55.35	AAAA N
ATOM	3821	C	GLN	400	33.113	63.008	34.052	1.00 52.08	AAAA C
ATOM	3822	O	GLN	400	33.197	61.783	33.942	1.00 51.90	AAAA O
ATOM	3823	N	LEU	401	34.073	63.580	34.751	1.00 49.58	AAAA N
ATOM	3825	CA	LEU	401	35.175	62.844	35.334	1.00 49.57	AAAA C
ATOM	3826	CB	LEU	401	36.378	63.803	35.260	1.00 47.94	AAAA C
ATOM	3827	CG	LEU	401	36.636	64.237	33.772	1.00 46.61	AAAA C
ATOM	3828	CD1	LEU	401	37.658	65.329	33.677	1.00 39.09	AAAA C
ATOM	3829	CD2	LEU	401	36.919	63.060	32.869	1.00 40.72	AAAA C
ATOM	3830	C	LEU	401	34.866	62.357	36.734	1.00 51.23	AAAA C
ATOM	3831	O	LEU	401	34.258	61.299	36.892	1.00 49.06	AAAA O

Figure 1A-36

```
ATOM  3832  H   TRP  402      35.297  63.140  37.690  1.00 54.58      AAAA H
ATOM  3834  CA  TRP  402      34.975  63.090  39.097  1.00 59.76      AAAA C
ATOM  3835  CB  TRP  402      36.279  62.954  39.933  1.00 59.56      AAAA C
ATOM  3836  CG  TRP  402      36.971  61.624  39.737  1.00 58.17      AAAA C
ATOM  3837  CD1 TRP  402      37.981  61.243  38.784  1.00 53.18      AAAA C
ATOM  3838  CE2 TRP  402      38.286  59.897  39.002  1.00 56.61      AAAA C
ATOM  3839  CE3 TRP  402      38.643  61.917  37.764  1.00 43.25      AAAA C
ATOM  3840  CD1 TRP  402      36.719  60.517  40.459  1.00 53.50      AAAA C
ATOM  3841  NE1 TRP  402      37.488  59.467  40.032  1.00 57.66      AAAA N
ATOM  3843  CZ2 TRP  402      39.212  59.166  38.249  1.00 51.44      AAAA C
ATOM  3844  CZ3 TRP  402      39.546  61.199  37.026  1.00 53.69      AAAA C
ATOM  3845  CH2 TRP  402      39.820  59.857  37.263  1.00 50.75      AAAA C
ATOM  3846  C   TRP  402      34.223  64.389  39.429  1.00 64.09      AAAA C
ATOM  3847  O   TRP  402      34.408  65.449  38.808  1.00 61.98      AAAA O
ATOM  3848  N   ASP  403      33.503  64.418  40.551  1.00 68.85      AAAA N
ATOM  3850  CA  ASP  403      32.947  65.668  41.068  1.00 67.83      AAAA C
ATOM  3851  CB  ASP  403      31.918  65.343  42.151  1.00 72.19      AAAA C
ATOM  3852  CG  ASP  403      30.853  66.417  42.306  1.00 73.08      AAAA C
ATOM  3853  OD1 ASP  403      31.177  67.625  42.297  1.00 71.67      AAAA O
ATOM  3854  OD2 ASP  403      29.693  65.979  42.454  1.00 75.08      AAAA O
ATOM  3855  C   ASP  403      34.065  66.607  41.607  1.00 66.63      AAAA C
ATOM  3856  O   ASP  403      34.245  66.672  42.811  1.00 67.18      AAAA O
ATOM  3857  N   TRP  404      34.449  67.588  40.846  1.00 69.29      AAAA N
ATOM  3859  CA  TRP  404      35.412  68.588  41.291  1.00 77.11      AAAA C
ATOM  3860  CB  TRP  404      35.859  69.409  40.063  1.00 79.10      AAAA C
ATOM  3861  CG  TRP  404      36.504  68.509  39.047  1.00 82.59      AAAA C
ATOM  3862  CD2 TRP  404      37.294  67.348  39.322  1.00 84.82      AAAA C
ATOM  3863  CE2 TRP  404      37.686  66.813  38.081  1.00 84.56      AAAA C
ATOM  3864  CE3 TRP  404      37.793  66.710  40.506  1.00 80.95      AAAA C
ATOM  3865  CD1 TRP  404      36.460  68.622  37.694  1.00 83.37      AAAA C
ATOM  3866  NE1 TRP  404      37.165  67.617  37.111  1.00 80.33      AAAA N
ATOM  3868  CZ2 TRP  404      38.477  65.662  37.982  1.00 85.91      AAAA C
ATOM  3869  CZ3 TRP  404      38.471  65.573  40.392  1.00 86.36      AAAA C
ATOM  3870  CH2 TRP  404      38.860  65.051  39.133  1.00 85.05      AAAA C
ATOM  3871  C   TRP  404      35.034  69.517  42.420  1.00 81.60      AAAA C
ATOM  3872  O   TRP  404      35.387  70.709  42.504  1.00 84.57      AAAA O
ATOM  3873  N   ASP  405      34.281  69.063  43.393  1.00 84.45      AAAA N
ATOM  3875  CA  ASP  405      33.771  69.861  44.496  1.00 87.48      AAAA C
ATOM  3876  CB  ASP  405      32.352  70.365  44.262  1.00 88.04      AAAA C
ATOM  3877  CG  ASP  405      32.274  71.612  43.409  1.00 92.54      AAAA C
ATOM  3878  OD1 ASP  405      33.306  72.285  43.207  1.00 94.82      AAAA O
ATOM  3879  OD2 ASP  405      31.130  71.854  42.955  1.00 95.26      AAAA O
ATOM  3880  C   ASP  405      33.730  68.906  45.693  1.00 87.80      AAAA C
ATOM  3881  O   ASP  405      34.245  69.224  46.743  1.00 92.10      AAAA O
ATOM  3882  N   ALA  406      33.239  67.709  45.460  1.00 84.46      AAAA N
ATOM  3884  CA  ALA  406      33.176  66.671  46.451  1.00 82.87      AAAA C
ATOM  3885  CB  ALA  406      31.943  65.805  46.133  1.00 76.32      AAAA C
ATOM  3886  C   ALA  406      34.445  65.840  46.459  1.00 85.77      AAAA C
ATOM  3887  O   ALA  406      34.470  64.823  47.185  1.00 89.38      AAAA O
ATOM  3888  N   ARG  407      35.433  66.073  45.577  1.00 83.74      AAAA N
ATOM  3890  CA  ARG  407      36.541  65.151  45.400  1.00 79.60      AAAA C
ATOM  3891  CB  ARG  407      36.105  64.140  44.297  1.00 77.84      AAAA C
ATOM  3892  CG  ARG  407      35.457  62.950  44.921  1.00 81.91      AAAA C
ATOM  3893  CD  ARG  407      35.362  61.688  44.113  1.00 86.97      AAAA C
ATOM  3894  NE  ARG  407      36.281  60.669  44.607  1.00 86.94      AAAA N
ATOM  3896  CZ  ARG  407      37.564  60.583  44.279  1.00 92.14      AAAA C
ATOM  3897  NH1 ARG  407      38.169  61.441  43.469  1.00 97.06      AAAA N
ATOM  3900  NH2 ARG  407      38.369  59.616  44.779  1.00 96.33      AAAA N
ATOM  3903  C   ARG  407      37.880  65.749  45.048  1.00 76.72      AAAA C
ATOM  3904  O   ARG  407      37.989  66.774  44.410  1.00 77.47      AAAA O
ATOM  3905  N   ASN  408      38.958  65.081  45.453  1.00 75.75      AAAA N
ATOM  3907  CA  ASN  408      40.311  65.556  45.173  1.00 73.79      AAAA C
ATOM  3908  CB  ASN  408      40.938  66.240  46.388  1.00 74.46      AAAA C
ATOM  3909  CG  ASN  408      41.986  67.242  45.947  1.00 82.51      AAAA C
ATOM  3910  OD1 ASN  408      41.913  68.429  46.240  1.00 90.33      AAAA O
ATOM  3911  ND2 ASN  408      43.028  66.821  45.253  1.00 84.46      AAAA N
ATOM  3914  C   ASN  408      41.297  64.468  44.654  1.00 65.97      AAAA C
ATOM  3915  O   ASN  408      41.251  63.374  45.151  1.00 63.82      AAAA O
ATOM  3916  N   LEU  409      42.041  64.793  43.659  1.00 61.41      AAAA N
ATOM  3918  CA  LEU  409      42.896  63.872  42.947  1.00 60.90      AAAA C
ATOM  3919  CB  LEU  409      42.153  63.250  41.768  1.00 62.98      AAAA C
ATOM  3920  CG  LEU  409      42.992  62.553  40.704  1.00 59.77      AAAA C
ATOM  3921  CD1 LEU  409      43.488  61.205  41.197  1.00 54.06      AAAA C
ATOM  3922  CD2 LEU  409      42.094  62.445  39.486  1.00 55.74      AAAA C
ATOM  3923  C   LEU  409      44.151  64.599  42.485  1.00 61.19      AAAA C
ATOM  3924  O   LEU  409      44.141  65.809  42.370  1.00 60.64      AAAA O
ATOM  3925  N   THR  410      45.281  63.903  42.424  1.00 63.74      AAAA N
ATOM  3927  CA  THR  410      46.588  64.462  42.131  1.00 60.44      AAAA C
ATOM  3928  CB  THR  410      47.454  64.676  43.385  1.00 67.08      AAAA C
ATOM  3929  OG1 THR  410      46.870  65.746  44.157  1.00 74.29      AAAA O
ATOM  3931  CG2 THR  410      48.909  65.103  43.162  1.00 48.56      AAAA C
ATOM  3932  C   THR  410      47.426  63.565  41.218  1.00 56.62      AAAA C
ATOM  3933  O   THR  410      47.382  62.354  41.317  1.00 54.99      AAAA O
ATOM  3934  N   ILE  411      48.077  64.245  40.288  1.00 53.97      AAAA N
ATOM  3936  CA  ILE  411      48.897  63.562  39.291  1.00 53.29      AAAA C
```

Figure 1A-37

ATOM	3937	CB	ILE	411	48.409	63.854	37.864	1.00	49.91	AAAA C
ATOM	3938	CG2	ILE	411	49.216	63.129	36.806	1.00	30.86	AAAA C
ATOM	3939	CG1	ILE	411	46.911	63.489	37.729	1.00	40.83	AAAA C
ATOM	3940	CD1	ILE	411	46.322	63.547	36.339	1.00	38.51	AAAA C
ATOM	3941	C	ILE	411	50.319	64.018	39.569	1.00	55.38	AAAA C
ATOM	3942	O	ILE	411	50.656	65.179	39.291	1.00	57.59	AAAA O
ATOM	3943	N	SER	412	51.073	63.182	40.270	1.00	54.26	AAAA N
ATOM	3945	CA	SER	412	52.434	63.502	40.689	1.00	54.46	AAAA C
ATOM	3946	CB	SER	412	53.071	62.210	41.248	1.00	55.78	AAAA C
ATOM	3947	OG	SER	412	53.756	62.536	42.434	1.00	67.12	AAAA O
ATOM	3949	C	SER	412	53.326	63.910	39.523	1.00	55.52	AAAA C
ATOM	3950	O	SER	412	54.081	64.876	39.527	1.00	55.04	AAAA O
ATOM	3951	N	ALA	413	53.254	63.124	38.438	1.00	50.12	AAAA N
ATOM	3953	CA	ALA	413	54.064	63.402	37.281	1.00	50.01	AAAA C
ATOM	3954	CB	ALA	413	55.334	62.529	37.365	1.00	34.96	AAAA C
ATOM	3955	C	ALA	413	53.301	63.078	35.994	1.00	49.71	AAAA C
ATOM	3956	O	ALA	413	52.495	62.168	35.998	1.00	48.81	AAAA O
ATOM	3957	N	GLY	414	53.675	63.690	34.895	1.00	47.92	AAAA N
ATOM	3959	CA	GLY	414	53.057	63.454	33.607	1.00	51.75	AAAA C
ATOM	3960	C	GLY	414	52.017	64.524	33.294	1.00	52.77	AAAA C
ATOM	3961	O	GLY	414	51.684	65.370	34.114	1.00	53.23	AAAA O
ATOM	3962	N	LYS	415	51.385	64.406	32.138	1.00	56.31	AAAA N
ATOM	3964	CA	LYS	415	50.289	65.317	31.759	1.00	52.49	AAAA C
ATOM	3965	CB	LYS	415	50.884	66.358	30.833	1.00	50.94	AAAA C
ATOM	3966	CG	LYS	415	51.198	65.855	29.429	1.00	54.39	AAAA C
ATOM	3967	CD	LYS	415	52.288	66.691	28.765	1.00	53.96	AAAA C
ATOM	3968	CE	LYS	415	52.785	66.151	27.441	1.00	56.01	AAAA C
ATOM	3969	NZ	LYS	415	52.426	67.032	26.284	1.00	66.36	AAAA N
ATOM	3973	C	LYS	415	49.110	64.576	31.155	1.00	50.94	AAAA C
ATOM	3974	O	LYS	415	49.077	63.337	31.036	1.00	49.77	AAAA O
ATOM	3975	N	MET	416	48.091	65.353	30.771	1.00	48.34	AAAA N
ATOM	3977	CA	MET	416	46.890	64.734	30.186	1.00	46.77	AAAA C
ATOM	3978	CB	MET	416	45.629	65.186	30.949	1.00	42.79	AAAA C
ATOM	3979	CG	MET	416	45.836	65.880	32.273	1.00	40.91	AAAA C
ATOM	3980	SD	MET	416	44.511	65.636	33.517	1.00	56.20	AAAA S
ATOM	3981	CE	MET	416	44.002	67.366	33.690	1.00	35.94	AAAA C
ATOM	3982	C	MET	416	46.623	65.064	28.729	1.00	40.40	AAAA C
ATOM	3983	O	MET	416	46.963	66.137	28.247	1.00	34.84	AAAA O
ATOM	3984	N	TYR	417	45.893	64.169	28.104	1.00	38.49	AAAA N
ATOM	3986	CA	TYR	417	45.355	64.387	26.765	1.00	39.50	AAAA C
ATOM	3987	CB	TYR	417	46.156	63.471	25.831	1.00	32.02	AAAA C
ATOM	3988	CG	TYR	417	45.583	63.430	24.429	1.00	39.48	AAAA C
ATOM	3989	CD1	TYR	417	45.730	64.501	23.511	1.00	39.29	AAAA C
ATOM	3990	CE1	TYR	417	45.196	64.429	22.253	1.00	34.56	AAAA C
ATOM	3991	CD2	TYR	417	44.884	62.321	24.005	1.00	36.81	AAAA C
ATOM	3992	CE2	TYR	417	44.379	62.241	22.722	1.00	38.80	AAAA C
ATOM	3993	CZ	TYR	417	44.535	63.292	21.872	1.00	44.20	AAAA C
ATOM	3994	OH	TYR	417	44.053	63.361	20.552	1.00	58.10	AAAA O
ATOM	3996	C	TYR	417	43.853	64.065	26.698	1.00	44.18	AAAA C
ATOM	3997	O	TYR	417	43.376	62.974	27.135	1.00	42.19	AAAA O
ATOM	3998	N	PHE	418	43.068	64.971	26.100	1.00	45.84	AAAA N
ATOM	4000	CA	PHE	418	41.644	64.701	25.910	1.00	45.67	AAAA C
ATOM	4001	CB	PHE	418	40.772	65.657	26.720	1.00	47.19	AAAA C
ATOM	4002	CG	PHE	418	40.675	65.264	28.177	1.00	43.44	AAAA C
ATOM	4003	CD1	PHE	418	41.552	65.686	29.132	1.00	38.43	AAAA C
ATOM	4004	CD2	PHE	418	39.638	64.417	28.544	1.00	51.21	AAAA C
ATOM	4005	CE1	PHE	418	41.402	65.291	30.440	1.00	46.44	AAAA C
ATOM	4006	CE2	PHE	418	39.486	64.023	29.845	1.00	46.63	AAAA C
ATOM	4007	CZ	PHE	418	40.358	64.454	30.801	1.00	44.68	AAAA C
ATOM	4008	C	PHE	418	41.251	64.730	24.440	1.00	44.64	AAAA C
ATOM	4009	O	PHE	418	41.375	65.762	23.812	1.00	47.60	AAAA O
ATOM	4010	N	ALA	419	40.554	63.713	23.936	1.00	43.06	AAAA N
ATOM	4012	CA	ALA	419	40.015	63.793	22.607	1.00	39.21	AAAA C
ATOM	4013	CB	ALA	419	41.090	63.562	21.555	1.00	30.88	AAAA C
ATOM	4014	C	ALA	419	38.837	62.846	22.366	1.00	41.77	AAAA C
ATOM	4015	O	ALA	419	38.871	61.628	22.557	1.00	36.08	AAAA O
ATOM	4016	N	PHE	420	37.829	63.398	21.618	1.00	40.41	AAAA N
ATOM	4018	CA	PHE	420	36.742	62.621	21.070	1.00	40.03	AAAA C
ATOM	4019	CB	PHE	420	37.157	61.430	20.180	1.00	45.54	AAAA C
ATOM	4020	CG	PHE	420	37.832	61.909	18.912	1.00	54.18	AAAA C
ATOM	4021	CD1	PHE	420	39.221	61.987	18.751	1.00	49.23	AAAA C
ATOM	4022	CD2	PHE	420	37.006	62.345	17.871	1.00	47.65	AAAA C
ATOM	4023	CE1	PHE	420	39.783	62.496	17.567	1.00	46.00	AAAA C
ATOM	4024	CE2	PHE	420	37.572	62.833	16.725	1.00	51.19	AAAA C
ATOM	4025	CZ	PHE	420	38.964	62.928	16.549	1.00	44.01	AAAA C
ATOM	4026	C	PHE	420	35.762	62.146	22.126	1.00	41.65	AAAA C
ATOM	4027	O	PHE	420	35.352	60.991	22.215	1.00	38.35	AAAA O
ATOM	4028	N	ASN	421	35.459	63.024	23.049	1.00	45.35	AAAA N
ATOM	4030	CA	ASN	421	34.477	62.960	24.112	1.00	46.86	AAAA C
ATOM	4031	CB	ASN	421	35.184	63.276	25.449	1.00	43.60	AAAA C
ATOM	4032	CG	ASN	421	36.407	62.401	25.654	1.00	47.90	AAAA C
ATOM	4033	OD1	ASN	421	36.426	61.147	25.714	1.00	44.83	AAAA O
ATOM	4034	ND2	ASN	421	37.541	63.101	25.732	1.00	27.46	AAAA N
ATOM	4037	C	ASN	421	33.432	64.069	23.835	1.00	47.83	AAAA C
ATOM	4038	O	ASN	421	33.617	65.233	24.237	1.00	38.95	AAAA O

Figure 1A-38

ATOM	4039	N	PRO	422	32.459	63.777	22.969	1.00	47.86	AAAA N
ATOM	4040	CD	PRO	422	32.213	62.423	22.372	1.00	44.11	AAAA C
ATOM	4041	CA	PRO	422	31.463	64.776	22.605	1.00	47.85	AAAA C
ATOM	4042	CB	PRO	422	30.731	64.084	21.446	1.00	44.86	AAAA C
ATOM	4043	CG	PRO	422	30.947	62.623	21.606	1.00	43.01	AAAA C
ATOM	4044	C	PRO	422	30.577	65.284	23.735	1.00	51.16	AAAA C
ATOM	4045	O	PRO	422	30.223	66.486	23.744	1.00	48.54	AAAA O
ATOM	4046	N	LYS	423	30.320	64.487	21.774	1.00	52.90	AAAA N
ATOM	4048	CA	LYS	423	29.431	64.908	25.865	1.00	58.82	AAAA C
ATOM	4049	CB	LYS	423	28.556	63.721	26.360	1.00	52.93	AAAA C
ATOM	4050	CG	LYS	423	28.209	62.810	25.196	1.00	70.55	AAAA C
ATOM	4051	CD	LYS	423	26.743	62.448	24.996	1.00	73.79	AAAA C
ATOM	4052	CE	LYS	423	26.030	63.374	24.021	1.00	77.06	AAAA C
ATOM	4053	NZ	LYS	423	25.949	64.748	24.614	1.00	64.99	AAAA N
ATOM	4057	C	LYS	423	30.158	65.482	27.071	1.00	57.43	AAAA C
ATOM	4058	O	LYS	423	29.582	65.478	28.152	1.00	55.22	AAAA O
ATOM	4059	N	LEU	424	31.425	65.859	26.862	1.00	55.95	AAAA N
ATOM	4061	CA	LEU	424	32.261	66.162	28.017	1.00	57.07	AAAA C
ATOM	4062	CB	LEU	424	33.463	65.250	28.237	1.00	49.16	AAAA C
ATOM	4063	CG	LEU	424	34.390	65.748	29.370	1.00	68.27	AAAA C
ATOM	4064	CD1	LEU	424	33.821	65.362	30.734	1.00	60.66	AAAA C
ATOM	4065	CD2	LEU	424	35.825	65.276	29.123	1.00	60.35	AAAA C
ATOM	4066	C	LEU	424	32.709	67.585	27.878	1.00	56.29	AAAA C
ATOM	4067	O	LEU	424	33.696	67.861	27.201	1.00	59.98	AAAA O
ATOM	4068	N	CYS	425	31.995	68.488	28.492	1.00	58.76	AAAA N
ATOM	4070	CA	CYS	425	32.342	69.916	28.406	1.00	60.39	AAAA C
ATOM	4071	C	CYS	425	33.771	70.119	28.810	1.00	62.59	AAAA C
ATOM	4072	O	CYS	425	34.288	69.665	29.831	1.00	64.45	AAAA O
ATOM	4073	CB	CYS	425	31.249	70.644	29.214	1.00	68.23	AAAA C
ATOM	4074	SG	CYS	425	29.916	71.303	28.086	1.00	81.03	AAAA S
ATOM	4075	N	VAL	426	34.529	70.953	28.102	1.00	65.31	AAAA N
ATOM	4077	CA	VAL	426	35.943	71.149	28.358	1.00	65.49	AAAA C
ATOM	4078	CB	VAL	426	36.644	72.022	27.310	1.00	66.66	AAAA C
ATOM	4079	CG1	VAL	426	36.715	71.413	25.925	1.00	62.49	AAAA C
ATOM	4080	CG2	VAL	426	35.962	73.365	27.239	1.00	60.92	AAAA C
ATOM	4081	C	VAL	426	36.105	71.711	29.757	1.00	65.99	AAAA C
ATOM	4082	O	VAL	426	37.180	71.724	30.388	1.00	64.51	AAAA O
ATOM	4083	N	SER	427	35.090	72.361	30.267	1.00	67.67	AAAA N
ATOM	4085	CA	SER	427	35.091	72.927	31.599	1.00	66.85	AAAA C
ATOM	4086	CB	SER	427	33.685	73.499	31.864	1.00	61.16	AAAA C
ATOM	4087	OG	SER	427	34.088	74.860	32.098	1.00	67.05	AAAA O
ATOM	4089	C	SER	427	35.515	71.972	32.701	1.00	64.24	AAAA C
ATOM	4090	O	SER	427	36.332	72.328	33.573	1.00	63.66	AAAA O
ATOM	4091	N	GLU	428	34.965	70.771	32.618	1.00	58.75	AAAA N
ATOM	4093	CA	GLU	428	35.384	69.753	33.585	1.00	63.39	AAAA C
ATOM	4094	CB	GLU	428	34.594	68.485	33.240	1.00	68.67	AAAA C
ATOM	4095	CG	GLU	428	33.115	68.560	33.537	1.00	66.59	AAAA C
ATOM	4096	CD	GLU	428	32.785	68.560	35.023	1.00	72.33	AAAA C
ATOM	4097	OE1	GLU	428	32.729	67.522	35.722	1.00	81.62	AAAA O
ATOM	4098	OE2	GLU	428	32.501	69.688	35.517	1.00	70.97	AAAA O
ATOM	4099	C	GLU	428	36.970	69.485	33.429	1.00	61.63	AAAA C
ATOM	4100	O	GLU	428	37.671	69.696	34.397	1.00	62.03	AAAA O
ATOM	4101	N	ILE	429	37.265	69.262	32.165	1.00	62.26	AAAA N
ATOM	4103	CA	ILE	429	38.631	69.038	31.789	1.00	61.09	AAAA C
ATOM	4104	CB	ILE	429	38.759	68.933	30.263	1.00	59.32	AAAA C
ATOM	4105	CG2	ILE	429	40.257	68.915	29.895	1.00	45.93	AAAA C
ATOM	4106	CG1	ILE	429	37.968	67.719	29.794	1.00	57.66	AAAA C
ATOM	4107	CD1	ILE	429	38.038	67.555	28.285	1.00	53.48	AAAA C
ATOM	4108	C	ILE	429	39.498	70.166	32.323	1.00	61.90	AAAA C
ATOM	4109	O	ILE	429	40.592	70.017	32.867	1.00	61.28	AAAA O
ATOM	4110	N	TYR	430	38.987	71.384	32.200	1.00	65.34	AAAA N
ATOM	4112	CA	TYR	430	39.729	72.543	32.719	1.00	68.10	AAAA C
ATOM	4113	CB	TYR	430	39.180	73.822	32.099	1.00	71.02	AAAA C
ATOM	4114	CG	TYR	430	39.538	74.006	30.639	1.00	75.98	AAAA C
ATOM	4115	CD1	TYR	430	38.653	73.821	29.599	1.00	77.60	AAAA C
ATOM	4116	CE1	TYR	430	38.953	73.977	28.270	1.00	75.72	AAAA C
ATOM	4117	CD2	TYR	430	40.810	74.401	30.260	1.00	75.95	AAAA C
ATOM	4118	CE2	TYR	430	41.155	74.575	28.937	1.00	74.81	AAAA C
ATOM	4119	CZ	TYR	430	40.221	74.359	27.952	1.00	78.51	AAAA C
ATOM	4120	OH	TYR	430	40.564	74.542	26.616	1.00	85.40	AAAA O
ATOM	4122	C	TYR	430	39.779	72.634	34.241	1.00	63.72	AAAA C
ATOM	4123	O	TYR	430	40.654	73.321	34.758	1.00	58.26	AAAA O
ATOM	4124	N	ARG	431	38.819	72.017	34.907	1.00	65.53	AAAA N
ATOM	4126	CA	ARG	431	38.747	72.043	36.356	1.00	68.15	AAAA C
ATOM	4127	CB	ARG	431	37.348	71.748	36.898	1.00	73.32	AAAA C
ATOM	4128	CG	ARG	431	37.345	71.815	38.430	1.00	82.99	AAAA C
ATOM	4129	CD	ARG	431	37.270	73.279	38.860	1.00	88.39	AAAA C
ATOM	4130	NE	ARG	431	37.698	73.472	40.258	1.00	92.48	AAAA N
ATOM	4132	CZ	ARG	431	36.835	73.258	41.259	1.00	94.93	AAAA C
ATOM	4133	NH1	ARG	431	35.610	72.872	40.872	1.00	87.40	AAAA N
ATOM	4136	NH2	ARG	431	37.021	73.371	42.567	1.00	95.17	AAAA N
ATOM	4139	C	ARG	431	39.718	70.986	36.677	1.00	67.75	AAAA C
ATOM	4140	O	ARG	431	40.637	71.292	37.629	1.00	66.74	AAAA O
ATOM	4141	N	MET	432	39.541	69.791	36.395	1.00	63.87	AAAA N
ATOM	4143	CA	MET	432	40.437	68.703	36.652	1.00	64.46	AAAA C

Figure 1A-39

ATOM	4144	CB	MET	432	40.237	67.522	35.719	1.00	54.25	AAAA C
ATOM	4145	CG	MET	432	41.254	66.426	35.971	1.00	40.18	AAAA C
ATOM	4146	SD	MET	432	40.829	64.925	35.112	1.00	52.21	AAAA S
ATOM	4147	CE	MET	432	41.582	63.681	36.137	1.00	54.99	AAAA C
ATOM	4148	C	MET	432	41.891	69.170	36.626	1.00	64.65	AAAA C
ATOM	4149	O	MET	432	42.530	68.992	37.653	1.00	65.99	AAAA O
ATOM	4150	N	GLU	433	42.331	69.811	35.556	1.00	65.78	AAAA N
ATOM	4152	CA	GLU	433	43.622	70.469	35.510	1.00	69.16	AAAA C
ATOM	4153	CB	GLU	433	43.704	71.506	34.401	1.00	69.58	AAAA C
ATOM	4154	CG	GLU	433	44.121	70.967	33.048	1.00	76.91	AAAA C
ATOM	4155	CD	GLU	433	44.623	72.149	32.242	1.00	82.02	AAAA C
ATOM	4156	OE1	GLU	433	44.718	73.224	32.874	1.00	86.82	AAAA O
ATOM	4157	OE2	GLU	433	44.965	72.050	31.042	1.00	88.26	AAAA O
ATOM	4158	C	GLU	433	44.016	71.219	36.781	1.00	71.29	AAAA C
ATOM	4159	O	GLU	433	45.153	71.083	37.294	1.00	74.29	AAAA O
ATOM	4160	N	GLU	434	43.178	72.120	37.280	1.00	72.93	AAAA N
ATOM	4162	CA	GLU	434	43.505	72.873	38.485	1.00	72.86	AAAA C
ATOM	4163	CB	GLU	434	42.458	73.916	38.840	1.00	81.36	AAAA C
ATOM	4164	CG	GLU	434	41.191	73.956	38.032	1.00	83.34	AAAA C
ATOM	4165	CD	GLU	434	40.191	75.001	38.437	1.00	87.32	AAAA C
ATOM	4166	OE1	GLU	434	39.521	74.929	39.505	1.00	97.34	AAAA O
ATOM	4167	OE2	GLU	434	40.080	75.941	37.583	1.00	99.95	AAAA O
ATOM	4168	C	GLU	434	43.675	71.886	39.632	1.00	71.46	AAAA C
ATOM	4169	O	GLU	434	44.728	71.858	40.251	1.00	78.49	AAAA O
ATOM	4170	N	VAL	435	42.670	71.095	39.926	1.00	66.34	AAAA N
ATOM	4172	CA	VAL	435	42.711	70.129	41.001	1.00	62.49	AAAA C
ATOM	4173	CB	VAL	435	41.451	69.217	40.932	1.00	60.38	AAAA C
ATOM	4174	CG1	VAL	435	41.547	68.214	42.104	1.00	52.32	AAAA C
ATOM	4175	CG2	VAL	435	40.203	70.073	41.029	1.00	50.79	AAAA C
ATOM	4176	C	VAL	435	43.939	69.253	40.818	1.00	60.74	AAAA C
ATOM	4177	O	VAL	435	44.607	69.165	42.034	1.00	62.37	AAAA O
ATOM	4178	N	THR	436	44.282	68.506	39.988	1.00	60.67	AAAA N
ATOM	4180	CA	THR	436	45.335	67.516	39.936	1.00	56.36	AAAA C
ATOM	4181	CB	THR	436	45.199	66.565	38.736	1.00	50.92	AAAA C
ATOM	4182	OG1	THR	436	44.913	67.283	37.503	1.00	47.03	AAAA O
ATOM	4184	CG2	THR	436	44.108	65.526	38.901	1.00	54.38	AAAA C
ATOM	4185	C	THR	436	46.701	68.184	39.930	1.00	60.55	AAAA C
ATOM	4186	O	THR	436	47.714	67.490	40.024	1.00	60.61	AAAA O
ATOM	4187	N	GLY	437	46.836	69.496	39.835	1.00	60.65	AAAA N
ATOM	4189	CA	GLY	437	48.102	70.164	39.749	1.00	59.47	AAAA C
ATOM	4190	C	GLY	437	48.800	69.864	38.424	1.00	64.78	AAAA C
ATOM	4191	O	GLY	437	49.983	70.254	38.245	1.00	62.70	AAAA O
ATOM	4192	N	THR	438	48.112	69.387	37.380	1.00	63.79	AAAA N
ATOM	4194	CA	THR	438	48.731	69.169	36.076	1.00	65.09	AAAA C
ATOM	4195	CB	THR	438	47.967	68.027	35.411	1.00	66.87	AAAA C
ATOM	4196	OG1	THR	438	46.600	68.385	35.731	1.00	62.22	AAAA O
ATOM	4198	CG2	THR	438	48.208	66.659	36.019	1.00	68.74	AAAA C
ATOM	4199	C	THR	438	48.590	70.415	35.220	1.00	66.14	AAAA C
ATOM	4200	O	THR	438	49.003	70.543	34.070	1.00	68.95	AAAA O
ATOM	4201	N	LYS	439	48.089	71.481	35.822	1.00	67.37	AAAA N
ATOM	4203	CA	LYS	439	47.927	72.757	35.154	1.00	71.08	AAAA C
ATOM	4204	CB	LYS	439	47.114	73.708	36.034	1.00	69.23	AAAA C
ATOM	4205	CG	LYS	439	46.677	74.938	35.265	1.00	77.26	AAAA C
ATOM	4206	CD	LYS	439	45.832	75.942	36.014	1.00	81.65	AAAA C
ATOM	4207	CE	LYS	439	44.385	75.475	36.182	1.00	87.39	AAAA C
ATOM	4208	NZ	LYS	439	43.667	76.431	37.100	1.00	93.85	AAAA N
ATOM	4212	C	LYS	439	49.249	73.396	34.752	1.00	73.01	AAAA C
ATOM	4213	O	LYS	439	49.996	73.986	35.541	1.00	74.60	AAAA O
ATOM	4214	N	GLY	440	49.517	73.453	33.441	1.00	73.33	AAAA N
ATOM	4216	CA	GLY	440	50.733	74.167	33.014	1.00	71.39	AAAA C
ATOM	4217	C	GLY	440	51.716	73.204	32.389	1.00	71.20	AAAA C
ATOM	4218	O	GLY	440	52.684	73.650	31.822	1.00	72.70	AAAA O
ATOM	4219	N	ARG	441	51.445	71.908	32.436	1.00	72.99	AAAA N
ATOM	4221	CA	ARG	441	52.343	70.945	31.831	1.00	74.12	AAAA C
ATOM	4222	CB	ARG	441	52.617	69.740	32.716	1.00	69.44	AAAA C
ATOM	4223	CG	ARG	441	51.847	69.695	34.003	1.00	63.34	AAAA C
ATOM	4224	CD	ARG	441	52.060	68.311	34.595	1.00	67.54	AAAA C
ATOM	4225	NE	ARG	441	52.244	68.395	36.030	1.00	61.00	AAAA N
ATOM	4227	CZ	ARG	441	52.326	67.357	36.831	1.00	59.21	AAAA C
ATOM	4228	NH1	ARG	441	52.258	66.117	36.395	1.00	60.57	AAAA N
ATOM	4231	NH2	ARG	441	52.468	67.596	38.128	1.00	72.94	AAAA N
ATOM	4234	C	ARG	441	51.760	70.446	30.511	1.00	73.50	AAAA C
ATOM	4235	O	ARG	441	52.195	69.424	30.012	1.00	74.73	AAAA O
ATOM	4236	N	GLN	442	50.732	71.114	30.043	1.00	74.69	AAAA N
ATOM	4238	CA	GLN	442	49.959	70.646	29.914	1.00	75.13	AAAA C
ATOM	4239	CB	GLN	442	48.457	70.875	29.126	1.00	68.73	AAAA C
ATOM	4240	CG	GLN	442	47.669	69.576	29.195	1.00	71.20	AAAA C
ATOM	4241	CD	GLN	442	47.623	69.029	30.607	1.00	70.98	AAAA C
ATOM	4242	OE1	GLN	442	47.714	67.822	30.868	1.00	78.66	AAAA O
ATOM	4243	NE2	GLN	442	47.477	69.907	31.584	1.00	66.86	AAAA N
ATOM	4246	C	GLN	442	50.326	71.359	27.627	1.00	77.69	AAAA C
ATOM	4247	O	GLN	442	50.227	72.569	27.536	1.00	75.57	AAAA O
ATOM	4248	N	ALA	443	50.474	70.554	26.575	1.00	81.51	AAAA N
ATOM	4250	CA	ALA	443	50.643	71.148	25.236	1.00	82.95	AAAA C
ATOM	4251	CB	ALA	443	51.104	70.118	24.229	1.00	91.69	AAAA C

Figure 1A-40

ATOM	4352	C	ALA	443	49.259	71.706	24.952	1.00	83.73	AAAA C
ATOM	4353	O	ALA	443	49.398	71.744	25.830	1.00	83.87	AAAA O
ATOM	4354	N	LYS	444	48.914	72.052	23.713	1.00	86.20	AAAA N
ATOM	4356	CA	LYS	444	47.559	72.524	23.482	1.00	85.88	AAAA C
ATOM	4357	CB	LYS	444	47.426	73.987	23.128	1.00	83.99	AAAA C
ATOM	4358	CG	LYS	444	46.673	74.734	24.241	1.00	93.60	AAAA C
ATOM	4359	CD	LYS	444	45.883	73.841	25.186	1.00	95.14	AAAA C
ATOM	4360	CE	LYS	444	46.390	73.786	26.614	1.00	97.04	AAAA C
ATOM	4361	NZ	LYS	444	45.368	73.090	27.473	1.00	97.22	AAAA N
ATOM	4365	C	LYS	444	46.659	71.779	22.508	1.00	84.20	AAAA C
ATOM	4366	O	LYS	444	45.428	71.901	22.635	1.00	85.63	AAAA O
ATOM	4367	N	GLY	445	47.214	70.734	21.916	1.00	78.85	AAAA N
ATOM	4369	CA	GLY	445	46.368	69.786	21.208	1.00	75.06	AAAA C
ATOM	4370	C	GLY	445	45.803	68.844	22.260	1.00	72.30	AAAA C
ATOM	4371	O	GLY	445	44.963	67.993	21.940	1.00	74.90	AAAA O
ATOM	4372	N	ASP	446	46.300	68.981	23.492	1.00	67.97	AAAA N
ATOM	4374	CA	ASP	446	45.914	68.174	24.642	1.00	62.81	AAAA C
ATOM	4375	CB	ASP	446	46.754	68.552	25.873	1.00	55.24	AAAA C
ATOM	4376	CG	ASP	446	48.213	68.169	25.801	1.00	54.07	AAAA C
ATOM	4377	OD1	ASP	446	48.693	67.385	24.946	1.00	45.08	AAAA O
ATOM	4378	OD2	ASP	446	49.091	68.595	26.593	1.00	50.12	AAAA O
ATOM	4379	C	ASP	446	44.438	68.274	25.016	1.00	58.07	AAAA C
ATOM	4380	O	ASP	446	43.610	67.369	25.127	1.00	55.59	AAAA O
ATOM	4381	N	ILE	447	44.043	69.527	25.226	1.00	54.13	AAAA N
ATOM	4383	CA	ILE	447	42.652	69.822	25.510	1.00	54.09	AAAA C
ATOM	4384	CB	ILE	447	42.505	70.502	26.877	1.00	48.92	AAAA C
ATOM	4385	CG2	ILE	447	41.030	70.663	27.182	1.00	41.02	AAAA C
ATOM	4386	CG1	ILE	447	43.211	69.621	27.932	1.00	52.36	AAAA C
ATOM	4387	CD1	ILE	447	43.468	70.323	29.237	1.00	48.47	AAAA C
ATOM	4388	C	ILE	447	42.027	70.591	24.364	1.00	53.06	AAAA C
ATOM	4389	O	ILE	447	41.718	71.772	24.423	1.00	56.08	AAAA O
ATOM	4390	N	ASN	448	41.625	69.915	23.307	1.00	53.17	AAAA N
ATOM	4392	CA	ASN	448	41.013	70.642	22.202	1.00	54.61	AAAA C
ATOM	4393	CB	ASN	448	41.283	69.982	20.863	1.00	49.17	AAAA C
ATOM	4394	CG	ASN	448	40.415	68.786	20.577	1.00	49.40	AAAA C
ATOM	4395	OD1	ASN	448	39.287	68.977	20.113	1.00	52.34	AAAA O
ATOM	4396	ND2	ASN	448	40.990	67.622	20.871	1.00	52.49	AAAA N
ATOM	4399	C	ASN	448	39.518	70.824	22.402	1.00	56.44	AAAA C
ATOM	4400	O	ASN	448	38.816	69.974	22.939	1.00	55.83	AAAA O
ATOM	4401	N	THR	449	39.071	71.917	21.764	1.00	58.52	AAAA N
ATOM	4403	CA	THR	449	37.682	72.351	21.901	1.00	58.62	AAAA C
ATOM	4404	CB	THR	449	37.497	73.845	22.169	1.00	55.90	AAAA C
ATOM	4405	OG1	THR	449	37.913	74.485	20.943	1.00	68.89	AAAA O
ATOM	4407	CG2	THR	449	38.354	74.352	23.310	1.00	59.06	AAAA C
ATOM	4408	C	THR	449	36.920	72.053	20.628	1.00	56.82	AAAA C
ATOM	4409	O	THR	449	35.750	72.381	20.473	1.00	60.87	AAAA O
ATOM	4410	N	ARG	450	37.539	71.304	19.757	1.00	55.76	AAAA N
ATOM	4412	CA	ARG	450	36.887	70.935	18.507	1.00	54.66	AAAA C
ATOM	4413	CB	ARG	450	37.845	71.179	17.377	1.00	48.33	AAAA C
ATOM	4414	CG	ARG	450	38.385	69.975	16.645	1.00	54.81	AAAA C
ATOM	4415	CD	ARG	450	39.487	70.561	15.696	1.00	44.92	AAAA C
ATOM	4416	NE	ARG	450	40.706	70.719	16.488	1.00	52.49	AAAA N
ATOM	4418	CZ	ARG	450	41.544	69.757	16.882	1.00	39.08	AAAA C
ATOM	4419	NH1	ARG	450	41.176	68.572	16.466	1.00	41.07	AAAA N
ATOM	4422	NH2	ARG	450	42.601	70.001	17.619	1.00	45.18	AAAA N
ATOM	4425	C	ARG	450	36.267	69.553	18.557	1.00	56.82	AAAA C
ATOM	4426	O	ARG	450	35.186	69.303	17.992	1.00	58.15	AAAA O
ATOM	4427	N	ASN	451	36.800	68.583	19.324	1.00	56.66	AAAA N
ATOM	4429	CA	ASN	451	36.107	67.311	19.434	1.00	50.27	AAAA C
ATOM	4430	CB	ASN	451	36.725	66.127	18.760	1.00	48.54	AAAA C
ATOM	4431	CG	ASN	451	38.243	66.143	18.764	1.00	60.51	AAAA C
ATOM	4432	OD1	ASN	451	38.779	66.279	19.855	1.00	53.45	AAAA O
ATOM	4433	ND2	ASN	451	38.707	65.976	17.506	1.00	54.88	AAAA N
ATOM	4436	C	ASN	451	35.849	66.854	20.869	1.00	52.97	AAAA C
ATOM	4437	O	ASN	451	35.330	65.750	21.096	1.00	49.71	AAAA O
ATOM	4438	N	ASN	452	36.126	67.668	21.951	1.00	51.98	AAAA N
ATOM	4440	CA	ASN	452	35.769	67.485	23.229	1.00	55.88	AAAA C
ATOM	4441	CB	ASN	452	36.947	67.873	24.136	1.00	54.62	AAAA C
ATOM	4442	CG	ASN	452	37.936	66.736	24.285	1.00	60.96	AAAA C
ATOM	4443	OD1	ASN	452	37.646	65.633	24.735	1.00	51.30	AAAA O
ATOM	4444	ND2	ASN	452	39.153	67.098	23.855	1.00	56.75	AAAA N
ATOM	4447	C	ASN	452	34.603	68.385	23.689	1.00	58.11	AAAA C
ATOM	4448	O	ASN	452	34.785	69.629	23.657	1.00	55.07	AAAA O
ATOM	4449	N	GLY	453	33.444	67.813	24.985	1.00	55.08	AAAA N
ATOM	4451	CA	GLY	453	32.313	68.658	24.296	1.00	59.47	AAAA C
ATOM	4452	C	GLY	453	31.500	69.269	23.174	1.00	64.95	AAAA C
ATOM	4453	O	GLY	453	30.302	69.603	23.276	1.00	65.71	AAAA O
ATOM	4454	N	GLU	454	31.910	69.109	21.910	1.00	67.44	AAAA N
ATOM	4456	CA	GLU	454	31.266	69.543	20.690	1.00	63.63	AAAA C
ATOM	4457	CB	GLU	454	31.739	68.818	19.401	1.00	53.71	AAAA C
ATOM	4458	CG	GLU	454	32.349	67.430	19.739	1.00	49.50	AAAA C
ATOM	4459	CD	GLU	454	32.368	66.629	18.454	1.00	54.61	AAAA C
ATOM	4460	OE1	GLU	454	31.368	66.637	17.702	0.01	54.10	AAAA O
ATOM	4461	OE2	GLU	454	33.412	66.003	18.159	0.01	54.17	AAAA O
ATOM	4462	C	GLU	454	29.762	69.301	20.787	1.00	65.41	AAAA C

Figure 1A-41

ATOM	4363	O	GLU	454	29.922	79.089	26.169	1.00	67.86	AAAA O
ATOM	4364	N	ARG	455	29.298	69.187	21.333	1.00	66.45	AAAA N
ATOM	4366	CA	ARG	455	27.843	67.997	21.371	1.00	69.33	AAAA C
ATOM	4367	CB	ARG	455	27.448	66.733	20.652	1.00	73.38	AAAA C
ATOM	4368	CG	ARG	455	28.467	65.912	19.924	1.00	74.27	AAAA C
ATOM	4369	CD	ARG	455	27.775	64.740	19.240	1.00	79.54	AAAA C
ATOM	4370	NE	ARG	455	27.301	63.638	20.052	1.00	86.31	AAAA N
ATOM	4372	CZ	ARG	455	27.802	62.412	20.189	1.00	88.60	AAAA C
ATOM	4373	NH1	ARG	455	28.990	61.997	19.538	1.00	84.52	AAAA N
ATOM	4376	NH2	ARG	455	27.225	61.523	21.003	1.00	87.36	AAAA N
ATOM	4379	C	ARG	455	27.213	67.934	22.756	1.00	67.35	AAAA C
ATOM	4380	O	ARG	455	26.423	67.025	22.961	1.00	66.26	AAAA O
ATOM	4381	N	ALA	456	27.499	68.879	23.623	1.00	66.52	AAAA N
ATOM	4383	CA	ALA	456	26.947	68.906	24.964	1.00	72.01	AAAA C
ATOM	4384	CB	ALA	456	27.832	68.147	25.939	1.00	61.84	AAAA C
ATOM	4385	C	ALA	456	26.802	70.379	25.371	1.00	75.25	AAAA C
ATOM	4386	O	ALA	456	27.706	71.219	25.202	1.00	81.30	AAAA O
ATOM	4387	N	SER	457	25.653	70.720	25.939	0.50	71.91	AAAA N
ATOM	4389	CA	SER	457	25.431	72.095	26.358	0.50	69.64	AAAA C
ATOM	4390	CB	SER	457	23.991	72.247	26.836	0.50	73.30	AAAA C
ATOM	4391	OG	SER	457	23.422	73.294	26.060	0.50	73.31	AAAA O
ATOM	4393	C	SER	457	26.418	72.510	27.437	0.50	69.27	AAAA C
ATOM	4394	O	SER	457	26.458	71.957	28.530	0.50	67.32	AAAA O
ATOM	4395	N	CYS	458	27.197	73.531	27.117	0.50	70.44	AAAA N
ATOM	4397	CA	CYS	458	28.287	73.960	27.972	0.50	72.57	AAAA C
ATOM	4398	C	CYS	458	27.949	75.205	28.757	0.50	72.54	AAAA C
ATOM	4399	O	CYS	458	27.065	75.128	29.606	0.50	76.63	AAAA O
ATOM	4400	CB	CYS	458	29.527	74.171	27.089	0.50	75.38	AAAA C
ATOM	4401	SG	CYS	458	30.844	73.032	27.490	0.50	72.18	AAAA S
ATOM	4402	N	ALA	459	28.607	76.306	28.441	0.50	70.13	AAAA N
ATOM	4404	CA	ALA	459	28.445	77.572	29.116	0.50	70.05	AAAA C
ATOM	4405	CB	ALA	459	27.046	78.149	28.996	0.50	70.57	AAAA C
ATOM	4406	C	ALA	459	28.826	77.461	30.601	0.50	70.13	AAAA C
ATOM	4407	O	ALA	459	29.080	78.556	31.154	0.50	69.96	AAAA O
ATOM	4407	OT	ALA	459	28.855	76.301	31.054	0.50	68.22	AAAA O
ATOM	4522	C1	NAG	461	59.581	7.102	61.119	1.00	88.13	AAAA C
ATOM	4524	C2	NAG	461	59.964	7.338	59.697	1.00	91.94	AAAA C
ATOM	4526	N2	NAG	461	58.738	7.699	58.920	1.00	92.72	AAAA N
ATOM	4528	C7	NAG	461	58.400	9.020	58.999	1.00	96.97	AAAA C
ATOM	4529	O7	NAG	461	58.879	9.774	59.726	1.00	98.62	AAAA O
ATOM	4530	C8	NAG	461	57.323	9.390	58.043	1.00	100.60	AAAA C
ATOM	4534	C3	NAG	461	60.725	6.225	59.085	1.00	94.77	AAAA C
ATOM	4536	O3	NAG	461	61.417	6.725	57.930	1.00	98.51	AAAA O
ATOM	4538	C4	NAG	461	61.873	5.869	60.064	1.00	96.01	AAAA C
ATOM	4540	O4	NAG	461	62.661	4.821	59.484	1.00	99.20	AAAA O
ATOM	4542	C5	NAG	461	61.359	5.529	61.474	1.00	95.13	AAAA C
ATOM	4545	C6	NAG	461	62.465	5.321	62.495	1.00	93.66	AAAA C
ATOM	4548	O6	NAG	461	62.745	6.364	63.354	1.00	92.13	AAAA O
ATOM	4544	O5	NAG	461	60.625	6.648	61.949	1.00	91.92	AAAA O
ATOM	4550	C1	NAG	463	33.054	15.249	72.938	1.00	43.58	AAAA C
ATOM	4552	C2	NAG	463	31.644	15.282	73.412	1.00	43.62	AAAA C
ATOM	4554	N2	NAG	463	30.709	14.527	72.541	1.00	42.16	AAAA N
ATOM	4556	C7	NAG	463	29.912	13.584	73.099	1.00	40.84	AAAA C
ATOM	4557	O7	NAG	463	29.928	13.406	74.222	1.00	40.10	AAAA O
ATOM	4558	C8	NAG	463	28.975	12.694	72.394	1.00	35.47	AAAA C
ATOM	4562	C3	NAG	463	31.150	16.675	73.448	1.00	45.40	AAAA C
ATOM	4564	O3	NAG	463	29.979	16.555	74.196	1.00	45.99	AAAA O
ATOM	4566	C4	NAG	463	32.117	17.617	74.171	1.00	50.36	AAAA C
ATOM	4568	O4	NAG	463	31.596	18.919	73.891	1.00	53.97	AAAA O
ATOM	4569	C5	NAG	463	33.589	17.477	73.725	1.00	48.50	AAAA C
ATOM	4572	C6	NAG	463	34.490	17.996	74.742	1.00	48.34	AAAA C
ATOM	4575	O6	NAG	463	34.906	18.739	75.671	1.00	57.11	AAAA O
ATOM	4571	O5	NAG	463	33.942	16.120	73.583	1.00	48.58	AAAA O
ATOM	4576	C1	FUC	464	34.544	19.954	76.083	1.00	81.45	AAAA C
ATOM	4578	C2	FUC	464	35.179	21.173	75.463	1.00	86.35	AAAA C
ATOM	4579	O2	FUC	464	35.153	21.169	74.021	1.00	92.94	AAAA O
ATOM	4582	C3	FUC	464	34.252	22.284	75.945	1.00	86.79	AAAA C
ATOM	4584	O3	FUC	464	34.691	23.613	75.599	1.00	87.83	AAAA O
ATOM	4586	C4	FUC	464	33.871	22.274	77.412	1.00	86.67	AAAA C
ATOM	4588	O4	FUC	464	34.508	23.297	78.115	1.00	87.06	AAAA O
ATOM	4590	C5	FUC	464	33.921	20.894	78.040	1.00	85.85	AAAA C
ATOM	4593	C6	FUC	464	34.279	20.768	79.512	1.00	83.37	AAAA C
ATOM	4592	O5	FUC	464	35.042	20.150	77.425	1.00	82.43	AAAA O
ATOM	4597	C1	NAG	465	31.575	19.813	74.940	1.00	64.68	AAAA C
ATOM	4599	C2	NAG	465	31.267	21.207	74.437	1.00	69.57	AAAA C
ATOM	4601	N2	NAG	465	32.480	21.642	73.690	1.00	71.25	AAAA N
ATOM	4603	C7	NAG	465	32.401	21.953	72.381	1.00	73.86	AAAA C
ATOM	4604	O7	NAG	465	31.373	21.835	71.881	1.00	74.80	AAAA O
ATOM	4605	C8	NAG	465	33.679	22.401	71.787	1.00	76.00	AAAA C
ATOM	4609	C3	NAG	465	31.050	22.214	75.546	1.00	72.71	AAAA C
ATOM	4611	O3	NAG	465	30.713	23.517	75.108	1.00	71.03	AAAA O
ATOM	4613	C4	NAG	465	30.035	21.654	76.560	1.00	75.71	AAAA C
ATOM	4615	O1	NAG	465	29.993	22.409	77.793	1.00	76.79	AAAA O
ATOM	4617	C5	NAG	465	30.498	20.238	76.977	1.00	75.45	AAAA C
ATOM	4620	O6	NAG	465	29.461	19.647	77.930	1.00	75.64	AAAA O

Figure 1A-42

ATOM	4623	O6	HAG	465	28.385	19.239	77.142	1.00	76.25	AAAA O
ATOM	4619	O5	HAG	465	30.514	19.425	75.807	1.00	71.44	AAAA O
ATOM	4625	C1	HAG	466	49.927	11.058	87.926	1.00	96.51	AAAA C
ATOM	4627	C2	HAG	467	50.538	11.751	89.109	1.00	99.92	AAAA C
ATOM	4629	N2	HAG	467	49.662	12.898	89.459	1.00	101.79	AAAA N
ATOM	4631	C7	HAG	467	49.299	13.021	90.759	1.00	103.63	AAAA C
ATOM	4632	O7	HAG	467	49.541	12.267	91.586	1.00	105.48	AAAA O
ATOM	4633	C9	HAG	467	48.526	14.239	91.102	1.00	105.92	AAAA C
ATOM	4637	C3	HAG	467	51.967	12.134	88.802	1.00	101.03	AAAA C
ATOM	4639	O3	HAG	467	52.535	12.761	89.949	1.00	100.89	AAAA O
ATOM	4641	C4	HAG	467	52.643	10.771	88.506	1.00	101.15	AAAA C
ATOM	4643	O4	HAG	467	54.067	10.834	88.441	1.00	101.35	AAAA O
ATOM	4645	C5	HAG	467	52.039	10.160	87.219	1.00	100.16	AAAA C
ATOM	4648	C6	HAG	467	52.746	8.852	86.934	1.00	99.75	AAAA C
ATOM	4651	O6	HAG	467	52.088	7.704	87.302	1.00	101.54	AAAA O
ATOM	4647	O5	HAG	467	50.671	9.918	87.503	1.00	98.59	AAAA O
ATOM	4653	C1	HAG	469	55.375	46.143	66.863	1.00	48.45	AAAA C
ATOM	4655	C2	HAG	469	56.601	46.993	66.861	1.00	50.42	AAAA C
ATOM	4657	N2	HAG	469	57.106	47.015	65.451	1.00	51.50	AAAA N
ATOM	4659	C7	HAG	469	57.235	48.143	64.746	1.00	48.89	AAAA C
ATOM	4660	O7	HAG	469	56.849	49.101	65.234	1.00	55.62	AAAA O
ATOM	4661	C8	HAG	469	57.838	48.134	63.394	1.00	43.70	AAAA C
ATOM	4665	C3	HAG	469	57.608	46.491	67.844	1.00	49.62	AAAA C
ATOM	4667	O3	HAG	469	58.640	47.461	68.031	1.00	47.76	AAAA O
ATOM	4669	C4	HAG	469	56.843	46.263	69.172	1.00	48.47	AAAA C
ATOM	4671	O4	HAG	469	57.826	45.800	70.134	1.00	50.06	AAAA O
ATOM	4672	C5	HAG	469	55.847	45.130	68.959	1.00	50.81	AAAA C
ATOM	4675	C6	HAG	469	55.190	44.720	70.239	1.00	53.92	AAAA C
ATOM	4678	O6	HAG	469	54.829	45.551	71.193	1.00	56.25	AAAA O
ATOM	4674	O5	HAG	469	54.914	45.599	68.043	1.00	55.45	AAAA O
ATOM	4679	C1	FUC	470	53.830	46.395	71.203	1.00	61.17	AAAA C
ATOM	4681	C2	FUC	470	53.642	47.121	72.534	1.00	59.23	AAAA C
ATOM	4682	O2	FUC	470	54.861	46.876	73.241	1.00	55.14	AAAA O
ATOM	4685	C3	FUC	470	53.421	48.429	71.757	1.00	58.39	AAAA C
ATOM	4687	O3	FUC	470	53.381	49.515	72.637	1.00	56.30	AAAA O
ATOM	4689	C4	FUC	470	52.245	48.255	70.809	1.00	61.24	AAAA C
ATOM	4691	O4	FUC	470	51.061	47.904	71.544	1.00	63.74	AAAA O
ATOM	4693	C5	FUC	470	52.455	47.086	69.828	1.00	62.20	AAAA C
ATOM	4696	C6	FUC	470	51.462	46.723	68.784	1.00	59.15	AAAA C
ATOM	4695	O5	FUC	470	52.567	45.889	70.781	1.00	64.68	AAAA O
ATOM	4700	C1	HAG	471	58.034	46.760	71.149	1.00	37.00	AAAA C
ATOM	4702	C2	HAG	471	58.977	46.225	72.186	1.00	40.30	AAAA C
ATOM	4704	N2	HAG	471	58.958	44.787	72.509	1.00	36.82	AAAA N
ATOM	4706	C7	HAG	471	57.856	44.183	72.903	1.00	44.21	AAAA C
ATOM	4707	O7	HAG	471	56.892	44.744	72.885	1.00	51.50	AAAA O
ATOM	4708	C8	HAG	471	58.202	42.814	73.323	1.00	46.02	AAAA C
ATOM	4712	C3	HAG	471	58.901	47.250	73.291	1.00	34.50	AAAA C
ATOM	4714	O3	HAG	471	59.698	46.917	74.385	1.00	35.84	AAAA O
ATOM	4716	C4	HAG	471	59.645	48.488	72.694	1.00	38.52	AAAA C
ATOM	4718	O4	HAG	471	59.754	49.464	73.694	1.00	37.44	AAAA O
ATOM	4719	C5	HAG	471	59.056	48.958	71.332	1.00	36.94	AAAA C
ATOM	4722	C6	HAG	471	60.116	49.692	70.525	1.00	36.14	AAAA C
ATOM	4725	O6	HAG	471	61.166	50.390	71.080	1.00	43.49	AAAA O
ATOM	4721	O5	HAG	471	58.853	47.785	70.530	1.00	34.98	AAAA O
ATOM	4727	C1	HAI	472	61.035	49.984	73.959	1.00	53.37	AAAA C
ATOM	4729	C2	HAI	472	60.920	51.497	74.260	1.00	56.72	AAAA C
ATOM	4730	O2	HAI	472	59.934	51.584	75.272	1.00	62.11	AAAA O
ATOM	4733	C3	HAI	472	62.216	52.031	74.840	1.00	60.70	AAAA C
ATOM	4735	O3	HAI	472	62.028	53.337	75.383	1.00	60.70	AAAA O
ATOM	4736	C1	HAI	472	62.787	51.161	75.932	1.00	55.46	AAAA C
ATOM	4738	O4	HAI	472	64.085	51.595	76.171	1.00	57.16	AAAA O
ATOM	4740	C5	HAI	472	62.797	49.685	75.511	1.00	52.10	AAAA C
ATOM	4743	C6	HAI	472	63.458	48.905	76.595	1.00	50.32	AAAA C
ATOM	4746	O6	HAI	472	62.990	48.969	77.885	1.00	51.02	AAAA O
ATOM	4742	O5	HAI	472	61.443	49.407	75.200	1.00	53.33	AAAA O
ATOM	4748	C1	HAI	473	62.594	54.401	74.672	1.00	72.61	AAAA C
ATOM	4750	C2	HAI	473	62.417	55.679	75.569	1.00	75.28	AAAA C
ATOM	4751	O2	HAI	473	63.378	56.709	75.348	1.00	74.98	AAAA O
ATOM	4754	C3	HAI	473	60.977	56.163	75.493	1.00	78.65	AAAA C
ATOM	4756	O3	HAI	473	60.841	57.447	76.148	1.00	79.16	AAAA O
ATOM	4758	C4	HAI	473	60.344	56.204	74.114	1.00	78.79	AAAA C
ATOM	4760	O4	HAI	473	58.983	56.571	74.178	1.00	78.93	AAAA O
ATOM	4762	C5	HAI	473	60.499	54.802	73.474	1.00	76.89	AAAA C
ATOM	4765	C6	HAI	473	59.968	54.490	72.091	1.00	74.73	AAAA C
ATOM	4768	O6	HAI	173	60.239	55.469	71.138	1.00	71.39	AAAA O
ATOM	4764	O5	HAI	473	61.916	54.562	73.463	1.00	74.97	AAAA O
ATOM	4408	CB	ALA	479	42.462	74.494	16.374	1.00	82.09	BBBB C
ATOM	4409	C	ALA	479	40.017	74.702	17.001	1.00	91.42	BBBB C
ATOM	4410	O	ALA	479	40.393	75.108	18.103	1.00	96.11	BBBB O
ATOM	4413	N	ALA	479	40.696	74.461	14.624	1.00	86.42	BBBB N
ATOM	4415	CA	ALA	479	41.033	74.100	16.033	1.00	89.85	BBBB C
ATOM	4416	N	ALA	480	38.749	74.752	16.619	1.00	92.12	BBBB N
ATOM	4418	CA	ALA	480	37.684	75.264	17.467	1.00	91.26	BBBB C
ATOM	4419	CB	ALA	480	37.925	76.731	17.769	1.00	86.84	BBBB C
ATOM	4420	C	ALA	480	36.306	75.030	16.849	1.00	91.39	BBBB C

Figure 1A-43

Application No. 09/555,275
Annotated Sheet Showing Changes


```
ATOM   4421  O   ALA   490      35.413   74.647   17.619  1.00 91.79      6588 O
ATOM   4422  N   GLN   491      36.135   75.304   15.564  0.91 89.69      7686 N
ATOM   4424  CA  GLN   491      34.832   75.164   14.915  1.00 87.19      2888 C
ATOM   4425  CB  GLN   491      34.471   76.492   14.221  0.91 92.74      8088 C
ATOM   4426  CG  GLN   491      34.237   77.627   15.220  1.00 99.93      0088 C
ATOM   4427  CD  GLN   491      34.067   79.003   14.626  1.00103.59      8888 C
ATOM   4428  OE1 GLN   491      35.011   79.777   14.381  1.00103.27      6888 O
ATOM   4429  NE2 GLN   491      32.792   79.328   14.398  1.00108.00      0886 N
ATOM   4432  C   GLN   491      34.755   73.947   14.005  1.00 85.31      6888 C
ATOM   4433  O   GLN   491      33.736   73.508   13.456  1.00 83.41      6888 O
ATOM   4434  N   LYS   492      35.849   73.188   13.908  1.00 82.85      8888 N
ATOM   4436  CA  LYS   492      35.982   71.990   13.089  1.00 73.49      6888 C
ATOM   4437  CB  LYS   492      37.377   71.930   12.480  1.00 73.13      8888 C
ATOM   4438  CG  LYS   492      38.287   73.128   12.494  1.00 76.33      6888 C
ATOM   4439  CD  LYS   492      39.413   72.968   11.471  1.00 80.62      8886 C
ATOM   4440  CE  LYS   492      39.985   74.310   11.027  0.91 76.66      6888 C
ATOM   4441  NZ  LYS   492      41.252   74.136   10.262  0.01 76.20      8888 N
ATOM   4445  C   LYS   492      35.779   70.701   13.872  1.00 67.70      8888 C
ATOM   4446  O   LYS   492      35.879   70.744   15.092  1.00 69.09      8888 O
ATOM   4447  N   LEU   493      35.539   69.585   13.199  1.00 61.47      8888 N
ATOM   4449  CA  LEU   493      35.193   68.356   13.896  1.00 59.03      8888 C
ATOM   4450  CB  LEU   493      34.256   67.529   13.039  1.00 55.20      8888 C
ATOM   4451  CG  LEU   493      32.779   67.860   12.875  1.00 61.94      8888 C
ATOM   4452  CD1 LEU   493      32.405   69.154   13.595  1.00 44.78      6886 C
ATOM   4453  CD2 LEU   493      32.433   67.707   11.395  1.00 44.63      8888 C
ATOM   4454  C   LEU   493      36.421   67.509   14.229  1.00 59.73      8888 C
ATOM   4455  O   LEU   493      36.465   66.709   15.165  1.00 57.22      8888 O
ATOM   4456  N   ILE   494      37.345   67.543   13.262  1.00 56.21      8888 N
ATOM   4458  CA  ILE   494      38.597   66.822   13.367  1.00 52.58      8888 C
ATOM   4459  CB  ILE   494      38.490   65.390   12.879  1.00 50.27      8886 C
ATOM   4460  CG2 ILE   494      37.769   65.319   11.524  1.00 44.85      8888 C
ATOM   4461  CG1 ILE   494      39.870   64.766   12.756  1.00 39.78      8888 C
ATOM   4462  CD1 ILE   494      39.888   63.291   12.404  1.00 30.43      8888 C
ATOM   4463  C   ILE   494      39.623   67.645   12.608  1.00 53.49      8888 C
ATOM   4464  O   ILE   494      39.158   68.568   11.942  1.00 48.33      8888 O
ATOM   4465  N   SER   495      40.911   67.499   12.887  1.00 50.86      8888 N
ATOM   4467  CA  SER   495      41.898   68.335   12.209  1.00 49.78      8888 C
ATOM   4468  CB  SER   495      41.969   69.753   12.747  1.00 46.06      8888 C
ATOM   4469  OG  SER   495      43.190   70.035   13.376  1.00 63.03      8888 O
ATOM   4471  C   SER   495      43.294   67.711   12.240  1.00 50.57      8888 C
ATOM   4472  O   SER   495      43.510   66.601   12.740  1.00 46.55      8888 O
ATOM   4473  N   GLU   496      44.246   68.389   11.604  1.00 52.16      8888 N
ATOM   4475  CA  GLU   496      45.624   67.874   11.509  1.00 59.12      8888 C
ATOM   4476  CB  GLU   496      46.547   68.683   10.598  1.00 59.71      8888 C
ATOM   4477  CG  GLU   496      46.221   70.162   10.568  1.00 76.75      8888 C
ATOM   4478  CD  GLU   496      47.370   71.045   10.983  1.00 80.53      8888 C
ATOM   4479  OE1 GLU   496      48.315   70.404   11.472  1.00 91.67      8888 O
ATOM   4480  OE2 GLU   496      47.480   72.289   10.897  1.00 86.00      8888 O
ATOM   4481  C   GLU   496      46.272   67.773   12.896  1.00 56.50      8888 C
ATOM   4482  O   GLU   496      46.768   66.747   13.326  1.00 49.83      8888 O
ATOM   4483  N   GLU   497      45.955   68.738   13.732  1.00 58.37      8888 N
ATOM   4485  CA  GLU   497      46.129   68.736   15.169  1.00 59.36      8886 C
ATOM   4486  CB  GLU   497      45.303   69.887   15.729  1.00 61.32      8888 C
ATOM   4487  CG  GLU   497      45.645   70.232   17.159  1.00 79.21      8888 C
ATOM   4488  CD  GLU   497      46.397   71.545   17.177  1.00 86.09      8888 C
ATOM   4489  OE1 GLU   497      45.768   72.610   17.320  1.00 92.00      8888 O
ATOM   4490  OE2 GLU   497      47.637   71.452   17.026  1.00 96.51      8888 O
ATOM   4491  C   GLU   497      45.735   67.436   15.841  1.00 58.84      8888 C
ATOM   4492  O   GLU   497      46.121   67.018   16.761  1.00 61.93      8888 O
ATOM   4493  N   ASP   498      44.748   66.661   15.474  1.00 56.59      8888 N
ATOM   4495  CA  ASP   498      44.446   65.347   15.932  1.00 55.61      8888 C
ATOM   4496  CB  ASP   498      42.947   64.977   15.699  1.00 51.22      8888 C
ATOM   4497  CG  ASP   498      42.047   66.008   16.267  1.00 45.27      8888 C
ATOM   4498  OD1 ASP   498      42.114   66.563   17.387  1.00 56.45      8888 O
ATOM   4499  OD2 ASP   498      41.151   66.395   15.492  1.00 55.11      8888 O
ATOM   4500  C   ASP   498      45.206   64.211   15.238  1.00 58.91      8888 C
ATOM   4501  O   ASP   498      44.967   63.042   15.634  1.00 57.00      8888 O
ATOM   4502  N   LEU   499      45.933   64.513   14.163  1.00 57.39      8888 N
ATOM   4504  CA  LEU   499      46.659   63.426   13.528  1.00 64.03      8888 C
ATOM   4505  CB  LEU   499      46.722   63.677   12.024  1.00 62.69      8888 C
ATOM   4506  CG  LEU   499      45.746   62.788   11.226  1.00 53.71      8888 C
ATOM   4507  CD1 LEU   499      44.324   63.243   11.514  1.00 51.88      8888 C
ATOM   4508  CD2 LEU   499      46.022   62.967    9.766  1.00 55.20      8888 C
ATOM   4509  C   LEU   499      48.017   63.355   14.210  1.00 68.12      8888 C
ATOM   4510  O   LEU   499      48.860   62.560   13.838  1.00 71.57      8888 O
ATOM   4511  N   ASN   500      48.306   64.318   15.063  1.00 68.24      8888 N
ATOM   4513  CA  ASN   500      49.497   64.424   15.855  1.00 75.04      8886 C
ATOM   4514  CB  ASN   500      49.734   65.910   16.187  1.00 84.46      8888 C
ATOM   4515  CG  ASN   500      51.191   66.105   16.589  1.00 98.83      8888 C
ATOM   4516  OD1 ASN   500      52.092   65.342   16.178  1.00 97.25      8898 O
ATOM   4517  ND2 ASN   500      51.459   67.129   17.407  1.00100.47      8888 N
ATOM   4520  C   ASN   500      49.350   63.610   17.139  1.00 80.30      8886 C
ATOM   4521  O   ASN   500      49.891   62.484   17.264  1.00 80.97      8888 O
ATOM   4521  OT  ASN   500      48.519   64.012   18.001  1.00 89.51      8888 O
ATOM   4770  S   SOL   493      37.254   -7.808   65.465  1.00108.87      8000 S
```

Figure 1A-44

ATOM	4771	O1	SUL	493	38.452	-7.021	66.315	1.00112.65	DDDD O
ATOM	4772	O2	SUL	493	37.611	-7.873	64.029	1.00110.21	DDDD O
ATOM	4773	O3	SUL	493	36.533	-6.555	65.856	1.00109.93	DDDD O
ATOM	4774	O4	SUL	493	36.335	-8.978	65.639	1.00107.58	DDDD O
ATOM	4775	S	SUL	494	56.567	19.753	66.302	1.00109.81	DDDD S
ATOM	4776	O1	SUL	494	56.597	19.128	67.659	1.00107.98	DDDD O
ATOM	4777	O2	SUL	494	57.964	20.027	65.795	1.00112.59	DDDD O
ATOM	4778	O3	SUL	494	55.749	21.006	66.267	1.00111.35	DDDD O
ATOM	4779	O4	SUL	494	55.886	18.792	65.379	1.00109.86	DDDD O
ATOM	4780	S	SUL	495	34.533	11.240	75.722	1.00114.67	DDDD S
ATOM	4781	O1	SUL	495	35.274	12.213	76.595	1.00111.38	DDDD O
ATOM	4782	O2	SUL	495	35.476	10.329	74.974	1.00113.60	DDDD O
ATOM	4783	O3	SUL	495	33.552	11.860	74.748	1.00112.77	DDDD O
ATOM	4784	O4	SUL	495	33.773	10.279	75.604	1.00113.18	DDDD O
ATOM	4785	S	SUL	496	35.466	24.844	59.093	1.00 50.73	DDDD S
ATOM	4786	O1	SUL	496	35.613	24.843	60.607	1.00 62.59	DDDD O
ATOM	4787	O2	SUL	496	36.002	23.581	58.571	1.00 48.59	DDDD O
ATOM	4788	O3	SUL	496	35.880	26.084	58.455	1.00 56.74	DDDD O
ATOM	4789	O4	SUL	496	33.958	21.953	59.034	1.00 59.34	DDDD O
ATOM	4790	S	SUL	497	47.653	-2.303	70.199	1.00 68.98	DDDD S
ATOM	4791	O1	SUL	497	47.849	-1.058	70.996	1.00 68.52	DDDD O
ATOM	4792	O2	SUL	497	48.594	-2.509	69.072	1.00 70.94	DDDD O
ATOM	4793	O3	SUL	497	46.187	-2.393	69.810	1.00 73.47	DDDD O
ATOM	4794	O4	SUL	497	47.799	-3.446	71.129	1.00 71.33	DDDD O
ATOM	4795	S	SUL	498	56.527	35.758	75.513	1.00 71.48	DDDD S
ATOM	4796	O1	SUL	498	55.870	35.013	76.621	1.00 72.97	DDDD O
ATOM	4797	O2	SUL	498	57.759	34.996	75.167	1.00 69.11	DDDD O
ATOM	4798	O3	SUL	498	56.619	37.237	75.785	1.00 72.45	DDDD O
ATOM	4799	O4	SUL	498	55.623	35.809	74.330	1.00 72.74	DDDD O
ATOM	4800	S	SUL	499	40.639	27.365	69.499	1.00 74.04	DDDD S
ATOM	4801	O1	SUL	499	40.219	26.039	70.048	1.00 76.00	DDDD O
ATOM	4802	O2	SUL	499	42.089	27.608	69.835	1.00 75.15	DDDD O
ATOM	4803	O3	SUL	499	39.823	28.467	70.098	1.00 77.27	DDDD O
ATOM	4804	O4	SUL	499	40.424	27.245	68.018	1.00 75.70	DDDD O
ATOM	4805	S	SUL	500	44.996	53.228	20.568	1.00 83.89	DDDD S
ATOM	4806	O1	SUL	500	45.080	54.400	21.461	1.00 84.79	DDDD O
ATOM	4807	O2	SUL	500	46.109	52.266	20.827	1.00 90.38	DDDD O
ATOM	4808	O3	SUL	500	45.032	53.674	19.135	1.00 92.23	DDDD O
ATOM	4809	O4	SUL	500	43.762	52.396	20.723	1.00 91.61	DDDD O
ATOM	4810	OW	WAT	501	29.970	6.904	77.713	1.00 34.84	DDDD O
ATOM	4813	OW	WAT	502	42.522	18.998	78.232	1.00 55.27	DDDD O
ATOM	4816	OW	WAT	503	37.561	21.003	67.518	1.00 41.63	DDDD O
ATOM	4819	OW	WAT	504	50.446	5.721	63.485	1.00 57.37	DDDD O
ATOM	4822	OW	WAT	505	56.668	24.854	72.729	1.00 57.34	DDDD O
ATOM	4825	OW	WAT	506	50.605	57.695	22.727	1.00 54.26	DDDD O
ATOM	4828	OW	WAT	507	55.123	37.781	61.204	1.00 43.71	DDDD O
ATOM	4831	OW	WAT	508	17.414	-9.070	74.793	1.00 48.79	DDDD O
ATOM	4834	OW	WAT	509	44.263	20.885	63.811	1.00 28.64	DDDD O
ATOM	4837	OW	WAT	510	45.085	19.708	84.433	1.00 49.09	DDDD O
ATOM	4840	OW	WAT	511	33.537	1.927	71.115	1.00 60.39	DDDD O
ATOM	4843	OW	WAT	512	19.279	4.902	75.254	1.00 55.23	DDDD O
ATOM	4846	OW	WAT	513	11.502	-9.835	68.996	1.00 57.51	DDDD O
ATOM	4849	OW	WAT	514	24.591	17.207	56.665	1.00 56.36	DDDD O
ATOM	4852	OW	WAT	515	56.947	34.914	62.552	1.00 36.47	DDDD O
ATOM	4855	OW	WAT	516	58.092	39.983	66.234	1.00 30.34	DDDD O
ATOM	4858	OW	WAT	517	48.308	40.726	56.768	1.00 81.69	DDDD O
ATOM	4861	OW	WAT	518	25.776	2.355	85.639	1.00 66.34	DDDD O
ATOM	4864	OW	WAT	519	30.644	68.108	30.765	1.00 82.28	DDDD O
ATOM	4867	OW	WAT	520	38.739	54.257	43.611	1.00 43.42	DDDD O
ATOM	4870	OW	WAT	521	22.996	4.470	64.871	1.00 48.71	DDDD O
ATOM	4873	OW	WAT	522	30.938	50.249	19.364	1.00 54.00	DDDD O
ATOM	4876	OW	WAT	523	32.413	9.061	42.441	1.00 44.45	DDDD O
ATOM	4879	OW	WAT	524	41.019	42.560	55.653	1.00 43.40	DDDD O
ATOM	4882	OW	WAT	525	54.268	51.393	37.513	1.00 55.10	DDDD O
ATOM	4885	OW	WAT	526	37.130	13.599	81.397	1.00 46.40	DDDD O
ATOM	4888	OW	WAT	527	42.585	10.244	84.472	1.00 35.95	DDDD O
ATOM	4891	OW	WAT	528	43.661	61.633	18.450	1.00 41.05	DDDD O
ATOM	4894	OW	WAT	529	27.990	19.862	53.348	1.00 54.59	DDDD O
ATOM	4897	OW	WAT	530	59.527	38.520	64.116	1.00 37.96	DDDD O
ATOM	4900	OW	WAT	531	22.451	1.046	57.437	1.00 59.31	DDDD O
ATOM	4903	OW	WAT	532	30.380	16.123	70.205	1.00 40.39	DDDD O
ATOM	4906	OW	WAT	533	46.835	27.888	65.854	1.00 52.34	DDDD O
ATOM	4909	OW	WAT	534	39.446	49.001	45.379	1.00 46.05	DDDD O
ATOM	4912	OW	WAT	535	46.992	51.272	50.722	1.00 52.62	DDDD O
ATOM	4915	OW	WAT	536	44.263	10.776	73.017	1.00 40.61	DDDD O
ATOM	4918	OW	WAT	537	33.670	58.861	20.848	1.00 51.56	DDDD O
ATOM	4921	OW	WAT	538	52.469	21.639	73.804	1.00 61.98	DDDD O
ATOM	4924	OW	WAT	539	49.985	44.871	37.324	1.00 45.45	DDDD O
ATOM	4927	OW	WAT	540	24.074	-1.791	60.077	1.00 40.40	DDDD O
ATOM	4930	OW	WAT	541	35.267	0.714	79.039	1.00 51.34	DDDD O
ATOM	4933	OW	WAT	542	31.231	-1.176	62.362	1.00 48.33	DDDD O
ATOM	4936	OW	WAT	543	41.728	-5.156	55.290	1.00 60.67	DDDD O
ATOM	4939	OW	WAT	544	48.564	37.335	72.612	1.00 71.65	DDDD O
ATOM	4942	OW	WAT	545	49.501	40.030	67.582	1.00 44.88	DDDD O
ATOM	4945	OW	WAT	546	54.851	7.987	69.018	1.00 49.91	DDDD O

Figure 1A-45

```
ATOM   1948  OH  WAT   547      39.459 -14.058  70.554  1.00 84.42      DDDD 0
ATOM   1951  OH  WAT   548      57.310  32.779  60.849  1.00 50.77      DDDD 0
END
```

Application No. 09/555,275
Annotated Sheet Showing Changes

Figure 1A-46

Figure 9: Sequence Alignment of hIGF-1R, hIR and hIRR ectodomains.

Derived by use of the PileUp program in the software package of the Genetics Computer Group, 575 Science Drive, Madison, Wisconsin, USA.

```
 Symbol Comparison table: GenRunData:PileUpPep.Cmp  CompCheck: 1254

                    GapWeight: 3.0
              GapLengthWeight: 0.1


 Name: Higflr          Len:   972  Check: 1781  Weight:  1.00
 Name: Hir             Len:   972  Check: 2986  Weight:  1.00
 Name: Hirr            Len:   972  Check: 9819  Weight:  1.00


                *                       *
Higflr  .....EICGP GIDIRNDYQQ LKRLENCTVI EGYLHILLIS K..AEDYRSY 43
  Hir   HLYPGEVC.P GMDIRNNLTR LHELENCSVI EGHLQILLMF KTRPEDFRDL 49
 Hirr   ....MNVC.P SLDIRSEVAE LRQLENCSVV EGHLQILLMF TATGEDFRGL 45

Higflr  RFPKLTVITE YLLLFRVAGL ESLGDLFPNL TVIRGWKLFY NYALVIFEMT 93
  Hir   SFPKLIMITD YLLLFRVYGL ESLKDLFPNL TVIRGSRLFF NYALVIFEMV 99
 Hirr   SFPRLTQVTD YLLLFRVYGL ESLRDLFPNL AVIRGTRLFL GYALVIFEMP 95

                                        *
Higflr  NLKDIGLYNL RNITRGAIRI EKNADLCYLS TVDWSLILDA VSNNYIVGNK 143
  Hir   HLKELGLYNL MNITRGSVRI EKNNELCYLA TIDWSRILDS VEDNYIVLNK 149
 Hirr   HLRDVALPAL GAVLRGAVRV EKNQELCHLS TIDWGLLQPA PGANHIVGNK 145

             *  *              *              *     *    *  *
Higflr  PPK.ECGDLC PGTMEEKPM. CEKTTINNEY NYRCWTTNRC QKMCPSTCGK 191
  Hir   DDNEECGDIC PGTAKGKTN. CPATVINGQF VERCWTHSHC QKVCPTICKS 198
 Hirr   LG.EECADVC PGVLGAAGEP CAKTTFSGHT DYRCWTSSHC QRVCPCPHG. 193

           *     **    *   *          *  *          *    *
Higflr  RACTENNECC HPECLGSCSA PDNDTACVAC RHYYYAGVCV PACPPNTYRF 241
  Hir   HGCTAEGLCC HSECLGNCSQ PDDPTKCVAC RNFYLDGRCV ETCPPPYYHF 248
 Hirr   MACTARGECC HTECLGGCSQ PEDPRACVAC RHLYFQGACL WACPPGTYQY 243

              *       *      *---------*          *   *
Higflr  EGWRCVDRDF CANILSAES. ...SDSEGFV IHDGECMQEC PSGFIRNGSQ 287
  Hir   QDWRCVNFSF CQDLHHKCKN SRRQGCHQYV IHNNKCIPEC PSGYTMNSSN 298
 Hirr   ESWRCVTAER CASLHSVPG. ....RASTFG IHQGSCLAQC PSGFTRNSS. 287

              *  *    *   *                  *
Higflr  SMYCIPCEGP CPKVCEEEKK TKTIDSVTSA QMLQGCTIFK GNLLINIRRG 337
  Hir   .LLCTPCLGP CPKVCHLLEG EKTIDSVTSA QELRGCTVIN GSLIINIRGG 347
 Hirr   SIFCHKCEGL CPKECKV..G TKTIDSIQAA QDLVGCTHVF GSLILNLRQG 335

Higflr  NNIASELENF MGLIEVVTGY VKIRHSHALV SLSFLKNLRL ILGEEQLEGN 387
  Hir   NNLAAELEAN LGLIEEISGY LKIRRSYALV SLSFFRKLRL IRGETLEIGN 397
 Hirr   YNLEPQLQHS LGLVETITGF LKIKHSPALV SLGFFKNLKL IRGDAMVDGN 385

                                                *
Higflr  YSFYVLDNQN LQQLWDWDHR NLTIKAGKMY FAFNPKLCVS EIYRMEEVTG 437
  Hir   YSFYALDNQN LRQLWDWSKH NLTITQGKLF FHYNPKLCLS EIHKMEEVSG 447
 Hirr   YTLYVLDNQN LQQLGSWVAA GLTIPVGKIY FAFNPRLCLE HIYRLEEVTG 435
```

Figure 9A

```
                                        *     !End of 1-462 fragment
Higflr  TKGRQSKGDI NTRNNGERAS CESDV  LHFTS TTTSKNRIII TWHRYRPPDY  487
  Hir   TKGRQERNDI ALKTNGDQAS CENEL  LKFSY IRTSFDKILL RWEPYWPPDF  497
 Hirr   TRGRQNKAEI NPRTNGDRAA CQTRT  LRFVS NVTEADRILL RWERYEPLEA  485
*
Higflr  RDLISFTVYY KEAPFKNVTE YDGQDACGSN SWNMVDVDLP .....PNKDV  532
  Hir   RDLLGFMLFY KEAPYQNVTE FDGQDACGSN SWTVVDIDPP LRSNDPKSQN  547
 Hirr   RDLLSFIVYY KESPFQNATE HVGPDACGTQ SWNLLDVELP L.....SRTQ  530

Higflr  EPGILLHGLK PWTQYAVYVK AVTLTMVEND HIRGAKSEIL YIRTNASVPS  582
  Hir   HPGWLMRGLK PWTQYAIFVK TL.VTFSDER RTYGAKSDII YVQTDATNPS  596
 Hirr   EPGVTLASLK PWTQYAVFVR AITLTTEEDS PHQGAQSPIV YLRTLPAAPT  580

Higflr  IPLDVLSASN SSSQLIVKWN PPSLPNGNLS YYIVRWQRQP QDGYLYRHNY  632
  Hir   VPLDPISVSN SSSQIILKWK PPSDPNGNIT HYLVFWERQA EDSELFELDY  646
 Hirr   VPQDVISTSN SSSHLLVRWK PPTQRNGNLT YYLVLWQRLA EDGDLYLNDY  630

        *                                 *   ** **  *
Higflr  CSKD.KIPIR KYADGTIDIE EVTENPKTEV CGGEKGPCCA C...PKTEAE  678
  Hir   CLKGLKLPSR TWS.PPFESE DSQKHNQSE. YEDSAGECCS C...PKTDSQ  691
 Hirr   CHRGLRLPTS N.NDPRFDGE DGDPEAEME. .....SDCCP CQHPPPGQVL  673

                                      α------->&lt;------β
Higflr  KQAEKEEAEY RKVFENFLHN SIFVPRPERK RRDVMQVANT TMSSRSRNTT  728
  Hir   ILKELEESSF RKTFEDYLHN VVFVPRPSRK RRSLGDVGNV TVAVP...TV  738
 Hirr   PPLEAQEASF QKKFENFLHN AITIPISPWK VTSINKSPQR D.SGRHRRAA  722

                                                           *
Higflr  AA..DTYNIT DPEELETEYP FFESRVDNKE RTVISNLRPF TLYRIDIHSC 776
  Hir   AAFPNTSSTS VPTSPEEHRP F..EKVVNKE SLVISGLRHF TGYRIELQAC 786
 Hirr   GPLRLGGNSS DFEIQEDKVP ........RE RAVLSGLRHF TEYRIDIHAC 764

              *
Higflr  NHEAEKLGCS ASNFVFARTM PAEGADDIPG PVTWEPRPEN SIFLKWPEPE 826
  Hir   NQDTPEERCS VAAYVSARTM PEAKADDIVG PVTHEIFENN VVHLMWQEPK 836
 Hirr   NHAAHTVGCS AATFVFARTM PHREADGIPG KVAWEASSKN SVLLRWLEPP 814

                                        *           *
Higflr  NPNGLILMYE IKYGS.QVED QRECVSRQEY RKYGGAKLNR LNPGNYTARI 875
  Hir   EPNGLIVLYE VSYRRYGDEE LHLCVSRKHF ALERGCRLRG LSPGNYSVRI 886
 Hirr   DPNGLILKYE IKYRRLGEEA TVLCVSRLRY AKFGGVHLAL LPPGNYSARV 864

Higflr  QATSLSGNGS WTDPVFFYVQ AKTGYENFIH L                     906
  Hir   RATSLAGNGS WTEPTYFYVT DYLDVPSNIA K                     917
 Hirr   RATSLAGNGS WTDSVAFYIL GPEEEDAGGL H                     895
```

Figure 9B